Edited by
Stefan Bäumer

Handbook of Plastic Optics

Related Titles

Gross, H. (ed.)

Handbook of Optical Systems

6 Volume Set

Hardcover
ISBN: 978-3-527-40382-0

Saleh, B. E. A., Teich, M. C.

Fundamentals of Photonics

2006
Hardcover
ISBN: 978-0-471-35832-9

Hornberg, A. (ed.)

Handbook of Machine Vision

2006
Hardcover
ISBN: 978-3-527-40584-8

Römer, H.

Theoretical Optics

An Introduction

2005
Hardcover
ISBN: 978-3-527-40429-2

Brown, T. G., Creath, K., Kogelnik, H., Kriss, M., Schmit, J., Weber, M. J. (eds.)

The Optics Encyclopedia

Basic Foundations and Practical Applications. 5 Volumes

2004
Hardcover
ISBN: 978-3-527-40320-2

Sinzinger, S., Jahns, J.

Microoptics

2003
Hardcover
ISBN: 978-3-527-40355-4

Handbook of Plastic Optics

Edited by
Stefan Bäumer

2nd, revised and enlarged edition

WILEY-VCH Verlag GmbH & Co. KGaA

Contents

List of Contributors

Stefan Bäumer
Philips Applied Technologies
Optics & Sensors
HTC 7 / 4A
NL – 5656 AE Eindhoven
The Netherlands

Thomas Bauer
Jenoptik Polymer Systems
Am Sandberg 2
D-07819 Triptis
Germany

Jukka-Tapani Mäkinen
VTT Technical Research Centre
of Finland
P.O. Box 1100
FI-90571 Oulu
Finland

Koji Minami
Zeon Corporation
Division of Specialty
Plastics & Components
1-6-2, Marunouchi, Chiyoda-ku
Tokyo, 100-8246
Japan

Michael Pfeffer
Optical Engineering
Physical Engineering Course
FH Ravensburg-Weingarten
Postfach 1261
D-88241 Weingarten
Germany

Ulrike Schulz
Fraunhofer Institut IOF
Albert Einstein Str. 7
D-07745 Jena
Germany

Thomas Walter
Arburg
Arthur-Hehl-Strasse
D-72290 Lossburg
Germany

Stefan Bäumer   is working at the Philips Applied Technologies as senior optical designer. Besides design of general optical system his main areas of interest are in design and metrology of injection molded optics.

Thomas Bauer   is working at Jenoptik Polymer Systems Triptis, a plastic optics manufacturer. He is currently head of the development department.

Dieter Marschall   is Area Sales & Service Manager for Germany, Austria & Switzerland at Precitech B.V., the European subsidiary of Precitech Inc. (USA), one of the worlds leading manufacturer of "Single Point Diamond Machining Systems" for turning-, milling- and grinding operation.

Koji Minami   is working at Zeon Corporation as senior researcher. His main responsibility is application development of Cyclo Olefin Polymer (COP): ZEONEX$^{®}$/ ZEONOR$^{®}$.

Michael Pfeffer   is teaching at the University of Applied Sciences in Weingarten as professor of optical engineering. His major areas of interest are finite element analysis in opto-mechanical engineering, diffractive optics and nanometric structuring of optical surfaces. He is currently dean of the master course Optical Systems Engineering.

Ulrike Schulz   received her diploma degree in chemistry in 1986 and her PhD (Dr. rer.nat.) in 1993 from the University of Jena, Germany. She is responsible for the group coatings on polymers at the Fraunhofer Institute of Applied Optics and Precision Engineering in Jena and has authored a number of papers and patents on processes for polymer coating and coating design.

Thomas Walther   is working at ARBURG GmbH & Co. KG, a manufacturer of plastic injection moulding machines. He is responsible for the applications engineering department

Jukka-Tapani Mäkinen   is working as a senior researcher at the Technical Research Centre of Finland. In addition to optical design work he is doing research on the topics of embedded optics in consumer devices and heterogeneous integration of electronics, optics and mechanics.

1
Introduction

Stefan Bäumer (Philips Centre for Industrial Technology (CFT), Eindhoven, The Netherlands)

Optics has been identified as one of the key technologies for the 21st century. Already now in our daily lives we come across optical technologies in several areas:

- at the supermarket most of the tills work in conjunction with bar code scanning;
- ink jet printers perform automatic calibration and media detection;
- most new mobile phones have an integrated camera;
- music and movies are available on CD and/or DVD players;
- computers store data on optical disks;
- blood sugar measurements are based upon optical technology; and
- LED illumination exists in several applications.

Looking at the examples above, it can be concluded that optical technologies are part of various market segments: consumer electronics, lighting, medical, automotive, sensors in general, security, and biometrics.

In order for these markets to further develop and emerge not only do smart inventions have to be made but also suitable manufacturing technologies have to be developed. For optical technology to really reach out and find applications in the mass market it is essential that optical components and systems can be manufactured in high volumes and at low prices. Many of the other components for high-volume applications as described above are based on silicon technology. Light sources such as LEDs and laser diodes can be manufactured using already developed silicon processing and manufacturing technology. The same holds for detectors such as photodiodes and CCD or CMOS cameras. These wafer-based technologies can cope with (very) high volumes and are of low cost. For integration of optical systems together with silicon devices in high-volume consumer optics, injection molding is the manufacturing method of choice. Once a design is cut into a tool and the proper processing for the application is developed, hundreds of thousand of virtually identical products can be made from that one master. Injection molding of optics is known for showing very little part-to-part variation once the proper process is defined. Also, using multi-cavity molding, low prices per piece and a fast production cycle can be achieved. Using 8-cavity – and

sometimes even 16-cavity – molding, production volumes of well above a hundred thousand parts per week can be achieved. These are the kinds of volumes needed to keep up with silicon manufacturing technologies, enabling the high-volume applications. For these lager volumes injection molded optics are highly cost effective. Compared to classic optics production with limited capital investment in machines and tooling, many parts can be produced. Furthermore the injection molding process can be automated and run with few operators.

As well as being cost effective in high-volume applications the other big advantage of injection molded optics is the possibility to also include mechanical features in the optics parts. This allows for cheaper, faster assembly. If reference marks are included in the optomechanical design, and the design is such that critical surfaces are referenced to each other through precision tooling, assembly can be done in a plug and play fashion. Parts can be stacked together without extra alignment of the components. There is even a possibility for (semi-) automated assembly. This is again a necessity for high-volume/low-cost production. Chapter 2 discusses various examples of integrated optomechanical design. By making use of combined optomechanical design, where in some cases the number of parts in a system can also be reduced. In particular, mounting rings and spacers can be eliminated quite easily. Although in some cases the price of the individual components might increase slightly by this integration, on the scale of the whole system costs can be reduced.

Injection molded optics is predestined for integration of functions – another advantage of optics produced by this process. Complex shapes can be realized using advanced tooling and molding. Mechanical functions can be combined with optical ones, and also electrical and chemical functions can be added. The last mentioned one is especially important for the emerging field of biosensing and biotechnology.

The overall drive for integration of functions is usually miniaturization. In classic manufacturing technology it can be fairly difficult to produce parts that are less than certain dimensions. Handling between polishing steps and working on front and back surfaces can become a problem. Molding these small parts can be of significant advantage, since fewer handling steps are involved.

Another advantage as regards injection molded optics is that packing of molded components can be made very effective. It is no problem to place molded optical components into a tape and reel package. The optical components can than be combined with silicon parts using standard pick and place machines, as they are common in the printed circuit board industry. Figure 1.1 shows a typical CMOS camera module in an exploded view and then packed in a tape.

Along with these many advantages, the challenges for plastic optical components lie mainly in the area of environmental resistance and durability. Plastic optical components have a limited temperature range in which they can operate. Water absorption, thermal expansion, and change of refractive index with temperature are other problems one encounters while working with injection molded optical components. Chapters 5 and 6 describe these problems in detail and also
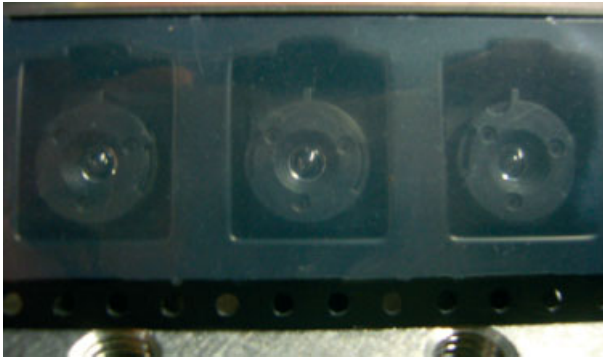
Figure 1.1 left: exploded view of a COMS camera module,
right: tape of CMOS camera modules[3]

ways to circumvent some of them. However, in most cases the benefits of using injection molded optics by far out weight the disadvantages.

Many advances in injection molded optics have been made, which started to really penetrate into the market with the advent of CD players. Besides defining ever more applications, research and development has been taking place in the following areas:

- molding machine development;
- tooling for optical inserts and molds;
- materials;
- coatings; and
- processes.

Taking all these developments into account it should become clear to the reader that injection molding of optical components is state-of-the-art manufacturing technology for high-volume optics. Precision and quality of molded optical components is at a level comparable to glass optics and certainly way beyond the level of toy-like applications.

This book attempts to give a coherent overview of the current status of injection molded optics. Since injection molded optics is a subject with many facets, it was decided to ask several experts in their fields to contribute to this book. This way the specific disciplines are covered in sufficient depth. Also, since injection molding is a manufacturing technology, all of the contributors either work in or have very close links to the industry. Therefore this book reflects practical molding experience rather than theoretical reflections. After going through the book, the reader should have a basic understanding of injection molded optics in all of the relevant areas. He or she should be able to enter a detailed and specific discussion about his/her application with an injection molding company. Also, engineers working in a specific area of injection molded optics can use the book for broadening their knowledge in other areas of injection molding. A designer can learn

more about metrology and a tooling engineer more about materials. By sharing experiences and knowledge the whole industry should profit and advance to the next level.

The basic idea that serves as a guideline throughout the book is the thought that all products have to go through a Design – Build – Test cycle. This idea has also been kept in the second edition of the book. Therefore, all the chapters of the first edition have been kept. Chapters 2, 3, and 5 have gone through some minor revisions and corrections. Chapters 4 and 6 have been substantially revised and updated. In order to make the book even more complete, three new chapters have been added: Process and Molding Equipment, Cost Modeling, and Applications. All the new chapters contain topics that are vital when talking about plastic optics, and deserve more attention than previously. With these additions and revisions of the previous chapter, this book is on its way to become more of a true handbook and reference for injection-molded optics.

Chapter 2, the first chapter after this introduction is devoted to optomechanic design of injection-molded optics. The unique opportunities in injection-molded optics to combine mechanical and optical features in one component are described. Special attention is paid to the thermal properties of the optical plastics and the proper design with these.

In Chapter 3 the building part of the cycle is covered. During the past few years immense advances in precision engineering and especially single-point diamond turning of optical surfaces have been made. The advances in tooling capability are essential for modern injection molded optics. While designing in glass gives the designer a freedom of material with preferably spherical forms, the designer of injection molded optics is left with very few materials but with freedom of form. However, in order to utilize fully the potential of free and aspherical forms optical tooling needs to be at a level such that these forms can be manufactured. In addition to advanced optical tooling, the whole variety of mold design and tooling is described. This ranges from prototype molding to multi-cavity series molds.

In Chapter 4 an overview of current state-of-the-art metrology is given. As in all of the other chapters the subtleties of injection molding are emphasized. A few generic metrology technologies are discussed and the conflict between these generic methods and custom metrology setups is described. Also the need for high-volume inspection is discussed.

Chapter 5 is devoted to materials. If currently or in the future there is one area that is or will be important for injection molded optics, then it is materials. At present it is very difficult to get reliable and coherent data on optical plastics. In the chapter an attempt is made to provide these data for the most common optical polymers. The most relevant properties of many optical plastics are listed and described. This chapter can serve as a reference for properties like refractive index, Abbe number, thermal expansion, etc.

Chapter 6 deals with coatings on polymers. Proper coatings can add value to injection molded optics. Besides that, coatings can enlarge the areas of application of polymer optics. Coatings can be used not only to enhance the optical performance of injection molded components but also make them more able to with-

stand a larger range of environments. In this way some of the traditional short-comings of injection molded optics can be compensated for. The chapter gives an overview of the current state-of-the-art of coatings on plastics. Also, the challenges of working with plastics are illustrated.

Chapter 7 is devoted to injection-molding equipment and processes. Besides proper design and tooling, suitable processes for the parts at hand are necessary as well. The processes used go mostly together with the injection-molding equipment available. Therefore, Chapter 7 gives a good overview on both: some of the most common equipment and on injection molding processes. Since processes are usually a core competence of the injection molding companies, this chapter gives an overview on basic principles; not recipes to follow.

A reoccurring topic in injection molding is costs. When it is cost effective to start molding? What are initial costs involved? These are only two of several common questions asked. Chapter 8 shines some light on cost modeling for injection molding. The chapter gives a review on several of the most important parameters that determine the cost of injection molding parts and products. As the other chapters of the book, this chapter can also be used and read from various perspectives: engineer, purchasing, and general interest.

The last chapter that was added to the second revision is a chapter on Applications. Sometimes in can be very useful and illustrative to see, how certain problems have been solved and how some of the solutions look like. In Chapter 9, several authors of companies and institutes have been willing to lift the tip of the veil and share their solutions with the reader. This chapter is intended more as an inspiration and food for thoughts on what is possible using injection-molded optics.

2
Optomechanics of Plastic Optical Components

Michael Pfeffer (Optical Engineering, FH Ravensburg-Weingarten, Germany)

2.1
Introduction

Citing Dan Vukobratovic, Willey and Parks [1] defined optomechanics "as the science, engineering, and/or art of maintaining the proper shapes and positions of the functional elements of an optical system so that the system performance requirements are satisfied." With respect to mechanical engineering this also implies "that the emphasis is on strain or deformation rather than stress."

Starting from this point of view, several new aspects arise when considering plastic optics, all of which have their origin in two fundamental differences. First, in comparison to glasses or metals, optical plastics have quite different material properties. Second, plastic optical parts and components are typically fabricated by methods and processes different from those applied to classic optics.

As a consequence, this gives rise to, on the one hand, various new possibilities such as:

- high-volume production capability and low relative manufacturing cost;
- freedom with respect to design, shaping, and structuring optically active surfaces, including aspheric, micro-optical refractive, and diffractive features;
- reduction of weight due to both smaller densities of plastic optical materials and facile realization of lightweight structures;
- higher shatter resistance due to the elastic behavior of most plastic optical materials; and
- implementation of cost-saving mounting methods for optical elements such as snapping, screwing, and welding techniques when dealing with thermoplastic resins.

The aspect with the highest overall impact with respect to the issues listed above is probably the monolithic integration of several optical, mechanical, or even electrical features.

On the other hand, there are also some optomechanical challenges [2]:

- Compared to glass, optical plastics show much higher photoelastic birefringence, which requires very careful study of both fabrication- and mounting-induced stress.
- Higher thermal expansion coefficients and lower thermal capacity and conductivity may cause important dimensional deformations. Therefore, athermalization becomes an important issue.
- Since service temperatures of almost all optical plastics are lower than those of glasses and metals, thermal management on a systems level has to be considered.
- Due to low mechanical hardness plastic optical materials are quite sensitive to scratching. This can be addressed by the use of hard, scratch-resistant surface coatings.
- Outgassing limits the use of plastic optical components in ultrahigh vacuum (UHV), since most polymers contain lubricants, colorants, and stabilizers, which may outgas.
- Another characteristic property of plastic optical materials is water absorption, which causes both dimensional changes by swelling and changes in the refractive index.
- Shrinkage due to cooling in an injection molding process is rather complicated to predict.
- When exposed to ionizing radiation, plastic optical materials show some fluorescence or even discoloration by polymer chain cross-linking.

All these items have to be taken into account when optimizing plastic optical parts and systems.

2.2
Configuration of Plastic Optical Elements

In general, an optical element has not only to fulfill optical functions but also mechanical and sometimes even electronic functions.

From a functional point of view optical elements generally can be divided into two groups: imaging and non-imaging optical devices. Of these two device groups, each may work with surfaces having refractive, reflective, diffractive, or stop functions.

Optical devices must also be considered as mechanical parts, which have to be mechanically aligned, centered, fixed, mounted, and assembled.

In some cases optical elements even must be considered as electric or electronic devices. For example, when using the surfaces of an optical element as substrate for integrated or printed circuits or in the case of electromagnetic compatibility (EMC), the electronic function aspect of such primarily optical devices may become an issue.

The following discussion starts with the configuration of single-function elements such as lenses and elements with integrated fixation features. This is followed by the consideration of some examples of plastic optical elements with high functional integration.

2.2.1
Single-Function Elements

Apart from plano window elements, the simplest plastic optical element is a lens with an integrated mounting flange, whether with a protrusion (Figure 2.1, top) or a flat (Figure 2.1, bottom) for both gating and orientation with respect to the mounting position.
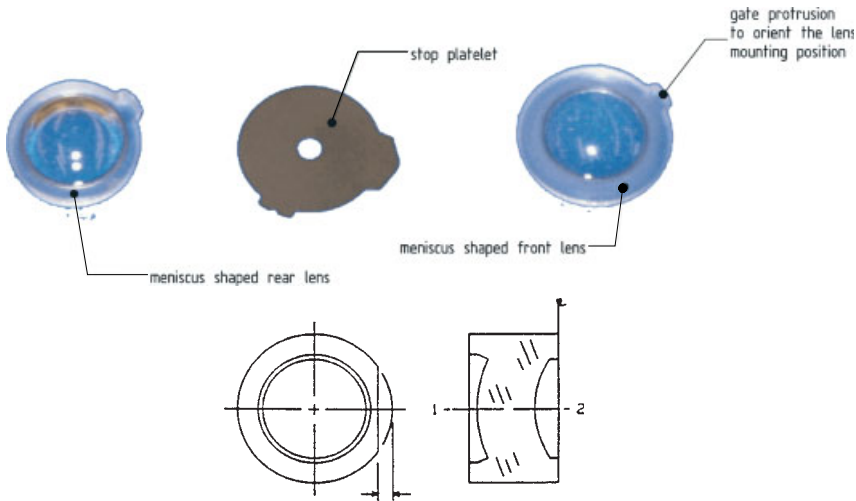
Figure 2.1 Top: components of the objective lens system of a single-use camera consisting of a meniscus-shaped rear lens, a stop platelet made of steel, and a meniscus-shaped front lens. Note the mounting flange and the gate protrusion to orient the lens mounting position. Bottom: meniscus lens with gate flat from Ref. [21]. Note the edge configuration serving for both lens centering and as a spacer with respect to other lens elements or the mounting barrel.

Particular attention has to be paid to the edge configuration. Higher stress levels at the edge of the optic cause birefringence and surface irregularities, the so-called "edge effect" [3]. Consequently, for standard-size lenses the effective aperture should be at least 1–2 mm beyond the clear aperture, i.e., the edge between flange and optical surface. To allow injection of molten plastic into the lens cavity, any increase in lens diameter should be accompanied by a proportional edge thickness increase. Typically the edge thickness varies between 1 and 3 mm.

Another feature to consider when designing edge configurations is the integral use of the flange as spacer requiring no additional spacers. If no flanges are incor-

porated, the same airspace may result in a spacer requirement that is too thin, particularly for robotic assembly (Figure 2.2, left). Extending the flange beyond the surface vertex of a convex surface protects the surface from damage when the lens is placed on a table or in a tray [21]. However, integrating flanges around a lens for mounting purposes requires thick flange walls designed with chamfers and radii that do not degrade the quality of the optics [3].
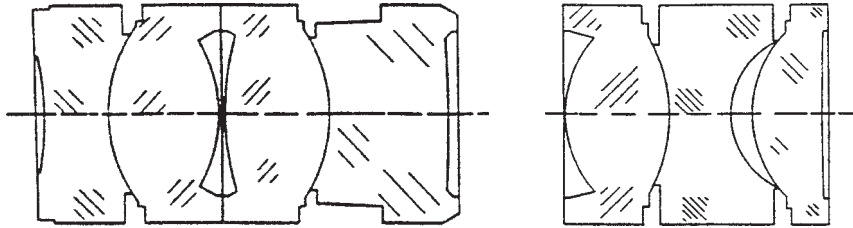
Figure 2.2 Edge configurations of plastic optical lenses. Left: flange spaced lenses; right: edge contact assembly (both from Ref. [20]). Note the possibility of achieving small airspace and protection of convex optical surfaces by extending the integrated flanges beyond the vertex (left).

Finally, plastic optical elements can often be designed to nest with one another, allowing the parts to be centered without the use of expensive mount designs (see Figure 2.2).

2.2.2
Elements with Integrated Fixation Features

Apart from simple flanges around lenses, there is a large variety of integral mounting and fastening features. In cases where a complete flange around a lens element is not possible, e.g., mounting/assembly problems or stress-induced birefringence, fastening pads with slots and holes can be applied (Figure 2.3, left). This is particularly the case for rotationally non-symmetric prismatic elements (Figure 2.3, center and right).
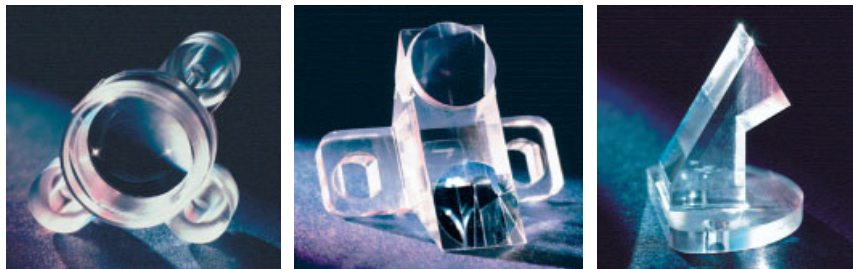
Figure 2.3 Plastic optical elements with integrated mounting slots and flanges. Left: lens assembly with three single slots; center: Small porro prism with two slotted mounting flanges; right: small prism with one-side cut circular flange and two fixation slots [4].

Generally, slots with an open end are preferred over mounting holes. This is because slots create less optical distortion during molding due to local shrinkage-induced deformation [3].

2.2.3
High Functional Integration

Deliberately integrating several optical, mechanical, and electrical features into one monolithic device could replace several discrete optical elements in an instrument. This, in turn, would decrease costs due to easier assembly and alignment, and lead to more reliable products, where in the case of failure the whole integrated module could be replaced. Thus, higher integrated optical devices would be of interest to many manufacturers dealing with optical assemblies.

Because of fabrication difficulties, until recently in classic glass optics it was difficult to integrate several optical and mechanical functions into one monolithic device. However, because of the totally different fabrication process, injection-molded optics offers an enormous variety of surface shapes and structures, easily allowing the implementation of several optical, mechanical, and electrical features.

Therefore, when dealing with plastic optics designers should aim for a high degree of feature integration. Here, it is important to resist the urge to emulate glass-based optomechanical design approaches. A fully optimized polymeric optical system not only makes use of aspheric technology and integrally molded features in the optical elements but also embodies an extension of this design philosophy into the lens housing concept and assembly strategy.

The best way to show the variety and the potential of functional and geometric integration of plastic optic elements is done through examples. In following some examples of highly integrated monolithic plastic optical elements for both imaging and non-imaging purposes are considered.

Figure 2.4 Monolithic plastic optical assembly made of poly(methyl methacrylate) (PMMA). The device is about 50 mm high and integrates a spherical and an aspherical lens, sensor alignment holes and locating ledges for sensors at the focal point of the lenses, and a mounting flange [3].

The first example is a highly integrated plastic optical device. This is a one-piece molded assembly with two integral lenses, interfaces for sensors, and a mounting flange (Figure 2.4).

Figures 2.5 and 2.6 show the viewfinder modules of different types of single-use, entirely plastic cameras. The assembly integrates an imaging path composed of two rectangular meniscus lenses, simple magnifying elements for the exposure counter wheel, and a light-guiding feature to collimate light of the flash control LED. Furthermore it incorporates several mechanical features such as snap hooks, alignment pins, and play-free flexible bearings. Interesting in these modules is the configuration, where the optical and mechanical features are almost all "mounted" on a baseplate. One advantage of this design is the clearly defined gating area and separation line.

A small integrated plastic optical module mounted on a flexible printed circuit is shown in Figure 2.7. Apart from an illumination path, also an imaging path, which runs over several beam-shaping surfaces, is integrated in this example.

Recently, Tan et al. [27] presented a highly integrated miniature plastic optical device to focus and monitor light from a VCSEL for bar-codes reading applications. With integrally-molded pins they realized improved mounting, alignment and fixation functionalities.

An example of a highly integrated plastic optical imaging device is shown in Figure 2.8. This illustrates an integrated waveguide optic structure to detect fingerprint patterns [7] by imaging the evanescent coupled light of an LED. In total the device integrates monolithically seven surface elements between the light source and the two-dimensional CCD imaging device.

The region between the illumination asphere and the output asphere is solid acrylic. Thus, the device can be regarded as a waveguide, where total internal
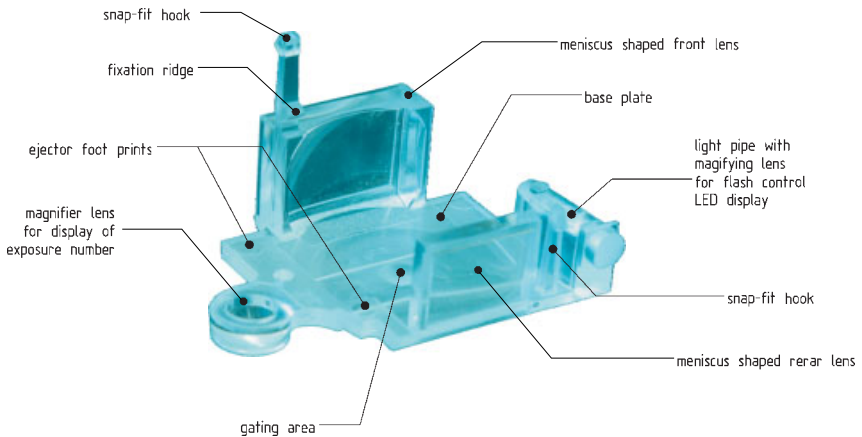
Figure 2.5 Monolithic viewfinder module of a single-use, totally plastic camera. The module integrates three optical features (viewfinder lens pair, exposure number magnified display, and LED flash control display) and several mechanical features, such as a baseplate structure to hold all optical elements and snap-fit hooks and ridges to fix and position the module in a suitable assembly.
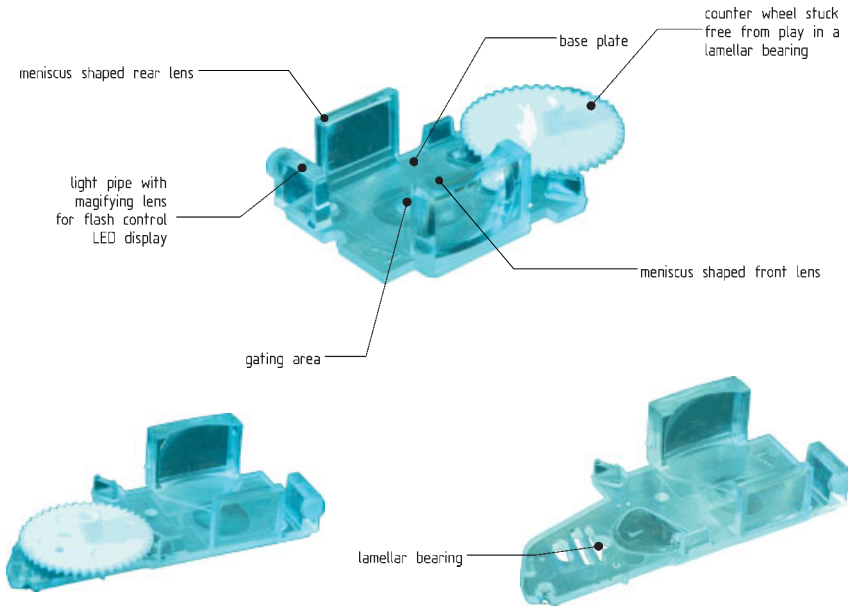
Figure 2.6 Monolithic viewfinder assembly of a similar type of one-use, totally plastic camera to that shown in Figure 2.5. This module additionally integrates a play-free lamellar bearing to hold the cogwheel of the exposure counter. View from left top (top), view from right top (bottom left), and view from top with the lamellar bearing (bottom right).
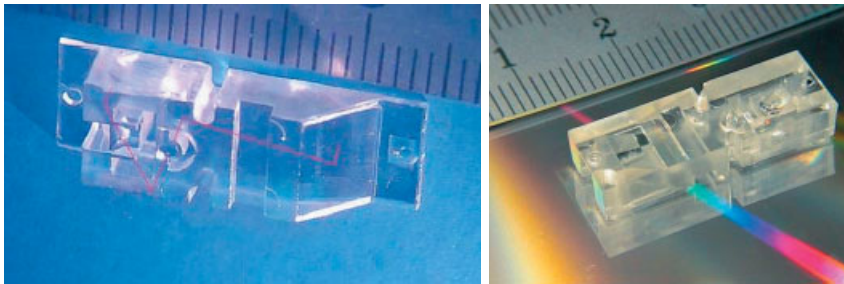
Figure 2.7 Small monolithic plastic optical module (from Ref. [5]). Left: two different configurations of the optical module; right: optical module mounted on a flexible printed circuit.

reflection (TIR) occurs at well-defined surfaces to shape the light bundle: first for illumination purposes (aspheric illuminator surface), and second to relay the image from the sensor area onto the two-dimensional CMOS camera mainly using TIR.

To achieve TIR almost all optical surfaces of the device are strongly off-axis. This, however, results in significant geometric distortions and especially astigmatism, which are accommodated with toroidal elements and differential x–y apertures.
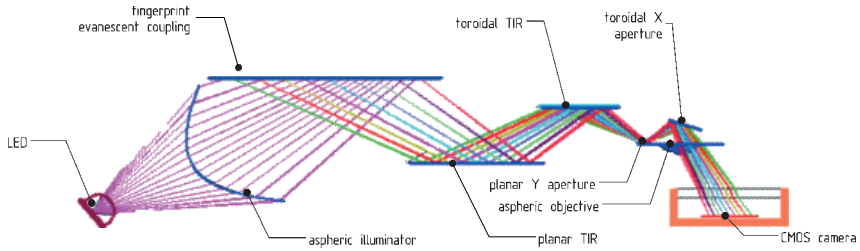
Figure 2.8 Fingerprint waveguide optic structure (from Ref. [7]). Optical layout including LED, aspheric illuminator, and planar, aspheric, and toroidal surfaces or apertures.

According to Hebert [6] this example was a particularly challenging design in that it required image-quality resolution, which only could be achieved in tooling with diamond-turning technology.

Figure 2.9 shows a further example of a highly integrated plastic optical element. This optical module is the functional kernel of a four-channel reflectometer of a single-use device for testing hemoglobin A1c [8]. It monolithically incorporates single and dual off-axis aspheres and toroidal and planar surfaces and apertures.
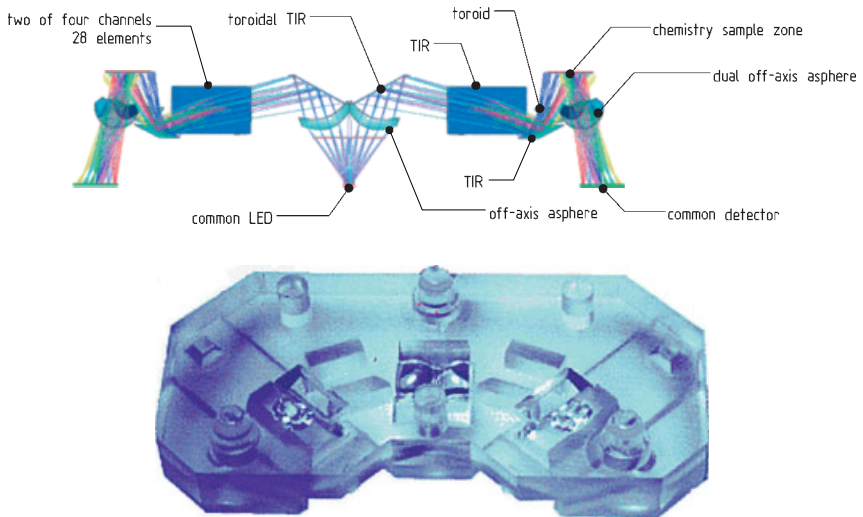
Figure 2.9 Four-channel reflectometer of a single-use device for testing hemoglobin A1c [8]. Top: optical layout including a common LED (for both reference and measurement paths), off-axis aspheres for light collimation, toroidal and dual off-axis aspheres, as well as several planar surfaces or apertures. Bottom: monolithic realization as one highly symmetric plastic optical module.

2.3
Mounting Plastic Optical Elements

As mentioned in Section 2.2, mounting features can easily be incorporated into the optics themselves. Cells and housings can also be configured to minimize the number of parts and assembly labor, and to allow the use of mechanical fasteners, adhesives, or heat sealing.

The design flexibility and the cost-saving potential of polymer optics can only be fully realized when the optical as well as the mechanical design is approached in a fundamentally different manner from that of glass-based optomechanical design. This means that a fully optimized plastic optical system implies not only integrated mechanical features and aspheric and diffractive surfaces, but extends this different design philosophy to mounting and assembly issues. The earlier the housing concept and assembly strategy are considered together, the better is the chance of not hindering parallel innovation concerning other aspects of the development process.

Since the thermal and mechanical properties of most plastic optical materials differ greatly from those of metallic materials typically used in glass-based assemblies, for mounting plastic optical elements one should primarily consider plastic or reinforced plastic materials. There are basically three different types of mounts made of plastic:

- Clamshell mounts. This type of mount consists of two identical half-shells made, for example, by injection molding of plastic material. When assembling, the optical elements are simply inserted in the seats of one half-shell. The second half-shell then serves as a top cover which can be attached by snap-fixations, UV-curing adhesive or ultrasonic bonding, or C-type expansion rings. In particular, the last method mentioned allows expansion of the optical elements, e.g., due to thermal changes. A typical example of this type is shown in Figure 2.10 (left). The internal configuration of the clamshells typically consists of half-ring-shaped local pads which determine the centric position, solid integrally molded tabs defining the axial position of the plastic optical element and serving as aperture stop, and flexible tabs allowing one to clamp the optical element axially (Figure 2.10, right). Benefits of this mounting type are the minimum number of parts and easy assembly. However, according to Ref. [3], control of centering and tilt is considered to be of moderate quality.
- Collet cap-type lens housing. This type of mounting for plastic optical elements is based on a slotted Collet sleeve into which the lens elements are filled and stacked. The orientation tappets of the lens elements are then inserted into the slots of the sleeve. Axially the lenses lean against the shoulders of the seats and are fixed by means of an ultrasonically bonded cap (Figure 2.11).

flexible
tab

molded
aperture
stop

anti-reflection
thread

lenses on local
pads to allow for
mold adjustment
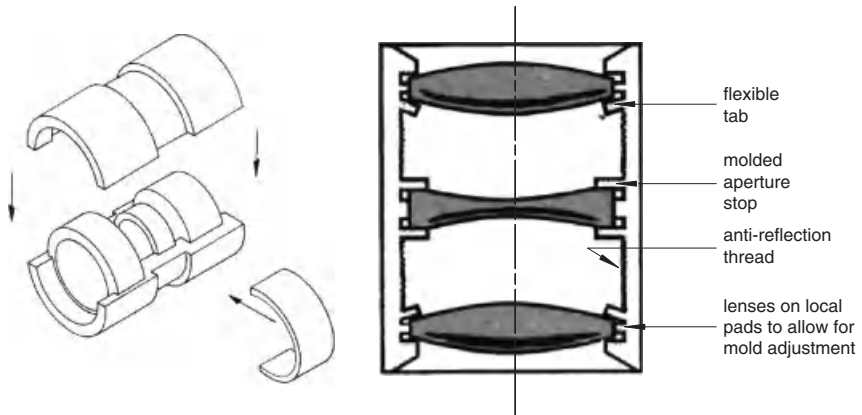
Figure 2.10 Clamshell lens housing. Left: the device consists of two identical housing half-shells, between which the lenses are inserted. The whole assembly is clamped by an expansion C-ring, which is snapped in the slot [2]. Right: internal mounting details [9] such as flexible tabs, integrated aperture stops, antireflection threads, and load pads to allow for mold adjustment [3].

• Barrel-type lens housings. These are similar to glass-based barrel-type lens housings but are made of plastic. Providing better accuracy than clamshell mounts, barrel-type mounts typically require retainers, which can be screwed, adhesively or ultrasonically bonded, or heat-sealed. However, excessively long mounts and wall-thickness variations resulting from draft-angle allowance make it more difficult to mold mounting barrels with high accuracy. An important issue in this context is the definition of the parting line as shown in Figure 2.12, bottom. In the upper section of the figure the parting line is axially set to the aperture stop location, allowing an integral molded aperture stop and few accessory parts. However, accuracy with respect to the concentricity of the elements left and right of the aperture stop may be inferior to the mounting method shown in the lower section of the figure, where the parting line is set to the right.
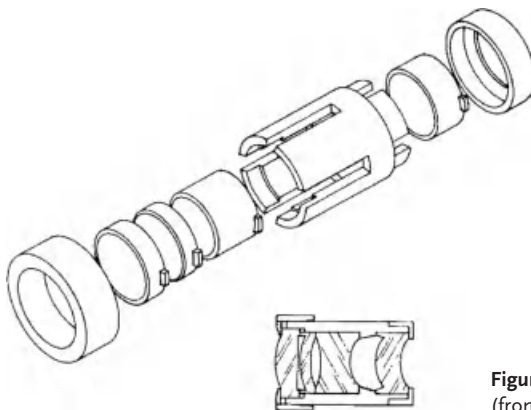
Figure 2.11 Collet-type lens housing (from Ref. [2]).

external
threads
can be
molded

one piece
mount

maintain constant
wall thickness

retainer: cemented in,
screwed in,
ultrasonically bonded

molded
spacers

parting line
upper diagram

better concentration
between elements

parting line
lower diagram
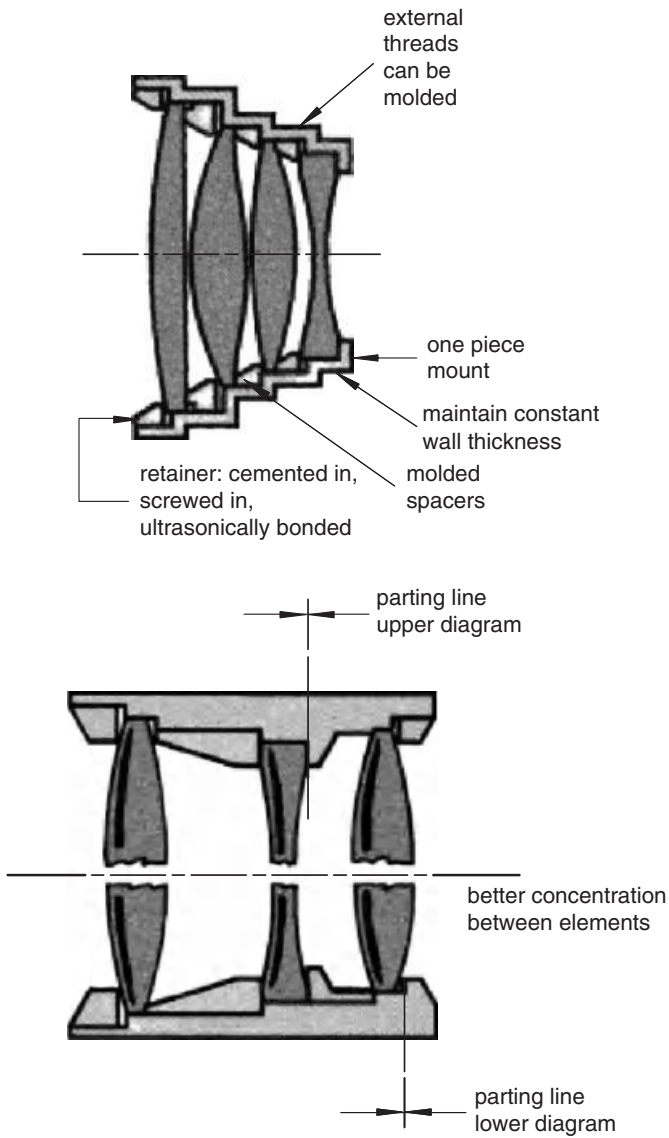
Figure 2.12 Barrel-type lens housing (from Ref. [3]). Top: one-piece lens
barrel with various shoulders, requiring retainer and spacer rings.
Bottom: barrel-type lens housing with two different axial positions of
the parting line.

2.4
Dimensional Stability

Dimensional stability relates to the ability of a material or part to retain its shape when subjected to varying temperature, moisture, pressure, or other stress. With respect to optical instruments, many properties of plastic optical materials have to be considered; however, first among these is the dimensional stability [10] of the plastic material, both the intrinsic stability of the base material and the instabilities attributed, for example, to injection molding.

Concerning the dimensional stability of plastic optical components, we will mainly focus on structural and thermal stability as well as on moisture expansion issues.

2.4.1
Structural Stability

Structural stability, with respect to both static and dynamic load, is a basic requirement for most optical systems. Therefore the choice for a certain geometric configuration of a component, its constituent material, and the applied fabrication processes must be carefully studied.

Structural stability as regards static and dynamic load can be characterized by the following parameters:

• Resonant frequency.
• Deflection at constant thickness.
• Deflection at constant mass.
• Mass at constant deflection.

2.4.1.1 **Resonant Frequency**
Concerning dynamic load, i.e. vibrations, the resonant frequency is the corresponding specific parameter. The higher the resonant frequency of a certain component, the stiffer it is. The further the resonant frequency is from the excitation frequency, the smaller is the oscillation amplitude (Figure 2.13), i.e., the dimensional changes of the component.
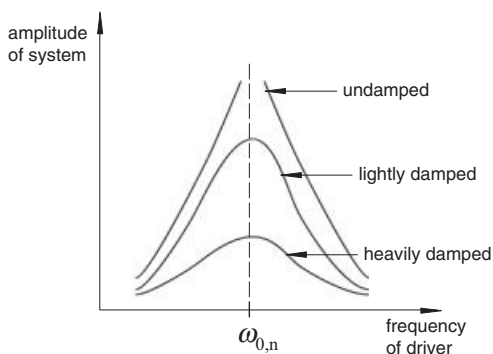
Figure 2.13 Amplitude–frequency characteristic of a system: undamped, lightly damped, and heavily damped.

Apart from the geometry of the component, the choice of the material plays an important role. This can easily be shown, taking the example of a vibrating beam. The motion of a vibrating beam with one side fixed is given by the following linear homogeneous differential equation:

$$\ddot{x}(t) + \frac{c}{m} \cdot x(t) = 0 \tag{2.1}$$

where the coefficient c/m is related to the resonant frequency ω_0 by

$$\omega_0 = \sqrt{\frac{c}{m}}. \tag{2.2}$$

The parameter c is the spring constant of the beam. For a homogeneous beam with rectangular cross-section it is determined by

$$c = \frac{EI}{l^3} \tag{2.3}$$

where E is Young's modulus, l is the length of the beam, and I is the geometrical moment of inertia. For a beam of width b and height h it is given by

$$I = \frac{bh^3}{12}. \tag{2.4}$$

The mass m of the beam can simply be calculated using $m = \rho bhl$, where ρ is the density of the beam material. Substituting these expressions in Eq. (2.2) gives the resonant frequency as

$$\omega_0 = \frac{h}{2\sqrt{3l^3}} \cdot \sqrt{\frac{E}{\rho}}. \tag{2.5}$$

Assuming constant geometry, the resonant frequency ω_0 is directly proportional to $\sqrt{E/\rho}$. Therefore, according to Paquin [11], the corresponding structural *figure of merit* concerning resonant frequency is $\sqrt{E/\rho}$. For large plastic optical components with protruding parts, in order to get high resonant frequencies this means that the square root of the ratio E/ρ should be as large as possible.

2.4.1.2 Deflection at Constant Thickness

When the self-weight deflections of identical geometries or plates of equal thickness are to be evaluated the corresponding structural figure of merit is ρ/E. However, it has to be noted that each component will have a different mass.

Contrary to the resonant frequency figure of merit, here one prefers the lowest possible ratio ρ/E in order to minimize deflection.

2.4.1.3 Deflection at Constant Mass

In the case where the deflections of components of equal mass but independent thickness are to be compared the factor ρ^3/E serves as an appropriate figure of merit.

2.4.1.4 Mass at Constant Deflection

A comparison of the mass of different plastic structures when keeping deflection constant and independent of thickness leads to the expression $\sqrt{\rho^3/E}$ as a figure of merit.

Table 2.1 lists some mechanical properties and the structural figures of merit discussed above for a selection of optical plastic materials.

Table 2.1 Structural properties and figures of merit for plastic optical materials.

property, figure of merit			density, ρ	Young's modulus, E	intrinsic birefringence, $\Delta n_0 \alpha$	photo-elastic coefficient	$\sqrt{(E/\rho)}$	ρ/E	ρ^3/E	$\sqrt{(\rho^3/E)}$
compares							resonant frequency	deflection	deflection	mass
constant							geometry	thickness	mass	deflection
independent variable							mass	mass	thickness	thickness
unit			g/cm^3	GPa	–	10^{-8}/MPa	$(10^6\ \text{Nm/kg})^{0.5}$	10^{-6} kg/Nm	kg^3/Nm^7	$(\text{kg}^3/\text{Nm}^7)^{0.5}$
preferred			small	large	small		large	small	small	small
material	abbrev.	trade name								
cyclic olefin copolymer	COC	Topas	1.02	3.1			1.73	0.33	0.35	0.59
cycloolefin polymer	COP	Zeonex, Zeonor	1.01	2.2		6.5	1.46	0.47	0.48	0.69
polycarbonate	PC	Makrolon, Lexan	1.2	2.4	0.106	72	1.41	0.50	0.72	0.85
poly(methyl methacrylate)	PMMA	Plexiglas	1.16	3	−0.0043	−6	1.59	0.40	0.56	0.75
polystyrene	PS	Styron	1.05	2.89	−0.1	−55	1.66	0.36	0.40	0.63
allyl diglycol carbonate	CR39		1.31	3			1.51	0.44	0.75	0.87
poly(styrene-co-acrylonitrile)	SAN		1.07	3.3			1.76	0.32	0.37	0.61
poly(styrene-co-methacrylate)	NAS		1.14	2.34			1.43	0.49	0.63	0.80
poly(4-methyl-1-pentene)	PMP	TPX	0.833	1.28			1.24	0.65	0.45	0.67
amorphous nylon		Grilamid TR90	1.183	1.6			1.16	0.74	1.03	1.02
poly(ether sulfone)	PSU	Udel	1.24	2.48			1.41	0.50	0.77	0.88
poly(ether imide)	PEI	Ultem	1.27	3			1.54	0.42	0.68	0.83

2.4.2
Thermal Stability

Thermal stability, with respect to both steady-state and transient thermal load, is a further requirement for optical systems. Dimensional stability with respect to thermal load is directly related to the following material properties:

- Coefficient of linear thermal expansion.
- Thermal conductivity.
- Specific heat.
- Thermal diffusivity.
- Steady-state and transient distortion.

2.4.2.1 Coefficient of Linear Thermal Expansion

The coefficient of linear thermal expansion a is the ratio of linear expansion caused by a rise in temperature of 1 °C. In the literature the abbreviation CTE is frequently used.

Over small temperature ranges, the linear nature of thermal expansion leads to expansion relationships for length, area, and volume in terms of the linear thermal expansion coefficient:

$$\frac{\Delta L}{L_0} = a \cdot \Delta T; \quad \frac{\Delta A}{A_0} = 2a \cdot \Delta T; \quad \frac{\Delta V}{V_0} = 3a \cdot \Delta T. \tag{2.6}$$

It should be noted that the coefficients of linear thermal expansion of plastic optical materials are typically a factor of ten higher than those of glasses. In comparison to metals they are about a factor of five higher.

2.4.2.2 Thermal Conductivity

Thermal conductivity is a property of materials that expresses the heat flux Φ_Q (W/m^2) that flows through the material if a certain temperature gradient ΔT (K/m) exists over the material. The heat flux is given by

$$\Phi_Q = k \cdot \Delta T. \tag{2.7}$$

The thermal conductivity k is usually expressed in W/(m K). It is related to the density ρ, the specific heat c_p, and the thermal diffusivity D by

$$k = \rho c_p D. \tag{2.8}$$

The thermal conductivity of plastic optical materials is relatively small. Values of k range between 0.14 and 0.22 W/(m K). This is about three orders of magnitude smaller compared to metals, and compared to glasses it is still about five times smaller. This means that plastic materials are good thermal insulators.

High thermal conductivity of optical components has two effects. For passive optical components absorbed heat can rapidly flow to heat sinks, whereas for active optical components, which create heat, e.g., laser diodes, heat cannot flow away.

2.4.2.3 Specific Heat

The specific heat, also called specific heat capacity, is the amount of heat Q required to increase the temperature of a unit mass m of a substance by one degree. Q is given by

$$Q = c_p m \Delta T. \tag{2.9}$$

Therefore, the specific heat has units of energy per mass per degree, and at constant pressure is commonly denoted c_p. For typical optical polymers at constant atmospheric pressure c_p varies between 1.2 and 1.97 kJ/(kg K). Compared to metals (~0.12–0.8 kJ/(kg K)) and glasses (~0.75–0.85 kJ/(kg K)) this is two times greater; however, compared to water (4.19 kJ/(kg K)) it is two to three times smaller. With respect to optical components it follows from Eq. (2.9) that the greater c_p, the greater the heat necessary to change the temperature of the component by one degree. Thus for a given amount of heat, in order to keep the temperature change of a certain optical element low, the c_p value should be as high as possible.

2.4.2.4 Thermal Diffusivity

A measure of the rate at which a temperature disturbance at one point in a body travels to another point is expressed by the diffusivity, found by rearranging Eq. (2.8):

$$D = \frac{k}{\rho c_p} \tag{2.10}$$

where k is the coefficient of thermal conductivity, ρ is the density, and c_p is the specific heat at constant pressure. Values for metals are typically three orders of magnitude higher than those for plastic optical materials. Diffusivities of glasses are about five times higher than typical values for plastic optical materials.

Since for optical components homogeneous temperature distributions are required, large diffusivity values are desirable. Among optical plastics poly(4-methyl-1-pentene) (PMP) shows the highest value (1.97×10^{-6} m^2/s) whereas for polycarbonate (PC) the value is only 1.2×10^{-6} m^2/s).

2.4.2.5 Distortion Coefficients

When comparing plastic optical materials with respect to thermal distortion one has to distinguish between steady-state and transient temperature characteristics.

In the steady-state case only the linear thermal expansion and heat conductivity are taken into account. The corresponding figure of merit is given by the ratio a/k. Thus, in order to minimize thermally induced distortion a small a/k ratio should be chosen. The values for the materials listed in Table 2.2 vary between 56 mm/W for amorphous nylon up to 700 mm/W for PMP. Typical optical plastic materials such as COC, PC, and PMMA for high-quality optical components have a/k values between 390 and 450 mm/W. CR39 has a value of only 218 mm/W.

In the case of transient thermal changes heat storage, linear thermal expansion, material density, and heat capacity parameters are involved. The equivalent figure of merit is then the ratio a/D. Similar to the steady-state regime, for minimum

thermal distortion a small ratio should be chosen. Here again amorphous nylon shows excellent values (108 s/(m^2 K)), whereas components made of PMP and SAN again are prone to thermally induced distortion (having relatively high values). Typical values for commonly used plastic optical materials vary between 332 s/(m^2 K) for CR39 and 573 s/(m^2 K) for PMMA.

Table 2.2 Thermal properties and figures of merit of plastic optical materials.

property			max. service temperature, air	refractive index change per degree	coefficient of linear thermal expansion	thermal conductivity	specific heat	thermal diffusivity	steady-state distortion coefficient	transient distortion coefficient
symbol			T_{max}	dn/dT	a	k	c_p	D	a/k	a/D
unit			°C	10^{-6}/K	10^{-6}/K	W/(m K)	W s/(kg K)	10^{-6} m^2/s	mm/W	s/(m^2 K)
preferred			large	small	small	large	large	large	small	small
material	abbrev.	trade name								
cyclic olefin copolymer	COC	Topas	130	−104.3	63	0.16			394	
cycloolefin polymer	COP	Zeonex, Zeonor	123	−126	67					
polycarbonate	PC	Makrolon, Lexan	130	−143	70	0.2	1.2	0.14	348	500
poly(methyl methacrylate)	PMMA	Plexiglas	86	−85	72	0.21	1.4	0.13	344	573
polystyrene	PS		80	−120	70	0.17	1.45		411	
allyl diglycol carbonate		CR39	100		120	0.55		0.36	218	332
poly(styrene-co-acrylonitrile)	SAN		77		65	0.14	1.7	0.07	464	916
poly(styrene-co-methacrylate)	NAS		95	−140	65					
poly(4-methyl-1-pentene)	PMP	TPX	180		117	0.167	1.97	0.1	700	1150
amorphous nylon		Grilamid TR90	118		9	0.16	1.8	0.08	56	108
poly(ether sulfone)	PSU	Udel	160		56	0.26				
poly(ether imide)	PEI	Ultem	210		55.8	0.22				
borCrown glass		BK7	138		7.1		858	0.5	6.4	13.7
aluminum		AlMg1Si	580		22.5	167	896	69	0.13	0.33

2.4.3
Moisture Expansion

For most optical plastic materials values of moisture or water absorption at equilibrium and saturation are given by material suppliers. However, as regards dimensional stability the coefficient of moisture expansion (CME) should be known. This is defined as the fractional increase in length per unit mass variation due to moisture desorption or absorption.

The CME is determined by measuring the moisture content change and the strain change between two moisture equilibrium states. Unfortunately, until now there has not been much published on typical CME values for optical plastics. As an order of magnitude, for PMMA a value of about 0.5% can be assumed.

2.5
Tolerancing

One of the most critical issues in determining the performance and cost of an optical system is the assignment of tolerances to both the material-related optical parameters and the dimensional parameters. Even though much effort has been expended on scientifically describing the tolerancing process [12], in practice, however, tolerancing is mainly based on experience, or can even be considered an art.

Much more than in classic optics, tolerancing of plastic optical systems requires strong interaction between the optical designer, the optomechanical engineer, and the production engineer. A key here is optomechanical engineering, since it can take advantage of the possibility of integrating optical and mechanical features, and therefore inherently integrating to a large extent the alignment tolerances into the fabrication tolerances.

In plastic optics the aim is for a system such that each of the components is fabricated to an accuracy that will ensure that an instrument will be adequately precise and aligned to give the required performance by simple assembly with almost no alignment or adjustment.

2.5.1
Tolerance Budgeting and Allocation

In order to achieve the performance requirements under any of the functional and environmental conditions a tolerance budget may help determine how to distribute the totally allowable wavefront error (WFE) among the many facets and tolerances of the system. The various theories as to how to combine error effects in an optical system are discussed in the literature (e.g., Ref. [12]). Although some authors, e.g., McLaughin [13], show that a simple root sum of the squares (RSS) approach to compute the total allowable WFE from the single error sources tends to be too pessimistic, it is a simple and quite useful first-order approach.
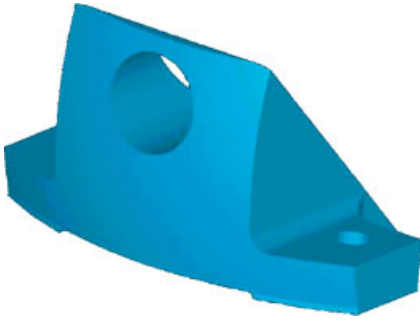
Figure 2.14 Monolithic 45° prism with two spherical surfaces and integral mounting flange of an airborne optical sensing device.
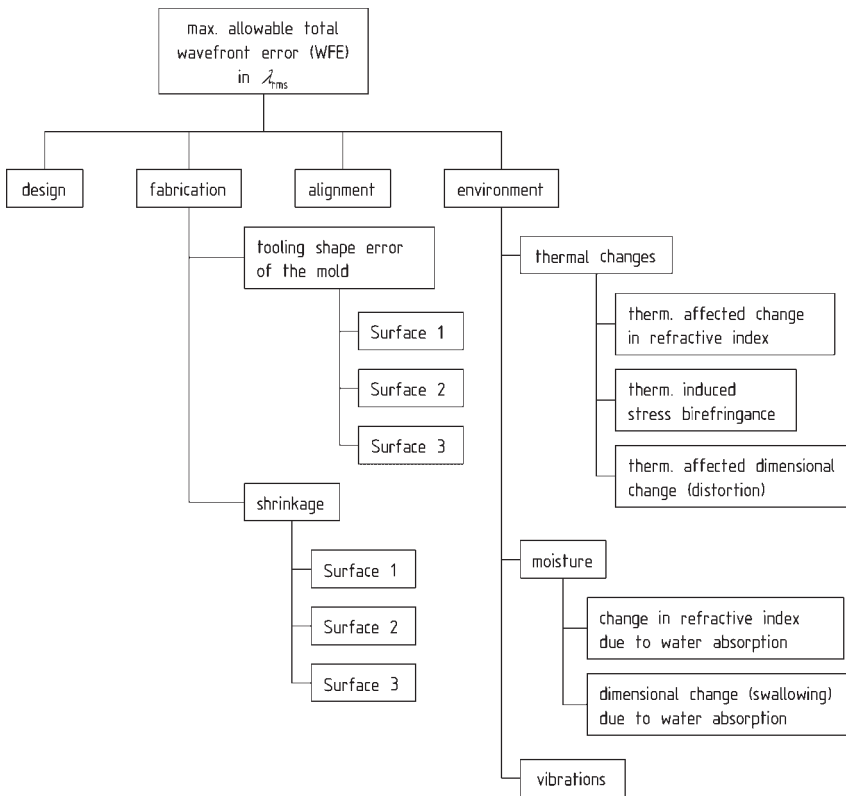
Figure 2.15 Wavefront error (WFE) budget for the plastic optical component shown in Figure 2.14.

Let us now consider as an example for a WFE budget a typical plastic optical component: a monolithic 45° prism with two spherical surfaces and integral mounting flange of an airborne optical sensing device, as shown in Figure 2.14. As depicted in Figure 2.15, the principal error sources of such a plastic optical device are:

- Residual optical design error. This error source corresponds to the remaining error after all optimization processes. It is typically expressed as an RMS value of the WFE in units of the corresponding wavelength. Almost all optical design software easily allows the quantifying of this error.
- Fabrication error. All optical components of a real optical system are never perfect, since the processes to manufacture them have limited precision. The maximum amount of fabrication error is directly related to the manufacturing tolerances. In the case of injection molded plastic components there are typically two principal fabrication-related error sources: tooling shape error of the mold and shrinkage.

High precision molds are made by cutting processes such as single-point diamond turning, grinding, and polishing, all of which are limited in precision. Consequently, these limited precision processes create plastic optical components with deviations from the perfect geometry.

Besides tooling errors, surface tension and volumetric shrinkage are the most important error sources. According to previous work [2, 14, 15], the accuracy to which a precision optical surface can be molded may be strongly influenced by surface tension effects. Especially in corners and edges where the ratio of surface area/volume is locally high, surface tension may create non-uniform shrinkage. Surface tension and volumetric shrinkage may, however, actually aid in the production of accurate surfaces. In spite of much activity on injection mold simulation, an interferometrically precise prediction of the WFE created by both volumetric shrinkage and surface tension effects is hardly possible.

It may often be helpful to break down the fabrication-related errors to each of the optically active surfaces, i.e., in the present example surface 1 (convex), surface 2 (plano), and surface 3 (concave).

- Alignment error. The geometrical position of the plastic optical element with respect to other optical elements or the mechanical datum axis is a further error source to be considered. This error is mainly determined by the accuracy of the alignment process, which, in principle, is quite well determined.
- Environment-related error. Optical systems or monolithic plastic optical devices are normally designed under theoretically ideal conditions. However, in practice they are used under various environmental conditions such as, for the present example, thermal changes, variations in humidity, and vibrations.

Among the thermal effects the following three aspects have to be taken into account: thermally induced change in refractive index (dn/dT); thermally induced stress birefringence, when, for example, due to thermal expansion of the chassis or housing, stress and consequently birefringence is introduced; and thermally induced geometric changes caused by thermal expansion and distortion.

A second environmental influence on the optical performance is moisture. In contrast to glass, plastic optical materials are quite sensitive to moisture absorption, which is a form of mass diffusion and is governed by Fick's law:

$$\frac{\dot{m}}{A} = -D_{\text{moist}} \frac{\partial C}{\partial x}$$

where D_{moist} is the diffusion coefficient, C is the moisture concentration, and $\dot{m}$ is the mass flux per unit time. Moisture absorption has two effects: first, there is a slight change of the refractive index; and second, dimensional changes and thus changes in the optical performance have to be expected.

A third environmental influence is vibrations. Due to vibrations being induced from the chassis or the housing, periodic dimensional changes occur, which may greatly affect the optical performance.

The effect of these environmental influences on the WFE can be quantified by finite element analysis, as discussed in Section 2.6. The difficulty here is mainly the lack of information with respect to boundary conditions such as material properties, or temperature distributions at the interface between plastic optical elements and housing, chassis, etc.

Once the error sources for a certain optomechanical configuration with the corresponding assumed fabrication tolerances are identified and quantified, a targeted optimization can start. Representing the influence of a certain optomechanical parameter p_i on the total wavefront error WFE_{tot} (sensitivity = $\partial\text{WFE}_{\text{tot}}/\partial p_i$) using sensitivity tables helps to distribute and allocate the corresponding fabrication tolerances.

2.5.2
Typical Tolerances and Specifications for Plastic Optics

To optimize the design of an optical system most types of optical design software use self-optimizing algorithms. The boundary conditions of such a multi-parameter optimizing process are normally given by the achievable manufacturing and material tolerances, which have to be entered by the optical designer.

The more loosely these tolerances are chosen, the more difficult it becomes to meet the optical performance requirements. Thus, in order to achieve a high-performance optical system with realistic design, reasonable values for the tolerances have to be chosen. The tolerance values in Table 2.3 give a first approximation for four tolerance levels: low cost, commercial, state of the art, and extremely tight.

In any case, discussion drawings of the elements, with powers and apertures based on the paraxial layout, and reasonable shapes and edges, should be prepared and sent to various molders for comments on feasibility to help direct the design effort.

Table 2.3 Typical tolerances and specifications for injection molded plastic optical parts [16–19].

	low cost	commercial	state of the art	extremely tight
focal length (%)	±3–5	±2–3	±0.5–1	±0.5
radius of curvature (%)	±3–5	±2–3	±0.8–1.5	±0.3
power (fringes)	10–6	5–2	1–0.5	
irregularity (fringes/10 mm)	2.4–4	0.8–2.4	0.8–1.2	
scratch/dig	80/50	60/40	40/20	
centration	±3′	±2′	±1′	
center thickness (mm)	±0.1	±0.05	±0.01	±0.015
flange diameter (mm)	±0.1	±0.05	±0.005/⌀10	±0.015
radial displacement (mm)	0.1	0.05	0.02	
repeatability (%)	1–2	0.5–1	0.3–0.5	
diameter/thickness ratio	2:1	3:1	5:1	
bubbles and inclusions (ISO 10110–3)		1 × 0.16	1 × 0.10	1 × 0.06
surface imperfections (ISO 10110–6)		2 × 0.10	2 × 0.06	2 × 0.04
surface roughness (nm$_{RMS}$)	10	5	2	

Ning [20] quoted for lenses with a diameter less than 8 mm surface figures of better than 3/1. For larger parts as a rule of thumb a value of 5/3 fringes per 10 mm is given. Tribastone et al. [21] reported in 1995 that surface figures of most optical molders cannot achieve 10-fringes surfaces on parts of about 75 mm diameter, except for plano windows. On smaller parts, they stated, they may come close to 0.5 fringes irregularity. Depending on the steepness curve and degree of asphericity, Bäumer et al. [17] presented in 2003 wavefront aberrations of 300 nm$_{PV}$ (60 nm$_{RMS}$) as standard, 150 nm$_{PV}$ (30 nm$_{RMS}$) as tight, and 75 nm$_{PV}$ (15 nm$_{RMS}$) as extremely tight tolerances, assuming a factor of 5 between RMS and PV values of the optical path difference.

Concerning the determination of the relative irregularity tolerance for a first-order (Gaussian) layout, the following relation was given in Ref. [21]:

$$\text{Relative irregularity tolerance} = \left(\frac{\text{Clear aperture}}{\text{Axial beam diameter}} \right)^2.$$

Furthermore, a maximum clear aperture of 90% of the physical diameter should not be exceeded.

Regarding the refractive index tolerance, for injection molded optics a minimum refractive index variation within one component of ±10^{-3} can be assumed.

Finally it is important to note that the following are difficult to mold to precision tolerances: plano shapes, prisms, noncircular elements, strong surfaces, or elements with high ratios of center to edge thickness and diameters greater than 75–100 mm.

2.6
Optomechanical Simulation of Plastic Optical Elements

In comparison to classic glass-based optics, plastic optical materials are much more sensitive to thermal changes, mechanical stress, or moisture. This is mainly due to material properties such as the coefficient of linear thermal expansion a, the stress-optical coefficient k, and the thermo-optic coefficient dn/dT, all of which are up to factors of ten higher than comparable glasses or metals. The CME, quantifying dimensional changes due to moisture absorption, is not even relevant for classic optical materials. Furthermore, especially for injection molded optical elements, fabrication-related material imperfections are a critical issue for high-quality applications.

To predict or improve the optical performance of a plastic optical device under all of these influences requires corresponding analysis tools. Based on finite element models, this technique was initially developed by Genberg [22], and later applied to a variety of optomechanical problems [23].

2.6.1
Integrated Optomechanical Analysis

The principal aspect of an integrated optomechanical analysis is to transfer environmental- or fabrication-related dimensional or material-specific changes computed in the finite element model into values that allow quantifying of the increase/decrease in optical performance. Such values could be, for example, Zernike polynomials or other standard surface fitting mathematical functions.

To obtain the optical performance metrics, such as WFE, point spread function, modulation transfer function, or encircled energy, the transferred data from the thermal and the structural analysis must be processed and evaluated by an optical analysis (Figure 2.16). Regarding polymer optical systems and components the following analysis types in particular have to be taken into account:

- Thermoelastic analysis.
- Stress birefringence analysis.
- Thermo-optic analysis.
- Moisture absorption analysis.

Material and dimensional imperfections are caused to a large extent by the fabrication method, e.g., injection molding. Here, a corresponding mold flow simulation could provide spatially resolved actual material properties and the surface profile.
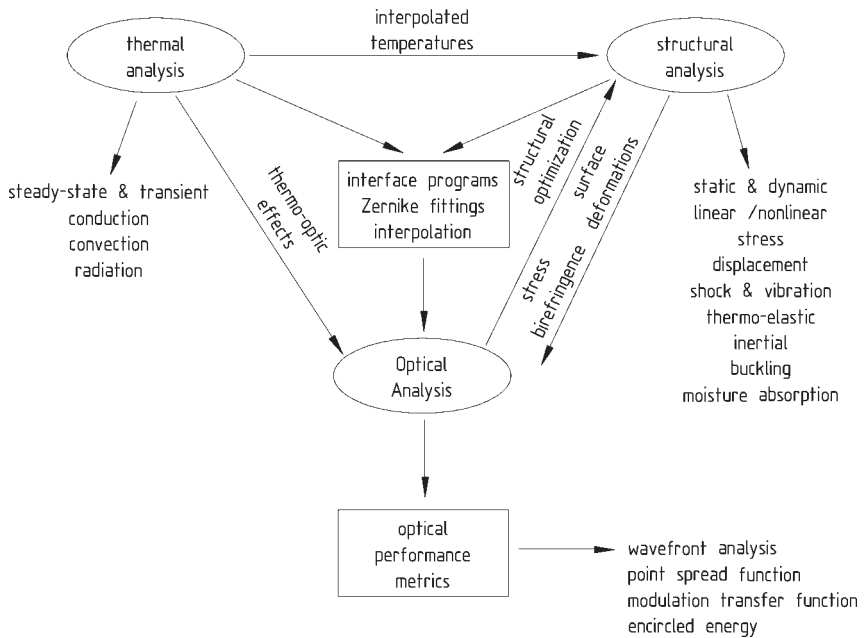
Figure 2.16 Optomechanical analysis interaction similar to that of Ref. [23].

2.6.2
Thermoelastic Analysis

A thermoelastic analysis is applied when thermally induced dimensional and positional changes, such as change of element thickness, radii of curvature, or higher-order surface deformations, in optical systems are to be determined. In most cases these dimensional changes may severely affect the optical performance of a plastic optical component.

The governing material property here is the coefficient of linear thermal expansion (CTE). Plastic optical materials typically show CTE values 10 times higher than those of metals or even 20 times higher than those of glasses.

Aspects to consider here are first that for most optical plastics the CTE increases slightly with increasing temperature, and second that spatial variations of the CTE of plastic optical elements and mounting structures might be critical for sensitive optical systems. Using thermal load vectors in the thermal finite element model, these CTE variations can be taken into account [23].

Finally, in order to evaluate the resulting change in optical performance the results from such a thermoelastic analysis have then to be transferred, e.g., via Zernike polynomials, into the corresponding optical metrics.

2.6.3
Stress Birefringence Analysis

Stress birefringence is a quite typical phenomenon of plastic optical materials, and due to the higher stress-optical coefficient is more important in polymeric materials than, for example, in optical glasses. This accounts for the importance of methods to quantify stress birefringence. To predict the optical performance of a plastic optical component under stress the updated dielectric impermeability tensor has to be known at each point in the optical element. A first method is to compute the corresponding three-dimensional index ellipsoid map from the spatial stress distribution of the finite element model, using the stress-optical coefficient matrix and the nominal optical properties [23]. Together with interpolation routines the optical properties for an arbitrary ray can then be determined.

A second method applies the system Jones matrix $\mathbf{M}_s$ representing the effective optical retarder properties to determine the values of birefringence, orientation, and ellipticity for a grid of rays. In some optical design software stress birefringence interferogram files may be derived from the birefringence and orientation values [24].

As regards optical software such as CODE V, Refs. [25, 26] provide some examples of computing optical errors due to mechanical stress using stress birefringence interferogram files.

2.6.4
Thermo-optic Analysis

A further analysis concerns the investigation of the change in optical performance caused by the thermo-optic effect, i.e., the change of refraction index due to a change in temperature. Here, the governing material parameter is the thermo-optic coefficient dn/dT. It has to be noted that, depending on the application, either the relative or the absolute value must be applied [23].

Changes in the refractive index of an optical material lead to differences in the optical path length (OPD), and therefore to wavefront errors. To evaluate this effect a thermo-optic finite element model has to be built up. With this technique for complex temperature profiles OPD maps of an optical element can be computed. According to Genberg [22] such a model is realized by modifying the material properties and boundary conditions of a three-dimensional finite element model of the optical element. In order to decouple in-plane and out-of-plane effects the following replacements and changes concerning material properties have then to be performed:

- CTE $\rightarrow$ thermo-optic coefficient, dn/dT
- Young's modulus $\rightarrow E = 1$
- shear modulus $\rightarrow G = 0$
- Poisson ratio $\rightarrow v = 0$.

As boundary conditions, Genberg proposes to constrain the nodes of the front surface concerning translation and to constrain the remaining nodes normal to the optical axis. The load vector here is the temperature field. The resulting displacement profile at the rear surface corresponds to the OPD map for an entering wavefront. Similar to the techniques described before, fitting the OPD map by Zernike polynomials will then allow one to quantify, for example, the resulting WFE.

2.6.5
Moisture Absorption Analysis

According to Doyle et al. [23] dimensional changes in plastic optics due to moisture absorption can be simulated by a thermal-to-moisture analogy, where thermal modeling tools may be used to compute the moisture concentration. The following parameters of the thermal model are replaced by the corresponding parameters of the moisture diffusion model:

- temperature, $T \rightarrow$ moisture concentration, C
- thermal conductivity, $k \rightarrow$ moisture diffusivity, D_{moist}
- temperature gradient, $\partial T/\partial x \rightarrow$ moisture gradient, $\partial C/\partial x$
- thermal flux, $\Phi_Q \rightarrow$ moisture flow, $\dot{m}$.

For a known moisture concentration, dimensional changes are computed, performing a thermoelastic analysis, where the parameters become:

- CTE $\rightarrow$ CME
- thermal load, $T \rightarrow$ moisture concentration, C.

2.6.6
Mold Flow Analysis

Mold flow finite element techniques allow the simulation of the plastic injection molding process. This aids in ensuring the quality and efficiency of the injection molding process. The simulation is usually conducted during the product design stage or the early stages of the tool design, and helps to reduce or eliminate many of the problems associated with commissioning an injection mold, before construction and major investment in the mold has even begun. The processing characteristics of the plastic injection mold are investigated during the course of the mold flow simulation allowing optimization of the part and mold design by adjusting areas such as gate positions, wall thickness, and cooling parameters. The results of such a mold flow analysis can be used as a database for the analysis techniques described above.

References

1 R.R. Willey and R.E. Parks, Optical fundamentals, in: *Handbook of Optomechanical Engineering*, edited by A. Ahmad (CRC Press, Boca Raton, 1997).

2 J.D. Lytle, Polymer optics, in: *Handbook of Optics*, 2nd edition, Vol. 2, edited by M. Bass, E.W. Van Stryland, Optical Society of America, D.R. Williams, and W.L. Wolfe (McGraw-Hill, New York, 1995).

3 *Handbook of Plastic optics*, 2nd edition (Corning Precision Lens Inc., Cincinnati, OH, 2000).

4 Wahl Optoparts GmbH, Triptis, Germany, 2004.

5 CSEM, Optical microsystems, *Replication Technology. Injection Moulding*, http://www.csem.ch/fs/micro_optics.htm, Zürich, Switzerland, 2004.

6 R.T. Hebert, Off-axis optical elements in integrated, injection-molded assemblies, *Proc. SPIE* **2600**, 129 (1995).

7 Prisma Optics, R. Hebert, Example: 4-channel reflectometer, http://www.prisma-optics.com/, Los Gatos, CA, 2004.

8 Prisma Optics, R. Hebert, Example: Electronic fingerprint detector, http://www.prisma-optics.com/, Los Gatos, CA, 2004.

9 E.I. Betensky and B.H. Welham, Optical design and evaluation of large aspherical-surface plastic lenses, *Proc. SPIE* **193** 78 (1979).

10 R.A. Paquin, Advanced materials: an overview, in: *Advanced Materials for Optics and Precision Structures*, SPIE Critical Reviews of Optical Science and Technology, Vol. CR67, edited by M.A. Ealey, R.A. Paquin, and T.B. Parsonage (SPIE Press, Bellington, WA, 1997), pp. 3–18.

11 R.A. Paquin, Dimensional instability of materials: how critical is it in the design of optical instruments, in: *Optomechanical Design*, SPIE Critical Reviews of Optical Science and Technology, Vol. CR43, edited by P.R. Yoder (SPIE Press, Bellington, WA, 1992), pp. 160–180.

12 G.W. Wiese, ed., *Selected Papers on Optical Tolerancing*, SPIE Milestone Series, Vol. MS36 (SPIE Press, Bellington, WA, 1991).

13 P.O. McLaughin, A primer on tolerance analysis, *Sinclair Optics Design Notes* **2**, 3 (1991).

14 E.C. Bernhardt and G. Bertacchi, New tool for mold design: computerized shrinkage analysis, *Plastics Technol.* Jan., 81 (1986).

15 G.R. Smoluk, *Plastics Eng.* July, 107 (1966).

16 G-S Plastic Optics – Custom Optics: Charts, Design guidelines for injection molded optics, http://www.gsoptics.com/custom_optics/charts.html, Rochester, NY, 2002.

17 S. Bäumer, L. Shulepova, J. Willemse, and K. Renkema, Integral optical system design of injection molded optics, *Proc. SPIE* **5173**, 38 (2003).

18 D.J. Butler, Plastic optics challenge glass, *Photonics Spectra* May, 168 (2000).

19 B.G. Broome, Optical Products Development Inc., 301 East Center Street, Elmira NY 14901

20 A. Ning, Plastic glass optics: factors to consider, part of SPIE Precision Plastic Optics short course note, www.sunex.com, Carlsbad, CA, 1998.

21 C. Tribastone, C. Gardner, and W.G. Peck, Precision plastic optics applications from design to assembly, *Proc. SPIE* **2600**, 6 (1995).

22 V.L. Genberg, Optical pathlength calculations via finite elements, *Proc. SPIE* **748**, 14 (1987).

23 K.B. Doyle, V.L. Genberg, and G.J. Michels, Integrated optomechanical analysis, in: *Tutorial Texts in Optical Engineering*, Vol. TT58, edited by A.R. Weeks Jr. (SPIE Press, Bellington, WA, 2002).

24 K.B. Doyle, V.L. Genberg, and G.J. Michels, Numerical methods to compute optical errors due to stress birefringence, *Proc. SPIE* **4769**, 34 (2002).

25 K.B. Doyle and W. Bell, Wavefront and polarization error analysis of telecommunication optical circulator, *Proc. SPIE* **4093**, 18 (2000).

26 K.B. Doyle, J.M. Hoffman, V.L. Genberg, and G.J. Michels, Stress birefrin- gence modelling for lens design and photonics, *Proc. SPIE* **4832**, 436 (2002).

27 C. Tan, M. Stern, and V. Bhargava, Vertical cavity surface emitting laser focusing using a miniature precision molded plastic lens, *Optical Engineering* Oct., 2478–2483 (2004).

3
Tooling for Injection Molded Optics

Thomas Bauer (Sections 3.1–3.4) (Jenoptik Polymer Systems GmbH, Triptis, Germany)
Dieter Marschall (Section 3.5) (Precitech Ultra Precision Technology, Haundorf, Germany)

3.1
Introduction

A high-quality injection mold is obviously essential for precise plastic optic parts. Parts can never be better than the tool; however, good tooling does not guarantee good parts. A thorough understanding of the whole manufacturing process is essential to produce precision plastic optical components [1, 2].
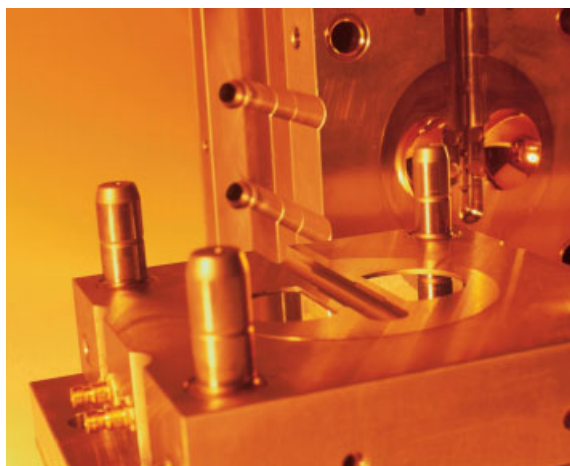
Figure 3.1 Injection mold.

In the production process the mold is as essential as the molding machine itself – and often costs as much. The main factors affecting a mold's price and lead time are

- choice of material for mold and optical inserts;
- number of cavities and expected production volumes and product life time; and
- part size and complexity, texture of surface finish, accuracy needed.

3.2
Principles

Mold design is a diverse and complicated subject. However, it is essential to understand basic design features and construction rules of injection mold tools.

3.2.1
Main Parts of an Injection Mold

In general an injection mold consists of two halves commonly referred to as the moving (core) half and the fixed (hot or cavity) half. The injection-side platen next to the nozzle is stationary while the other half moves for clamping and product release (fixed to the ejector-side platen and the mold-ejection mechanism). The melt material flows through the nozzles into the mold cavities.
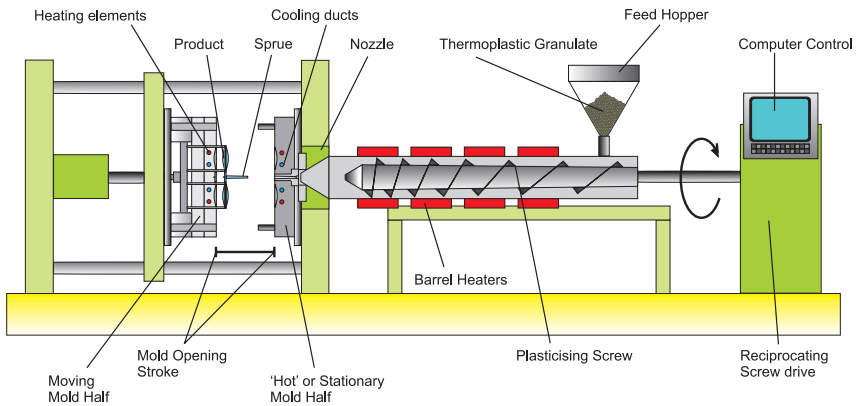
Figure 3.2 Injection molding machine.
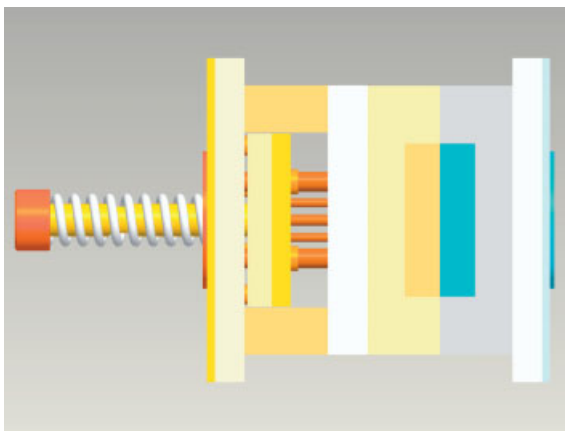
Figure 3.3 Side view, closed mold.
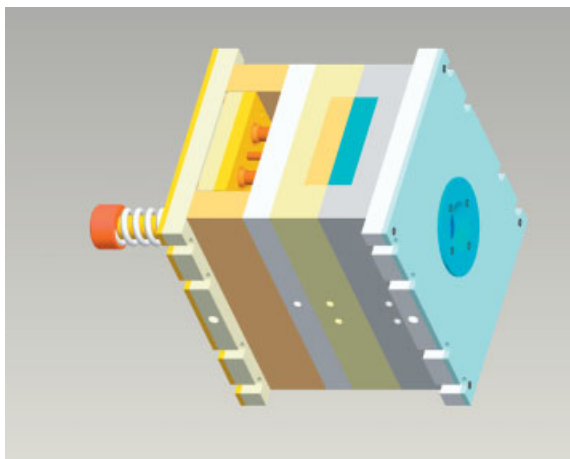
Figure 3.4 Nozzle side view in perspective.

At the end of a molding cycle the moving mold half moves back, pulling the product out of the stationary mold half. Guide pins and taper locks ensure proper alignment of the mold halves. An ejection system is built in at the end of the platen stroke to push the molded parts off the moving mold half so that they can easily be taken off the machine either manually or by an automatic collection system.
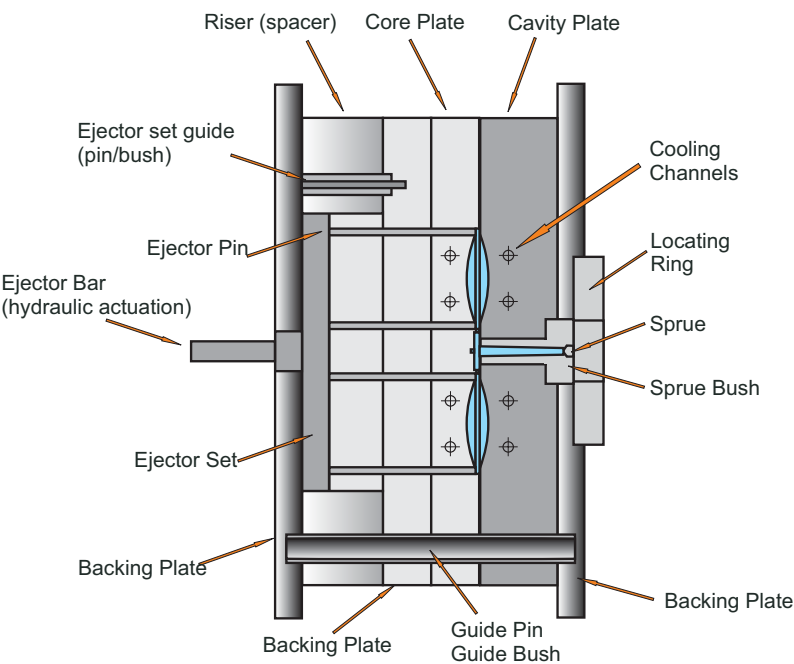
Figure 3.5 Detailed sectional view.

Starting from the injection side, a location ring is fitted to the back of the rear backing plate. It locates and guides the mold into the fixed platen. A sprue bush is positioned through the locating ring. The sprue bush is profiled with a radius to match up with the injection unit nozzle so that material can be directly transferred from the injection unit through to the mold cavity. In the case of a single-cavity mold, the sprue may feed directly onto the component; in the case of a multi-cavity mold, the sprue feeds onto a runner system machined into the tool face that acts as a transfer system to the cavity for the molten material [3].

The sprue and the cavity form in the mold the component shapes. These may be machined directly into solid steel plates. More common for optical components are separately made inserts which may be subsequently fitted to the core and cavity supporting plates.

Many different types of gating may be used to connect the runner system to the mold cavities. Typically gates are preferably as small as possible in order to minimize the potential "witness" mark on the component.

Cooling channels are machined into the core and cavity plates in order to remove the process heat from the tool. The complete tool is held together with a
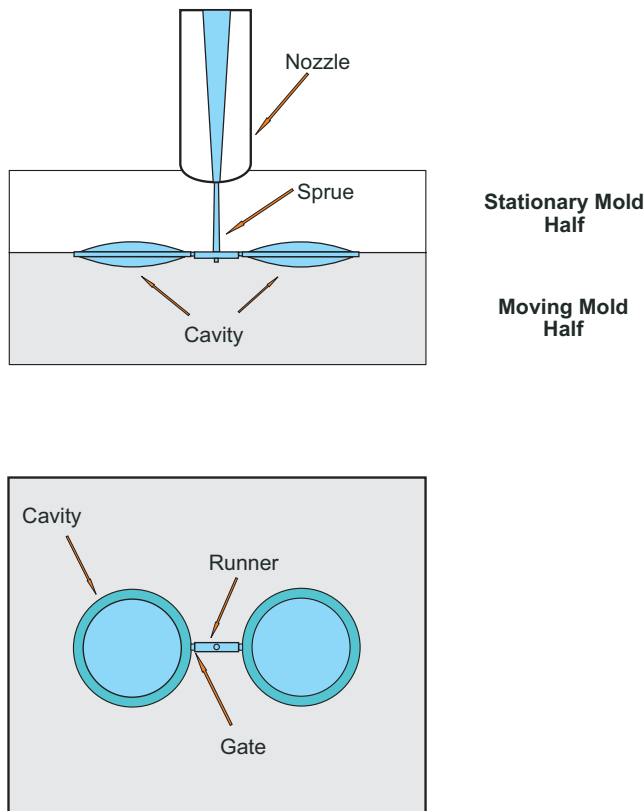
Figure 3.6 Schematic representation of melt delivery system in a two-cavity mold.

system of spacer blocks and bolster and backing plates such that it may be bolted directly to the machine platens and is completely rigid and able to resist injection forces.

3.2.2
Gate and Runner Design for Optical Molded Parts

Injection molds for optical parts often have relatively massive gate cross-sections (Figure 3.7). For molding precise plastic optical components it is essential to apply pressure into the mold during cooling of the melt until the gate freezes off.

To avoid shrink marks and voids, especially during the production of lenses and prisms, the material shrinkage (some percentage of the melting in a firm condition) needs to be balanced by injection of additional material during the cooling period. The diameter of the runner needs to be of a sufficient size to prevent the sprue from freezing too early.

The edges of the injection molding parts should not be too thin, since there needs to be enough space for the gate. This should be at least three-quarters of the edge thickness. The edges of the gates are rounded off to avoid flow lines. The form has to be fed slowly and the sprue channels should be preferably short.
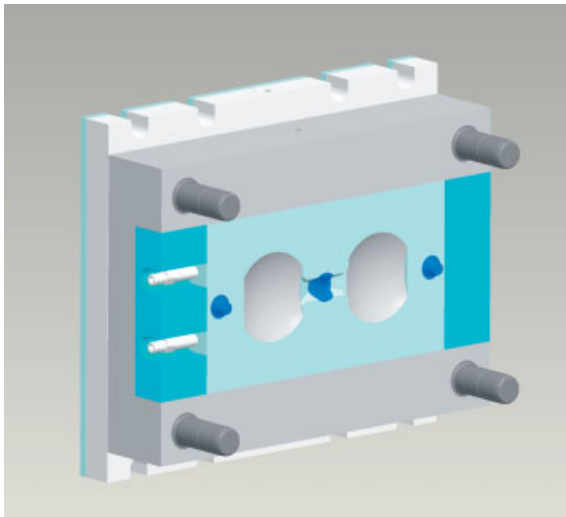
Figure 3.7 View of gating channels of a two-cavity lens mold.

3.2.3
Hot and Cold Runner Molds

A runner is the channel in the mold that conveys the plastic from the barrel of the injection molding machine to the part (Figure 3.6). There are two main types of injection molds: cold runner and hot runner molds.

3.2.3.1 **Cold Runner**

In a cold runner mold, the runner is cooled and ejected with the part. For every cycle, a part and a runner are molded. The obvious disadvantage of this system is the necessity to separate the runner from the part by an additional sawing, milling, or mechanical, thermal, or ultrasonic cutting step. For optical parts with high demands of melt purity the runners are normally disposed of and there is a substantial waste of plastic [4].

Despite these disadvantages, there are many significant advantages to using a cold runner mold. The mold design is simple and much cheaper than a hot runner system. Above all a cold runner allows the application of a post-pressure to the cavity. This will prevent the optical shape from deforming during cooling and shrinking of the part and leads to more precise optical shapes.

3.2.3.2 **Hot Runner**

In a hot runner mold, the runner is situated internally in the mold and kept at a temperature above the melting point of the plastic. The major disadvantage of a hot runner is that it is much more expensive than a cold runner. It requires costly maintenance and more skill to operate [5].

Hot runners have many advantages. They can completely eliminate runner scrap, so there are no runners to be separated from the parts. Hot runners are popular for high volume application, especially for multi-cavity tools with moderate accuracy demands and small part size.

3.2.4
Ejector Design

The most common ejector designs are ejector pins (round, flat, etc.), ejector tubes, and ejector plates. Ejector pins are reasonably easy to install; ejector tubes have
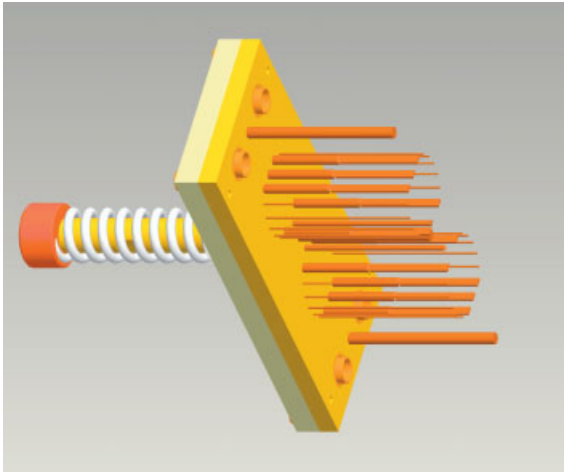
Figure 3.8 Package of flat and round ejector pins for a two-cavity lens mold (core half).

the advantage of enabling good ventilation for circular parts; ejector plates can be effective over large surface areas.

Figure 3.8 shows several hardened pins used to eject a two-cavity molded lens at the edge. The ejector pins are fixed into the rear ejector plate which is connected to a hydraulic actuator behind the moving platen.

Smaller optical parts can also be ejected over the whole optical insert, especially if no edge area is available.

3.2.5
Heating and Cooling

As thermoplastic products have to cool before the mold can be opened, water or oil cooling systems are incorporated in the mold design. Heating and cooling mechanisms guarantee a homogeneous temperature distribution over the cavity surface.

The ideal tempering of the tool defines considerably the cooling time and with it also the cycle time. It has a great influence on the distortion incline, dimensional accuracy, and with that also an influence on the quality of the injection molded parts.

Several microstructured parts (e.g., gratings, diffractive structures, moth-eye structures) sometimes have to be cooled or heated in a certain precise controlled regime during the molding cycle to guarantee exact structure replication. These so-called variotherm molding systems may have to incorporate separate heating and cooling equipment.

Cooling channels should pass as close as possible to the cavity surface and should be located close together. Cooling should be given priority over ejector sets during mold design.

The temperature difference between inflow and outflow should not exceed 5 °C (1 °C for high-precision parts). Cooling time generally dominates cycle time – and as a result part price.
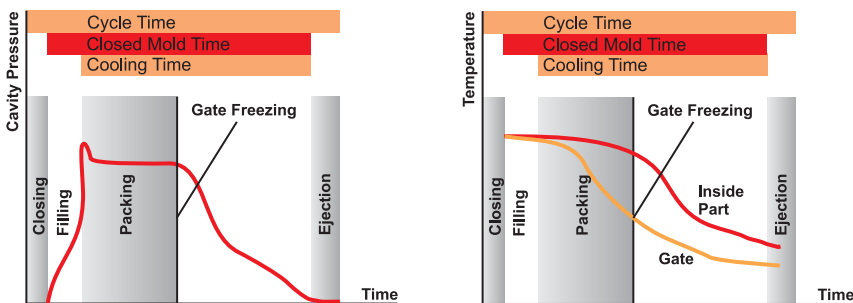
Figure 3.9 Pressure and temperature history for an injection molded part.

3.2.6
Mold Height, Opening Stroke, and Ventilation

The mold height actually means the thickness of the mold. Injection molding machines are normally adjustable and can be adapted to several mold heights – expressed in the machine specifications as the minimum and maximum mold height.

The mold opening stroke (see Figure 3.2) is the distance that the moving mold half slides from the mold closed to mold open position. Because the injection molded part has to clear the mold and should have room to be removed from the machine, the opening stroke must be greater than twice the mold height added by the length of the sprue and possibly the room needed for automatic collection systems.

During filling of the mold the molten polymer has to replace air in the cavity as quickly as possible. Locked air may prevent the perfect filling of the cavity. The immense compression heats up the air, which can lead to combustion of the melt. Sufficient ventilation can be achieved by selecting the right sprue position or additional separation joints, pins, or channels.

3.2.7
Number of Cavities

Production volume and precision required from a tool influence the selection of mold materials, built-in maintenance features, and the optimum number of cavities.

Single-cavity and multi-cavity molds from 2 to 8, 16, or even 32 cavities are used for plastic optic parts. Typically single-cavity tools are used for prototype molds and two- to four-cavity tools for production molds with medium production quantities.
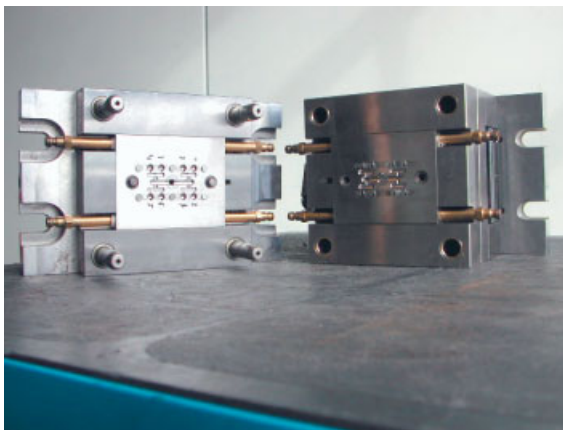
Figure 3.10 Multi-cavity lens mold.

Higher cavity numbers are associated with:

- high production volumes (parts per molding cycle);
- cost-sensitive mass production (low part price, automated production); and
- complex (and expensive) mold design, mold adjustment, and maintenance.

Lower cavity numbers are associated with:

- small and medium production volumes;
- high-precision parts (small differences between cavities); and
- robust mold design, lower mold price, faster mold manufacturing process.

The higher the cavity number the more difficult is it to achieve accurate and similar parts from all cavities.

3.2.8
Consideration of Shrinkage

Thermoplastic shrink rates of most optical polymers lie in the range 0.2–1%. It is important to compensate for material shrinkage in the mold design process.

Unfortunately it is often difficult to calculate exact shrink rates because of the effects of component geometry and the unique molding process used for a part. In such cases the molds are built with smaller dimensions than the nominal final dimensions of the part. The process can be run, molded parts can be measured, actual shrink rates can be calculated, and the tool can be optimized. With one ore more optimization cycles a more precise level of optical shape tolerance can be consistently maintained once the molding process has been established and appropriate mechanical adjustments are completed [6].

3.2.9
Materials for Injection Molds

Molds are usually made from stainless steel, hardened tool steel, or a combination of both. Steel qualities for injection molding tools in the optical field comply with steel qualities for highly strained tools. The tool and the components have to withstand injection pressures of up to 900 bar (injection pressure in the cylinder). Further strains are the cyclic clamping force of the injection molding machine, flashings because of the polymer material, corrosion because of the required cooling liquids, out-gassing of the melt, or the strain of maintenance, repair, and cleaning.

Steels with good polishing properties and preferably few inclusions and voids are used for optical polished and mirror finished tool inserts. Through-hardened steels for increased bear resistance as well as hardness and toughness are used for components with increased strain (such as sprue bushes) [7].

As already mentioned, mold tempering has a great influence on cycle time and part quality. Non-ferrous metals such as copper, cobalt–beryllium, copper–chrome–zirconium, and others are used to improve the heat conductivity of the mold partitions.

3.2.9.1   **Coatings**

Coatings of components in the injection mold are used for quite different requirements. A coating can, for example, avoid the cold welding of metallic friction partners. Coatings may also increase the ease of separation of injection molded parts from steel surfaces. Furthermore, they can be used as wear indicators, corrosion protection, or scratch protection of a polished surface.

All steel types for manufacturing injection molds can be coated on condition that the surface to be coated is metallic bright, or ground, or polished. The layer has a thickness of only some thousandths of a millimeter and reproduces the ground surface exactly. Absolute cleanness is the first priority to avoid coating errors.

In addition to the well-known thermochemical (nitration) and galvanic (hard chrome plating, nickel plating) procedures, processes of thin layer metallurgy such as CVD (chemical vapor deposition) and PVD (physical vapor deposition) are used. For injection molds PVD coatings have become accepted. The coating is done below the starting temperature of many tool steels which avoids loss of hardness. The risk of distortion and dimensional changes is very low, as the coating is done after the treatment.

Additionally, TiN (titanium nitride) coatings are used to achieve longer tool lifetimes, less undesirable cavity surface films, and better melt-filling and part-release properties of the cavities.

3.2.10
Design Steps of Injection Molds for Plastic Optics

3.2.10.1   **Diamond-Turned Prototypes**

After designing a plastic optical system, lens prototypes can be made by direct diamond point turning in various plastic materials. The best surface finishes can be obtained with poly(methyl methacrylate) (PMMA). Materials such as polycarbonate (PC), Pleximid, or cycloolefin polymer (COP) can be machined but do not yield such smooth surface finishes as acrylic.

Because of the high manufacturing costs, diamond point turning is only recommended for making a limited number of prototypes to verify functionality of the optical design and to perform initial tests.

At this stage optical systems are normally assembled from single elements. Housing parts often are made from aluminum. The resulting surface quality and system performance cannot be a validation of the manufacturability by injection molding.

3.2.10.2   **Prototype Mold**

To get reliable knowledge about molded parts, making a molded prototype from a single-cavity prototype mold is recommended. This pre-production stage allows checking of the manufacturing process and determining of the optimal molding conditions.

Optical and mechanical design can be verified with real molded components and design revision is possible to give appropriate operating conditions.

Optical inserts at this stage often are made from non-ferrous materials like aluminum or various alloys like nickel silver or Ampcoloy (trademark of Ampco Metal Inc.). These materials can be machined directly by diamond point turning and allow easy optimization of surface shapes. Often the prototype molds are used to start limited production, since production tooling may take much more time.

3.2.10.3 Production Mold

After the tool has been initially sampled, the tool manufacturer makes mechanical modifications to particular dimensions; the mold is usually designed to allow individual cavities to be adjusted for thickness control.

For series production of high volumes, multi-cavity production molds are required. Depending on quality, volume, throughput, and cost the production tool may have 2, 4, 8, or up to 32 cavities. The production molds function for at least several hundreds of thousands of injection cycles.

3.2.10.4 Production Mold Optimization

Process optimization for a production mold has to include always reproducibility tests. If a constant deviation from the target shape is reached, further compensation can be obtained by correction of the optical shape of the mold.

Figure 3.11 shows three optimization stages of the surface fit for a spherical lens insert.
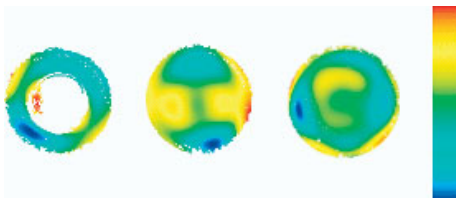
Figure 3.11 Optimization steps (−1.5 to 1.5 μm scale – blue to red).

3.3
Molding Variations

3.3.1
Two-Component Injection Molding

Molded parts consisting of different plastics (e.g., different colors) often are manufactured by so-called more-component injection molding processes. This means that in one molding cycle with only one machine and one tool more than one function can be integrated in a part and assembling costs can be reduced.

In rotary table injection molding, for example, a number of different mold cavities are mounted on the stationary half of the machine and a rotating mold with a number of identical cavities is mounted on the moving platen. After the first

injection the moving platen rotates, taking the part with it, so that on the second injection a new element in a different material is added to the part.

All moldable polymers can be molded by more-component processes in principle. For optical parts the process is usually limited to two components; for example, transparent lenses can be combined with black housing components.
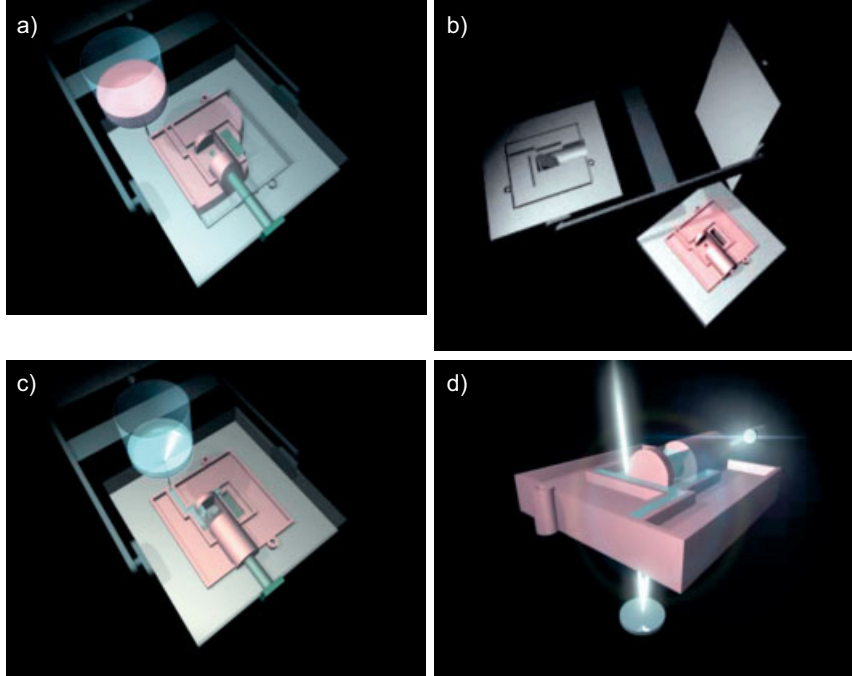
Figure 3.12 Two-component injection molding. a) Step 1: molding of the frame component; b) step 2: mold rotation; c) step 3: molding of the transparent component; d) optical function.

3.3.2
Compression Molding

One of the earliest forms of plastic molding was compression molding. In this method a fixed amount of plastic is placed in the lower half of a mold and heated before the upper half of the mold is closed over the top of it. The mold remains closed while the part cools and when it is taken off the excess material that seeps between the two halves of the mold is removed.

This production method is still used for large-area flat parts like Fresnel lenses and display windows, often in combination with microstructured surfaces [8]. Tools for compression molded Fresnel lenses can be produced using processes such as diamond turning, laser writing, lithography, and e-beam writing. Master tooling can be replicated using electroforming processes.

Tooling costs are usually less than injection-mold costs. Relatively little material is wasted (no sprue is required).

Specialized versions of compression processes are used to make DVDs and laser disks.

3.3.3
Injection-Compression Molding (ICM)

Injection-compression molding combines injection molding with a compression stage often under variothermal tempering conditions. The thermoplastic melt is injected into the lightly opened tool with a simultaneous or following compression by an additional stamping stroke. This stoke can be applied by the machine movement or an embossing stamp in the tool.

The advantages are short cycle times, high flow, and small cavity pressures.

Therefore, the process is excellent suitable for the fabrication of large-area optical parts with small thickness variations (significant decrease of birefringence) and microstructured surfaces.

The mold must be designed or adapted to the ICM (vertical flash-face, female mold/male, core compression concept). The molding machine requires an additional ICM controller.

3.3.4
Variothermal Injection Molding

In the variothermal molding cycle, the cavity wall temperature at first is increased to a level between the glass transition and the melting temperature of the plastic. The melts viscosity remains low during cavity filling. This improves the cavity filling. The required injection pressure and clamping force are reduced. This allows a good surface replication for structures like gratings and other microstructures. Cooling starts not until the cavity is filled equally.

Mold designs for variothermal processes always use classical liquid tempering systems. For the temporary heating of the cavity walls, various additional heating systems are implemented. Especially metallic or ceramic resistance heating elements are integrated. Other methods are heating by infrared radiation, induction, or microwaves.

Variothermal tempering leads to improved structure replication and surface quality of molded parts. Self-cleaning (lotus effect) and antireflective (moth eye like) surface structures, micro- and nanostructures like channels and cell structures for micofluidic applications can be made by variothermal tempering.

The major disadvantages are the increase in tooling expense, need of peripheral heating equipment, higher energy consumption, and an extension of the cycle time.

3.3.5
Micro-Injection Molding

Micro-injection molding is used for small parts in the mass range of 10 mg to 1 g. The shot weight is very low and has to be adjusted very accurately to fill the small cavity. Commercially available plastic granule grains weight approx. 20 to 30 mg. Therefore, the material has to be homogenized very carefully during melt formation.

To minimize dwell time and melt volume, the injection unit combines a screw-type plastication unit with an injection plunger and a melt volume monitoring.

To assure quality and productivity of a micro-injection molding machine, it typically includes integrated handling systems, cameras with image processing, and clean room modules.

Both the molding machine setup and the mold have to be adapted to the small part dimensions. Among the established precision tool engineering methods like micro grinding, micro milling, and micro drilling new technologies are required.

Micro erosion techniques like electric discharge machining (EDM), LIGA (a combination out of lithography, electroplating, and various replication techniques) and laser conditioning methods are used to realize the mold inserts.

Micro-injection molds have small outer dimensions (10 cm edge length) and filigree inner structures (see Figure 3.13). So a sensor-based active tool protection system compares the effective clamping force with a control curve. Even minor changes force the clamping unit to retard.
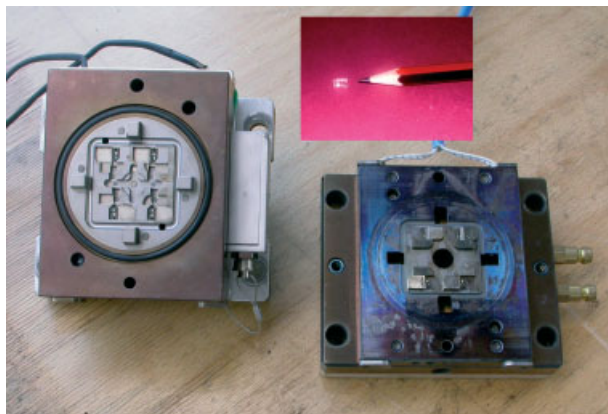
Figure 3.13 Micro-injection mold, typically part size.

3.3.6
Liquid Silicone Rubber (LSR) Injection Molding

Liquid silicone rubber (LSR) polymers are two-component mixtures belonging to the group of high-temperature vulcanizing rubbers. One component has an inhi-

bitor added to define the processing window; the other component contains a cata-
lyst. Vulcanization starts under the influence of the mold temperature, usually be-
tween 160 °C and 220 °C. The reaction is very fast with approximately 5 s/mm wall
thickness.

Molded LSR components are physiologically inconspicuous, unaffected by
weather and aging, high-temperature stable (continuous working temperature up
to 180 °C) and can be made for optical applications with very high transparency
(up to 95%) and low haze. So the material is excellent for the manufacturing of
high-power LED lenses. They withstand the high operating temperatures (up to
150 °C) and the high percentage of blue radiation.

Other important features of LSR materials are their low viscosity during pro-
cessing (perfect for microstructures), the short cycle times, very good release prop-
erties, and an almost waste free (sprue is not necessary) processing.

The low viscosity during processing makes design of the mold challenging. To
obtain flash free parts, extreme close tolerances are obligatory. Furthermore, it is
required to evacuate the cavities (made by additional vacuum pumps) to avoid
entrapped air.

3.4
Optical Mold Inserts

Typically the mold features that create the optical surfaces are fabricated as sepa-
rate inserts. The optical surfaces of the mold inserts are fabricated as negative
shapes of the final component surfaces – generally spherical, plano, or aspherical
shapes. Diffractive, conical, lenticular, and cylindrical surfaces are also generated
as inserts.

Optical inserts can be manufactured by steel polishing, galvanic replication of
certain structures, or single-point diamond turning (see Figure 3.14).
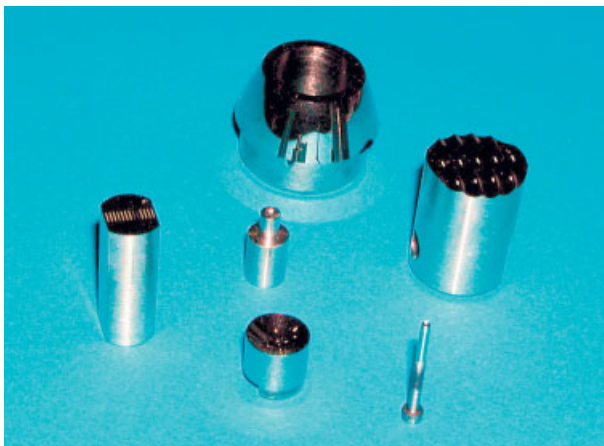
Figure 3.14 Optical mold inserts.

3.4.1
Steel Polishing

3.4.1.1 Mirror Finish

Spherical and plano inserts are produced and polished to the same accuracy as glass surfaces. They are generally fabricated from chromium-alloy stainless steel.

For optical surfaces the roughness needs to be approximately 10–20 times smaller than light wavelengths. This means that for plastic optical components that are typically used in the infrared and near-infrared regions the roughness has to be better than 30 nm. In practice target values for the tool are about 5–10 nm.

A steel that has preferably few structural defects and an extremely fine and consistent microstructure is preconditioned for this kind of surface quality. The steel has to be prepared by an appropriate pre-treatment such as several re-melts in ESU (electro slag re-melt process).

The steel inserts are hardened to a Rockwell C-hardness rating range of 50–54 prior to polishing. This degree of hardness is required to maintain a surface finish that will not degrade under the heat and pressure of the molding cycle.

Polishing should be carried out in dust- and draught-free places. Hard dust particles can easily contaminate the abrasive and ruin an almost finished surface. Each polishing tool should be used for only one paste grade and kept in a dust-proof container.

3.4.1.2 Computer-Controlled Polishing

This process means numerically controlled diamond grinding. Unlike diamond turning, this process can be used on ferrous metals such as stainless steel. It yields inserts with surface accuracies close to but not as good as diamond-turned inserts.

Continuing development work is being conducted in the areas of finishing and polishing of aspheric steel inserts. Conical, cylindrical, and toroidal inserts can be manufactured using grinding methods similar to those used to produce these types of surfaces in glass. The surface quality and finish of these inserts typically are poorer when compared with spherical steel inserts.

3.4.2
Galvanic Replication

Even small structures like gratings can be replicated by galvanic processes. A galvanic replication of the grating original (e.g., made by holographic processes in a photoresist layer on a glass substrate) is required for manufacturing an insert for an injection molding tool. This process makes high demands on the chemical resistance of the resist layer, its adhesion on the substrate, as well as on the processing conditions.

A gold conductive starting layer is sputtered on the resist structure with a thickness of approximately 100 nm. The galvanic process takes place with low current densities to guarantee a microcrystalline deposition that is required for molding of microstructured surfaces (see Figure 3.15).
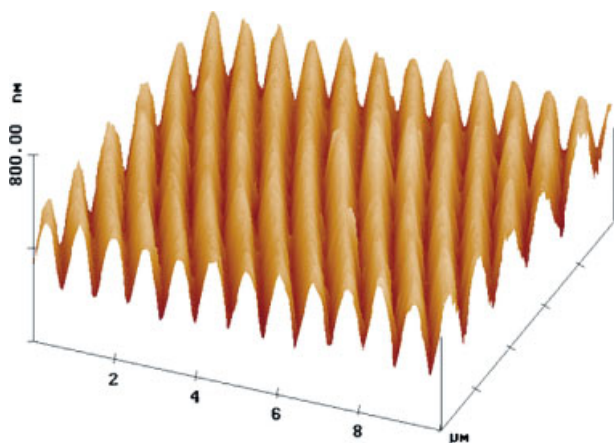
Figure 3.15 Molded grating with 0.7 µm grating constant (AFM image).

Due to the required minimal inner stress a nickel sulfamate electrolyte with a highly surface-active agent is used. A very high positioning accuracy can be achieved by the mutual manufacture of tool inserts and master retainer plate.

The galvanic molding is done directly into the mold insert to eliminate possible residual stresses (see Figure 3.16).
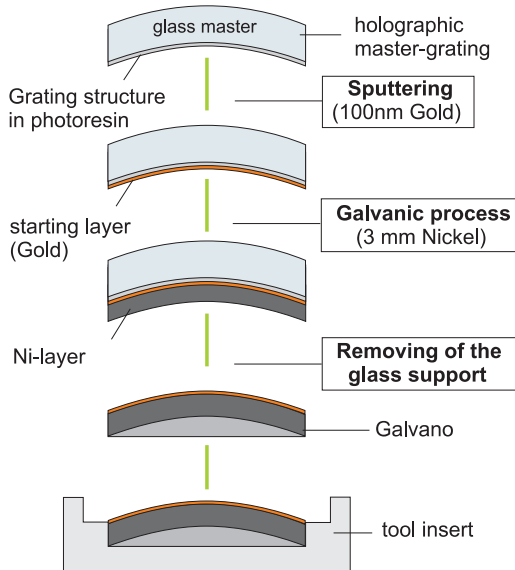
Figure 3.16 Tool insert manufacturing by galvanic replication.

3.4.3
Diamond-Turning Technology

Aspheric inserts, for instance, are manufactured in two steps. In the first step a best-fit curve is generated on a stainless steel substrate. The substrate is then subjected to a nickel-plating process (electroless nickel) that deposits a thin layer of nickel (up to 500 μm). In the second step single-point diamond turning produces the final aspheric or diffractive curve in the nickel (see Section 3.5).

Because the surface hardness of a nickel-plated insert is less than that of a spherical steel insert, it will be more susceptible to scratches and cosmetic defects.

The diamond-turning process can produce inserts to very close surface deviation tolerances, although it can leave residual grooving in the finish. Diamond-turned inserts typically exhibit root mean square surface roughness values of less than 5 nm.

3.4.4
Insert Quality and Molded Parts

Figures 3.17–3.19 show atomic force microscopy (AFM) images of machined tool surfaces for mold inserts made from different materials [9]. All the structures have a height of a few nanometers and an R_q value of less than 5 nm and are all suitable for optical applications.
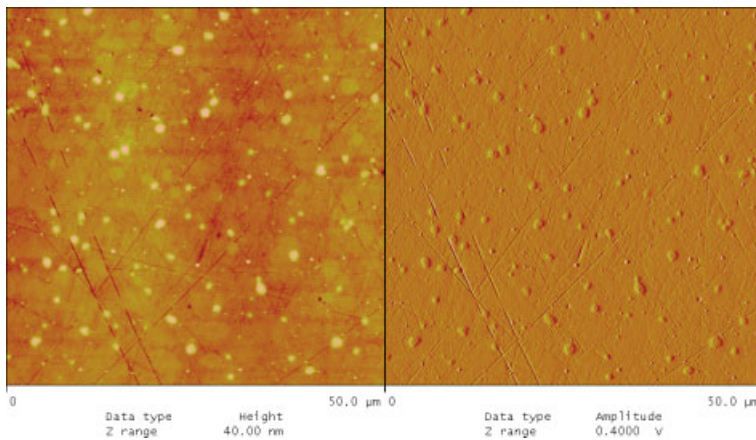
Figure 3.17 AFM image; optical polished steel insert – $R_q = 2.07$ nm.
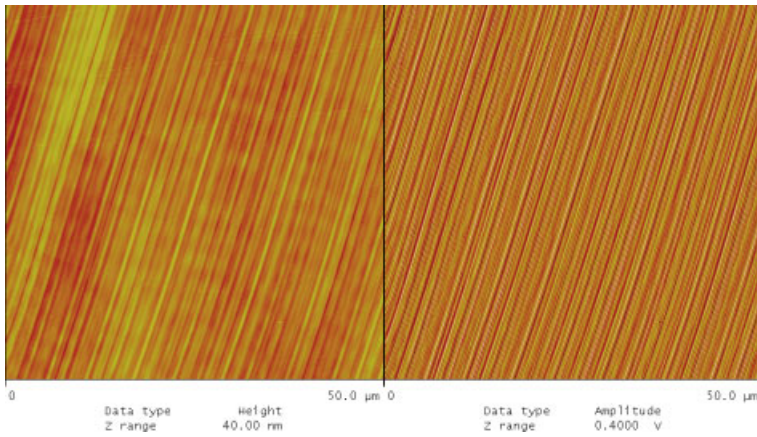
Figure 3.18 AFM image; nickel-coated steel insert, diamond turned – $R_q = 2.33$ nm.
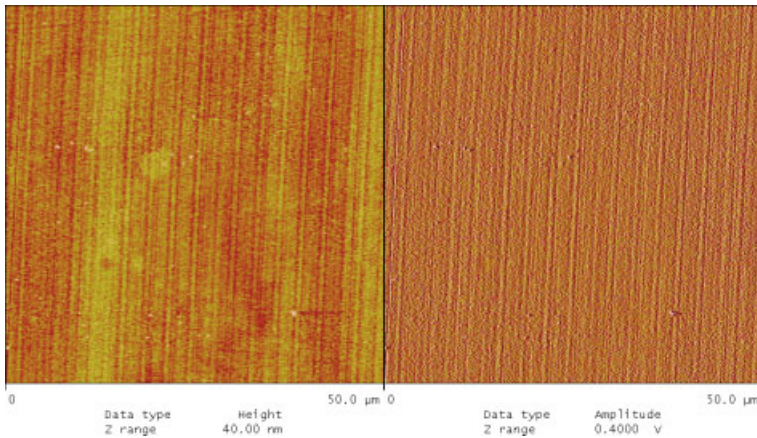
Figure 3.19 AFM image; nickel–copper alloy insert, diamond turned – $R_q = 3.72$ nm.

Figure 3.20 compares the achievable surface roughness for different materials. Polished steel and diamond-turned nickel on steel give the best results.

Figures 3.21 and 3.22 show the molding results of a polished steel insert (Figure 3.17) in PMMA and PC. All defect structures in a nanometer range are replicated almost identically. This behavior is also shown by other polymers (Figure 3.23). The observed differences reach a maximum of 0.5 nm. The replication of the surface is almost perfect.
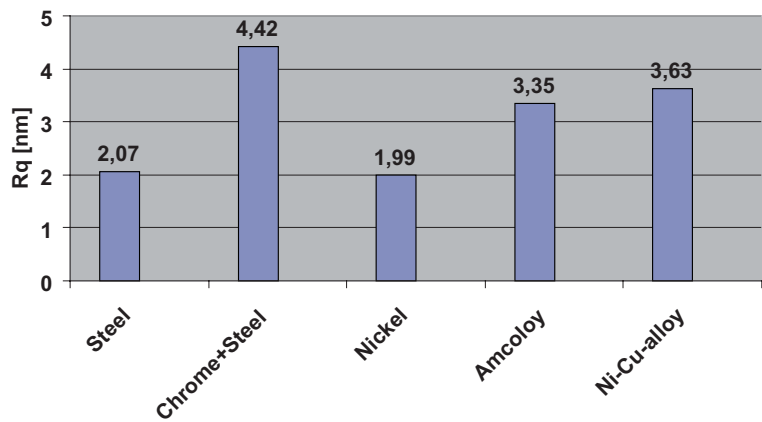
Figure 3.20 Surface quality of different mold inserts.
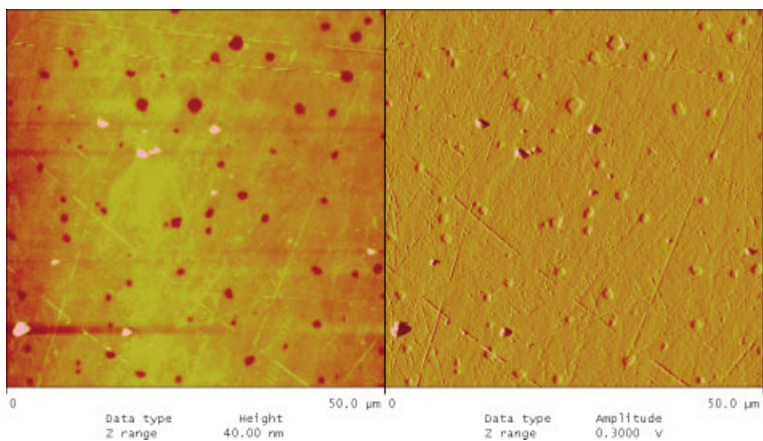
Figure 3.21 AFM image; PMMA replication of steel insert (Figure 3.17) – $R_q = 2.13$ nm.
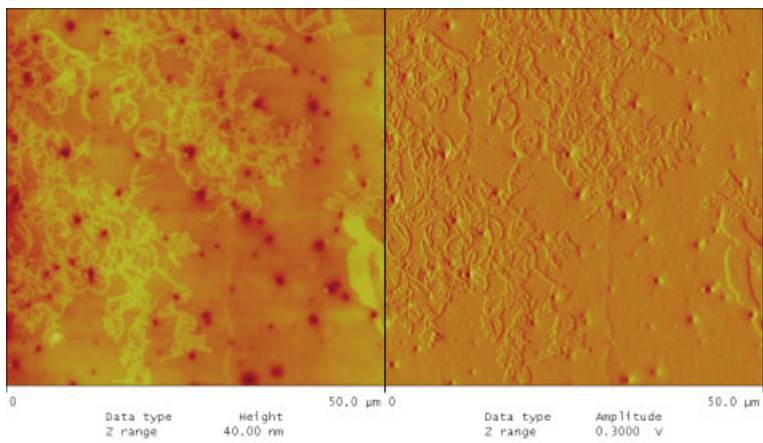
pcst2307.001

Figure 3.22 AFM image; PC replication of steel insert (Figure 3.17) – $R_q = 2.52$ nm.
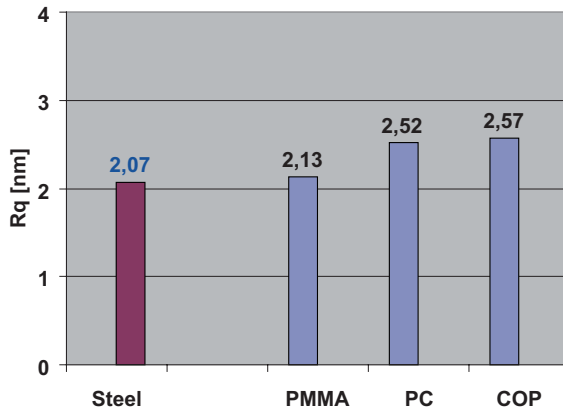
Figure 3.23 Replication of a steel insert in different polymers.

3.5
Ultra-precision Machine Tools for Mold-Making

It has been the author's experience that in many cases people hear about this technology, with impressive-sounding numbers on achievable accuracies for form and surface finish, are very excited, but need to be informed about what it takes to get there and where the limitations are. Although nowadays this is not a new technology, having been around for over 30 years, it is still associated with notions like "very expensive," "just for scientists," or "for laboratory use only." In the past this was quite true, but over the last decade the technology has gradually moved out of its niche of exotic aeronautic, space, and defense applications towards consumer markets. Because of this the total number of installed units worldwide has probably multiplied several times, from a view hundred in the early 1990s to probably more then a thousand nowadays, depending what one defines as an ultra-precision (UP) machine tool.

3.5.1
Characteristics of an UP Machine Tool

Basically a machine tool consists of at least one linear slide and some kind of spindle, both regulated by an appropriate "computer numeric control" (CNC). The linear slide must at least be equipped with a positioning feedback system for a closed loop control system. In some cases, e.g., ruling processes, the spindle might not be required, but we do not consider that case for now.

In order to fall into the category of an UP machine (state of the art), certain minimum criteria must be met:

- Linear slide overall straightness error < 0.5 μm (causes form errors).
- Linear slide sectional straightness error (any 25 mm) < 0.1 μm (causes waviness).

- Linear positioning feedback system resolution < 10 nm.
- Fast CNC system, capable of handling the huge amount of feedback information due to the high feedback resolution.
- Tool- or work-holding spindle with radial and axial error motion < 0.05 μm.
- Optimized drive motors for minimum energy consumption to avoid heat sources.
- Athermal mounting of critical components (thermal expansion errors).
- Axis mounted on a solid platform, with very good damping characteristics (mostly granite).
- Appropriate vibration insulations between platform and ground (causes extra roughness).

3.5.2
Some Words about the Environment

In order use an UP machine tool to its full extent special attention should be focused on the immediate environment. Ideally, such a machine should be placed in a room where the floor never vibrates, the temperature never varies, and the surrounding is noise-free. These perfect conditions may be hard to realize, but a reasonable attempt to get close to them is desirable. Floor vibrations always seem to be the biggest problem when deciding where to position a machine tool.

General considerations are:

- Whenever possible the tool should be sited in a basement and in a room that is furthest away from heavy traffic.
- Consideration should be given to heavy vehicles entering the premises for loading/unloading, even when it happens only once a day.
- The tool should be positioned away from any heavy machinery, like stamping or punching machines.
- Facility traffic should be avoided, like forklift trucks or pump trucks setting or lifting pallets.
- Banging doors or sources of low-frequency noise should be avoided.

3.5.3
Basic Process Features

The most distinctive feature of an UP application, which often is not understood by conventional machinists, is the small amount of material to be removed. As such, all blanks must be pre-machined to a precision level. Machine time is much too valuable for wasting hours nagging off material. Typical removal rates of 0.01 mm for roughing and 0.002 mm for finish are indications of what is required for good efficiency.

Expecting sub-micrometer accuracies from a machine tool can be justified only if operators appreciate all the relevant factors in the process. Fixtures for the blanks can be very critical, depending on size, form, and thickness. Maintaining

machined accuracies after components have been taken out of the fixture can be very difficult, especially when material thickness is small. Sometimes it can be useful to machine extra surfaces on the component for better alignment in successive processes or unit assembly. If component size and shape are variable, as is quite often the case in this technology, a universal vacuum chuck has been proven as the best solution. As long as the blanks (or adapter plates for holding the blanks) feature a flat lapped back surface, with sufficient area for establishing the required vacuum force for holding, no jaw or membrane device is necessary.

3.5.4
Tooling for Precision

Compared to other tool materials, the single-crystal diamond tool has unique characteristics:

- the highest possible hardness;
- low friction;
- high stiffness;
- good thermal conductivity; and
- atomic-level sharp edges are possible.

Depending on application requirements, the cutting edge of the tool can vary in shape and size, within the physical limitations of the crystal (Figure 3.24). Usually a radius-shaped and sharpened section of the diamond crystal represents the cutting zone. This section is defined as the "tool sweep" and specified by an angle. Any tool has more or less waviness superimposed on the nominal tool radius. Depending on the process, this waviness is reflected in the generated surfaces more or less by reducing form accuracies and surface finish. While in fly-cutting
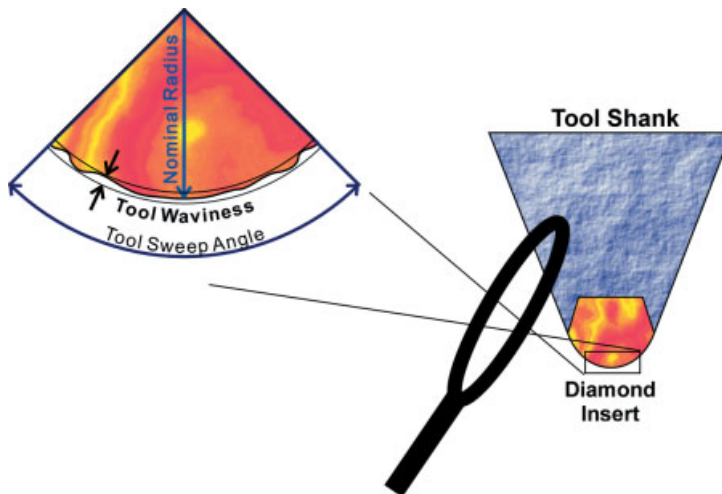
Figure 3.24 Single-crystal diamond tool.

processes the cutting point is stationary, in two-axis single-point diamond turning (SPDT) operations this point moves along the tool sweep line. Since the tool radius compensation (TRC) of the machine control assumes a perfect nominal tool radius, tool errors (waviness) are more critical in two-axis SPDT. Since errors introduced by tool waviness are rather consistent, compensation methods can be applied.

3.5.5
Typical Machine Configurations

3.5.5.1 Single Axis
This configuration (Figure 3.25) consists of one linear slideway on which the component resides. The cutting tool is mounted on the face of a spindle (just like a single tooth), usually with a comparable large disc mounted on the spindle shaft. The spindle height can be adjusted manually or via CNC for positioning only. This is most appropriate for generating flat components, since the surface speed of the tool is constant during the entire process. The common name for this process is fly cutting.
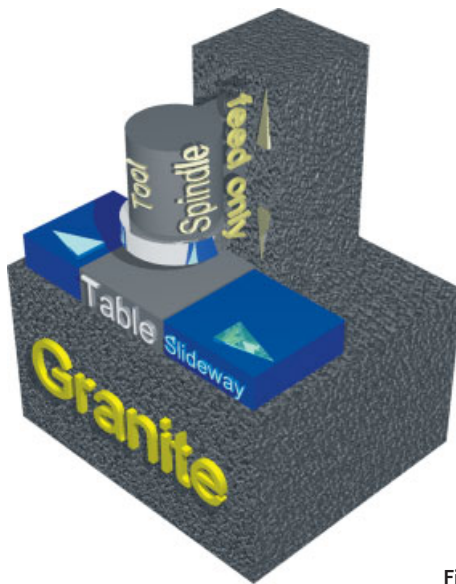
Figure 3.25 Single-axis machine configuration.

3.5.5.2 Two-Axis SPDT
Two linear slideways (X and Z) are orientated perpendicular to each other, usually forming a "T" with more or less offset allowing equal or unequal travel of either side (Figure 3.26). One slide tabletop carries the work piece spindle and the other the tooling plate. Featuring two CNC slideways, any rotationally symmetric shape can be generated within the working envelope of the machine.
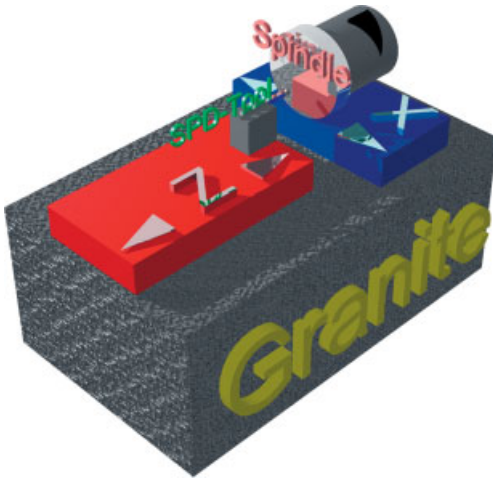
Figure 3.26 Two-axis SPDT machine configuration.

3.5.5.3 Three-Axis SPDT

In addition to the two-axis version, the tool sits on a CNC turning table, usually defined as the B-axis (Figure 3.27). The main purpose of this configuration is to maintain the same angle between tool and work piece surface (normal) during the entire process. This method is known as "tool normal cutting." Unfortunately the working envelope of same-sized machines is reduced and, due to greater technical effort, the machine price is significantly higher. Figure 3.28 shows the operating principle of this method. By means of the B-axis, the angle between the surface and tool is held nearly constant over the entire contouring process. The X- and Z-slide must be offset (X-move and Z-move) in real time to ensure correct tool tip compensation.
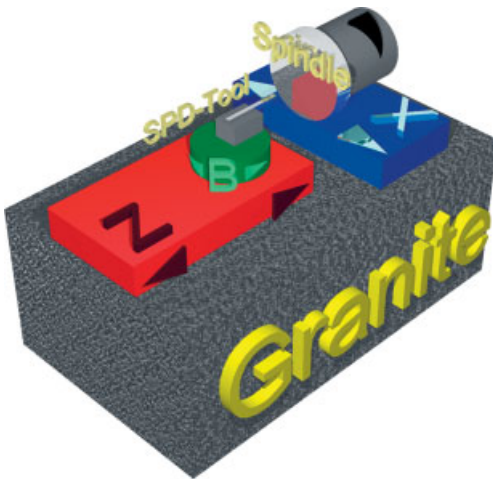
Figure 3.27 Three-axis SPDT machine configuration.
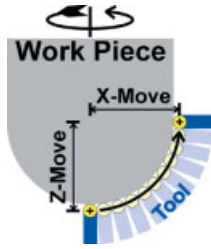
Figure 3.28 Principle of tool normal cutting.

3.5.5.4 Off-Axis SPDT

Quite often it is not realized that the required form might be machined in an off-axis set-up, by offsetting the components within the swing of the work-holding spindle chuck, and using so-called "freeform machining methods" (see below), although the form could also be machined on a two-axis lathe. Figure 3.29 shows one typical example, in which the tool path is dominated by a radial X-move. Figure 3.30 shows another example, but with a predominant Z-move in the tool path.
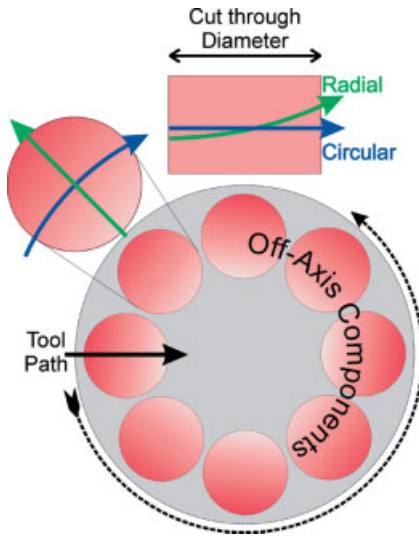
Figure 3.29 Principle of off-axis SPDT.

If the spindle rotates, the two components build a drum shape, on the inner diameter of which the machining process takes place. The offset of the component in the work-holding spindle chuck determines a concave radius (only a radius is possible, of course) while in the other coordinate any shape can be machined (e.g., aspherical). If the machining takes place on the outside of the "drum," convex radii can be machined in one coordinate. The size of these radii is limited by the swing capacity of the machine.
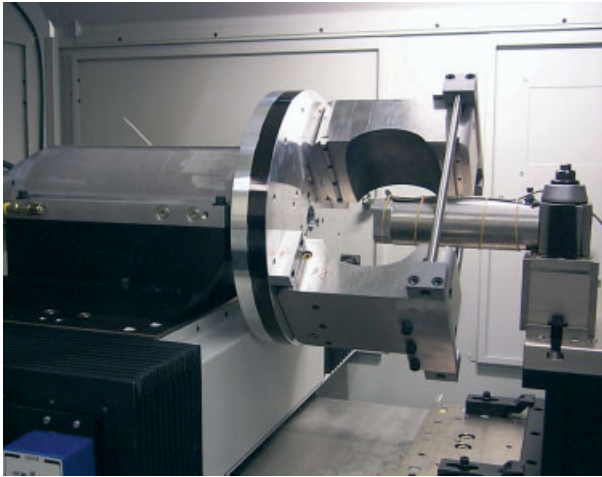
Figure 3.30 Off-axis machining of large molds. (Courtesy of Precitech Inc.)

3.5.5.5 Multi-Axis Freeform Operation

Raster Milling or Grinding

Three linear slides, configured as in Figure 3.31, form a typical platform for the multi-axis configuration. Basically this consists of a two-axis SPDT set-up as in Figure 3.26, but without the work piece spindle, where the vertical slide rides on the X-slide tabletop. Typical applications with this configuration would be raster milling or raster grinding, by mounting a vertically orientated tool-spindle on the Y-slide and holding the components by means of an L-shape vacuum chuck on the Z-slide tabletop, as shown in Figure 3.31.
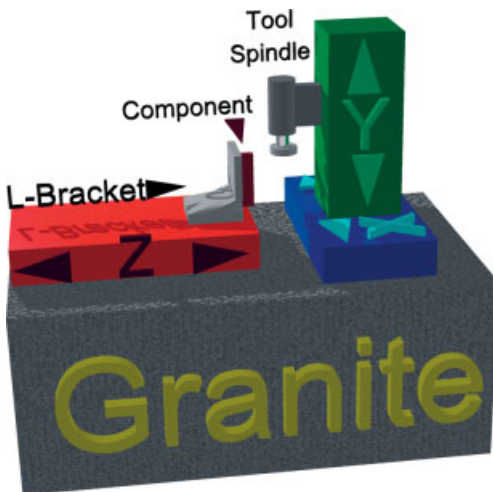
Figure 3.31 Three-axis raster machining configuration.
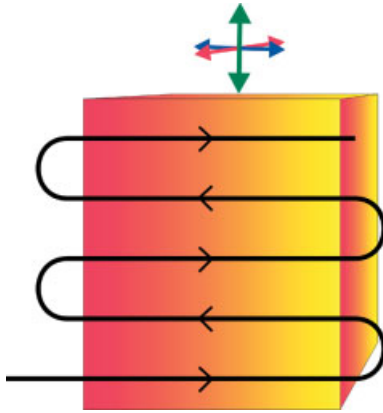
Figure 3.32 Principle of raster machining.

The principle of the tool path is shown in Figure 3.32. Depending on component size and vertical step width, the process time for generating freeform shapes by raster methods may be as long as days. As such, thermal stability to a maximum 1 °C drift, over such a long time frame, becomes a real challenge.

End-Ball Milling

Additional CNC turning axes can be added to a three-linear-axis base (Figure 3.31) in order to increase the amount of freedom. This could be the A- and B-axis, as shown in Figure 3.33. A typical application for this kind of configuration would be end-ball milling.
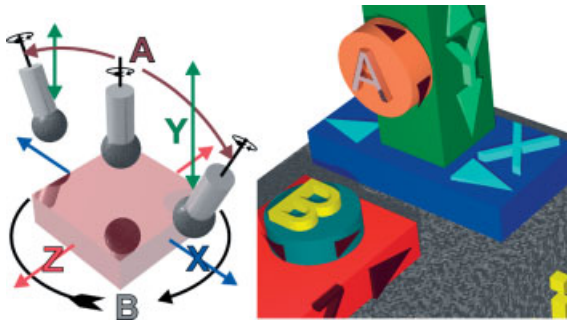
Figure 3.33 a) Five-axis end-ball milling set-up; b) detail of axes.

Tool tip compensation for this kind of application becomes very difficult. Available CNC systems cannot compensate as required; hence compensation must already be implemented when generating the part program. This, of course, makes part programming somewhat inflexible, because every time the tool changes, another part program must be generated with the new tool data.

Spiral Milling

If the surfaces to be machined represent a freeform in a sense of minor deviation from a rotational symmetric shape, for instance a "toric" as shown in Figure 3.34, a two-axis SPDT configuration (Figure 3.26) could be a more economical method.
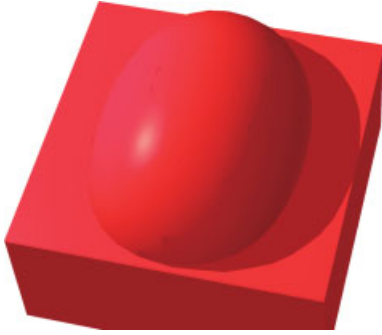
Figure 3.34 Toroidal shape (squeezed ball).
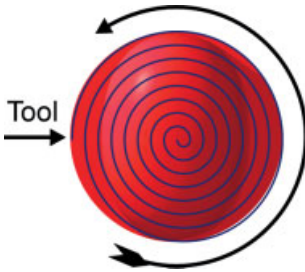
Figure 3.35 Spiral tool path.

The work piece spindle must be designed as a C-axis and fully integrated in the CNC system. As such, any X- and Z-slide movement is carried out in conjunction with the angular position of the component on the C-axis. Typically this results in a spiral tool path over the component surface (Figure 3.35). Depending on the machine slide dynamics and surface requirements, a SPDT or milling operation can be chosen for the cutting method.

Slow Tool and Fast Tool Servo Systems

If moving a tool axial (Z) and synchronous to angular (C) positions of the work piece during the turning process, one refers to "tool servo" systems. In order to cope with physical limitations given, two basic variations are known as slow tool servo (STS) and fast tool servo (FTS). While in STS systems the entire slide table carries out the Z-stroke, only the tool moves in FTS systems. By carrying much less mass, FTS systems are much more dynamic and can be used to significantly higher frequencies (kHz) than STS systems (Hz). Unfortunately the maximum stroke of this kind of system is limited to less than one millimeter, depending on design. While STS is more suitable for generating freeform geometries (as in spiral milling), FTS is the choice when fine structures (Figure 3.36) have to be machined in rotational symmetric contours (e.g., optical diffusion).

Figure 3.36 Typical surface generated in fast tool servo mode. (Courtesy of Precitech Inc.)

3.5.6
Material-Related Limitations

Typical diamond-turnable materials are: metals like aluminum alloys, copper, copper–nickel alloys, brass, and electroless nickel; crystals like germanium, zinc selenite, calcium fluoride, and silicon; and polymers like acrylics and PMA.

As has been discussed, the most accurate tool available is the single-crystal diamond. Unfortunately not all materials can be machined with this type of tooling (SPDT). Due to chemical reactions of all ferrous metals, causing excessive tool wear, common materials for molding tools, such as hardened steel or steel alloys, cannot be machined directly. A typical work-around would be to nickel plate the steel substrate and generate the final form and finish in this material, which represents the hardest metal (ca. 550 HV) for SPDT. Because of its high phosphor content (> 10%), electroless nickel yields the best results for surface finish ($R_a < 5$ nm) and tool life. The nickel plating can be as thick as 0.2 mm, which ample for the SPDT process. The quality of the coating (adhesion, purity) is of great importance for good results.

3.5.6.1 Overcoming Material Limitations

If the material does not allow the use of a SPDT process, generating the contour by a grinding process should be considered. By replacing the holder for the SPDT tool with a vertical grinding spindle, the machine set-up is almost identical (Figures 3.37 and 3.38). As with the diamond-turning process, the position of the grinding wheel in X-direction and height is very critical and therefore accurate tool-setting and dressing (on the machine) is important. Once the grinding process has been optimized, deterministic machining of hardened steel as well as glass, quartz, ceramic, and many other crystals, close to diamond-turning quality, becomes possible.
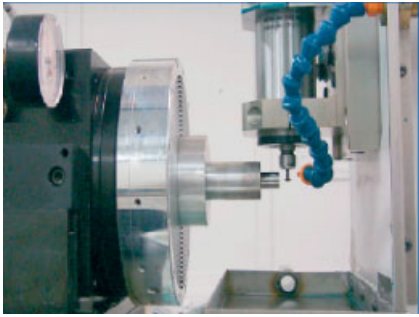
Figure 3.37 Steel mold grinding set-up. (Courtesy of Precitech Inc.)
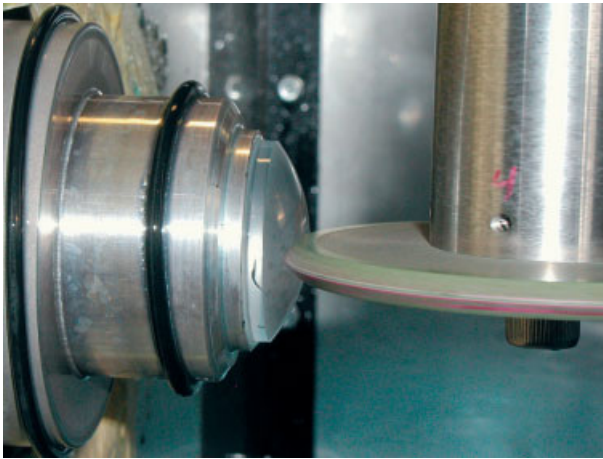
Figure 3.38 Direct glass grinding set-up. (Courtesy of Precitech Inc.)

References

1 B. G. Broome, The design of plastic optical systems, SPIE Short Course (SC384), San Diego, 2001.

2 Xiaohui Ning and R. T. Hebert, eds., Design, fabrication and application of precision plastic optics, *SPIE Proc.* **2600** (1995).

3 An introduction to the design, manufacture and application of plastic optics, Optical Coating Laboratory Inc., technical information, 2001.

4 *DIAKON – Technical Handbook* (Imperial Chemical Industries, 1986).

5 Technical Information by EMS-CHEMIE (Germany) GmbH, www.emsgrivory.com, July 2001.

6 *The Handbook of Plastic Optics*, 2nd edition (Corning Precision Lens, 2000).

7 P. Zimmermann, Moulds for optical disc substrates, *Spritzgießen 2004*, VDI-Tagung Baden-Baden, 2004, pp. 243–259.

8 A. Davis, R. Bush, J. Harvey, and M. Foley, Fresnel lenses in rear projection displays, Technical Paper of Fresnel Optics, Rochester, NY.

9 J. Hamann, Characterization of significant surface parameters of optical functional surfaces of plastic optic elements and optically polished and diamond turned tool inserts. Diploma thesis, University of Applied Sciences, Jena, 2002.

4

Metrology of Injection Molded Optics

Stefan Bäumer (Philips Applied Technologies, Eindhoven, The Netherlands)

4.1
Introduction

All products have to go through a design–build–test cycle. Every single step in this process is equally important. Only if all steps of the whole product development cycle are filled in at a sufficient level, a quality product can emerge. Metrology is an item that is often forgotten or filled in at a late stadium in the product development cycle. In this chapter, an attempt is made to emphasize the importance of metrology. It should also be stated in the beginning that metrology is more than having a room full of measurement equipment and knowing how to use it. Metrology is a discipline just like designing optics or molds! In order to perform quality metrology, one needs to have a thorough understanding of the product (and its function) and on the other hand be familiar with state-of-the-art measurement technologies and equipment. Someone working in metrology needs to be able to translate the relevant (optical) functions of a product into measurable quantities. Most of the time, this is a learning process and requires some practical experience that cannot be conveyed by written text. However, this chapter is an attempt to support that process by giving an overview of the state-of-the-art metrology techniques and equipment. Since it is still a very broad field, a selection has been made. Guiding the selection are the special requirements of injection molded optics.

For injection molded optics, there are several tasks in metrology.

First, the molding tool needs to be measured. This is usually dimensional metrology for mold and mold base. Since these form the basis for many products coming out of the tools, they need to be characterized to a very high accuracy. Depending upon the products, submicron accuracy is required. Other parts that usually need to be measured with very high precision are the insert pieces that form the optical surfaces. These parts need to be better or at least as good as the parts they will form. The advantage is that the molding tool together with the insert needs to be measured only once (or after maintenance). Therefore, measurement time is not so critical – accuracy is more of an issue. More elaborated and time-consuming measurement methods can be applied.

Then the molded products need to be characterized as well. Injection molding is a mass production technology. Molded products usually run in high volumes. Therefore, metrology for injection molding needs to be fit for mass production. This can be achieved along various paths. A very first step is to set up a good metrology plan. In the metrology plan, all critical dimensions and parameters are listed. Then, depending on product function, tool design, process stability, molding conditions, etc., it has to be decided which parameters need to be measured and how often. The two main approaches are to measure every single part manufactured or to rely on statistical process control (SPC). The choice is depending upon the molder, his process, and sometimes also on the nature of the product and/or customer. Security relevant parts probably need to be measured 100%, while many other parts can perfectly well be manufactured using SPC. In any case, a good metrology plan can save lots of effort in metrology and should always be in place, preferably already during the design phase of the product. It should also be quite evident that metrology equipment, which is released for mass production, i.e., able to handle high volumes, should have been qualified by a suitable R&R study (repeatability & reproducibility).

A subtlety in injection molding is that in many cases the dimensions of the molding tool are slightly different than the ones of the product itself. The reason for this lies in the shrinkage of the polymer material. Therefore, easy conclusions between mold- and product dimensions are sometimes misleading or more complex than at first sight. For a good metrology plan, the molder should have sufficient knowledge and experience in the shrinkage behavior of the material being used.

Another very specific factor for metrology of injection molding comes for one of the big advantages of injection molding: integration of functions. For generic parts, one usually can make use of generic metrology. An example is producing a collimating lens for a CD or DVD optical pick-up unit. This kind of single lens element can be characterized using a standard interferometer system. However if more functions are added, such as beam splitting and shaping, metrology needs to be more and more customized toward relevant functions of the part. Either one plastic part has to pass several generic metrology instruments or a custom setup has to be built. Metrology could be the price one has to pay for the advantage of integrated functions in one product!

The ultimate challenge for metrology for injection-molded *optics* is the characterization of (steep) aspheric surfaces. While traditional optical designs based upon glass usually have got the freedom of material within mostly spherical surfaces, injection molding knows only a handful of materials but uses the freedom of form for the designs. This is even more so, since ultra precision single point diamond turning became readily available during the last years. Therefore many plastic optics designs contain aspheric surfaces, some of them with steep slopes and large deviations from sphericity.

In all the sections, the emphasis is on optical metrology. The main advantage of optical metrology is that it is noncontact and usually fast. The noncontact feature is a valuable asset in characterizing the inserts used in molding. This way they

stay in their original shape and do not get touched (and possibly scratched) by any probe. In optical metrology, there are several generic techniques available to characterize high-precision optical parts. Good reviews of most of these techniques are given in [1–3]. Furthermore, rich resources on various measurement principles are the international standards published by ISO. For optical metrology, one of the most important ones is ISO 10110 [4]. This standard covers many of the standard parameters that should be known for a particular optical component. Although not referenced at each place in this chapter, the ISO 10110 standard forms a basis for optical metrology.

It should also be pointed out that there is plenty of good literature on each and single one of the metrology topics mentioned. It is not the aim of this chapter to double these efforts. An attempt has been made to reference literature that zooms in on the specific topics. The purpose of the current work is to put all these techniques in perspective to injection-molding optics and to mass production, giving the reader a guideline in which direction he or she might be able to find solutions for the problems they are facing.

Capturing all previously described tasks in one chapter has been a true challenge. As a structure of the chapter, the following has been chosen. First a short review on dimensional metrology is given. This type of metrology is essential for mold and tool characterization. However for some optical surfaces, it can be used as well. Next, surface metrology is described. Optical surfaces are most important for all optical parts. Therefore, they need to be known to upmost precision. If optical components are characterized as a whole, the measurement of the transmitted wavefront is often being used. Therefore, wavefront metrology is reviewed in more detail. It should also be mentioned that wavefront metrology in some cases can be used as well for surface characterization. A specific problem of injection-molded optics is birefringence. An extra section is devoted to that problem. Another specific item of injection-molded optics is centration. The optical part is formed using two different mold parts, so the orientation of the two surfaces with respect to each other is important. In injection-molded optics, aspheres are used in many systems. In general, aspheres are more sensitive to tilt and decenter than their spherical counterparts. This is another reason to cover methods for measuring centration. The last section of this chapter is devoted to examples of custom setups and high-speed metrology for mass production.

Before starting the actual review of various metrology technologies, Table 4.1 will give a short overview on typical specifications of injection-molded optics [5]. Metrology should be able to characterize the optical components to at least this level.

A similar table is found in Chapter 2 and also published by Beich [6].

Table 4.1 Selected tolerances.

lens attribute	normal tolerance	tight tolerance	extra tight tolerance
surface radius	± 1%	± 0.5%	± 0.3%
focal length	± 2%	± 1%	± 0.5%
lens thickness	± 0.03 mm	± 0.02 mm	± 0.015 mm
flange diameter	± 0.03 mm	± 0.02 mm	± 0.015 mm
surface wavefront aberration	60 nm RMS	30 nm RMS	15 nm RMS
(depending on steepness curve (NA)	300 nm PV	150 nm PV	75 nm PV
and degree of asphericity)			
bubbles/inclusions/scratches	1×0.16	1×0.10	1×0.06
	2×0.10	2×0.06	2×0.04

4.2
Dimensional Metrology

Good optics always needs good mechanics. Having this idea in mind, a good opti-cal system always needs to have not only a solid optical design but also a good mechanical construction. For injection molding, this is even more the case since all optical parts come out of a mechanical tool. Figure 4.1 shows the schematics of a typical optical mold.
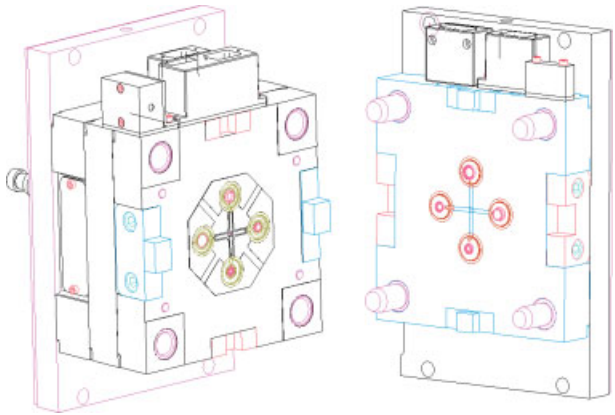
Figure 4.1 Schematic optical 4 cavity mold.

While designing the mold, the mold designer needs to have a couple of refer-ence points and lines in mind. It is important to define these references in such a way that they are accessible for metrology. That way the mold can be measured and the results of the measurements can be directly compared to the drawings. Also experience shows that it is of high value for tool and product if the metrology points are physically present. Many times it happens that metrology lines are the-

oretical references on the drawing. There they make perfect sense. However in reality, such theoretical references have proven to be very impractical, because they cannot be measured directly. In Figure 4.1, the metrology points are designed along the process of closing the mold. First important reference points are the four centering pins. The next step in centering is the cross in the middle and at last the centering and alignment on the insert locations itself. All these three locations are used as metrology reference marks.

The main tool for this kind of measurement is a 3D coordinate measuring machine (3D CMM). With this kind of machines, all geometric dimensions of a part can be measured. While these machines form the backbone of dimensional metrology and are already in place for many years, there are still recent developments to further increase the accuracy of these devices [7]. Many of these efforts go into the direction of thermal management, compensation of Abbe error, and of course even more sophisticated software. Good reviews on the use and capabilities of the CMMs can be found in the literature [8, 9]. Depending on the measurement volume, different kinds of accuracies in the three dimensions can be reached. State-of-the-art standard equipment can measure in a volume of 400 mm × 400 mm × 400 mm with a resolution of 0.5 μm and an accuracy of about 4 μm/mm stroke. There are also high-precision machines available that perform even better than this standard equipment, see for example [10, 11]. For smaller measurement volumes, an ultra high precision CMM has been developed at Philips Applied Technologies. Figure 4.2 shows a photograph of the machine that measures in a measurement volume of 100 mm × 100 mm × 40 mm (*x, y, z*) with a volumetric machine uncertainty of 30 nm and a point-to-point position accuracy of 0.1 μm.

Besides the machine construction, the choice of probe plays a very important role as well. On most CMMs, various probes reaching from mechanical to capacitive probes can be mounted.

(a)   (b)
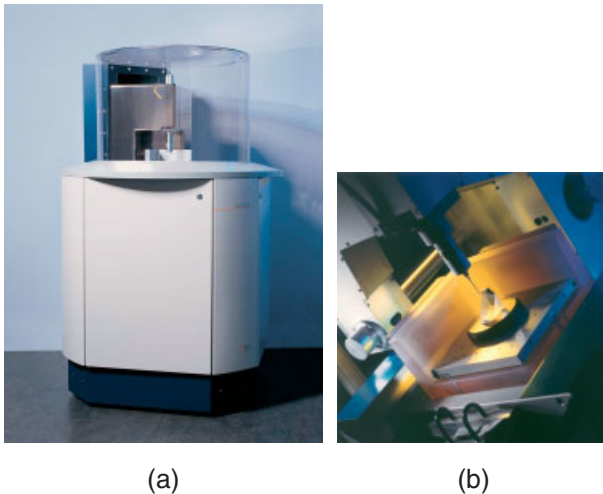
Figure 4.2 Philips Applied Technologies Isara; (a) machine total, (b) metrology chamber [12].

3D CMMs can not only be used to measure molds and mold bases, but also they can sometimes be very useful in profiling optical surfaces. Especially larger lens surfaces, like for molded spectacle lenses, can be measured perfectly well with such a 3D CMM.

4.3
Surface Metrology

4.3.1
General Concepts

Talking about (optical) metrology, a distinction can be made between surface metrology and wavefront metrology. Surface metrology – as the name suggests – is the accurate characterization of the optical surfaces. This is of upmost importance, since optical surfaces form the basis of all optical systems. Lenses are formed of two optical surfaces, and in case of reflective optics all optical functionality is placed in one surface. For injection-molded optics, surface metrology has yet got another dimension: since the optical surfaces are formed using a mold, all optical inserts need to be characterized as well. Therefore, surface metrology is very important.

Before reviewing some of the most common techniques of surface metrology, it is important to understand that there are different types of surface domains that have to be distinguished: surface figure or shape, surface finish, and surface waviness. These three domains are distinguished because of their spatial extend [13]. Surface figure is the general shape of the surface. With surface figure, long spatial wavelengths are associated; it is measured over the entire product. For surface figure measurements, metrology tools do not need to have extreme spatial resolutions. Surface finish is also called surface roughness. This is a surface parameter that is determined over small length, usually 1 mm. In order to measure this parameter accurately, metrology should have very high spatial resolutions. The last surface quality parameter is the so-called waviness. At the same time, in many cases this is also the most difficult one to determine accurately. Figure 4.3 shows the different contributions of shape, waviness, and roughness to the surface.

Waviness is a parameter that is relevant in the mid-spatial frequency region. Therefore, metrology tools used for surface figure measurements would need a higher spatial resolution to determine waviness and tools for roughness measurements a larger range. In today's metrology equipment, these two opposing requirements are usually battled by introducing high-resolution cameras in imaging metrology systems, and more sophisticated lengths scales in scanning systems. A good method for comparing and checking the performance of metrology instruments is the so-called A–W diagram or Stedman diagram as it is called sometimes as well [14, 15]. In this diagram, the log of the surface wavelength versus the log of the surface amplitude is plotted. An area in such a diagram depicts the usable region of a metrology instrument.
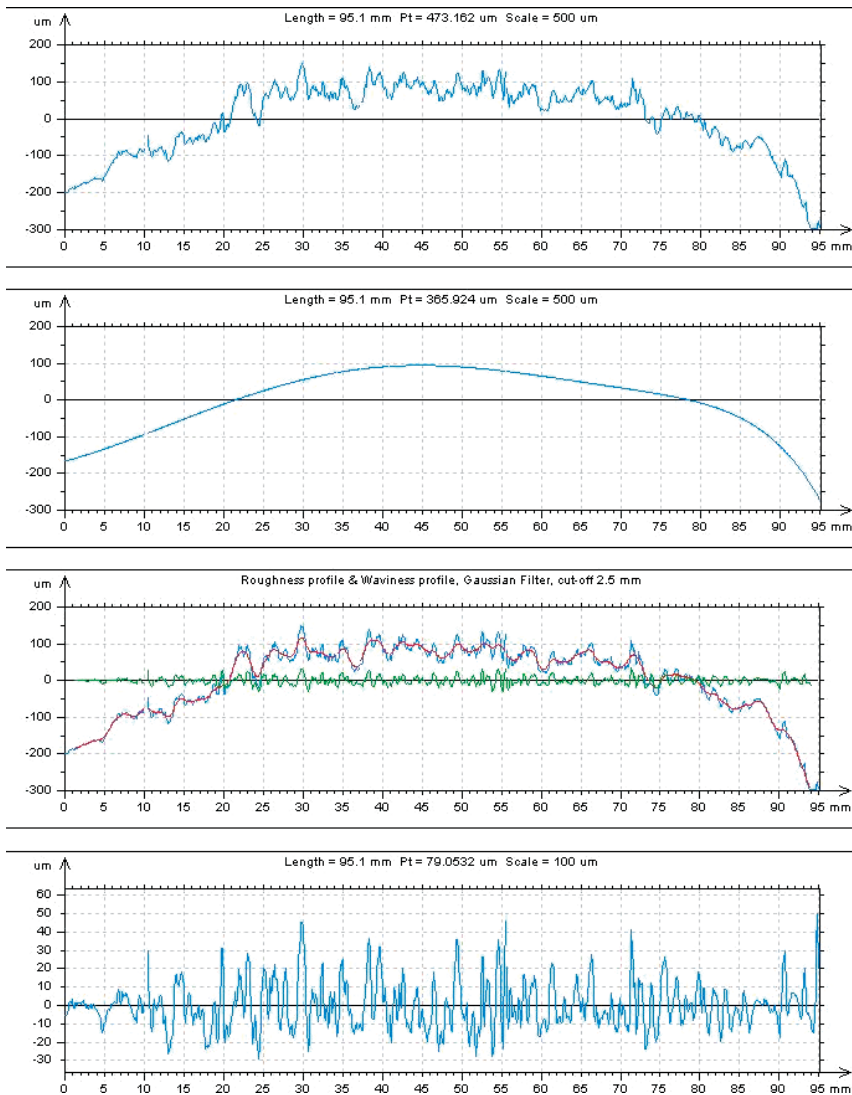
Figure 4.3 Different surface parameters: top profile, 2 shape only, 3 all parameters together (blue line: profile; read line: waviness; green line: roughness), 4 (bottom) roughness only.

Yet another classification of metrology tools is to look at the way the data are acquired: there are scanning systems that acquire measurement points in a sequential mode, and there are imaging systems that take in data points in parallel. Scanning type systems for surface metrology are systems where the sample under test is mechanically moved with respect to a probe that measures the height of the surface. The above-mentioned 3D CMMs are a perfect example of such a

surface metrology application. Note that advanced CMMs can be used very well to probe optical surfaces as well. Especially for larger surfaces, the application of a CMM is a good idea. Usually these machines can handle larger volumes and for some shapes the accuracy is sufficient. For smaller optical surface, a good x–y scan stage can be used as well. If the stage is then equipped with an optical probe that has got a sufficient height range/resolution for surface under test, optical surface can be measured as well with good quality. As noncontact probes, chromatic probes and so-called conoscopic probes have to be mentioned [16, 17].

Taking that basic idea a step further, a trend in optical surface metrology, especially for steeply curved surfaces and aspheres, is to use the basis of a CMM and adopt it to the specific requirements of optical metrology [18]. In general, the CMM base is used to provide an accurate global position of the probe with respect to the surface under test, while the probe itself delivers high accurate surface profile data, usually height data. In this way, best use is being made of global position measurements, usually backed by displacement measuring interferometers (DMI), and high-resolution local data off the probe. Some specific examples of this more general principle are discussed in the following paragraphs.

4.3.2
NANOMEFOS

A recent development of a metrology system that is especially geared toward measuring larger optical surfaces with extreme accuracy is the so-called NANO-MEFOS (Nanometer Accuracy NOn-contact MEasurement of Freeform Optical Surfaces) [19]. Although not a commercial product yet and in the first place geared toward larger optical elements, the machine concept is such that it has got several advantages over Cartesian scanning of most CMMs. Therefore, it is mentioned here and maybe in the future a special machine that takes the subtleties of injection-molded optics into account will emerge, based upon this general concept. Figure 4.4 shows the basic machine setup.
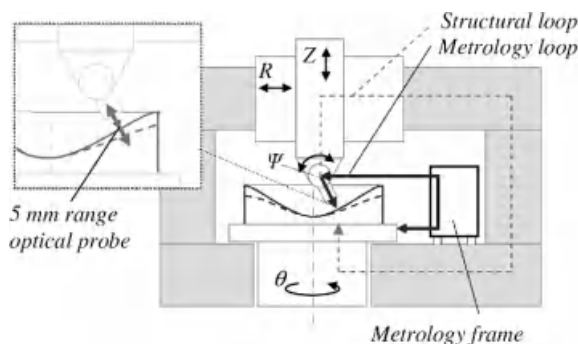
Figure 4.4 Machine concept of NANOMEFOS [20].

The sample under test is rotated, while an optical probe is scanned across the rotating sample (*R*- and *Z*-direction). The neat thing about this metrology setup is that:

- It measures in a cylindrical system (*R*, *Θ*, *h*), which is a lot better suited to describe optical surfaces (who are very often manufactured using some turning movement as well)
- The optical probe is placed in such a way that it is positioned as much as possible perpendicular to the surface under test

That way it is used under limited angles and distances, which intrinsically increases the accuracy. One could say that by positioning the probe in this way, a best-fit sphere is subtracted mechanically and the asphericity is measured locally with the probe. In the current prototype, a differential confocal probe is applied [21a].

The very high accuracy of the whole machine is then achieved by clever design and engineering of the various subsystems and the overall architecture. The prototype machine achieved the following specifications:

- Sample under test, lateral dimensions: 500 mm × 100 mm, measurement uncertainty of 30 nm in height, measurement time ~15 min.

A similar approach is realized in the Panasonic UA3P; however there the focus is on rather small surfaces. And the probe used is an atomic force probe [21b].

4.3.3
Deflectometry

During the last years, developments in the area of deflectometry have taken place, turning the deflectometer potentially into a very powerful metrology tool for not only injection-molded optics. A deflectometer is a local slope sensor. One way of implementing such a local slope sensor is to work with a single-point sensor. Figure 4.5 illustrates the operating principle. A small light bundle is sent onto the surface under test. The light bundle is reflected and an optical angle senor measures the local deviation from the surface normal. If the light bundle is scanned over the entire surface under test, a slope map of the surface under test is generated. By using a 2D detector, both slopes in the *x*- and *y*-direction can be recorded. Using smart algorithms, the surface under test can be reconstructed by means of integration [22, 23]. Also the intensity data of the returning measuring spot can be

Figure 4.5 Measurement principle of local slope.

recorded. In some cases, this data can be used to identify erroneous measurement points.

Using the deflectometer for characterizing injection-molded optics, in many cases the challenge is to cope with large slopes. This can be achieved by applying a similar device architecture as used in NANOMAFOS. Figure 4.6 depicts the principle applied here. The deflectometer head is scanned along the best-fit sphere, while the sample under test is rotating around its center. Applying this configuration, a large portion of the slope range is taken out by the geometry of the setup. The remaining slope measurement range has to be captured in the design of the deflectometer head. The advantage of such a deflectometer is that the lateral resolution of the device can be made very high. Furthermore, measurements in the slope domain can usually handle steeper aspheres better than interferometers without compensation optics. In this respect, the Shack–Hartmann sensor and the deflectometer are very similar.

Besides the large slope range that can be covered with the deflectometer, it is very flexible. By moving the deflectometer head in the *z*-direction, the best-fit sphere can be adjusted easily. Furthermore, both concave and convex surfaces can be measured without any hardware changes.
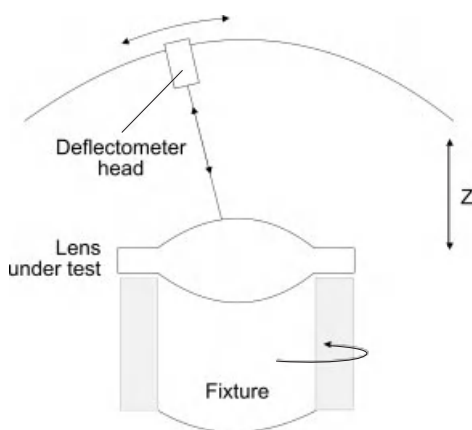
Figure 4.6 Schematic setup of the deflectometer.

At Trioptics, feasibility studies of such a device are ongoing. Figure 4.7 shows the layout of an industrial preprototype. For measurements of inserts, it has been proven a very powerful tool. Measurement of plastic surfaces is under investigation.

Besides being a noncontact and fast technology, a big advantage is that deflectometers can measure so-called free-form surfaces. Since the whole surface under test is scanned during one measurement, it is possible to reconstruct free-form surfaces. The integration algorithms are suitable to fit all data point together to one continuous surface. Figure 4.8 shows a typical reconstruction of a toric form. The deviation from the best-fit sphere is displayed.
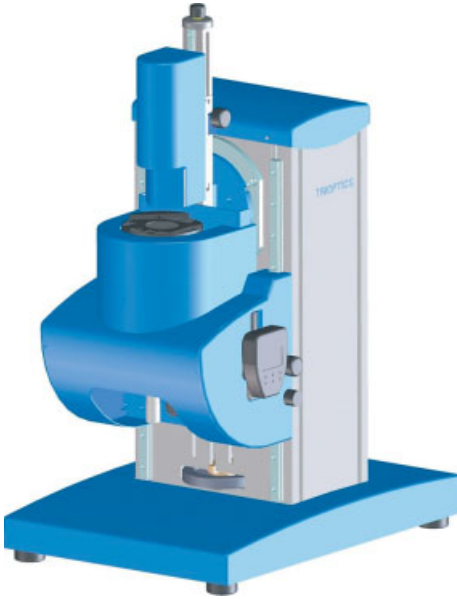
Figure 4.7 Trioptics asphere deflectometer (illustration courtesy of Trioptics GmbH [24]).
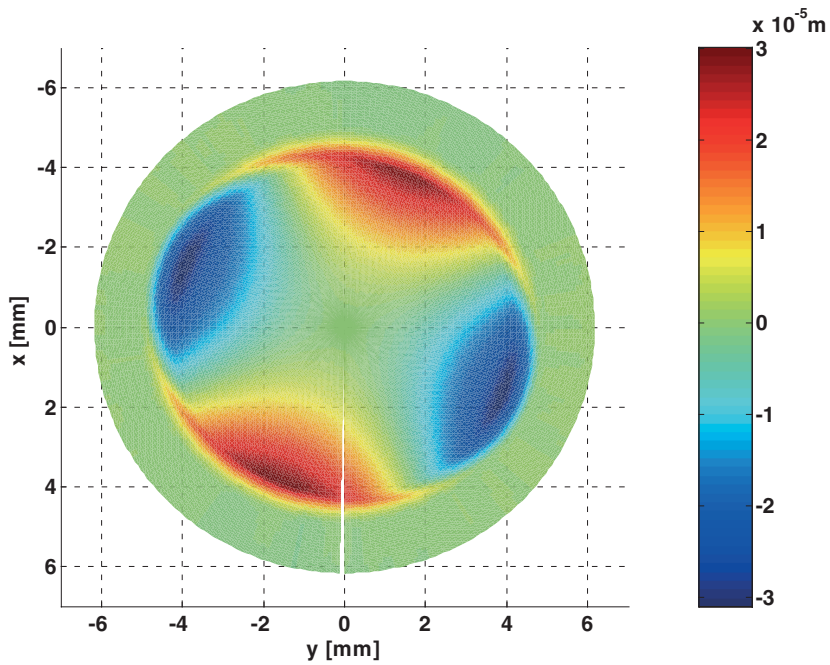
Figure 4.8 Typical deflectometer output, surface topography of a toric insert.

An imaging version of the deflectometer has been implemented and industrialized as well [25]. This implementation is specially suited and geared toward fast and precise measurement of spectacle lenses [26].

4.3.4
Tactile Profiling

The classical way of measuring surface profiles is using mechanical tactile instruments. The most widely used and known one is the Form Talysurf of Taylor Hobson. The instrument was introduced first in 1984 and since then became an industry standard in surface profiling. The Form Talysurf is a tactile sensor with a very fine tip. The tip is brought in contact with the surface under test, and then the surface is profiled along lines. This is done by scanning the tip across the surface under test. Figure 4.9 illustrates the contact of the fine tip with the surface under test.

Figure 4.9 Contact profiling (photo courtesy of Taylor Hobson Ltd. [27]).

The main advantage of this technology is that the surface is profiled in direct contact, leaving no ambiguities on where the surface under test is. Furthermore with this method, most free-form and aspheric surfaces can be handled. Figure 4.10 shows the example of an aspheric surface that is very difficult to measure with optical metrology. This type of surface is quite common in recent designs for camera modules for cell phone cameras.

One of the problems of measuring this type of surfaces is the changing curvature of the surface and the fairly steep slopes. Therefore, an optical profiler would have to have a considerable measurement range. The Talysurf can handle this type of surfaces easily. Depending on the instrument, scans up to 200 mm in the
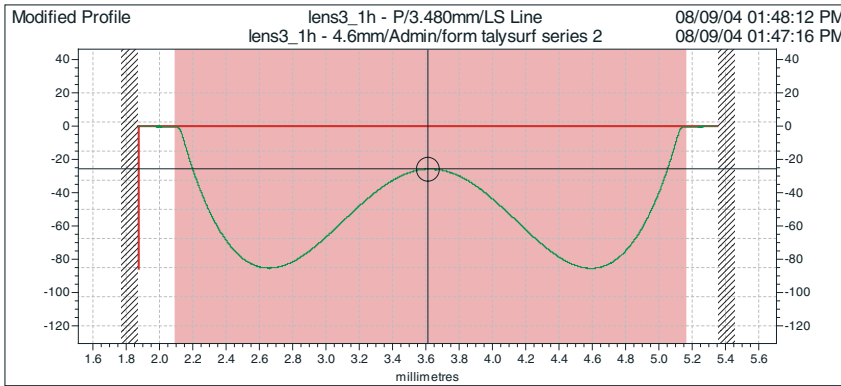
Figure 4.10 W-shaped aspheric surface (vertical scale in micrometer).

lateral (*x*-) direction can be done. Using the newest model PGI 1240 (Figure 4.11), the range in the *z*-direction is 12.5 mm. The sampling rate in the *x*-direction lies between 0.125 and 1.0 μm (depending on the scan length) with and uncertainty of 0.3 μm + 0.03× scan length. The repeatability in height can be as good as 0.04 μm at a resolution of 0.8 nm. Maximum slope angles that can be measured lie between ±35°. As with many other instruments, also for the Form Talysurf proper calibration of the system is the key. Over the years, Taylor Hobson has developed sophisticated calibration routines that enable the instrument to perform at a high level. Since this is a contact-probing instrument, both inserts and molded optical components can be measured with this technique.

A new member in the Talysurf family is the PGI BLU [29]. This new instrument was especially developed to cope with very high numerical aperture lenses as used
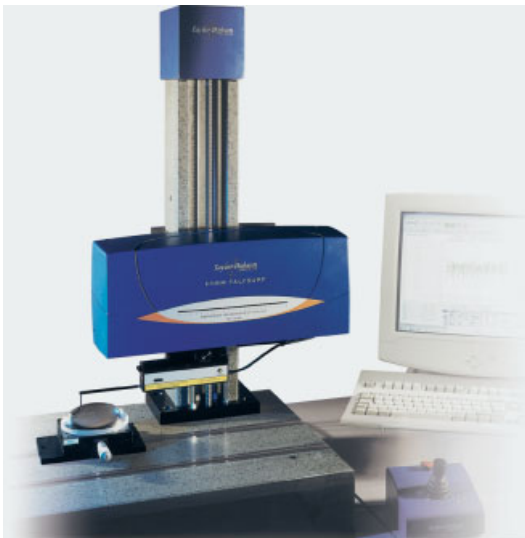
Figure 4.11 Form Talysurf PGI 1240 (photo courtesy of Taylor Hobson Ltd. [28]).

in BluRay technology and also in cell phone cameras. The main difference between this one and the PGI1240 is that the instrument is moving relative to the part under test. By doing so, the actual probe can stay well within its measurement and accuracy range, while sophisticated software puts the probe data and mechanical scan data together to one continuous (aspheric) surface. Again, precision mechanical movements are combined with high accurate probes, giving locally the required resolution. Figure 4.12 illustrates this principle.

Typical Ø 1-5 mm

Aspheric mould example

❶ Accurately machined mold face
❷ Very steep sides towards edge of lens
❸ High Aspheric departure in this region
❹ Minimal Aspheric departure in this region

(a)   (b)
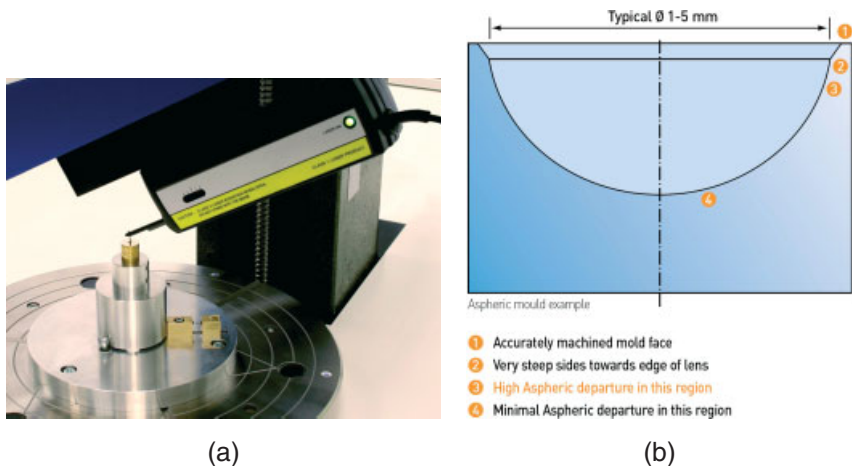
Figure 4.12 (a) PGI BLU.(b) Different measurement regions of an aspheric mold (courtesy of Taylor Hobson Ltd [30]).

The main disadvantages of the Form Talysurf are the measurement speed and the fact that during the measurement the surface under test is in contact with the probe. Although the forces applied to the measurement tip are usually in the millinewton range, traces of the measurement will be visible. For the injection-molded lenses, this is usually not a problem, since in molding many lenses can be produced. However, qualifying the inserts that are used for molding the optical components is more critical. Figure 4.13 shows the intensity map of an optical insert after mechanical profiling. The traces of the probe are clearly visible, as a cross in diagonal direction. Although in absolute height they are only on the order of a couple of nanometers, but they are present.

Another problem encountered when applying tactile probing is the measurement of nonrotational symmetric surfaces. Tactile profiling is producing 2D scans of a surface. If one wants to know the complete 3D form of the surface, the different profiles have to be stitched together.

Up to now, the Talysurf-like instruments are still the standard for characterizing optical surfaces that cannot be profiled in any other way, despite this disadvantage. Also for all other surfaces, the Talysurf is a very useful instrument, provided one has got the time for the measurement. In process control for a limited amount of samples and for initial tool characterization, this is a very valid measurement
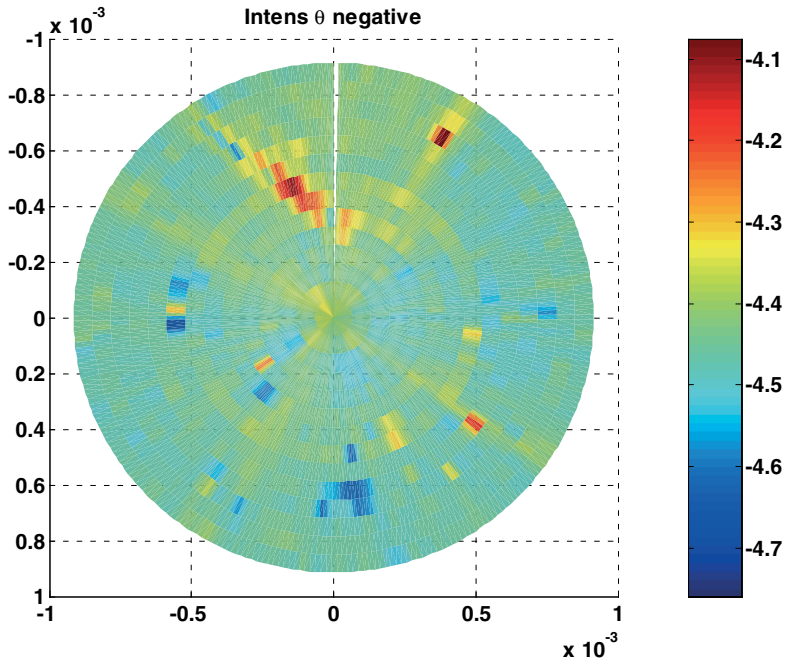
Figure 4.13 Intensity image of a nickel surface.

option. For high-throughput applications, it is advisable to check the other options mentioned.

4.4
Wavefront Metrology

4.4.1
General Concept

In wavefront metrology, a wavefront after interacting with a sample under test is analyzed. In general, for wavefront metrology matrix detectors are used, and hence 3D information is captured fast. The advantage of wavefront metrology is that it can be used not only for surfaces but also for characterizing whole components. In the latter case, optical parts are measured in transmission. Sometimes that opens the way for a functional measurement, where pure surface metrology could have been difficult. In some cases, the combined effect of two surfaces on a wavefront might be less steep or complex than on one of the surfaces alone. This is not only the power measuring the wavefront of components but also a point of attention. When measuring the combined effect of two or more surfaces, it is not always straightforward to single out the root cause of a potential defect. In order

to do so, other means of inspection have to be utilized or simply experience of the molder can help as well to pinpoint the surface with the largest defect. For quality control of a production, transmissive interferometry or wavefornt sensing are very useful techniques, since they measure the optical function of a part. Therefore pass/fail criteria can easily be applied. Also only one measurement has to be done instead of two surface measurements. In the following, interferometry and other wavefront-sensing techniques will be explored. If not explicitly stated differently, these metrology techniques can be applied to both surface and transmissive wavefront measurements.

4.4.2
Interferometry

The most often applied technology for characterizing optical components is interferometry. During the past 30 years, huge advances in interferometry have been made leveraging this measurement technique to an industry standard. In an interferometer, the wavefronts coming off a surface or traversing through an optical element are measured. A very good review of interferometry as measurement technology is given by Schwider [30]. For this chapter, it is important to review a couple of basic properties of interferometry. Although interferometers are highly accurate measurement instruments, the instrument itself does not guarantee perfect measurements. The boundary conditions, such as setup, handling, and operator knowledge, need to be at sufficient level as well [31].

In optical testing, most of the times so-called amplitude dividing interferometers are being used. Fizeau-, Michelson-, and Twyman–Green interferometers are of this kind. In the following, the Michelson configuration will be used for explanation. All items can be easily converted to the other types mentioned. Figure 4.14 shows a schematic drawing of a Michelson interferometer as a typical example of this kind.
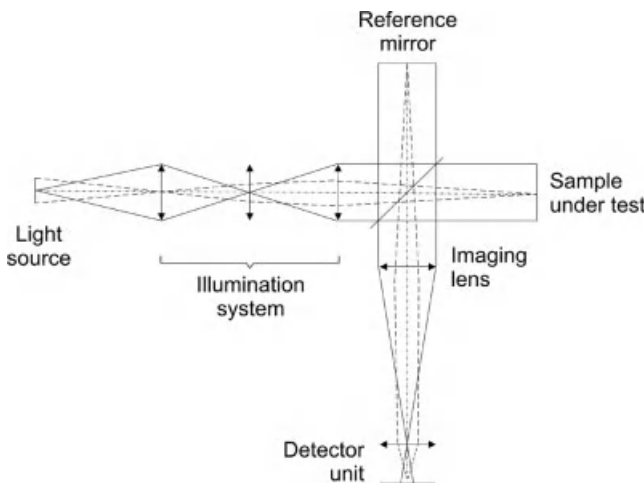
Figure 4.14 Michelson interferometer.

Light coming from a source is collimated, and then split into reference- and measurement beam. The light entering into the reference arm of the interferometer is reflected off the reference surface and sent back to the beam splitter. The light in the measurement arm is reflected off the surface under test and passes through the beamsplitter to recombine with the reference beam. The interference pattern emerging after the recombination of measurement- and reference beam is a coding of the phase difference between reference- and measurement beam. Mathematically, this can be described as follows:

The incoming beam with amplitude $E(x,y,t)$

$$E(x,y) = E_0(x,y)\, e^{i(\varphi(x,y)-\omega t)}, \tag{4.1}$$

with the phase $\varphi(x,y)$ of the beam, is split into measurement- and reference beam, E_m, E_r.

$$E_m(x,y;t) = E_{0m}(x,y)\, e^{i(\varphi_m(x,y)-\omega t)} \tag{4.2}$$

$$E_r(x,y;t) = E_{0r}(x,y)\, e^{i(\varphi_r(x,y)-\omega t)} \tag{4.3}$$

with E_{0m} and E_{0r} the amplitudes of the measurement- and reference beam, respectively. After recombination, the two beams are added up coherently for the resulting interference beam.

$$E_i(x,y;t) = E_{om}(x,y)\, e^{i(\varphi_m(x,y)-\omega t)} + E_{or}(x,y)\, e^{i(\varphi_r(x,y)-\omega t)}. \tag{4.4}$$

On the detector, the intensity I_i of the interfering wave E_i is recorded.

$$I_i(x,y;t) = E_i(x,y;t)\, E_i^*(x,y;t). \tag{4.5}$$

After regrouping and taking into account that on the detector, a time-averaged signal is recorded; the intensity on the detector is [12]

$$I_i(x,y) = I_{0m}(x,y) + I_{0r}(x,y) + 2\sqrt{I_{0m}(x,y)I_{0r}(x,y)}\cos(\Delta\varphi(x,y)), \tag{4.6}$$

with I_{0m} and I_{0r} the intensities of the measurement and reference beams, respectively, and

$$\Delta\varphi(x,y) = \varphi_m(x,y) - \varphi_r(x,y). \tag{4.7}$$

The last equation is of great importance, since it shows clearly that all interferometric measurements with these kinds of interferometers are relative measurements. The measurement beam is compared with the reference beam. There are several publications dealing with resulting accuracies of interferometric measurements [30–32]. For the application of measuring injection-molded optics, one can make use of the relative measurement by modifying the reference wavefront accordingly. This will be covered later in this chapter, when metrology of aspheres is discussed.

Going back to the basic setup of the Michelson interferometer, it is important to not only understand how the interference pattern is generated but also where it is located. Looking at the setup of Figure 4.14, starting right behind the beamsplitter interference patterns can be observed. However in order to perform a meaningful

measurement, the interference pattern needs to be mapped onto the sample under test. Therefore, besides having generated the interference pattern, an image of the exit pupil of the system under test should be created at the detector: the fringes have to be localized. Only if there is proper localization of the fringes, the interferogram can be interpreted correctly. In fact, the phase in the exit pupil of the system under test is imaged onto the detector and coded in the interference pattern. This is to keep in mind while an attempt is made to build an interferometer from scratch. Most commercially available interferometers are designed carefully and the proper imaging of the sample under test can be achieved. Commonly CCD cameras are used as detectors in modern interferometers. They offer the advantage of low noise, high sensitivity, high sampling, and fast data acquisition. Depending on the type and the features of the interferometer, cameras ranging from VGA – chip size up to several megapixels – chips can be bought. Interpretation of the interferogram is done by modern software using various kinds of phase shift algorithms for interferogram analysis [33]. Once the wavefront is reconstructed from the raw interference data, several display options for the data are available. These options depend largely on the used interferogram analysis package. However, the following analysis items are standard for all interferogram analysis software: RMS wavefront error, PV wavefront error, cross-section through the wavefront (2D profile), 3D wavefront map, and Zernike coefficient analysis. All these items serve their specific purpose in characterizing the quality of particular optical components.

In daily practice of quality control of injection-molded optics, interferometers can be used in several different configurations. In the following, the basic configurations will be explained using the Michelson type interferometer as an example. In most of the cases, a flat reference mirror will be used. Therefore, the measurement beam needs to be configured such that before entering the beamsplitter for recombination with the reference beam, a more or less plane wavefront should be generated. Figure 4.15 shows some common interferometer configuration schemes for the measurement arm of the interferometer.

- *Flat surfaces*: If flat surfaces need to be tested, the basic configuration is given in Figure 4.15(a). The sample under test is placed in the interferometer and after proper alignment surface shape can be measured.
- *Curved surfaces*: If a curved surface needs to be inspected, an auxiliary high-quality objective is inserted in the measurement path in order to generate a spherical wavefront that is reflected off the curved surface. For curved surfaces, the focus of the auxiliary lens is made to coincide with the center of curvature of the sample under test. In this configuration, one can measure concave and convex optical elements, see Figures 4.15(b) and (c).
- *Optical components in transmission*: For testing optical components in transmission (i.e., lenses), the lens under test (LUT) is placed in the measurement arm of the interferometer. Now a spherical reference mirror is placed as an additional component. In fact, this configuration is identical to the configuration in
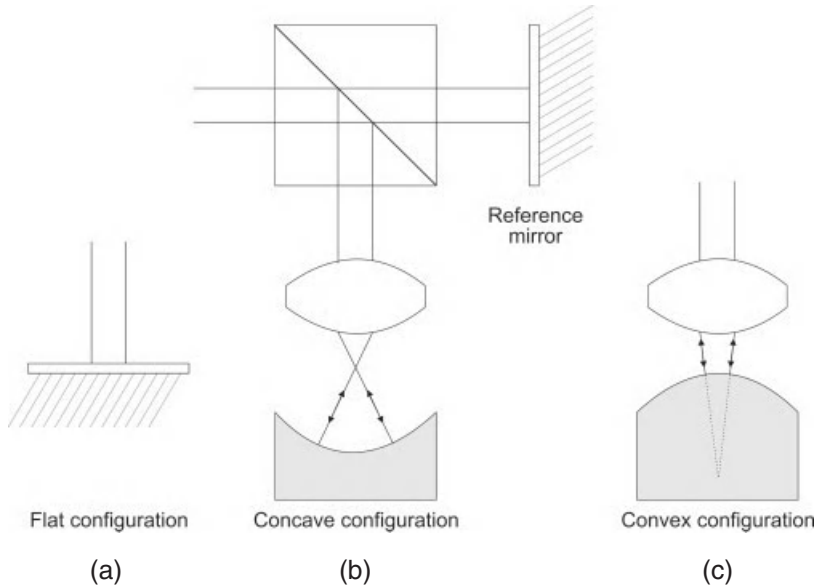
Figure 4.15 Different interferometer configurations.

curved surfaces with the difference that now the lens is tested and the auxiliary mirror is known.

As with the reference mirror, whenever auxiliary optics are used in measurement- and/or probe beam, these auxiliary elements need to be either of such a quality that they do not significantly influence the measurement or their effect has to be taken out by means of calibration. In most practical cases, certified spherical reference mirrors are used. Also most state-of-the-art interferogram analysis software does have the capability of subtracting a stored wavefront from the measured data. One way of using this feature is to perform a measurement using calibrated reference objects in place of the system under test. This way the system-signature can be determined and subtracted.

Besides localization of the fringes, proper alignment of the sample under test is another very important issue for measuring with an interferometer. In all amplitude dividing interferometers, the sample is a part of the device. Therefore, the alignment of the sample plays a key role in the accuracy of the measurement. In this respect, one should make use of the big advantage of injection-molded optics: it is easily possible to design into the product reference- and alignment marks. In the following example, a flat reference ring is designed around the clear aperture of the lens. The reference ring is diamond turned together with the optical clear aperture. Thus there is an accurate relation between reference ring and optical clear aperture. The sample is aligned such that the tilt of the reference ring of the lens is minimized with respect to the incoming beam. In Figure 4.16, the large ring with almost no fringes is the reference ring. The small zone in the center
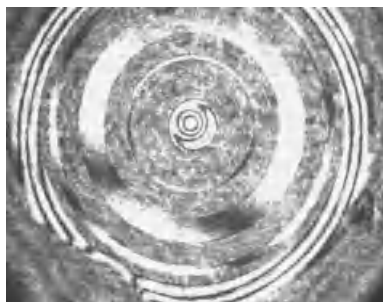
Figure 4.16 Interferogram of a lens with reference ring.

represents the center of the asphere under test. Although in this example the complete clear aperture cannot be measured, the principle is clear.

Furthermore, the reference ring can be used for the definition of the center of the clear aperture. If the lens is aligned free of tilt using the reference ring, it is possible to indirectly measure decentration. If the lens surfaces are decentered with respect to each other, there will be a coma in the interferogram. The magnitude of the coma is directly related to decentration. Figure 4.17 shows the geometry of a decentered lens.
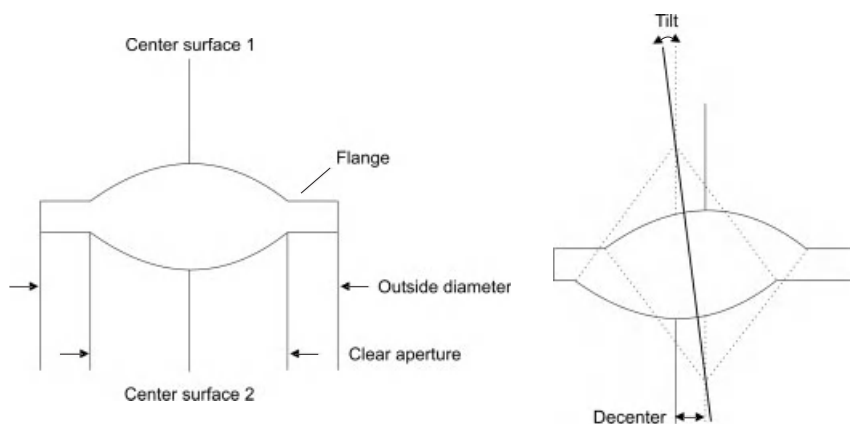
Figure 4.17 Lens geometry, nominal and decentered.

In case the lens is not aligned tilt free, coma can be compensated by the setup. This can be done by aligning the optical axis of the lens with the axis of the interferometer. The resulting interferogram will give a distorted image of the lens performance. The following series of interferograms will illustrate the effect of tilt, decenter, and coma in an interferogram.

In Figure 4.18, the left interferogram represents the nominal lens. In the middle interferogram, the lens surfaces are decentered by 20 μm with respect to each other; coma is clearly visible. In the right interferogram, most of the coma is compensated by tilting the lens in the interferometer.

Figure 4.18 Interferogram: nominal, decenter of surface 1, tilted reference mirror.

4.4.3
Interferometer and Aspheres

Besides spherical wavefronts, an interferometer can also be used to measure weak aspheres. When there are only modest deviations from sphericity, the interferometer will provide an accurate quantification of the aspheres. The relevant parameter is slope of the asphere. Looking at the detector used in the interferometer and the lateral resolution given by the imaging system in the interferometer, the Nyquist criterion of sampling should always be fulfilled. From that we can derive that at least one interferometric line should be sampled by 2 pixel. Translating this into slope of the wavefront under test, the optical path difference (OPD) sampled by 4 pixel should be always less than $\lambda/4$ (one dark and one white fringe in a double pass configuration).

In the previous discussion, it was always assumed that the sample under test is ultimately compared with a flat reference surface. In case of a reflecting surface, an ideal (calibrated) lens is used to transform the wavefront that needs to be measured into a flat one (see Figure 4.15). If a lens should be measured, a spherical reference mirror is used to perform this task. However if the LUT produces an aspherical wavefront, there is the possibility to use a known aspherical mirror to transform the wavefront back into a flat one. With this technique, it is possible to extend the capabilities of standard interferometers beyond the usual capabilities. Figure 4.19 shows the difference.

In Figure 4.19(a), a common spherical reference mirror is used. The large deviation from sphericity of the wavefront under test causes strong deviations from the common path on the return. Therefore, the wavefront can only be evaluated close to the center. In Figure 4.19(b), the same lens with an aspherical reference mirror is illustrated. Now the lens can be characterized up to the edge of the clear aperture. The difference between the two situations can also be seen in the raytrace diagram of both situations (Figures 4.20(a) and (b)). In case of the spherical reference mirror, there is a clear difference between the rays coming back into lens for the second pass and the emerging rays. This huge path difference is the source of the large fringe density at the edges and a large source of error. In case of an aspherical reference mirror, this path difference (almost) vanishes. The attractive
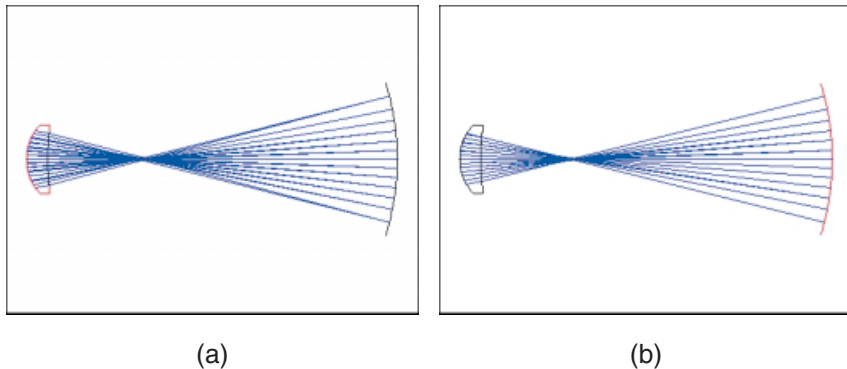
Figure 4.19 Difference between spherical (a) and aspherical (b) reference mirror.

feature for testing injection-molded aspheres in this way is that the injection molding company needs to have access to aspherical tooling for the lens inserts already. Therefore, supply of an aspherical reference mirror is not a problem.

Besides the obvious advantages of using aspherical reference mirrors, there are a couple of issues that have to be addressed and considered. First, the reference mirror should be verified and well known. At present, the only way of doing so is by means of a tactile surface profiling, and by deflectometry (see Section 4.3). Another point is that using the aspherical reference implies that the mechanical construction of the measurement arm of the interferometer needs to be well defined. Small differences in distance between the sample under test and the reference mirror can lead to nontrivial disturbances in the interferogram. Depending upon the actual design, a variation of less than 20 μm can be sufficient to lead to vast misinterpretations of the interferogram. Also tilt of the reference mirror needs to be controlled very tightly. One way of solving that problem is to include a flat reference ring outside the aspherical mirror. If this reference ring is manufactured (diamond turned) in the same setup of the machine, there is a well-defined
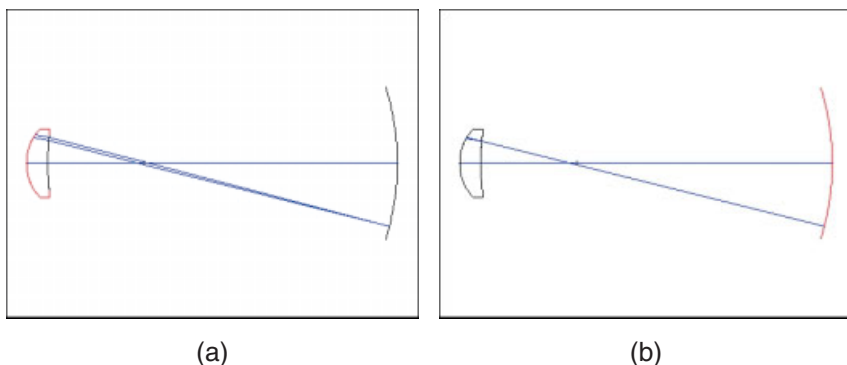
Figure 4.20 Ray trace diagrams of spherical and aspherical reference mirror.

correlation between the mirror surface and the ring. The ring can then be used to align the aspherical reference mirror to be without tilt in the system (using the interferometer itself).

4.4.4
Interferometry and Strong Aspheres

If the asphericity becomes even larger or an aspherical reference mirror cannot be obtained, there is the possibility to introduce a synthetic compensation element, a computer generated hologram (CGH). The CGH is a theoretically calculated diffractive element that compensates the asphericity of the wavefront under test. Sometimes combined with normal refracting elements, the CGH is mostly applied in a null-configuration [34]. With a CGH in such a null-configuration, a standard interferometer can be used to measure stronger aspheres. Figure 4.21 shows a typical configuration for such a CGH setup.
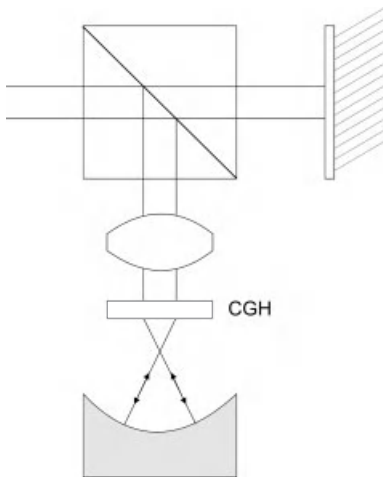
Figure 4.21 Schematic set up of a CGH interferometer configuration.

In one configuration, the light is passing through a strong asphere, and then through the compensation CGH onto a spherical reference mirror. In the other configuration, the lens is a spherical one while the mirror surface is the strong asphere. In the first setup, molded lenses can be tested, while in the second one inserts can be tested.

In terms of extending the capabilities of a standard interferometer, the same considerations regarding optomechanical setup for the interferometer as in case of the aspherical reference mirror have to be made. Also for the CGH approach, it is true that setup tolerances are a lot tighter than that for a standard interferometer. Luckily the major suppliers of CGHs put reference- and alignment marks on their CGHs. This makes alignment of these elements a lot easier. A summary of some other concerns using compensation optics for measuring aspheres can be found in the literature [35–37].

Another issue that goes together with CGHs has to be addressed as well. For every different lens design, a new CGH needs to be fabricated. While for small series of lenses this is quite costly and time consuming, for injection-molded optics, CGHs are certainly a consideration. If large series of aspherical lenses at a critical quality level have to be produced, the initial investment for a CGH setup can easily be earned back. The one big advantage of the CHG in a null-test configuration is the fact that standard interferometers can be used. So in terms of capital equipment, the investments are for the CGH and the knowledge in setup. Figure 4.22 shows such a real-life application of a CGH using a commercially available Fisba interferometer.
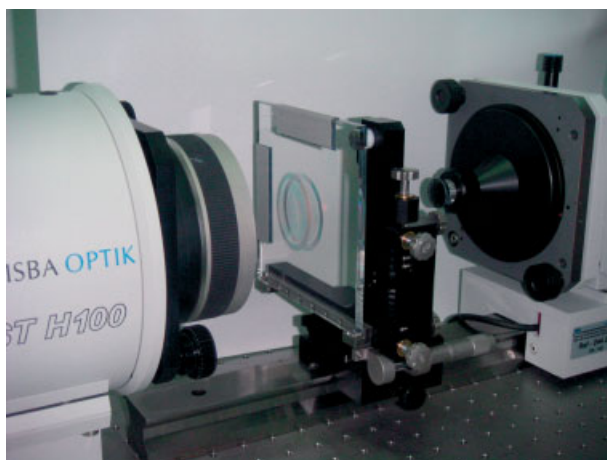
Figure 4.22 Photo of the Fisba CGH technology (photo courtesy of Fisba Opik AG [38]).

A more elaborated view on measuring aspheric lenses and molding tools can be found in the Fisba μnew of June 2004 [39].

Since measuring aspheres is such a big challenge, new ideas are always coming up and attempts are made to tackle the problem from different sides. Interferometry remains one of the principle tools to do so [37, 40].

One of the most interesting developments of the last years for using interferometers for metrology of aspheres has been done by Zygo. The Zygo VeriFire asphere instrument combines a state-of-the-art Fizeau interferometer with a DMI. As explained earlier, the main problem of interferometers while measuring aspheres is the high fringe density when deviating too much from the reference sphere. However by moving the Fizeau interferometer relative to the sample under test, in most cases a position can be found, in which the fringe density is small enough to be resolved. Stepping through the asphere under test, the sample can be characterized by several measurements at different positions. While the Fizeau Interferometer measures the optical surface and more specific the local curvature of the surface, the relative displacement of the Fizeau interferometer with respect to the probe is measured by the DMI. A thorough explanation of the idea and algo-

Figure 4.23 Zygo VeriFire Asphere (photo courtesy of Zygo [42]).
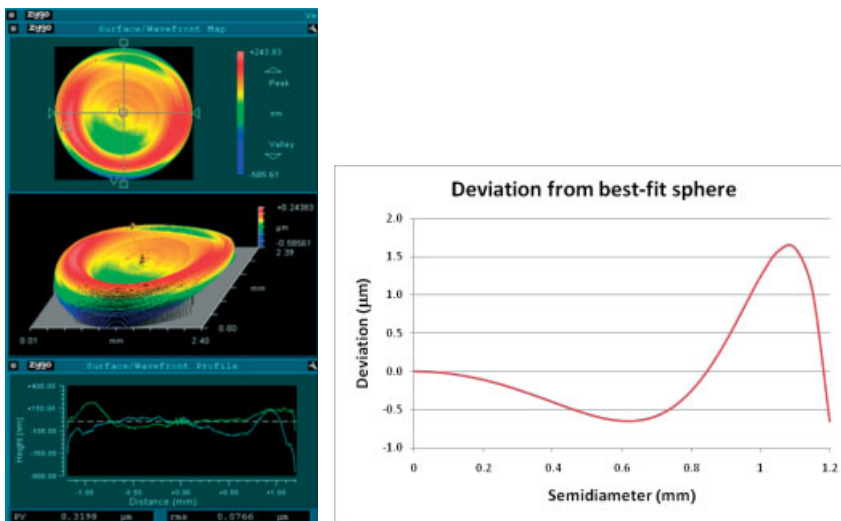
Figure 4.24 Results of a measurement with the ZygoVeriFire Asphere.

rithm behind the instrument is given by Kuechel [41]. Figure 4.23 shows a picture of the machine, and in Figure 4.24 a typical measurement of a plastic part is shown.

On the left-hand side, the result of the measurement of an injection molded lens surface is presented, while on the right-hand side the deviation from the best-fit sphere is shown. The total sag of the lens was $600\,\mu m$ with a best-fit

sphere of deviation of 2 μm. The interferometer shows a rest difference between design and measurement of 0.32 μm PV: a result that is within the expected tolerance range for this particular lens surface. For this measurement, seven different zones were measured and evaluated. In this system, the accuracy of standard interferometry is combined with the possibility to measure up to 10 μm deviation from best-fit sphere. The only condition that is implied upon the surface under test is that there is no change of sign in the curvature of the surface. The so-called w-shape lens surfaces can only be measured within the center zone.

After elaborating on several methods and instruments to characterize aspheres, a general comment on asphere metrology should be made: usually the result of an asphere measurement is the deviation of the shape from design or from best-fit sphere. Having said that it is evident, that asphere metrology always goes together with proper optical modeling and comparing measurement to design. Sometimes the design data have to be analyzed before in order to determine the proper setup of the metrology instrument. For example in the just described Zygo Verifire application, the design data were considered in order to come to a first estimate on how many measurement zones are needed. Also the metrology report shows difference with respect to design. What has been said about the interferometer is also true for the Shack–Hartmann sensors described later in this chapter. Also their developments are ongoing to directly link the metrology instrument to raytrace systems.

4.4.5
Double Pass–Single Pass Interferometers

All the configurations and examples so far discussed in this chapter are so-called double pass configurations. The main advantage of the double pass configurations is that they can be built very stable and compact. Furthermore they are readily available. The vast majority of the commercial interferometers are double pass interferometers (i.e., Fizeau or Twyman–Green type). Due to the fact that the light passes twice through the component under test, these interferometers are very sensitive to small aberrations. As soon as the aberrations (deviations from the best-fit asphere) become large – as in the case of the already discussed aspheres – this sensitivity advantage turns into a disadvantage. A solution would be the use of a single pass interferometer configuration. A Mach–Zehnder type interferometer would be such an interferometer. While successfully applied for testing microlenses, not much usage for testing (aspherical) optical components has been reported so far [43]. Maybe this is due to the fact that Shack–Hartmann wavefront sensors are measuring in single pass configuration and are very accurate as well [44].

4.4.6
Automated Interferometry – Jenoptik Example

If all design considerations are taken carefully into account, fast and efficient interferometric test setups can be built. A particular nice example has been realized at Jenoptik Polymer Systems (Jenoptik PS). The interferometer technology was supplied by Fisba Optik, and automation and handling was carried out by Jenoptik PS. Figure 4.25 shows an automated interferometric setup for testing weak aspherical optical components. The lenses under test are placed into the setup. Then the lenses are rotated under the interferometer. Before each measurement, the lenses are automatically aligned. This way misinterpretation due to alignment is minimized. When the lens is aligned, the interferogram is taken and evaluated. The data are stored on the PC.
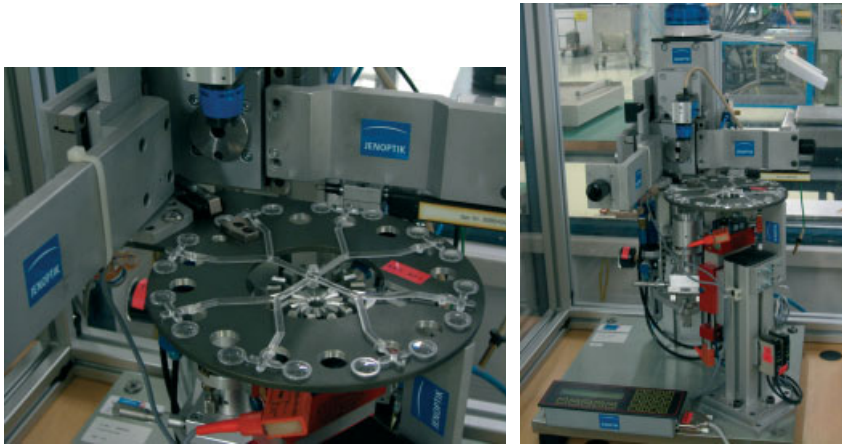
Figure 4.25 Pictures Jenoptik PS setup (photo courtesy of Jenoptik PS [45]).

4.4.7
Microscope Interferometers

In the range of measurement equipment, one highly sophisticated device needs to be mentioned as well: microscope interferometers. These devices are interferometers – mostly of the Mireau type – that are integrated into microscopes. In these devices, the lateral resolution of a microscope is combined with the height resolution of an interferometer. The microscope interferometers are especially useful for measuring small details as in integrated optics and also for measuring surface shape of these small optical parts. Surface roughness can be measured as well using the microscope interferometers. The latest generation of these devices is equipped with sophisticated scanning tables. Using white light illumination and mechanical scanning in z, large height differences can be dealt with. In the
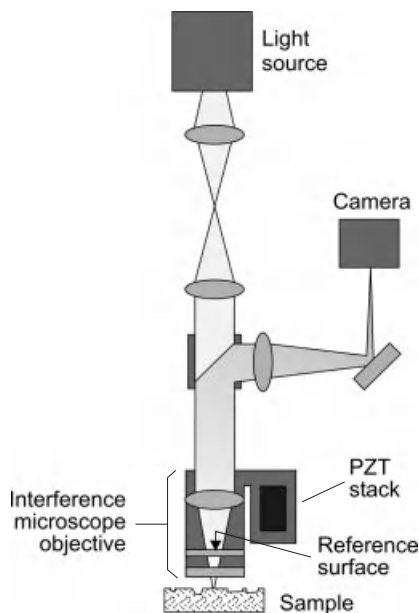
Figure 4.26 Microscope interferometer.

evaluation software, the data are put together to one common height map. Figure 4.26 shows a typical setup of such an interferometer.

Besides measuring surface roughness, small aspheric lenses can be measured as well. Since the interferometer uses stitching technology, ten possibly steeper aspheres can be measured. The reason for this lies in the fact that by changing the focus for each stitching field, optimal sampling for different regions of the interferogram is achieved. Therefore, virtually more pixels are used for sampling the interferogram. As an example, the lateral field of view of the Zygo NewView 7000 series lies between 0.05 and 21.9 mm, and the lateral resolution is between 0.36 and 9.5 μm (depending on the objective, zoom lens, and camera used) [46a]. Height resolution can be as small as 0.1 nm. Various scan ranges for vertical scanning are available.

It should be noted that the slope range of this microscope interferometer is limited as well. This is analog to the larger interferometers. Light reflecting off the surface under test has to be captured by the microscope objective. Therefore the numerical aperture of the objective poses one limit. If light is captured back and in some regions of the interferogram the fringe density becomes too large; the stitching capabilities can help to extend the measurement range in some cases. Alternatives to these microscope interferometers are so-called confocal microscopes. There a 3D surface profile is generated by vertically scanning the surface under test and evaluating the focus at each position [46b].

Surface figure and texture can also be measured using tactile instruments. For many years, this has been the standard in roughness measurement.

4.4.8
Shack–Hartmann Sensors

Originally Hartmann designed this test method for testing large optical compo-
nents for astronomy. Later with the addition of Shack's ideas, the Shack–Hart-
mann sensor was very often applied as wavefront sensor for active and adaptive
telescope systems. A good basic review of the Shack–Hartmann technology can be
found in the literature [47]. However in recent years, the Shack–Hartmann wave-
front sensing technology has found its way back into optical testing of not only
injection-molded components and systems. The Shack–Hartmann technology is a
wavefront sensing technology, not an interferometric one. As such, the system
under test is not part of the sensors itself. Systems under test and wavefront sen-
sor are in first approximation separated from each other. Figure 4.27 shows a
schematic layout of a Shack–Hartmann sensor.
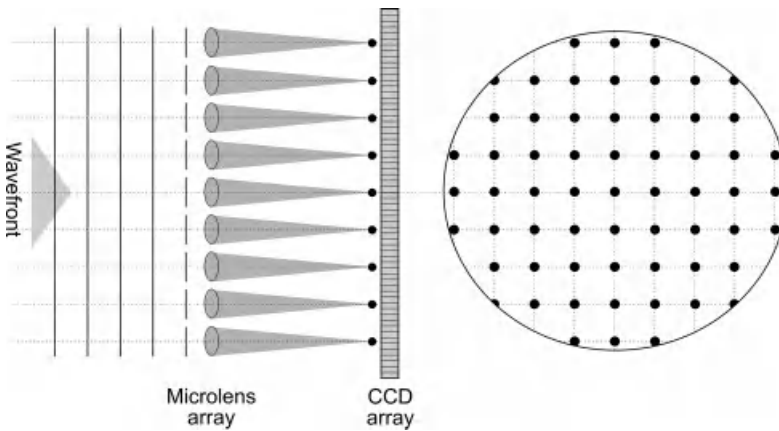
Figure 4.27 Schematic layout of the Shack–Hartmann sensor.

The wavefront that is to be analyzed enters the wavefront sensor. Subsequently
it is divided by microlenses into many small subapertures. The microlenses are
aligned with respect to the detector (usually CCD or CMOS camera) in such a way
that for a perfect plane wave they are focused on the detector. The resulting spot
pattern is a regular grid pattern of spots each one centered behind its microlens.
This regular grid pattern forms the reference for all subsequent measurements.
    Once the wavefront that has to be analyzed falls onto the microlens array, each
microlens measures the local tilt of the wavefront across the aperture of that spe-
cific microlens. As a consequence of the local tilt, the spot on the detector deviates
from its central reference position. All these deviations are analyzed and used to
reconstruct the wavefront of the wave under test. Figure 4.28 shows the principle
of the local tilt together with the reference grid. From the difference between the
grid pattern in Figures 4.27 and 4.28, the wavefront distortion can be determined.
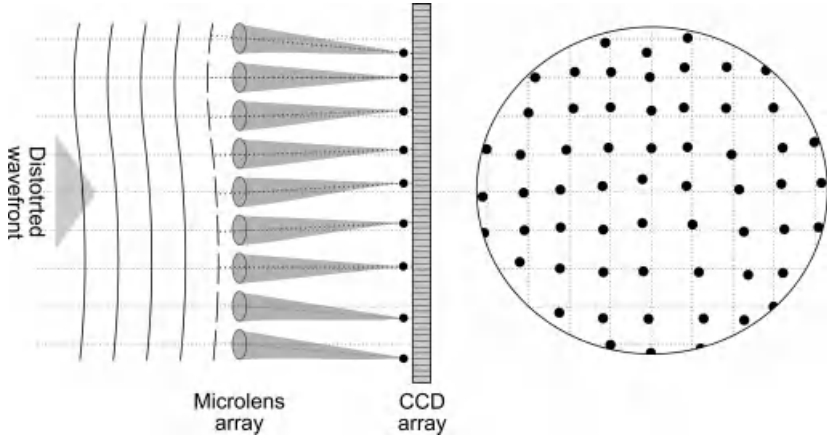
Figure 4.28 Shack–Hartmann sensor with distorted wavefront.

In mathematical terms, the Shack–Hartmann principle can be described as follows. A wavefront, $W(x,y)$, entering the microlens array is focused on the detector. The measured quantity is the deviation of the spot with respect to the reference spot, Δx and Δy.

$$\Delta x = f\,q\frac{\mathrm{d}W(x)}{\mathrm{d}x} \tag{4.8}$$

$$\Delta y = f\,q\frac{\mathrm{d}W(y)}{\mathrm{d}y}, \tag{4.9}$$

with f being the focal length of the microlens array and q a focus factor. Note that since most of the time a Cartesian coordinate system at the detector is present (i.e., CCD- or CMOS array) the wavefront is represented in Cartesian coordinates as well. Looking at the earlier equations, it can be observed that the sensitivity of the Shack–Hatrmann sensor depends largely on the focal length of the microlens array. The longer the focal length, the larger the deviation Δx and Δy from their reference positions. In other words with a long focal length, small deviation of the wavefront, $\mathrm{d}W$, can be measured. However there is a trade-off – if the lateral sampling of the wavefront has to be small, microlenses with a small diameter have to be selected. If these microlenses have got a long focal length, their numerical aperture becomes very small. Consequently the spots are not sharply defined anymore. It is very difficult to find the proper focal position and, therefore, make use of the extra sensitivity. As in all optical measurement systems, a careful analysis of the measurement setup with respect to the metrology task has to be done.

Besides choosing the proper microlenses for evaluating the wavefront under test correctly, there are two important limits. The first one is regarding the local tilt limit. The local tilt of the wavefront under test should always be such that the spot of the microlens that samples these local slopes stays within the subaperture

region on the detector. Only if this is the case, the spots can unambiguously be referenced to the proper microlens and wavefront portion.

The second limit is the curvature limit, expressed by the focus factor, q. Suppose the local wavefront is not only tilted but also curved. Besides the deviation in spot position, there will be an increased spot size due to defocus. Summarizing condition (i), the spot does not deviate more than the equivalent size of the microlens aperture, and condition (ii) the spot blur should also always stay within the microlens aperture should always be met.

Figure 4.29 illustrates the two conditions. The upper and lower spots stay just within the subaperture, while spot 3 is blurred due to a strong local curvature. If these two conditions are violated, it will be very difficult to reference the actual spots to their reference positions. If these two conditions are fulfilled, an unambiguous evaluation can be done. In certain cases, there are possibilities to extend the range of the Shack–Hartmann sensor such that the measured spots do not have to fall within the subaperture [48]. However the curvature limitation will remain.

The advantage of Shack–Hartmann sensors for testing injection-molded components is mainly in the scalable sensitivity for measuring (steep) aspheres. In most commercial interferometers, the injection-molded component is part of the interferometer and will be measured in double pass. Therefore, it is a very sensitive technique for measuring small aberrations. However for large deviations from the reference sphere, there are the well-known problems. A Shack–Hartmann sensor is a wavefront sensor and analyzes the wavefront exiting the system under test. In most cases, this is in single pass. Furthermore by choosing a suitable focal length of the microlenses, the sensitivity of the sensor can be adapted to cover most of the required measurement range. Consequently aspheres with fairly large deviations from the reference sphere can be characterized quite easily. Figure 4.30 shows the transmitted wavefront through an injection-molded system. If analyzed by an interferometer, only about 70% of the wavefront can be evaluated. Using a Shack–Hartmann sensor, more than 90% of the wavefront can be analyzed.

In order to fully exploit the potential of the Shack–Hartmann sensor, two issues need to be considered: alignment and configuration. On both issues some
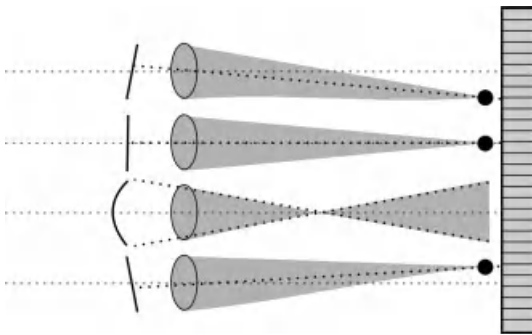
Figure 4.29 Local curvature limit of a Shack–Hartmann sensor.
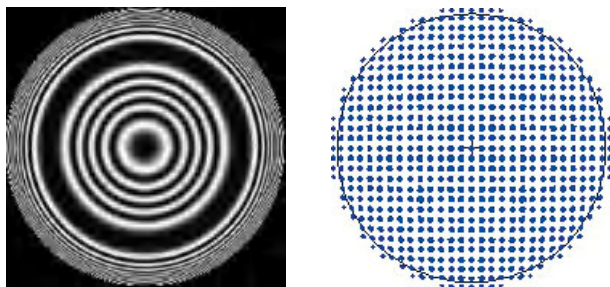
Figure 4.30 Interferogram and Shack–Hartmann pattern of a steep asphere.

research has been carried out [49, 50]. In the subsequent section, some ideas on configuration and alignment are added. In most published applications, the system under test is configured such that it produces a collimated or nearly collimated wavefront. This wavefront can subsequently be analyzed using the Shack–Hartmann sensor. In some applications, the LUT produces a collimated beam using only a small portion of the lens. In order to fully characterize these lenses, a different configuration and auxiliary optics have to be used in order to generate the flat wavefront for testing. Figure 4.31 illustrates the situation.

Figure 4.31(a) shows an LUT producing a collimated beam using only the center portion of the lens. For injection-molded optics, the center part of a lens usually comes out rather good. In many cases, the outer part of the clear aperture of a lens shows larger aberrations. This is due to process parameters, mold release, etc. Trying to test the molded optical system using the configuration on Figure 4.31(a) will leave just the critical outer parts of the lens undetected. Therefore, it is more advisable to create an illumination with a higher numerical aperture, place the LUT such that as much as possible of the lens surfaces is traversed by the light. The exiting wavefront is slightly diverging and can be collimated using auxiliary optics. This way a larger portion of the lens can be tested – including the more critical outer areas of the clear aperture. To a certain extent, this approach is

(a) (b)
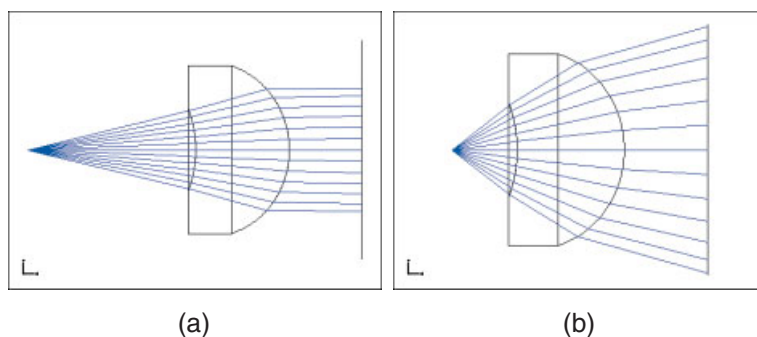
Figure 4.31 Different lens configurations for Shack–Hartmann testing.

very similar to the approach of testing optical components with compensating optics in an interferometer. Also here the issue of calibration remains an important one. Smart calibration strategies need to be employed in order to come to reliable results.

One necessary condition for good and reliable measurements is the mechanical setup and alignment of the sensor. Besides software that – similar to interferometer software – is able to subtract wavefront tilt and power, the setup should have some calibration and alignment aids. In the setup depicted in Figure 4.32, an additional autocollimation arm is added. Through this arm of the sensor, the sample under test can be aligned such that the tilt of the sample with respect to the wavefront sensor is minimized.
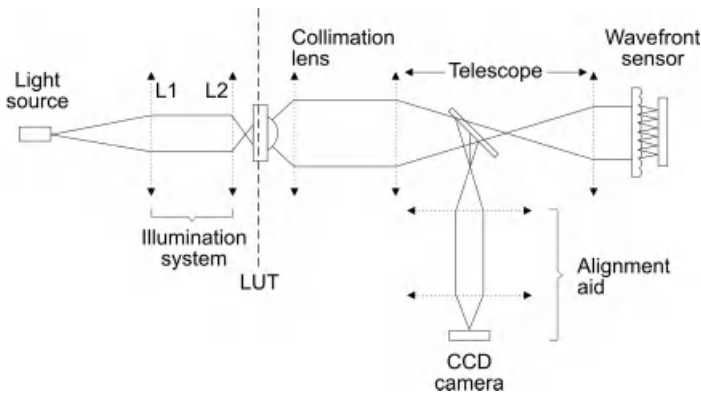
Figure 4.32 Shack–Hartmann sensor system with alignment aid.

Figure 4.33 Shack–Hartmann system implementation (photo courtesy of Trioptics GmbH [24]).

In the schematic setup displayed in Figure 4.32, it is also noteworthy that there is a flexible illumination system. By changing lenses L1 and/or L2, the light can be offered to the LUT in different forms, depending on the function of the lens. The telescope in the detection arm guaranties that the wavefront under test is conditioned in a way that it optimally fills the actual wavefront sensor. In Figure 4.33, commercial implementation of a Shack–Hartmann sensor with alignment aid is shown.

4.4.9
Other Wavefront Sensors – Shearing Interferometer

Besides the Shack–Hartmann sensor, there are several different kinds of wavefront sensors. Among these sensors, the shearing interferometer is of particular interest. In principle, the shearing interferometer works in a very similar way as the Shack–Hartmann senor. The wavefront under test is sent into the interferometer. In a lateral shearing interferometer, the wavefront is split and the two wavefronts are laterally sheared with respect to each other. The resulting interference pattern decodes the difference between the two wavefronts $\Delta W(x, y)$ into an interferogram.

$$\Delta W(x, y) = W(x - s, y) - W(x + s, y), \tag{4.10}$$

with s being the shear, the displacement, of the two wavefronts with respect to each other. The advantage of the shearing interferometer is that it is a wavefront sensor with interferometric accuracy. Furthermore, if the instrument is designed with a variable shear, the sensitivity of the instrument can be adapted. A large shear can make even very small changes in the wavefront visible. The disadvantage of the shearing interferometer is that in order to get the full wavefront information on an arbitrary wavefront, two measurements have to be taken with orthogonal shear. As can be seen from Eq. (4.10), there is no information in the interferogram perpendicular to the shear direction.

At Philips, a double grating shearing interferometer is used for testing injection-molded components of optical pick up units [51]. Figure 4.34 shows the principle of this interferometer.
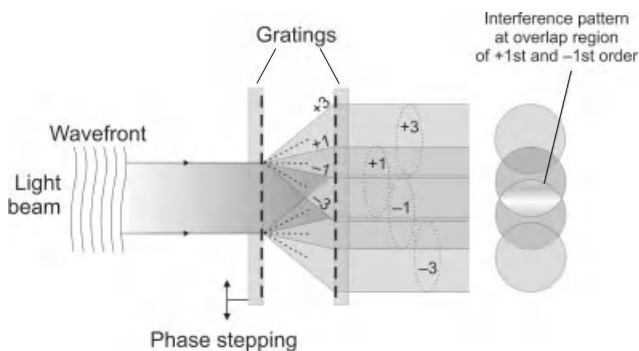
Figure 4.34 Operating principle of the Philips double grating shearing interferometer.

The wavefront under test is split into different diffraction orders by the first grating. Then the second grating splits the wavefront in the different diffraction orders once more. By choosing the appropriate gratings and the distances between the gratings, two different diffraction orders (+1 and –1) overlap and interfere. For the measurement with orthogonal shear, the whole grating unit is rotated 90°. Then a second measurement is taken. By moving the first grating perpendicular to the incoming light beam, phase shifting can be carried out. Using appropriate algorithms, the wavefront can be reconstructed [52]. Figure 4.35 shows a photo of the rotating grating head of the Philips shearing interferometer.
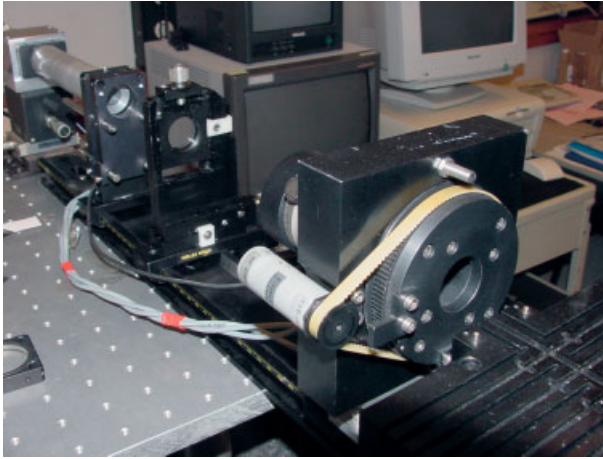
Figure 4.35 Philips shearing interferometer, grating shear head.

4.5
Birefringence

During injection molding, the optical plastics undergo large pressure and temperature changes. Due to the nature of this process and the properties of the material, (stress)birefringence is induced into the optical component (see Chapter 5). Especially for applications where polarized light is used, birefringence influences the performance of the part. Birefringence is an anisotropy in refractive index, showing different indices of refraction along different orientations of the optical part. Different polarizations experience different indices of refraction, depending upon the orientation of the optical component with respect to the light source. Especially for laser sensor applications, this is a very undesirable effect, since the focal position of such a sensor then depends upon orientation of the part – a nightmare for high-volume assembly.

Therefore birefringence is one of the parameters that are important for injection-molded optics and need to be measured. There are several ways of measuring birefringence, the most common one is to use polarization microscopy. Figure 4.36 shows the typical setup of a polarization microscope.

Modern Polarized Light Microscope
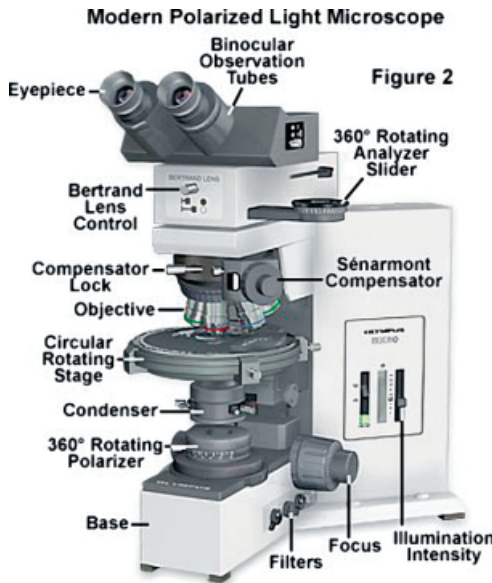
Figure 4.36 Schematic setup of a polarization microscope [53].

In a common microscope with high-quality stress–strain free optics, two polarizers are introduced. The one in the illumination path is called the polarizer, and the one in the imaging path is called the analyzer. During the initial setup, polarizer and analyzer are crossed, i.e., the resulting intensity in the image is zero. If the birefringened specimen is introduced into the light path, the intensity in the image will differ, depending upon the orientation of the sample under test with respect to the polarized light. If so-called conoscopic illumination is applied, a typical image in the microscope looks like in Figure 4.37.

(a) (b)
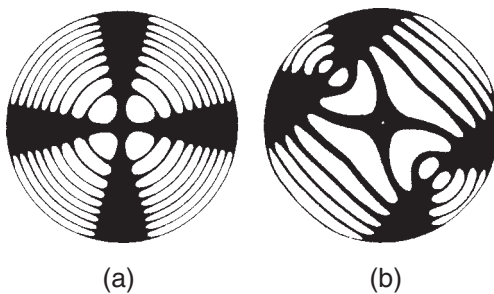
Figure 4.37 Typical conoscopic illumination patterns, (a) uniaxial crystal, (b) biaxial.

The origin of this figure can be explained by interference. Figure 4.38 gives schematic view of this illumination- and interference principle. In conocsopic illumination, an image of the light source is created in the font focal plane of the condenser (2). Therefore, bundles of parallel light under different angles pass
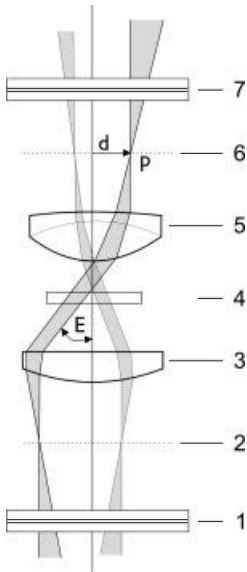
Figure 4.38 Schematic view of conoscopic illumination.
1, Polarizer; 2, first focal plane condenser; 3, condenser;
4, object; 5, objective; 6, rear focal plane objective; 7, analyzer.

through the object under test (4). In a conjugate plane to the condenser focal plane, angle-dependent OPDs can be observed (6).

Behind the crossed polarizers (1, 7), the interference pattern can be observed. The interference pattern is an indication of the axis of the optical material. Uniaxial materials show the pattern displayed in Figure 4.42 (a), where the main axis corresponds with the main axis of the material. The concentric rings are an indication of the OPD. Many rings are equal to more OPDs. Therefore an optical component with few rings has got little birefringence.

If this qualitative judgment is not sufficient, and measurements need to be done, a compensator has to be inserted into the optical path of the microscope. A compensator is usually a quartz plate with a particular geometry. Using the compensator for quantitative measurements works as follows:

The sample under test is placed in the light path of the microscope with polarizer and analyzer crossed. Then the sample under test is rotated by a compensator-depended amount. Usually this rotation is 45°. Then the compensator is used to restore the initial intensity patterns as good as possible. This is done for both directions of the compensator. The readings of the compensator can then be converted to retardation by means of a chart. Figure 4.39 shows a sequence of such images.

While this method is quantitative, it is still subjective, since the operator needs to judge the position of the compensator. There are automated systems available that can be placed as an addition – on to existing microscopes. With the aid of automated compensation and image processing, the measurement of birefringence can be made a lot more repeatable and accurate. The range of about
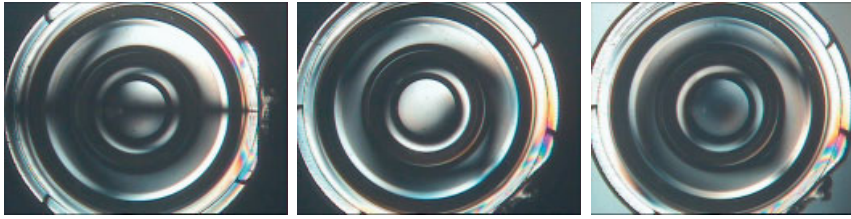
Figure 4.39 Sequence of birefringence images.

10 nm/cm up to several hundred nm/cm is more than sufficient for injection molding applications. For specification of birefringence, see ISO 10110–2 [4].

While automated birefringence measurement systems are in existence for quite some time (optical disks, LCD industry), most of these are scanning systems. The sample is mechanically scanned point by point and this way a polarization map of the system under test is composed. Recently systems came into the marked, where no mechanical scan is required. These systems fall into the category of imaging birefringence measurement systems. Figure 4.40 shows an example of such a system.
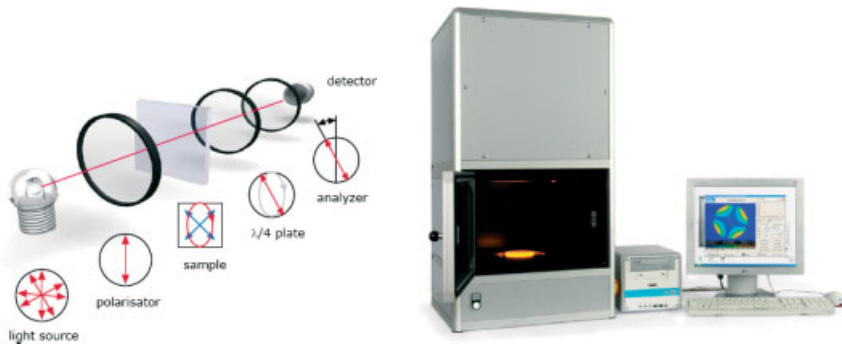
Figure 4.40 Birefringence metrology set up. (a) Principle of operation, (b) industrial measurement equipment (Photo courtesy of Ilis[54]).

The systems work according to a Sénarmont compensation technique [55, 56]. Linearly polarized light is sent through the sample under test. Birefringence causes the light to become elliptically polarized. By applying a quarter-wave plate, the light is again linearly polarized and analyzed with a rotating analyzer. If the detector is replaced by a matrix camera and images of the sample are taken at various positions of the analyzer, a complete laterally resolved polarization map of the sample can be composed. Figure 4.41 shows an example of the birefringence of an injection-molded lens.

It can clearly be seen that there is an increased amount of birefringence at the gate of the lens, and a radial decrease of birefringence centered on the gate. These kinds of images make it quite easy to visualize and understand what is going on
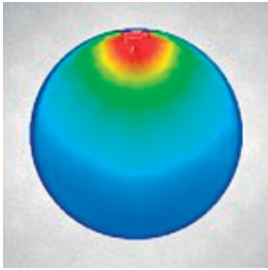
Figure 4.41 False color visualization of birefringence in an injection molded lens [54].

during the molding process. The standard equipment of Ilis can analyze surfaces up to 100 mm with a lateral resolution of up to 0.14 mm. Repeatability of the bire-fringence measurement is ±0.1 nm and measurement time less than a minute. As for other automated methods as well, with the shown instrument flat and slightly curved samples can be measured. Steeply curved lenses require a different approach, a more visual based one as described earlier.

4.6
Centration Measurement

Centration of an injection-molded lens is an important but difficult measurement. As with most optomechanical measurements, the choice of the proper reference is very important. Looking at the way injection-molded lenses are made, there are two types of centrations that are important:

- Centration of the optical centers of the two surfaces of a lens with respect to each other.
- Centration of optical center of the lens surfaces with respect to the outside di-ameter of the lens.

Figure 4.40 illustrates the different parameters of centration.

Optically relevant is the so-called optical axis, the line connecting the centers of curvature of the two lens surfaces. However in most practical cases, the optical axis is somewhat offset with respect to a mechanical reference. Figure 4.42(b) shows two examples: on the left-hand side the optical axis is tilted with respect to the outer diameter of the lens. On the right-hand side, the example of one lens surface being centered with respect to a cylindrical housing is displayed. This is a common example that occurs when lenses are mounted in mechanical housings. Exact definitions of centering tolerances can be found in ISO 10110–6 [4].

For injection-molded optics, the following items are of particular interest: the centration of the optical insert. Since many inserts are being manufactured by sin-gle point diamond turning (see Chapter 3), it needs to be checked if the center of the optical surface coincides with the diamond turning axis. Usually this can be seen while measuring the form of the insert, but a straight centration measure-ment can be done as well. The second interesting question for injection-molded
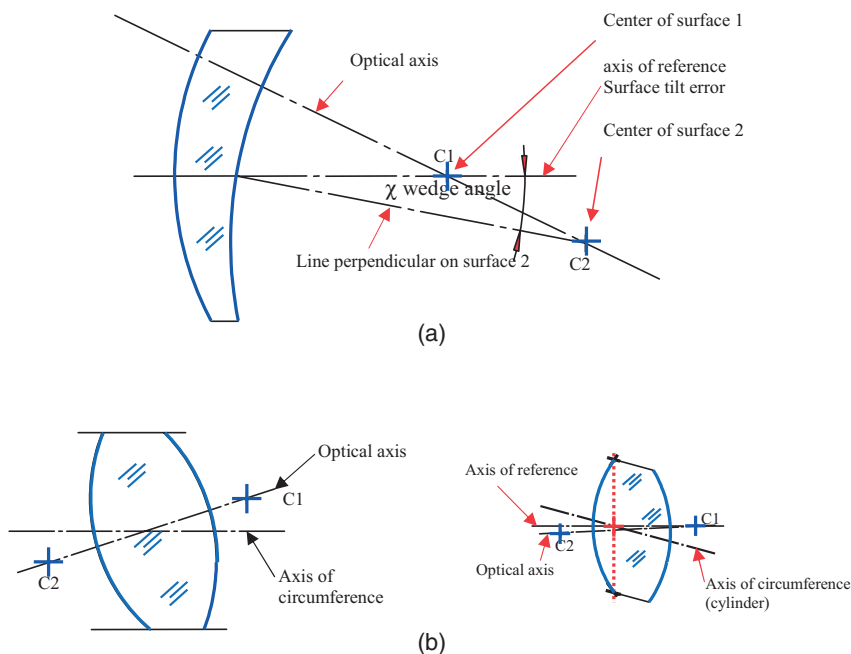
Figure 4.42 (a) Different parameters of lens geometry regarding centration of the two optical surfaces. (b) Different types of reference systems.

lenses is how well do the optical surfaces align with the mechanical outside of the lens or a particular flange. The difference between the two types of centration can be explained by looking at the way lens tools usually are constructed (Chapter 3).

Another difficulty in measuring centration of injection-molded optics lies in the fact that all injection-molded optical elements have got a sprue. Depending on the design of the mold, the sprue is either an appendix to a circular diameter or recessed a little bit such that it fits within the diameter of the lens. Since either one of the sprue locations forms a deviation from a circle, the classical method of measuring centration will not work. An adaptation of the classical centration method for injection-molded lenses will be discussed further.

4.6.1
Optical Centration Measurement

The classical method of measuring centration of a lens is to shine a small laser bundle onto the lens, rotate the lens over at least 180° back and forth, and observe the movement of the reflected light spot. The same is true for using a larger light bundle and then looking at the location of the focus generated by the surface under test.

A more sophisticated and quantitative method is based upon an autocollimator principle (Figure 4.43).

Autocollimator with additional lens

CCD with image of the target

Target (Cross Hair Reticle) + Illumination

Beam Splitter Plate

Objective of Autocollimator

Focusing Head lens

Surface under Test

Center of Curvature

R
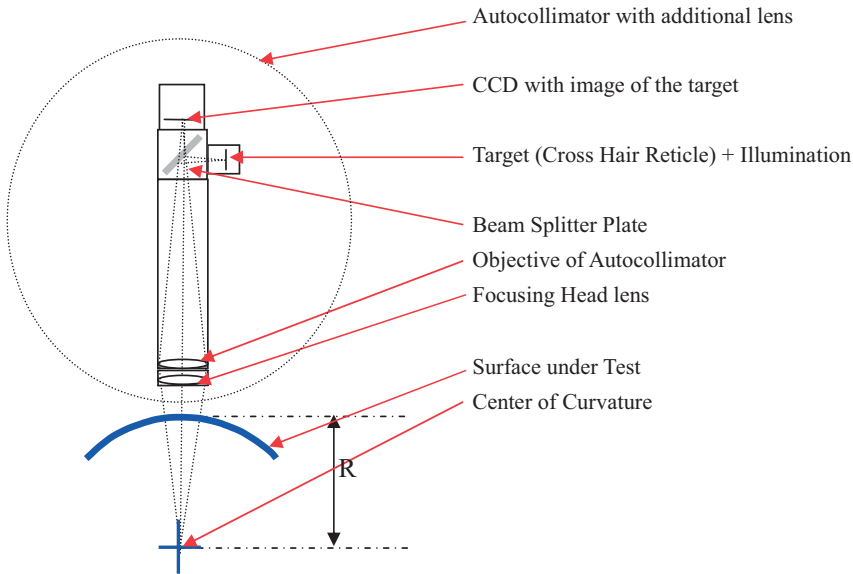
Figure 4.43 Autocollimator setup for measuring centration [57].

A (cross hair) target is imaged onto the center of curvature of the lens surface under test. Light is reflected back from the lens surface and forms an image on the CCD detector. If now the surface under test is rotated around a vertical axis, a displacement of the center of curvature from the rotation axis causes a circular movement of the target image on the detector. The radius of the circle is directly proportional to the decenter. If a lens should be measured, this method is first carried out for the first surface and then for the second surface. Evaluating both results will show the relative displacement of the centers of curvature of the two optical surfaces between each other and with respect to the reference axis of rotation. The quality of the rotation table is of essential influence on the measurement accuracy. Figure 4.44 shows a typical centration measurement device, with a typical measurement result next to it.

However for measuring the centration of the injection-molded lens elements, the above-described method needs a slight adaptation. The reason for this is the already mentioned sprue, which makes a defined 360° turn impossible. Figure 4.45 illustrates the procedure. The lens is first placed in a V-groove with the sprue part facing down, and then the lens is placed in the same V-groove with the sprue part up (referenced to drawing plane). This is done in both positions of the lens. From the difference, the centration is calculated. Through proper image analysis, both direction and magnitude of the centration error can be determined. Using high-precision air bearing for the rotation and vacuum chucks for the two positions, an accuracy of the measurement of about 1 μm can be achieved with a repeatability of about 0.2 μm.
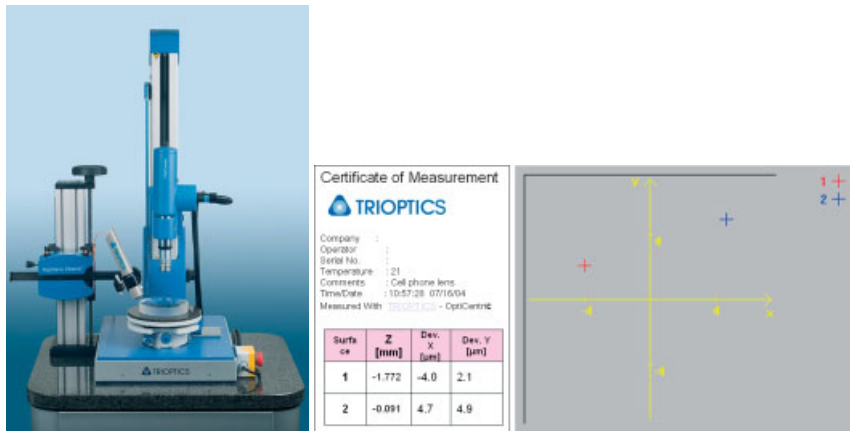
Figure 4.44 State-of-the-art centration measurement device (photo courtesy of Trioptics GmbH [24]).
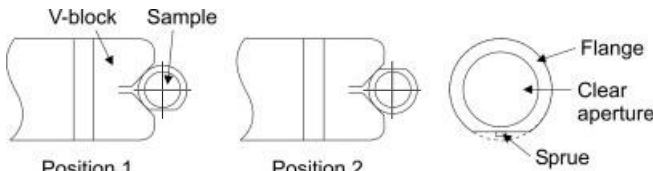
Figure 4.45 180° measurement principle.

4.6.2
Image Processing

Another very accurate way of measuring centration is using advanced image processing. With a CCD camera mounted on a 3D CMM, the image of the lens is taken. By using the proper illumination, usually the transition between the clear aperture and the flange can be made visible. Through this transition, a circle fit is done. In a next step, the camera is focused through the lens onto the second lens surface. Again the circle fit is done. Using this data, the centration of the optical surfaces can be computed. If the transition between clear aperture and flange or the lens rim can be brought into an image with sufficient contrast, this measurement provides centration data with submicron accuracy. Also this method is capable of measuring both types of centration. Figure 4.46 shows pictures with the circle fit through the transition zone. On the left-hand side, a circle segment is fitted through the upper lens surface, while on the right-hand side the lower lens surface is determined.

The real big advantage of this measurement is that the LUT can stay in position and does not have to be handled. That takes out the uncertainty in correlating top to bottom surface of the lens.

(a)   (b)
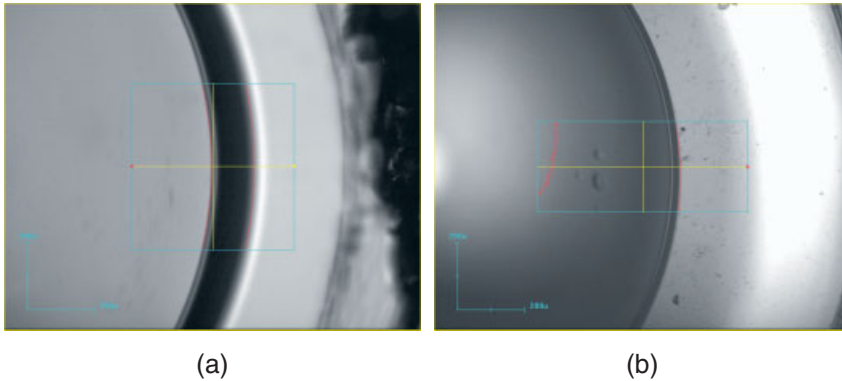
Figure 4.46 Centration measurement with image processing. (a) surface 1, (b) surface 2.

4.6.3
Mechanical Centration Measurement

If none of the described optical technologies work, there is still a possibility to perform mechanical centration measurements. Again the 3D coordinate measurement machine could be used in combination with a smart fixture and a very fine probing tip. The 3D CMM can measure the concentricity of the lens surface transition to the outside diameter easily. The problem is to relate the top surface of the lens to the bottom surface of the lens. For that, the lens has to be turned around and undergo at least one handling step. It is a matter of smart fixture and measurement strategy to eliminate the handling. Besides the 3D coordinate measurement machines, there also exists specialized equipment for measuring roundness and concentricity. An example of such a machine is the Talyrond equipment [58]. With this kind of equipment, centration in the submicron region can be measured as well.

4.6.4
Centration of Aspherical Surfaces

Measuring centration of spherical surfaces using the above-described optical method does not distinguish between a lateral displacement of the center of curvature or a tilt of the surface. For aspheres, this distinction between the two effects is very important, and can be measured as well. Using the centration measuring method described in Section 4.6.1, the decenter of the paraxial radius of curvature of the asphere can be measured. If a high-resolution distance sensor is added to the setup (see Figure 4.44 on the left-hand side and schematic figure below), the sag variation during one revolution of the surface can be monitored. Figure 4.47 shows that principle. Combing these two measurements enables the possibility to separate decenter from tilt of the aspheric surface [59]. Again, the accuracy of the rotation is of upmost importance for the result of the measurement.
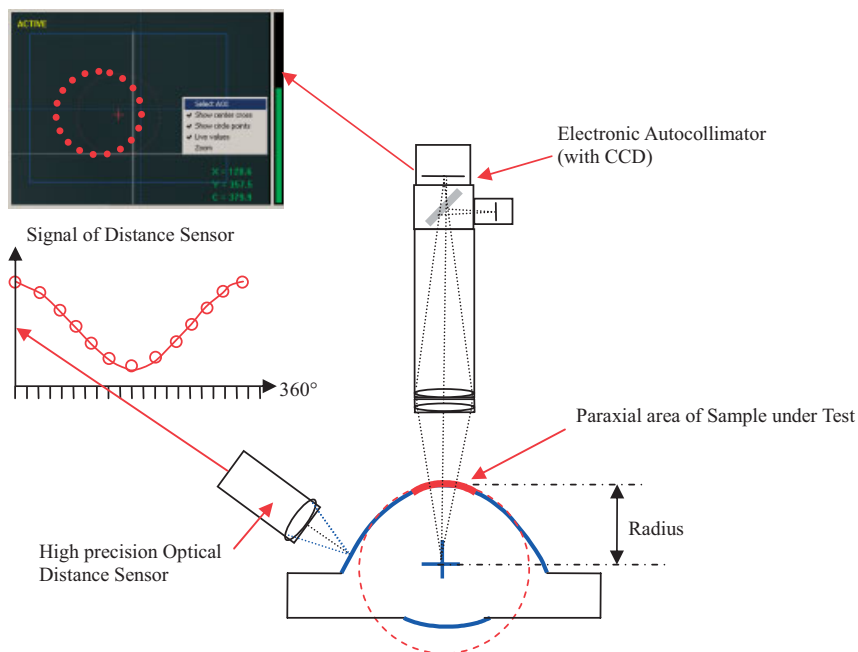
Figure 4.47 Radius of curvature measurement of an aspheric surface.

4.6.5
Centration of Multielement Systems

If the centration of a completely assembled objective needs to be measured, only optical techniques can be considered. For that, the classical method of locating the centers of curvature of the lens surfaces needs to be combined with the design data of the lens. Knowing the lens design data, one can work through a multi element system from top to bottom. Using the design data to estimate the location of the foci of the centers of curvature of the surfaces and compensating for the refraction effects, one works through the objective applying the method described earlier (see Section 4.6.1). This way all centers of curvature of an objective can be determined. This can give valuable information on the assembly of such a lens system.

Figure 4.48 shows a typical lens centration measurement device of Trioptics [60]. This device uses a high-precision air bearing for turning the lens. Also the air bearing has got a central hole. Using a second measurement head, the lens can be measured from both sides. This will increase accuracy and also enable the measurement of whole objectives, if some surfaces cannot be located from one side only.

Figure 4.48 Trioptics centration measurement stand, dual measurement head (photo courtesy of Trioptics GmbH [60]).

4.7
Custom Setups

So far in this chapter, fairly generic setups have been discussed. The big advantage of injection-molded optics is that several functions can be combined into one component. Multiple optical and mechanical features can be realized in one injection-molded part. In Chapters 2 and 9, several examples have been presented. Other examples can be found in the literature [61, 62]. The advantage of high integration sometime turns into a disadvantage for metrology. If there is a highly integrated component, measurement of all functions can be quite complex. In these cases, there are two possible approaches:

- use several standard instruments to check the component;
- build a custom measurement setup for the specific component.

As in many cases for injection-molded optics, the scale of the product plays an important role. If the component is manufactured in large numbers and contains critical functions, a specific setup is a better choice. If the production is of lower volume, it might be sufficient to test with a standard instrument and a special alignment jig. The same is true if the manufacturing process is very stable and only few parts have to be measured for SPC. At which point the custom setup is a

better solution depends to a large extend on economic facts as well. Engineering cost of the setup, measurement time, and of course quality level are the principle parameters that have to be considered. In the following, a couple of examples for integrated optical parts and their measurement setups are given. These are examples and many more setups can be thought of [61].

4.7.1
SALDO

First the special applications laser detection optics (SALDO) is described. Figure 4.49 shows the light path for a CD drive application.
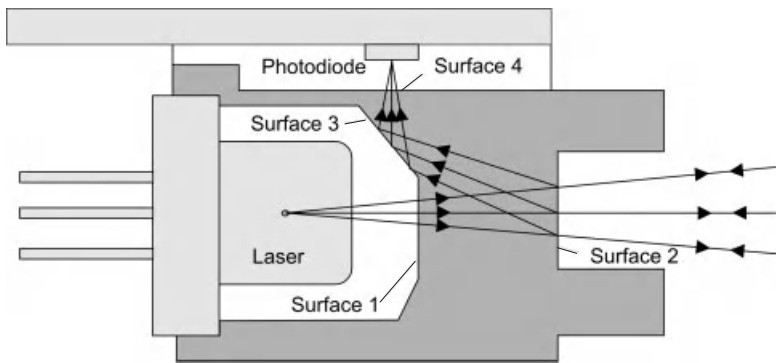
Figure 4.49 SALDO light path.

In the application, light from the laser diode falls onto surface 1, which is a linear phase grating producing three beams for spot tracking on the disk. Surface 2 is a fish-bone type linear grating that acts as a beamsplitter for the returning light and also subdivides the returning light bundle in two for dual knife edge focus detection. Surface 3 is a folding mirror surface and surface 4 the exit window. Table 4.2 gives an overview over the requirements for the surfaces.

Table 4.2 An overview of the required accuracies of the SALDO beam splitter.

	surface 1 3 spot	surface 2 fish bone	surface 3 mirror	surface 4 exit	unit	conditions
clear aperture	0.6	1.0	0.8	0.5	mm $\varnothing$	
shape accuracy (ISO 10110)	3/– RMSi <0.035	3/– RMSi <0.035	3/– RMSi <0.035	3/– RMSi <0.050	λ	$\lambda = 780$ nm
surface tilt	± 2	± 2	± 9	± 9	mrad	

Besides the surface shape, an additional requirement is given. Since there are two gratings in this component, the relative intensities between the different diffraction orders used are of interest as well.

For the prototype series of this product, the individual surfaces were measured using an interferometer with a short coherence length laser diode. That way, fringe patterns from the back surfaces could be avoided. For the test of all individual surfaces, special measurement holders were developed in order to verify the mechanical reference points as well. The relative intensity distributions were checked by building the component into a test CD drive. For mass production, the development of a custom setup was started. In that setup, the component was illuminated with a plane wave entering the component from surface 2. With several photocells at the correct reference positions, the relative intensity distribution between the spots was measured. The surface shape of all surfaces was still measured individually with an interferometer.

4.7.2
Double Mirror System

A second example of an integrated optical component is a dual mirror. In an off-axis parabolic mirror, a small flat mirror has been integrated. The surface normal of the parabolic mirror and the flat mirror make an angle with respect to each other. Figure 4.50 shows the geometry of the part.
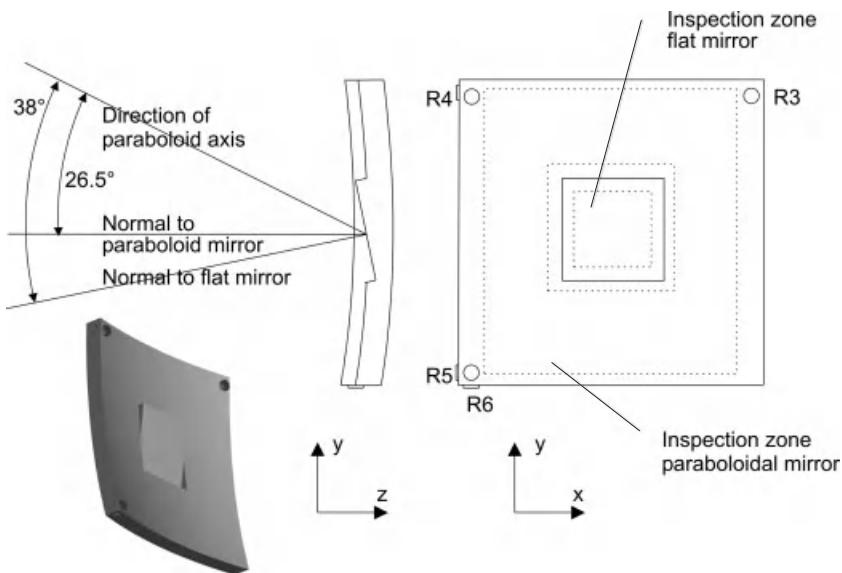
Figure 4.50 Schematic layout of a double mirror system.

The important functional parameters for this component are as follows:

- shape accuracy of parabolic mirror
- shape accuracy of flat mirror
- tilt of parabolic mirror with respect to the mechanical references
- tilt of flat mirror with respect to the mechanical references.

In Table 4.3, the important functional specifications are detailed out in measurable quantities.

Table 4.3 An overview of the required properties of the dual mirror.

	surface 1	surface 2	unit	conditions
surface type	off axis paraboloid	flat		
clear aperture	11.2×10.0	3×3	mm^2	
maximum spot diameter	250	–	μm	in focal point
PV shape accuracy	–	0.2	λ	$\lambda = 650$ nm
surface tilt w.r.t. mech. ref.	± 6	± 6	mrad	two orthogonal directions
surface tilt w.r.t. each other	± 6		mrad	two orthogonal directions

The difficulty in measuring this part is mainly in the tilt measurement of the two mirrors. For the shape accuracy, it was chosen to use spot diameters as a quality measure. The spot diameters can be linked to the mirror shape. Since all these parameters are important and linked to each other, it was chosen to build a custom setup. Figure 4.51 shows this setup.

The parabolic mirror is tested by illuminating the mirror with a parallel light bundle, and then measuring form and position of the focal spot. The flat mirror is tested in an autocollimation setup. An additional reference mirror is placed in the test setup. Once common illuminating beam passes the flat mirror, the additional reference mirror sends the light back into the test system. Passing the flat mirror a second time, the bundle is then focused on a second CCD camera. Again shape and position of the spot are measured. Using this setup and some data processing, the critical parameters of the double mirror can be measured.

However there is one very important item that has to be done before starting the routine measurements: calibration of the test setup. From the geometry of the test setup, it is evident that reference position of the mirror under test, the nominal position of the spots on the CCD cameras, and the nominal spot sizes (with their tolerances) need to be determined. The calibration that is used and described here is again an example on how to solve this kind of problem. It should explicitly be stated that a proper calibration scheme is absolutely necessary for carrying out reliable measurements. These calibration schemes are increasingly more impor-
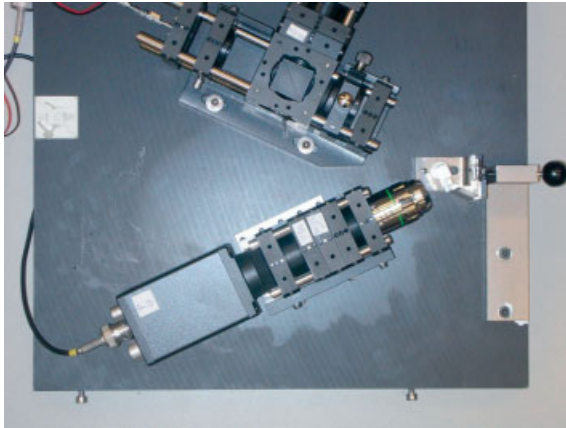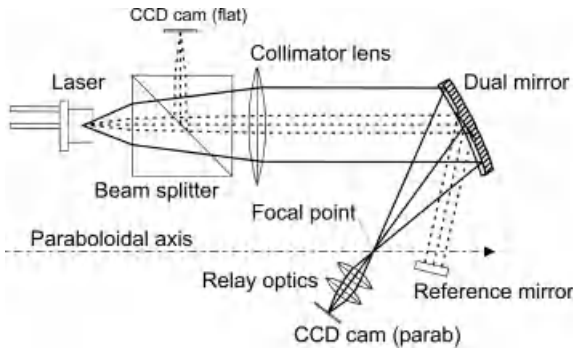
Figure 4.51 Custom setup for testing double mirror, layout, and actual setup.

tant as one decides to move to a custom and functional test setup. The standard metrics provided by the standard measurement instrument do not exist for custom setups. In the case of the dual mirror, it was chosen to follow a calibration scheme that requires three different calibration tools. In this case, it seemed easier to use the three pieces, since manufacturing a "golden" reference sample is almost impossible and certainly cost prohibitive. The calibration of both channels is done separately. The following items are calibrated:

- Zero tilt of the parabolic channel with calibrator 1.
- The tilt sensitivity of the parabolic channel with calibrator 2.
- Zero tilt of the flat mirror channel with calibrator 3.
- The tilt sensitivity of the flat mirror channel with a commercially available tilt stage.

A detailed description of the calibration steps can be found in Ref. [61].

4.7.3
High Throughput MTF Testing of CMOS Camera Modules

A different type of optical testing will be discussed in the third example of dedicated optical testing. CMOS camera modules are a high volume market. The vast amount of these camera modules consists of injection-molded optical components. The problem in testing these objectives is that the individual optical components can be characterized by interferometer, Shack–Hartmann sensor, or deflectometry, but the most meaningful specification for this type of optics is the modulation transfer function (MTF). Besides the quality of the individual optical components, assembly does have a great influence on the performance of the module as well. In order to deliver constant and reliable quality to the customers, one needs to test all camera modules after assembly and before shipping. Since the production volumes of the CMOS camera modules are of the order of several hundred thousands per month, the test equipment needs to be able to handle these volumes. Short measurement times and very high throughput are heavy boundary conditions for the testers. On top of that measuring, the MTF of an optical system correctly is not trivial since the MTF is a function of many variables such as focus, spectrum, field position, etc. Basic requirements for the MTF production setup are a follows:

- full MTF calculation (not only contrast measurement)
- multiple fields
- polychromatic
- autofocus
- fast (total measurement time less than 4 s)
- fast loading and unloading
- operator user interface.

The company Trioptics developed such MTF setups that are ready for MTF measurements in production and able to handle very high volumes [63]. Figure 4.52 shows such a high-volume MTF tester.

In this tester, the LUT images a test reticule with lines as test pattern to infinity. Under adjustable angles, CCD cameras with auxiliary optics are placed to capture the image that is projected by the LUT. Through image processing and FFT calculations, the MTF of the system is computed. In the current Pro Line 4 testers, up to nine cameras can be placed to capture the MTF at nine field positions simultaneously. Since one of the important parameters in measuring the MTF of a system is focus, the optimum focus in the center of the image is determined prior to measuring. This is done by a through focus scan in several steps. Focusing, measurement and evaluation of one lens module is performed in less than 4 s. With this kind of equipment, the very high volumes of injection-molded products can be handled, even at a 100% level as in this example [64]. In addition to measuring CMOS camera objectives, there are also MTF testers that can handle so-called wafer level produced objectives. In this production method, camera modules are

Figure 4.52 High throughput production MTF tester, Trioptics Image Master Pro Line 4.

assembled on a wafer level and then also tested on a wafer. The depicted MTF tester (Figure 4.52) does have this wafer level test capabilities.

4.8
Concluding Remarks

At the end of this chapter, it should be clear that metrology is a rich discipline with many facets to it. Metrology should be an integral part of the product creation process. The earlier metrology gets involved, the better it is. Injection-molded optics provides the unique opportunity to design reference marks into the product. This should be used as much as possible. The challenge of metrology for injection-molding optics is on one side to have high-precision metrology for the tools and on the other side metrology that is fit for mass production, that is, high throughput and high reliability. Another challenge is to cope with complex and (highly) integrated products. It should have become clear that the choice is either using as much standard equipment as possible and finding suitable parameters that characterize the product sufficiently, or building customized measurement equipment. In many cases, this decision is made not only on technical grounds but also on economical ones. For the generic measurement equipment described in this section, Table 4.4 represents an attempt to classify the techniques into various categories of measuring injection-molded optics. Table 4.4 focuses on surface and wavefront measuring techniques, leaving other measurements such as birefringence, centration, and geometrical measurements out. The reason for that is in the variety of different possibilities for surface- and wavefront measurements.

Table 4.4 Summary of surface and wavefront metrology techniques.

	surface insert	surface plastic	wavefront plastic	comments
interferometer	++	++	++	if slopes are not too strong, very good choice
interferometer with compensation optics	+	+	++	alignment and calibration are critical, compensation optics are custom for every lens
Shack–Hartmann sensor	+	+	++	flexible tool, alignment needs attention
deflectometer	++	++ (phase shift technique)	under development	very flexible, extended range
shearing interferometer	0	0	+	useful for special applications
tactile probing	++	++	not possible	standard for measuring surfaces

Looking at the table it can be said that standard interferometers are an excellent choice for characterizing standard optics, i.e., optical surfaces and components that do not deviate much form sphericity. For aspherical components, there is a variety of possibilities. Both, slope measuring devices and height measuring have got some advantages and disadvantages. It very much depends on the application which technique can be applied best. Up to now, tactile profiling still sets the standard for measuring (steep) aspheres. However among the optical technologies, there is lots of development going on in order to bring technologies such as Shack–Hartmann sensors and deflectometers commercially into the market. At university and institute level, some of the problems seem to be solved; however for high-volume production, extra effort is still needed.

Finally remarks need to be made about software. This chapter is reviewing several metrology techniques in relation to their relevance and application in measuring injection-molded optics. It is true that all setups need to be placed on solid optomechanical ground. Therefore, the emphasis of this chapter was placed on the metrology principles, and some hardware implementation. However in modern metrology equipment, the ratio between hardware and software is approximately 30:70. Intelligent algorithms, data pre- and postprocessing, and last but not least alignment and calibration tools are coded into metrology software. Furthermore, the software forms the interface to the user. Ease of use and access to analysis features are very important for the user, and sometimes decide upon use or not of a certain metrology tool. Therefore it is of essential interest that the software aspects of a metrology project are covered well. If one decides to build

own metrology setups, it is sometimes advisable to consult a software supplier in the early stage of the project. This becomes even more crucial as the metrology device is intended to be operated in production.

Another aspect of metrology is that it should be evident that correct interpretation of the metrology results is very important for improving products and processes. One should always remain critical about the hardware and software used. Even the most sophisticated hardware and software do not relief the operator/ designer from thinking and evaluating. Generating data is easy, while using the data for meaningful improvements is the challenge.

Finally a last aspect on metrology for injection-molded optics – for tooling, there is an ongoing movement to implement on machine measurement for characterization of the inserts directly on the lathe [65]. This could potentially help in reducing throughput time and also increasing accuracy of insert making. One will have to watch for a trend.

Acknowledgments

A last disclaimer: although specific instruments were named in their application, the author does not endorse or recommend any specific brand. Main purpose of the chapter is to show that certain principles have reached industrial maturity.

References

1 D. Malacara, *Optical Shop Testing*, 3rd edn (John Wiley & Sons, New York, 2007).

2 P.G. Cielo, *Optical Techniques for Industrial Inspection* (Academic Press, San Diego, 1988).

3 Joseph M Geary, *Introduction to Optical Testing* (SPIE TT15, Bellingham, WA, USA, 1993).

4 ISO 10110 "Optics and optical instruments – preparation of drawings for optical elements and systems – parts 1–12", International Organization for Standardization, Geneva, CH, 1996.

5 S. Bäumer, L. Shulepova, J. Willemse, and K. Renkema, Integral optical system design of injection molded optics, *Proc. SPIE* **5173**, 38–45 (2003).

6 W.S. Beich, Specifying injection-molded plastic optics, *Photonics Spectra*, **3** 2002, 127–132.

7 T. Ruijl, *Ultra Precision Coordinate Measuring Machine: Design, Calibration and Error Compensation*, 2nd edn (Ponsen & Looijen, Wageningen, NL, 2002).

8 J.A. Bosch, *Coordinate Measuring Machines and Systems* (Marcel Dekker, New York, 1995).

9 T. Pfeifer, *Koordinaten – Messtechnik für die Qualitätssicherung* (VDI Verlag, Düsseldorf, 1992).

10 Mitutoyo Coordinate Measuring Machines Legex, Mitutoyo American Cooperation, Aurora, IL, Brochure, May 2004.

11 Zeiss F25 Measuring Nanometers, Carl Zeiss Industrial Metrology GmbH, D-73446 Oberkochen, Germany, 2006, www,zeiss.de/imt.

12 Philips Applied Technologies, "Ultra precision coordinate measuring machine", Philips Applied Technologies HTC7, 5656AE Eindhoven, The Netherlands, 2004, www.apptech.philips.com.

13 J.M. Bennett, L. Mattsson, *Introduction to Surface Roughness and Scattering*, 2nd edn (OSA, Washington, USA, 1999).

14 M. Stedman, Basis for comparing the performance of surface-measuring machines, *Prec. Eng.* **9**, 149–152 (1987).

15 G.T. Smith, *Industrial Metrology: Surfaces and Roundness* (Springer, New York, 2002).

16 Precitec Optronic, www.precitec.com/ measuring-technology/contactless-measuring-sensor-chrocodile.html.

17 Fries Research and Technology, www.frt-gmbh.com/frt/upload/pdf_en/ FRT_Sensor_CSL_EN.pdf.

18 E. Savio, L. de Chiffre, and R. Schmitt, Metrology of freeform shaped parts, *Ann. CIRP* **56/2**, 810–835 (2007).

19 R. Henselmans, L.A. Cacace, G.F.I.J. Kramer, P.C.J.N. Rosielle, and M. Steinbuch, Development and performance demonstration of the NANO-MEFOS non-contact measurement machine for freeform optics, *Proc. EUSPEN International Conference*, San Sebastian, Spain, 2009.

20 R. Henselmans, "Non-contact Measurement Machine for Freeform Optics", PhD Thesis, Technische Universiteit Eindhoven, 2009.

21a L.A. Cacace, W.D. van Amstel, Henselmans, R.H. de Man, and P.C.J.N. Rosielle, Development of a new differential confocal optical probe with nanometer accuracy at large acceptance angles for measurement of free-form

aspherics, *Proc. EUSPEN International Conference*, Bremen, 168–171 (2007).

21b H. Takeuchi, K. Yosizumi, H. Tsutsumi, Ultrahigh accurate 3-D profilometer using atomic force probe of measuring nanometer, *Proc. ASPE Winter Topical Meeting on Free-Form Optics: Design, Fabrication, Metrology, Assembly*, 102–107 (2004).

22 J. Campos, L.P. Yaroslavsky, A. Moreno, and M.J. Yzuel, Integration in the Fourier domain for restoration of a function from its slope: comparison of four methods, *Opt. Lett.* **27** (22), 1986–1988 (2002).

23 L.P. Yaroslavsky, J. Campos, A. Moreno, and M.J. Yzuel, Comparison of three methods of integration to obtain the profile from its slope, *Proc. SPIE* **4829**, 902–904 (2003).

24 Trioptics GmbH, Hafenstrasse 35–39, 22880 Wedel, Germany, www.trioptics.com.

25 3D-Shape GmbH, Erlangen, www.3d-shape.com/produkte/pmd_e.php# ueberblick.

26 M.C. Knauer, J. Kaminski, and G. Häusler, Phase measuring deflectometry: A new approach to measure specular free-form surfaces, *Proc. SPIE* **5457**, 366–376 (2004).

27 Taylor Hobson Ltd, PO Box 36, 2 New Star Rd., Leicester, LE4 9JQ, UK, www.taylor-hobson.com.

28 Taylor Hobson Ltd, Form Talysurf PGI 1240 aspheric measurement system, Taylor Hobson Ltd, PO Box 36, 2 New Star Rd., Leicester, LE4 9JQ, UK (2004).

29 Taylor Hobson Ltd, Form Talysurf PGI BLU Aspheric Lens Mold Measurement System, Taylor Hobson Ltd, PO Box 36, 2 New Star Rd., Leicester, LE4 9JQ, UK, (2008).

30 J. Schwider, Advanced evaluation techniques in interferometry, in: *Progress in Optics*, Vol. XXVIII, pp. 271 – 359, edited by E. Wolf (North Holland, New York, 1990).

31 J.D. Briers, Interferometeric optical testing: considerations for the proposed new international standard, *Proc. SPIE* **3739**, 496–507 (1999).

32 P.E. Murphy, T.G. Brown, and D.T. Moore, Measurement and calibration of interferometric imaging aberrations, *Appl.Opt.* **39** (34), 6421–6429 (2000).

33 K. Creath, Phase-measurement interferometry techniques, in: *Progress in Optics*, Vol. XXVI, pp. 348–393, edited by E. Wolf (Elsevier, Amsterdam, 1988).

34 S.M. Arnold, L.C. Maxey, J.E. Rogers, C. Robert, and R.C. Yoder, Figure metrology of deep general aspherics using a conventional interferometer with CGH null, *Proc. SPIE* **2536**, 106–116 (1995).

35 F. Schillke, Critical aspects on testing aspheres in interferometeric setups, *Proc. SPIE* **3739**, 317–324 (1999).

36 S. Reichelt, C. Pruss, and H.J. Tiziani, New design techniques and calibration methods for CGH-null testing of aspheric surfaces, *Proc. SPIE* **4778**, 158–168 (2002).

37 B. Braunecker, R. Hentschel, and H.J. Tiziani, *Advanced Optics using Aspherical Elements* (SPIE Press, Bellingham, WA, USA, 2007).

38 Fisba Optik AG, Rorschacher Strasse 268, CH-9016 St.Gallen, Switzerland, www.fisba.ch.

39 Fisba Optik AG, FISBA μNews 10: Measuring aspheric surfaces of lenses or lens molding tools, Fisba Optik AG, st. Gallen, June 2004.

40 J.E. Greivenkamp and R.O. Gappinger, Design of a nonnull interferometer for aspheric wavefronts, *Appl. Opt.* **43** (27), 5143–5151 (2004).

41 M.F. Kuechel, Absolute measurement of rotationally symmetrical aspheric surfaces, in: *Optical Fabrication and Testing* (OSA, Washington, USA, 2006).

42 Zygo Corporation, Verifire Asphere specification sheet, Zygo Corporation, Middlefield, CT, USA, 2009, www.zygo.com.

43 H. Sickinger, J. Schwider, and B. Manzke, Fiber based Mach–Zehnder interferometer for measuring wave aberrations of microlenses, *Optik* **110** (5), 239–243 (1999).

44 J. Pfund, N. Lindlein, J. Schwider, R. Burow, T. Blümel, and K.E. Elssner, Absolute sphericity measurement: a comparative study of the use of interferometry and a Shack–Hartmann sensor, *Opt. Lett*, **23** (10), 742–744 (1998).

45 Jenoptik Polymer Systems, Breitwiesen, 73347 Muehlhausen, www.jenoptik-ps.de.

46a Zygo Corporation, NewView 7200 specification sheet, Zygo Corporation, Middlefield, CT, USA, 2008, www.zygo.com.

46b G. Ganesha Udupa, M. Singaperumal, R.S. Sirohi, and M.P. Kothiyal, Characterization of surface topography by confocal microscopy: I. Principles and the measurement system, *Meas. Sci. Technol.* **11**, 305–314 (2000).

47 Joseph M Geary. *Introduction to Wavefront Sensors* (SPIE TT18, Bellingham, WA, USA, 1995).

48 S. Groening, B. Sick, K. Donner, J. Pfund, N. Lindlein, and J. Schwider, Wave-front reconstruction with a Shack–Hartmann sensor with an iterative spline fitting method, *Appl. Opt.* **39** (4), 561–567 (2000).

49 J. Pfund, N. Lindlein, J. Schwider, Nonnull testing of rotationally symmetric aspheres: A systematic error assessment, *Appl. Opt.* **40** (4), 439–446 (2001).

50 J. Pfund, N. Lindlein, and J. Schwider, Misalignment effects of the Shack–Hartmann sensor, *Appl. Opt.* **37** (1), 22–27 (1998).

51 G.W.R. Leibbrandt, G. Harbers, and P.J. Kunst, Wavefront analysis with high accuracy by use of a double grating lateral shearing interferometer, *Appl. Opt.* **35** (31), 6151–6161 (1996).

52 G. Harbers, P.J. Kunst, and G.W.R. Leibbrandt, Analysis of lateral shearing interferograms by use of Zernike polynomials, *Appl. Opt.* **35**(31), 6162–6172 (1996).

53 http://micro.magnet.fsu.edu/primer/techniques/polarized/configuration.html.

54 ilis gmbh, Konrad-Zuse-Str. 12, D-91052 Erlangen, www.ilis.de.

55 H. Katte, Imaging measurement of stress birefringence in optical materials and components, Photonik International 1/2009, 39–41 (2009).

56 J.G. Delly, Sénarmont compensation: How to accurately measure small relative retardations (0–1 λ), in: "How To" tutorial series, *Mod. Microsc. J.*, **2**, 2004, www.modernmicroscopy.com.

57 J. Heinisch, E. Dumitrescu, and S. Krey, Novel technique for measurement of centration errors of complex, completely mounted multi-element objective lenses, *Proc SPIE* **6288**, 78–88 (2006).

58 Talylor Hobson Ltd, Tayrond 265/290, Talylor Hobson Ltd, PO Box 36, 2 New Star Rd., Leicester, LE4 9JQ, UK, (2004).

59 Trioptics GmbH, Data Sheet Opti-Centric®, AspheroCheck®, Trioptics GmbH, Hafenstrasse 35–39, 22880 Wedel, Germany (2009).

60 Trioptics GmbH, "OptiCentri – tool for production and lab", Trioptics GmbH, Hafenstrasse 35–39, 22880 Wedel, Germany (2004).

61 W. Timmers, S. Bäumer, B. van Iersel, A. Ras, R. de Schipper, and G. Verkade, Metrology of injection molded optical components with multiple optical functions, *Proc. SPIE* **3778**, 78–88 (1999).

62 O. Kinrot and U. Kinrot, Interferometry: transverse Doppler measurement by VCSEL-based optical translation measurement (OTM) sensor, Laser Focus World, March 2000.

63 M. Dahl, S. Bäumer, J. Heinisch, S. Krey, J. Lurquin, and L. Chen, Ultra fast MTF test for high volume productions of CMOS imaging cameras, *Proc. SPIE* **5180**, 293–300 (2003).

64 Trioptics GmbH, ImageMaster, Trioptics GmbH, Hafenstrasse 35–39, 22880 Wedel, Germany (2009).

65 M. Breukers, Cost effective manufacturing aspherical lens moulds using on-machine metrology, *Proc. EOS Conference Manufacturing of Optical Components,* June 2009.

5
Optical Plastics

Koji Minami (Zeon Corporation, Kawasaki, Japan)

5.1
Introduction

The innovative engineering development of optoelectronics has contributed to the expansion of information technology over the past 25 years. This development has been essential for modern information technologies through high-speed communication and information processing.

For example, there are lens technologies for optical fibers and discs; laser technologies for printers and copiers; light sensor technologies including digital processing for charge coupled devices (CCDs) and complementary metal oxide semiconductors (CMOSs); and flat panel display technologies for liquid crystal displays. These technologies are increasingly seen in digital cameras, cellular phones with cameras, DVD recorders/blue laser recorders, and various sensor cameras for automotive applications.

Optical devices are extremely important, since they play a central role in optical transmission, recording, replay, and display. For these optical parts, transparent materials with optical properties have been used. Glass materials have been conventionally used and are the most reliable, and are thus used in important parts for which high stability is required. However, they are not suitable for mass production. Plastic materials are suitable for mass production and, therefore, widely used for many optical devices. In addition to the mass-productivity, low weight is another attractive feature. As for transparent plastic materials, poly(methyl methacrylate) (PMMA) and polycarbonate (PC) have excellent transparency and are used extensively. In addition, alicyclic acrylates and cycloolefin polymers (COPs) with various optical properties have been developed. Furthermore, optical polyester (O-PET) and a certain series of polysulfones have recently been developed and used.

A notable example can be seen in the compact disc market where transparent plastic materials were accepted to the market in large quantities. The use of plastic pick-up lens for optical discs significantly lowered the total cost and thus greatly expanded the compact disc market. As information technology advances, sophistication in the use of transparent plastic materials for optical devices becomes more

important. Therefore the development of the technology of these materials is essential.

This chapter compares the physical properties of some of the transparent plastic materials currently in use.

5.2
Quality Requirements for Optical Plastics

5.2.1
Transparency

The most required property of optical plastics is high transparency at specific wavelengths. The transparency of a plastic is determined by (1) molecular structure, (2) molecular conformation formed by molding or other causes, and (3) impurities.

5.2.1.1 Molecular Structure
The transparency of a polymer is intimately related to its molecular structure. Various interatomic/intermolecular interactions in a polymer being exposed to light cause optical absorption in the ultraviolet to visible region due to electron transitions or optical absorption in the infrared region due to vibrational transitions. The absorption in the infrared region does not affect absorption in the visible region. For absorption due to electron transitions a_e mostly in the ultraviolet region, Urbach's rule is known [1, 2]:

$$a_e = A \exp \frac{B}{\lambda} \tag{5.1}$$

where A and B are inherent to each molecule and λ is the optical wavelength. At 500 nm, a_e of PMMA is reported as <1 dB/km whereas that of polystyrene is 98 dB/km from this formula [3]. The value of a_e is high when a polymer has a benzene ring structure, as in the phenyl groups that are found in most polycarbonates and polystyrenes. On the other hand, PMMA is a typical transparent material with excellent transparency because its molecular structure has no group that absorbs within the visible region. Thus, materials that are barely affected by electron transitions are desirable in order to obtain high transparency. Light absorptions occur, for instance, in $\pi \rightarrow \pi^*$ transitions in double bonds as typified by azo or phenyl groups, or n $\rightarrow \pi^*$ transitions in C=O bonds.

The reflectance (R) depends on refractive index (n) as follows:

$$R = \frac{(n-1)^2}{(n+1)^2} . \tag{5.2}$$

This formula indicates that materials with low refractive index show low reflectance and accordingly high light transmittance. Commonly, plastic lenses are coated with inorganic materials for which the refractive indices are lower than those
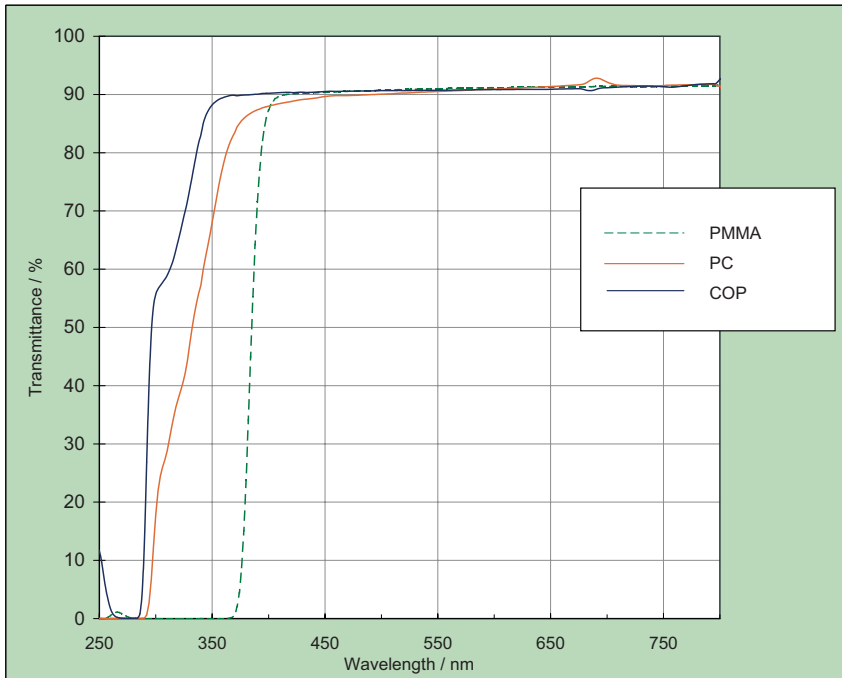
Figure 5.1 Comparison of light transmittance of PMMA, PC, and COP.
Sample thickness 3 mm. PC: PANLITE® AD5503, Teijin chem.;
PMMA: ACRYPET™ VH, Mitsubishi rayon; COP: ZEONEX® 330R.

of plastics. Figure 5.1 shows a comparison of light transmittance data for PMMA, PC, and COP.

5.2.1.2 Molecular Conformation

Randomness of molecular chains is essential for polymer transparency. Crystal and non-crystal regions of a crystalline polymer generally have different refractive indices. This causes scattering of light at the boundary between two such regions. A multicomponent polymer such as polymer alloy behaves similarly. There is also light scattering loss caused by isotropic and anisotropic density fluctuations called Rayleigh scattering [2, 4].

5.2.1.3 Impurities

Polymers may be colored due to various additives such as antioxidants, plasticizers, ultraviolet absorbers (UVAs), coloring agents (pigments and dyes), or oxidized resin damaged in thermoprocessing. Small amounts of residues such as catalysts that are added at the time of polymer synthesis may unintentionally cause coloring of the polymer.

5.2.2
Refractive Index

The refractive index varies depending on molecular polarizability and weight per unit volume (density) as in the Lorentz–Lorenz equation [5]:

$$\frac{n^2 - 1}{n^2 + 2} = \frac{4}{3}\pi N a \tag{5.3}$$

where n is the refractive index, a the polarizability, and N the number of molecules in 1 cm^3.

As the result of Eq. (5.3), the refractive index values depend on molecular refraction and molecular volume of macromolecules as follows:

$$n = \sqrt{\frac{1 + 2[R]/V}{1 - [R]/V}} \tag{5.4}$$

where $[R]$ is the molecular refraction and V the molecular volume.

The Abbe number is expressed as

$$V_{\mathrm{D}} = \frac{n_{\mathrm{D}} - 1}{n_{\mathrm{F}} - n_{\mathrm{C}}} . \tag{5.5}$$

This formula corresponds to Fraunhofer's D-line (589.2 nm), F-line (486.1 nm), and C-line (656.3 nm). The Abbe number is the wavelength dependence of refractive index. The higher the refractive index, the smaller the Abbe number and thus the larger the wavelength dispersibility, as shown in Figures 5.2 and 5.3 and
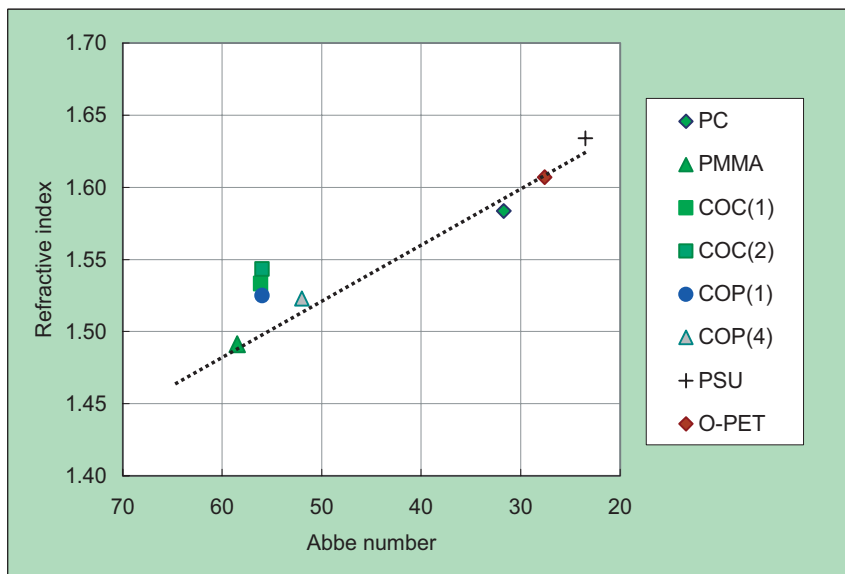
Figure 5.2 Relationship between refractive index and Abbe number for various polymers at 25 °C. PC: PANLITE® AD5503 at room temperature; PMMA: Parapet at 23 °C; COC(1): APEL™ 5104DP; COC(2): TOPAS® 5013; COP(1): ZEONEX® 480R; COP(4): ARTON® FX4727; PSU: Udel® P-1700; O-PET: OKP-4.
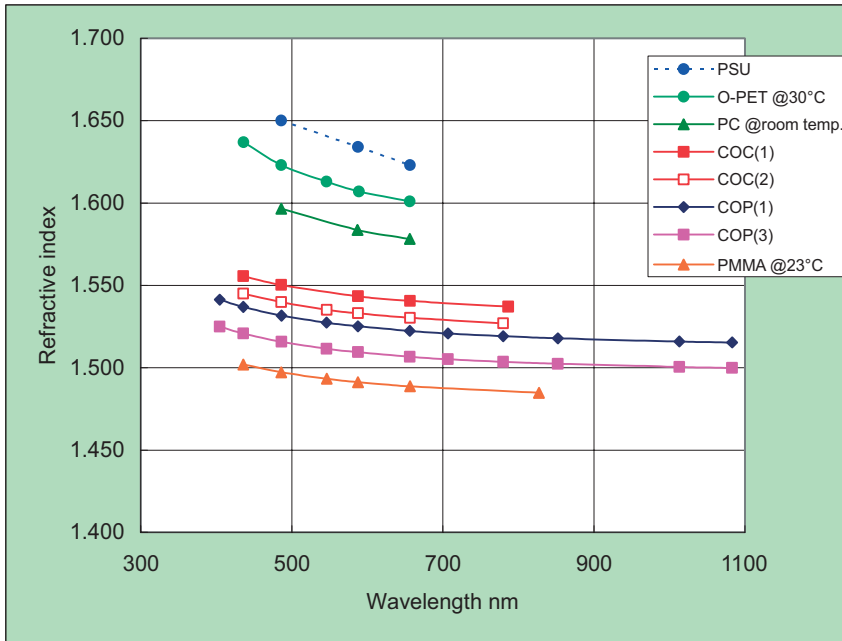
Figure 5.3 Wavelength dependence of refractive index for various polymers at 25 °C.
PC: Panlite at room temperature; PMMA: Parapet at 23 °C; COC(1): APEL™ 5104DP;
COC(2): TOPAS® 5013; COP(1): ZEONEX® 480R; COP(3): ZEONEX® 330R;
PSU: Udel® P-1700; O-PET: OKP-4.

Table 5.1 [6–12]. Usually an almost straight line can be observed for all polymers when plotting refractive index against Abbe number.

Table 5.1 Abbe numbers and refractive indices of optical polymers.

material	brand name	temperature (°C)	refractive index, D-line (587.6 nm)	Abbe number, V_D
polycarbonate	PANLITE®	room temp.	1.5836	31.7
poly(methyl methacrylate)	PARAPET®	23	1.4913	58.5
cycloolefin polymer	APEL™ 5014DP	25	1.5434	56.2
	TOPAS® 5013	25	1.5333	56.1
	ZEONEX® 480R	25	1.5251	56.0
	ARTON® FX4727	25	1.523	52.0
polysulfone	Udel® P-1700	–	1.634	23.5
optical polyester	OKP-4	30	1.6070	27.6

Plastics usually have a larger linear coefficient of expansion $(5 \times 10^{-5} - 10 \times 10^{-5})$ than glass $(5 \times 10^{-6} - 10 \times 10^{-6})$. Additionally, the specific volume of plastics is strongly affected by temperature and pressure, especially above the glass transition temperature (Figure 5.4). Commonly optical elements made from thermoplastics are fabricated by injection molding. In a certain molding process, melted plastic is pressed and flowed into the mold cavity and then cooled rapidly. Because this melted plastic is cooled from the skin layer to core in the injection molding process, temperature and pressure distributions occur in the molding. By this means, certain density distributions, i.e., refractive index distributions, are generated in the molding. These distributions are affected by sprue/runner shapes and injection and cooling conditions.

As mentioned above, it is important to control optical properties by specifying mold designs and molding conditions. Generally, one way to avoid nonuniformity of cooling is to keep the mold temperature high and to fill the mold with melted plastic in the shortest possible time. Recently, certain molding technologies have been under consideration in order to control refractive index distribution using molding techniques [13].
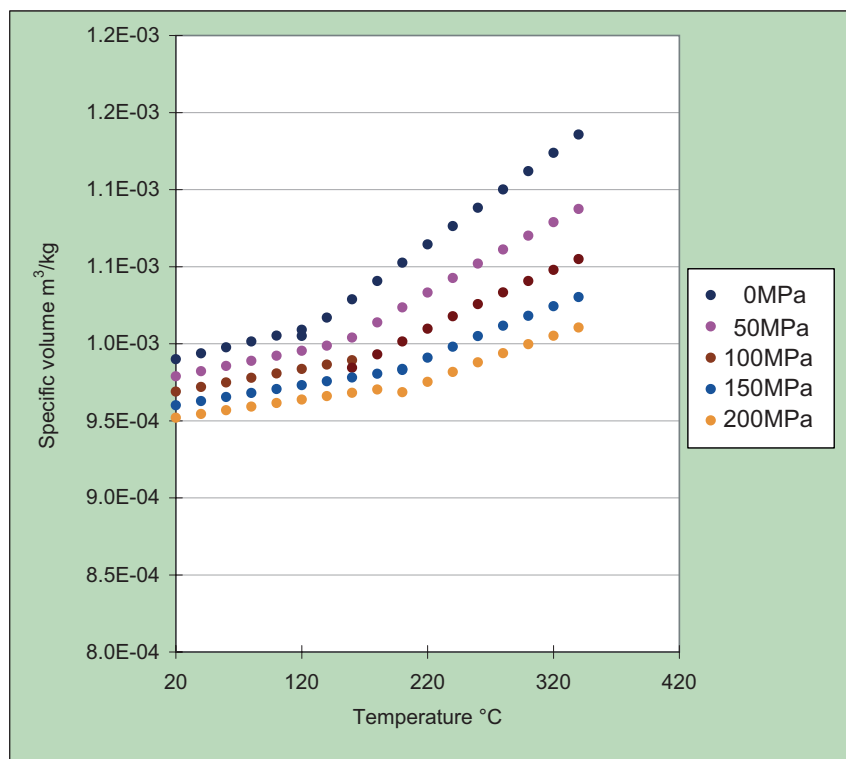
Figure 5.4 Dependence of specific volume on temperature and pressure. Polymer: ZEONEX® E48R.

5.2.3
Birefringence

Another important property of optical parts is the birefringence that appears in a molding. When light passes through a material, velocities of light differ between two orthogonally arranged vibrating surfaces. This is called birefringence. If this phenomenon occurs in lenses, they become sensitive to orientation when used in polarized light, or no image formation can be achieved around the focal area.

There are several explanations for the cause of birefringence of polymers. Generally birefringence is categorized into: (1) orientational birefringence given by

$$\Delta n = f \Delta n_0 \qquad (5.6)$$

where f is the orientational coefficient, n the average refractive index, and Δn_0 the intrinsic birefringence given by

$$\Delta n_0 = \frac{2\pi}{9} \frac{(n^2 + 2)^2}{n} \frac{\rho}{M} N_A \Delta a \qquad (5.7)$$

in which ρ is the density, M the molecular weight per unit, N_A Avogadro's number, and Δa the major difference of polarizability; and (2) stress birefringence given by

$$\Delta n_s = C\sigma \qquad (5.8)$$

where C is the photoelastic coefficient and σ the stress. In these cases, each polymer has characteristic constants of intrinsic birefringence and photoelastic coefficient. Tables 5.2 and 5.3 give the intrinsic birefringence and photoelastic coefficient, respectively, of several polymers [14].

Table 5.2 Intrinsic birefringence of polymers.

polymer	intrinsic birefringence, Δn_0
polystyrene	−0.1
PPE[a]	0.21
PC	0.106
PVC	0.027
PMMA	−0.0043
PET	0.105
PE	0.044

a)   Poly(phenylene ether).

Table 5.3 Photoelastic coefficients of polymers.

polymer	photoelastic coefficient, C ($\times 10^{-13}$ cm²/dyn)
PMMA	−6
PC	72
COP (ZEONEX® 480R)	6.5
PS	−55

As for a specific method to minimize the birefringence of polymers, the refractive index or polarizability may be minimized using Eq. (5.6). To minimize polarizability, various measures have been recently used such as the introduction of alicyclic structures into the main chain. In order to minimize the stress birefringence of Eq. (5.8), the synthesis of structures with positive and negative constant birefringence within the same macromolecule has been reported.

5.2.4
Stability

5.2.4.1   Heat Resistance
Heat resistance may be required depending on the intended service environment of optical plastics. Normally stability to 85 °C is required for laser beam printer (LBP), CD/DVD, and cameras for cellular phones. For automotive applications in the passenger area, the temperature specification is up to 100–110 °C; for applications in the engine area, it is up to 150 °C.

Optical polymers are required to have higher deflection temperature under load than 85 °C. Figure 5.5 shows a comparison of the deflection temperature under load for various optical polymers [6–12].

Some plastics cannot be used in situations involving large environmental changes, because the temperature dependence of refractive index, dn/dT, of plastics is about 10–100 times higher than that of glass. For instance, Table 5.4 gives a comparison of the focal shifts of plastic and glass lenses. Both lenses have a focal distance of approximately 20 mm and thickness of 2 mm with a temperature change from 20 to 80 °C calculated by

$$f = \frac{R_1 R_2 n}{(n-1)[n(R_1 - R_2) + (n-1)d]} \tag{5.9}$$

where n is the refractive index, R_1 and R_2 the radii of curvature of the lens, and d the thickness of the lens. In this case, the focal shift value of the plastic lens is approximately 19 times larger than that of the glass lens. It is necessary to consider this fact when designing optic elements made of plastics.
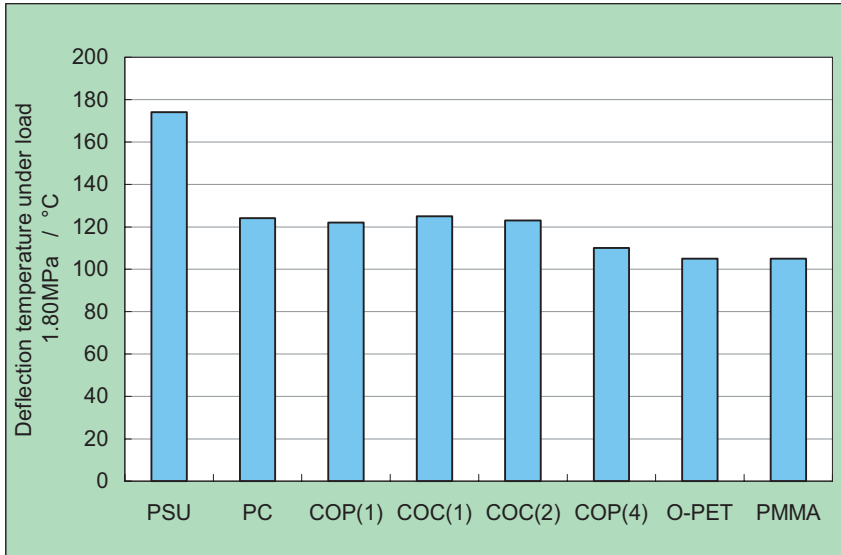
Figure 5.5 Comparison of the deflection temperature under load for various optical polymers. PC: PANLITE® AD5503; PMMA: ACRYPET™ VH; COC(1): APEL™ 5104DP; COC(2): TOPAS® 5013; COP(1): ZEONEX® 480R; COP(4): ARTON® FX4727; PSU: Udel® P-1700; O-PET: OKP-4.

Table 5.4 Comparison of focal shifts of plastic and glass lenses.

	plastic: ZEONEX® 480R		glass: Schott N-BK7	
linear expansion coefficient	6.0×10^{-5}		7.1×10^{-6}	
temperature (°C)	20	80	20	80
r_1 (mm)	34	34.122	32	32.014
r_2 (mm)	−15	−15.054	−15	−15.006
refractive index, n	1.52784	1.52140	1.51872	1.51891
thickness, d (mm)	2.0	2.0072	2.000	2.0009
focal distance, f (mm)	20.0	20.32	19.979	19.980
refractive index shift		−0.006		−0.0002
focal shift		0.318		0.001

5.2.4.2 Moisture Absorption

The influence of volume change on optical properties in high-temperature and high-humidity environments cannot be clearly expressed. Usually, the reliability of an optical device is evaluated by accelerated tests in high-temperature and high-

humidity environments. For example, it is determined using the performance change of an optical device under conditions of 60 °C, 90% RH, and 500 h duration as a reference. Figure 5.6 shows the water absorption of some major optical plastics [6–12].
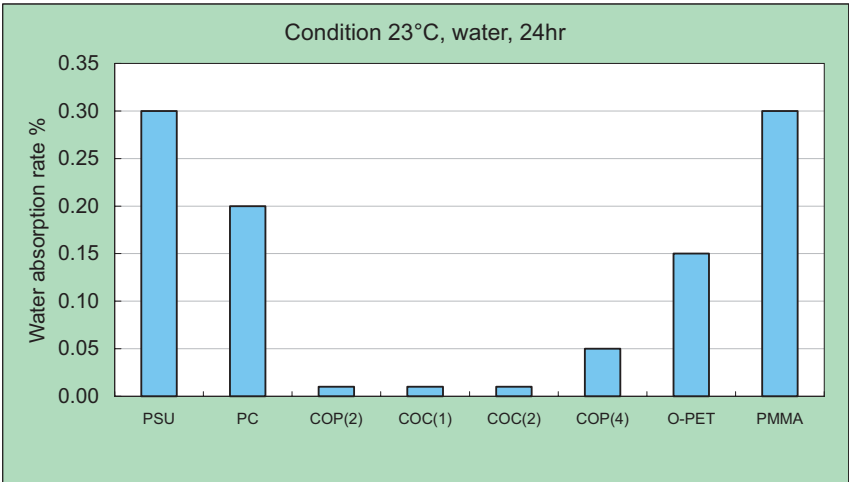
Figure 5.6 Comparison of the water absorption of some optical polymers. PC: PANLITE® AD5503; PMMA: ACRYPET™ VH; COC(1): APEL™ 5104DP; COC(2): TOPAS® 5013; COP(2): ZEONEX® E48R; COP(4): ARTON® FX4727; PSU: Udel® P-1700; O-PET: OKP-4.
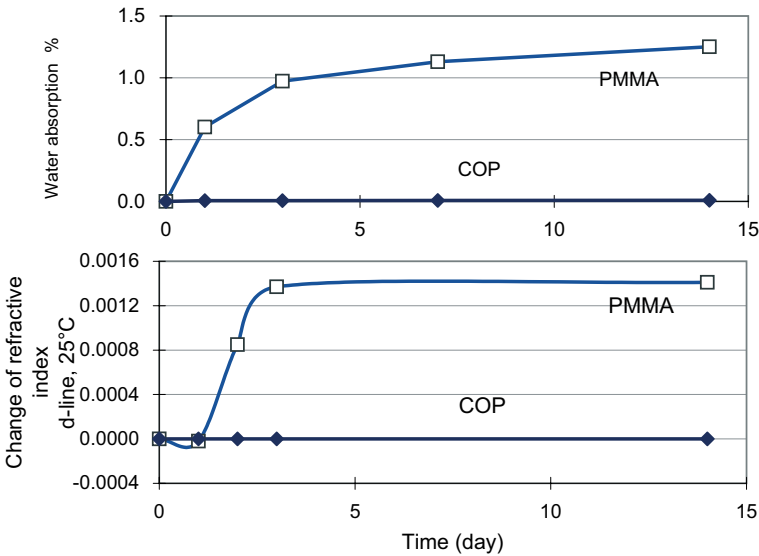
Figure 5.7 Change of refractive index due to water absorption for PMMA (DELPET® 80NH) and COP (ZEONEX® E48R). Sample thickness 3 mm; condition: 50 °C, 90% RH; measurement by V-block method at 23 °C, 50% RH; instrument: Kalnew precision refractometer KPR-200.

Even a relatively small water absorption affects size distortion and density. In order to obtain optically stable materials various developments have been attempted to reduce the water absorption. From recent actual examples, the introduction of alicyclic structures and the use of a polyolefin with alicyclic structure (cycloolefin polymer) have produced good results. Figure 5.7 shows the change of refractive index due to water absorption for PMMA and COP. From these data it can be seen that the refractive index is much affected by water absorption. The details are discussed later.

5.2.4.3 Residual Stress

It is also important to prevent size distortion and tilt due to the residual stress at the time of plastic molding. Optimization of molding conditions will minimize the residual stress of a molded item and, as a result, minimize warp progression. Large residual stress can also be removed by annealing below the glass transition temperature (see Figure 5.8).
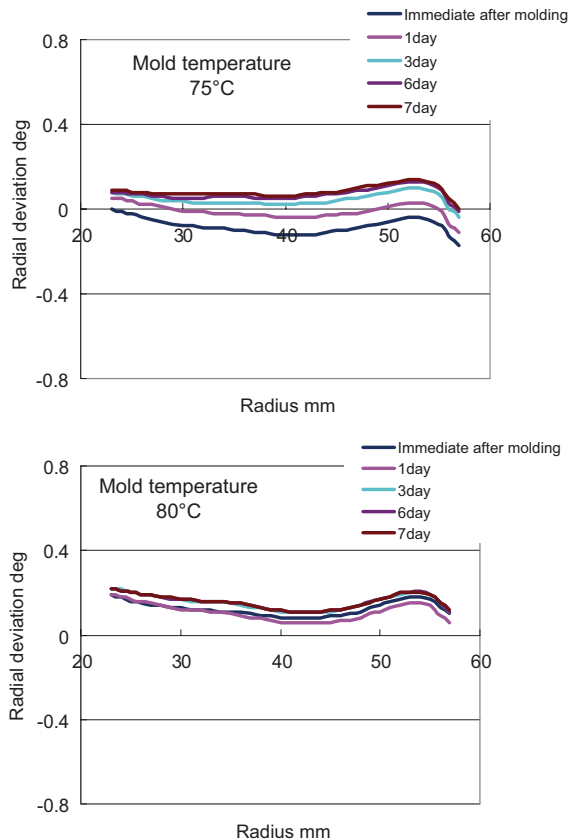
Figure 5.8 Change of radial deviation of optical disc. Sample thickness 0.6 mm, diameter 120 mm, optical disc substrates made from COP (ZEONOR® 1060R), measurements at room temperature.

**5.3
Plastics**

5.3.1
Acrylate Polymers

5.3.1.1 **PMMA**
This is one of the major materials used in optical plastics. It is made by polymerizing the monomer methyl methacrylate. It is used as a pellet-shaped material for processing or offered as cast board manufactured by polymerizing the monomer by pouring it into a mold sandwiched between glass boards. The chemical structure of PMMA is shown in Figure 5.9.
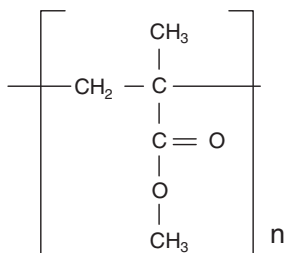
Figure 5.9 Chemical structure of PMMA.

The material characteristics are as follows:

- high transparency;
- low birefringence;
- outstanding hardness;
- high light deterioration resistance; and
- high Abbe number.

Tables 5.5 and 5.6 give catalog values for PMMA polymers offered by Mitsubishi Rayon Co. Ltd. and Kuraray Co. Ltd [7, 15]. With its high transparency and hardness, PMMA is used in various transparent parts.

As for optical use, PMMA is used in large lenses such as condensers, Fresnel lenses, projection TV lenses, and lenses for car lamps; it is also used for small- to medium-sized high-precision lenses such as optical lenses for LBP, lenses for disposable cameras, and optical pick-up lenses. With its high transparency it is also used in light guide plates for LCD backlights and in light diffusing devices for illumination in which elements are diffused. It is also used in cover materials for displays, instruments, and gauges, and for the covers of rear lights of automobiles.

Table 5.5 Typical properties of poly(methyl methacrylate): ACRYPET™ (Mitsubishi Rayon Co. Ltd).

property	test method	test condition	unit	standard grade					high-impact grade											
				VH	MD	MF	V	VH5	IR H70	IR H50	IR H30	IR D70	IR D50	IR D30	IR G504	IR G304	IR K304	IR S404	VR L40	VR L20A
physical																				
density	JIS K7112		g/cm³	1.19	1.19	1.19	1.19	1.19	1.14	1.16	1.17	1.14	1.16	1.17	1.16	1.17	1.17	1.16	1.16	1.17
light transmittance	JIS K7361	3 mm	%	92.5	93	93	93	93	92	92	92	92	92	92	92	92	92	92	92	92
haze	JIS K7136	3 mm	%	0.3	0.3	0.3	0.3	0.3	0.6	0.6	0.4	0.6	0.6	0.4	0.7	0.5	0.5	0.5	0.5	0.4
refractive index	JIS K7142	n_d	–	1.49	1.49	1.49	1.49	1.49	1.49	1.49	1.49	1.49	1.49	1.49	1.49	1.49	1.49	1.49	1.49	1.49
water absorbance	JIS K7209	24 h	%	0.3	0.3	0.3	0.3	0.3	0.3	0.3	0.3	0.3	0.3	0.3	0.3	0.3	0.3	0.3	0.3	0.3
thermal																				
specific heat	JIS K7123		J/g/°C	1.5	1.5	1.5	1.5	1.5	1.5	1.5	1.5	1.5	1.5	1.5	1.5	1.5	1.5	1.5	1.5	1.5
coefficient of linear expansion	JIS K7197		1/°C	6×10^{-5}	6×10^{-5}	6×10^{-5}	6×10^{-5}	6×10^{-5}	6×10^{-5}	6×10^{-5}	6×10^{-5}	6×10^{-5}	6×10^{-5}	6×10^{-5}	6×10^{-5}	6×10^{-5}	6×10^{-5}	6×10^{-5}	6×10^{-5}	6×10^{-5}
heat conductivity	JIS A1412		W/m/°C	0.2	0.2	0.2	0.2	0.2	0.2	0.2	0.2	0.2	0.2	0.2	0.2	0.2	0.2	0.2	0.2	0.2
heat deflection temp.	JIS K7191	1.80 MPa	°C	101	87	84	94	101	82	87	93	78	82	85	85	93	92	83	93	95
Vicat softening point	JIS K7206	50 N	°C	108	94	88	100	108	78	88	98	73	84	90	88	99	99	87	98	104
melt flow rate	JIS K7210	230 °C, 37.3 N	g/10 min	2	6	14	2.2	5.5	0.8	1.3	1.8	1.1	2.5	4.3	1.1	1.5	3.1	7.8	2.6	4.3
spiral flow length (2 mm thickness)	MRC	230 °C	mm	130	190	250	150	180	170	170	170	200	230	230	120	120	150	230	130	230
		250 °C	mm	220	290	370	230	290	260	260	260	290	310	320	200	210	270	330	220	320
mechanical																				
tensile stress at load	JIS K7162	1A/5	MPa	78	72	69	75	62	34	44	59	32	43	54	46	58	56	48	44	60
elongation at break	JIS K7162	1A/5	%	6	6	5	8	5	90	90	80	90	90	80	85	78	65	90	80	50

Table 5.5 Continued.

property	test method	test condition	unit	standard grade					high-impact grade											
				VH	MD	MF	V	VH5	IR H70	IR H50	IR H30	IR D70	IR D50	IR D30	IR G504	IR G304	IR K304	IR S404	VR L40	VR L20A
tensile modulus	JIS K7162	1A/1	GPa	3.3	3.3	3.2	3.3	3.3	1.5	1.9	2.5	1.5	1.9	2.5	1.9	2.5	2.5	2	2.2	2.5
flexural stress at yield	JIS K7171		MPa	127	117	114	126	92	48	68	93	45	66	90	70	90	79	78	71	89
flexural modulus at yield	JIS K7171		GPa	3.3	3.3	3.2	3.3	3.3	1.5	1.9	2.5	1.5	1.9	2.5	1.9	2.5	2.4	2	2.2	2.6
Izod impact strength	JIS K7110	1A	kJ/m^2	1.7	1.6	1.6	1.7	1.6	8.8	4.9	2.5	8.8	4.4	2	5.8	3.8	3.4	3.9	11	3.7
Charpy impact strength	JIS K7111	1eU un-notched	kJ/m^2	21	21	20	22	21	111	62	32	110	55	25	73	48	43	49	140	47
		1eAV notched	kJ/m^2	1.3	1.3	1.2	1.4	1.2	6.9	3.9	2	6.7	3.4	1.6	4.6	2.9	2.7	3.1	8.5	2.9
Rockwell hardness	JIS K7202	M scale	–	101	94	92	98	101	38	55	77	33	52	67	66	80	80	70	69	85
electrical																				
surface resistivity	JIS K6911		Ω	$>10^{16}$	$>10^{16}$	$>10^{16}$	$>10^{16}$	$>10^{16}$	$>10^{16}$	$>10^{16}$	$>10^{16}$	$>10^{16}$	$>10^{16}$	$>10^{16}$	$>10^{16}$	$>10^{16}$	$>10^{16}$	$>10^{16}$	$>10^{16}$	$>10^{16}$
volume resistivity	JIS K6911		Ω m	$>10^{13}$	$>10^{13}$	$>10^{13}$	$>10^{13}$	$>10^{13}$	$>10^{13}$	$>10^{13}$	$>10^{13}$	$>10^{13}$	$>10^{13}$	$>10^{13}$	$>10^{13}$	$>10^{13}$	$>10^{13}$	$>10^{13}$	$>10^{13}$	$>10^{13}$
dielectric breakdown strength	JIS K6911	4 kV/s	MV/m	20	20	20	20	20	20	20	20	20	20	20	20	20	20	20	20	20
dielectric constant	JIS K6911	60 Hz	–	3.7	3.7	3.7	3.7	3.7	3.7	3.7	3.7	3.7	3.7	3.7	3.7	3.7	3.7	3.7	3.7	3.7
dielectric loss	JIS K6911	60 Hz	–	0.05	0.05	0.05	0.05	0.05	0.05	0.05	0.05	0.05	0.05	0.05	0.05	0.05	0.05	0.05	0.05	0.05
arc resistance	JIS K6911		–	no trace	no trace	no trace	no trace	no trace	no trace	no trace	no trace	no trace	no trace	no trace	no trace	no trace	no trace	no trace	no trace	no trace

Table 5.6 Typical properties of poly(methyl methacrylate): PARAPET® (Kuraray Co. Ltd).

property	ISO	JIS	condi-tion	unit	GF high flow	G general purpose	EH extrusion	HR-L heat resistance	HR-G heat and solvent resistance	HR-F heat resistance, good flow	HR-S heat resistance	GH-S light conductor	GH-SN light conductor (UVA added)
					general purpose grade			standard (heat resistance) grade			optical grade		
optical													
light transmittance	ISO 13468-1	JIS K7361-1	3 mm	%	>92	>92	>92	>92	>92	>92	>92	>92	>92
haze	ISO 14782	JIS K7136	3 mm	%	<0.3	<0.3	<0.3	lt0.3	<0.3	<0.3	<0.3	<0.3	<0.3
refractive index	ISO 489	JIS K7142	n_d	–	1.49	1.49	1.49	1.49	1.49	1.49	1.49	1.49	1.49
mechanical													
tensile modulus	ISO 527-2	JIS K7162	1A/1	MPa	3300	3300	3300	3300	3300	3300	3300	3300	3300
tensile strength at break	ISO 527-2	JIS K7162	1A/5	MPa	67	70	75	77	78	65	77	62	62
tensile strain at break	ISO 527-2	JIS K7162	1A/5	%	3	4	7	5	7	3	5	2	2
flexural modulus	ISO 178	JIS K7171		MPa	3300	3300	3300	3300	3300	3300	3300	330	3300
flexural stress at break	ISO 178	JIS K7171		MPa	108	110	125	128	126	100	114	90	90
Charpy impact strength, unnotched	ISO 179	JIS K7111	1eU	kJ/m²	19	20	23	22	23	20	22	20	20
Charpy impact strength, notched	ISO 179	JIS K7111	1eA	kJ/m²	1.3	1.3	1.4	1.4	1.4	1.3	1.4	1.3	1.3
Rockwell hardness	ISO 2039-2	JIS K7202	M scale	–	94	98	99	102	99	102	103	100	100
thermal													
temperature of deflection under load, annealed	ISO 75-2	JIS K7191	1.82 MPa	°C	86	93	93	101	94	101	101	95	95
Vicat softening point	ISO 306	–	B50	°C	92	99	101	110	103	108	110	104	104
melt flow rate	ISO 1133	–	230 °C, 37.3 N	g/10 min	15	8	1.3	2	0.6	5.5	2.4	10	10

Table 5.6 Continued.

property	test method ISO	JIS	condition	unit	general purpose grade			standard (heat resistance) grade				optical grade	
					GF high flow	G general purpose	EH extrusion	HR-L heat resistance	HR-G heat and solvent resistance	HR-F heat resistance, good flow	HR-S heat resistance	GH-S light conductor	GH-SN light conductor (UVA added)
electrical													
surface resistivity		JIS K6911		Ω	$>10^{16}$	$>10^{16}$	$>10^{16}$	$>10^{16}$	$>10^{16}$	$>10^{16}$	$>10^{16}$	$>10^{16}$	$>10^{16}$
volume resistivity		JIS K6911		Ω m	$>10^{13}$	$>10^{13}$	$>10^{13}$	$>10^{13}$	$>10^{13}$	$>10^{13}$	$>10^{13}$	$>10^{13}$	$>10^{13}$
dielectric strength		JIS K6911	4 kV/s	MV/m	20	20	20	20	20	20	20	20	20
dielectric constant		JIS K6911	60 Hz	–	4	4	4	4	4	4	4	4	4
other													
density	ISO 1183	JIS K7112		g/cm^3	1.19	1.19	1.19	1.19	1.19	1.19	1.19	1.19	1.19
water absorption at 23 °C	ISO 62, method 1		24 h	%	0.3	0.3	0.3	0.3	0.3	0.3	0.3	0.3	0.3
shrinkage of moldings	ISO 8328	–		%	0.2–0.6	0.2–0.6	0.2–0.6	0.2–0.6	0.2–0.6	0.2–0.6	0.2–0.6	0.2–0.6	0.2–0.6
flammability	UL 94			class	HB	HB	HB	HB	HB	HB	HB	HB	HB

Note: Values reported are typical and should not be used for specification purposes.
Source: Molding Materials Sales Dept, Methacrylate Company, Kuraray Co. Ltd.

The problems of PMMA as an optical material include (1) water absorbing property: change of refractive index and size due to water absorption; and (2) heat resistance: glass transition temperature of 100 °C is insufficient in some environments. The development of various polymers is in progress to solve these problems.

Various companies have shown good results of their own efforts to minimize birefringence, ideally to zero. One well-known example is the development of an acrylate-containing alicyclic structure by Professor Koike of Keio University and Hitachi Chemical Co. Ltd [16].

5.3.2
Polycarbonate

5.3.2.1 Optical Polycarbonate

Polycarbonate (PC) is the most commonly used optical material. General PC is polymerized from bisphenol-A with carbonyl chloride or diphenylether. It is mostly used for CD-DA. It is also used for optical discs including CD-ROM, CD-R/RW, MD, DVD-ROM, DVD-Video, and DVD±R/RW. The chemical structure is shown in Figure 5.10.
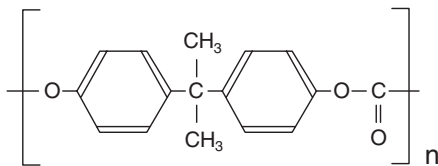

Figure 5.10 Chemical structure of PC.

The characteristics of PC are as follows:

- low levels of impurities;
- transparency;
- high refractive index, high scattering;
- heat resistance;
- moldability (transferability); and
- high intensity.

With these characteristics it is not only used for optical discs but also for optical lenses and optical films for liquid crystals. It has one of the best impact strengths among the various engineering plastics, and thus is used for multiple purposes. It is also used for grading of building materials and for lenses for car lamps. The suppliers are Sabic Innovative Plastics, Bayer, Dow Chemical, Teijin Chemicals, Mitsubishi Engineering Plastics, Idemitsu Petrochemical, Asahikasei, and others. It is the most widely used material for optical disc storage. Table 5.7 gives the physical properties of PANLITE® AD-5503 offered by Teijin Chemicals Co. Ltd [6].

Table 5.7 Typical properties of polycarbonate: PANLITE®
(Teijin Chemicals Ltd).

property	unit	test method	condition	AD-5503	L-1225Y
density	kg/m^3	ISO 1183	–	1200	1200
water absorption	%	ISO 62	in water; 23 °C, 24 h	0.2	0.2
light transmittance	%	ASTM D1003	3 mm thickness	89	88
refractive index	–	ASTM D542	–	1.585	1.585
Abbe number	–	ASTM D542	–	30	30
tensile modulus	MPa	ISO 527-1 and -2	1 mm/min	2450	2400
tensile yield stress	MPa	ISO 527-1 and -2	50 mm/min	63	62
tensile yield distortion	%	ISO 527-1 and -2	50 mm/min	6	6
tensile fracture designation distortion	%	ISO 527-1 and -2	50 mm/min	>50	>50
flexural modulus	MPa	ISO 178	2 mm/min	2400	2350
flexural strength	MPa	ISO 178	2 mm/min	96	92
load-deflection temperature	°C	ISO 75-1 and -2	1.80 MPa	124	128
			0.45 MPa	138	141
coefficient of linear expansion	×10^{-4}/°C	ISO 11359-2	parallel	0.7	0.7
			vertical	0.7	0.7

A problem with PC is that it has large birefringence. The photoelastic coefficient of PC is approximately 10 times greater than that of PMMA. Thus, for high-density optical discs, such as magnetic optical discs, when the incident angle is large, the birefringence becomes large. This may cause read errors. The following measures can be taken to reduce the birefringence [17]:

- improvement of fluidity;
- introduction of monomer with structure different from bisphenol-A; and
- mixing with other materials, such as polystyrene, that off-set the large photo-elastic coefficient.

5.3.2.2 Low-Birefringence Polycarbonate: ST-3000

Teijin-Bayer Polytec Ltd, jointly operated by Teijin Chemicals and Bayer, under-took a joint development and has now started marketing a new material called ST-3000, a low-birefringence PC [18, 19]. This is a material that solves the problems of the large birefringence of conventional PC. Compared to conventional PC it is characterized by the following:

- 50% lower birefringence than normal PC;
- 25% lower water absorption than normal PC; and
- high rigidity.

This material is used for some high-density optical discs and (optical) films that require a low birefringence, which can be achieved using this new material.

5.3.3
Cycloolefin Polymer

Recently COP, which was originally developed around 1990, has been used as an optical material for parts that require high quality. COP is a polymer with an alicyclic structure synthesized using a cycloolefin as a monomer. Its main chain has a bulky cyclic structure. This polymer is amorphous and has high transparency and heat resistance. It has also outstanding environmental durability and no hygroscopic property when it is composed only of hydrocarbons.

It has already been commercialized as ZEONEX® and ZEONOR® by Zeon Corporation, APEL™ by Mitsui Chemicals, TOPAS® by Topas Advanced Polymer GmbH, and, although not a complete carbon hydride, ARTON® by JSR.

These materials have high heat resistance and no property transformation due to moisture absorption. They are thus used in optical parts that would otherwise use PMMA.

5.3.3.1 ZEONEX®/ZEONOR® [20, 21]

The ZEONEX® materials are polymers obtained by ring-opening metathesis polymerization of norbornene derivatives and then complete hydrogenation of double bonds. The catalyst and other impurities used in the polymer synthesis have been almost completely removed. Its transparency is outstanding even among COPs. It is a transparent and colorless material with no light absorption in the visible region. The chemical structure is shown in Figure 5.11.
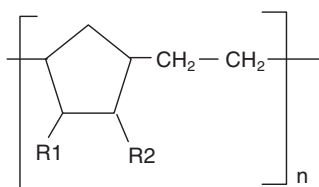

Figure 5.11 Chemical structure of COP.

The major characteristics are as follows:

- Low specific gravity (approximately 1.0). This is less than that of PMMA/PC.
- Transparent. No absorption in the whole visible region; almost the same transmittance as PMMA.
- Low water absorption. The lowest water absorption among optical plastics.

- Low scattering. Refractive index is approximately 1.51–1.53. The wavelength dependence is relatively weak.
- Low birefringence. Outstanding birefringence performance especially to diagonal incident light compared to PC. The optoelastic constant is the same as that of PMMA.
- Heat resistance. Glass transition temperature is 123–138 °C. This is sufficient for normal use.
- High processability. High fluidity and excellent and accurate moldability.

The general physical properties are given in Table 5.8. COP has the lowest water absorption among all transparent plastics. Thus distortion or change of optical properties due to water absorption is a minimum (Figure 5.12). This plastic is suitable for optical devices such as lasers used for the visible region.

The photoelastic coefficient of ZEONEX® or other COPs is less than that of PC and the same as that of PMMA. The actual birefringence is higher than that PMMA and lower than that of PC. The dependence on the incidence angle of birefringence is less pronounced than for PC, and thus it has been used for optical discs (Figure 5.13).
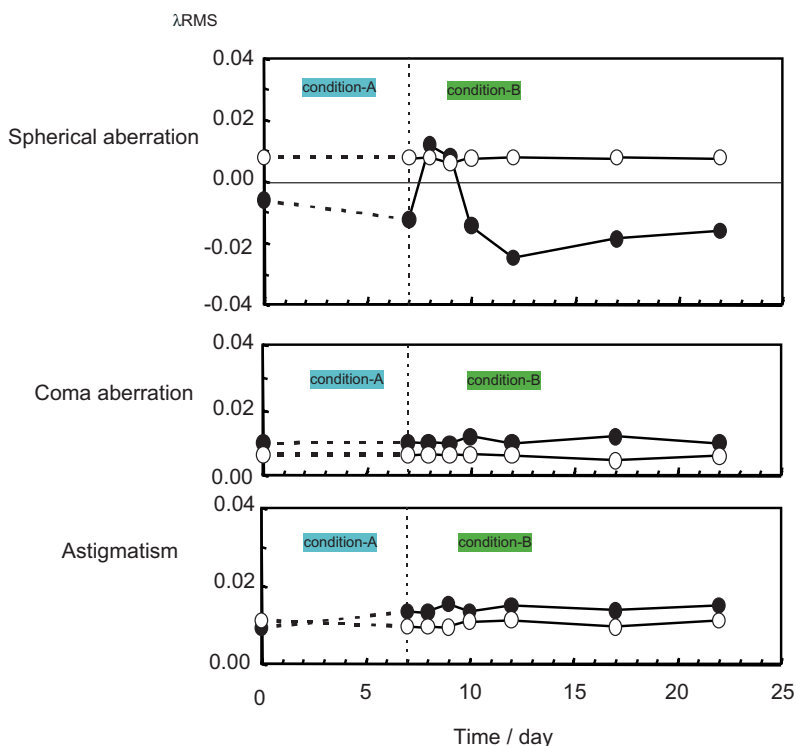

Figure 5.12 Change of the spherical aberration of optical lenses made from PMMA (filled circles) and COP (ZEONEX® 480R, open circles) under the condition of high temperature and humidity. Condition A: 60 °C, 90% RH, 168 hours; condition B: 25 °C, 50% RH.

Table 5.8 Typical properties of cycloolefin polymer: ZEONEX® (Zeon Corporation).

| property	unit	method	condition	480	480R	E48R	330R	F52R
specific gravity	–	ASTM D792	–	1.01	1.01	1.01	0.95	1.01
water absorbance	%	ASTM D570	–	<0.01	<0.01	<0.01	<0.01	<0.01
light transmittance	%	ASTM D1003	3 mm thickness	92	92	92	92	92
refractive index	–	ASTM D542	–	1.525	1.525	1.53	1.509	–
glass transition temperature	°C	JIS K7121	–	138	138	139	123	156
deflection temperature under load	°C	ASTM D648	1.80 MPa, no anneal	123	123	122	103	144
coefficient of linear expansion	1/°C	ASTM E831	–	6×10^{-5}	6×10^{-5}	6×10^{-5}	9×10^{-5}	6×10^{-5}
melt flow rate	g/10 min	JIS K6719	280 °C, 21.18 N 260 °C, 21.18 N	20 –	21	25 –	– 15	22 –
flexural modulus	MPa	ISO 178	–	2100	2100	2500	3100	2400
flexural strength	MPa	ISO 178	–	94	94	104	91	109
modulus of elasticity in tension	MPa	ISO 527	–	2200	2200	2500	–	3000
tensile strength	MPa	ISO 527	–	59	59	71	45	45
tensile elongation	%	ISO 527	–	40	40	10	3	2
Izod impact strength	J/m	ASTM D256	3.2 mm with notch	24	24	21	13	19
pencil hardness	–	JIS K5401	–	H	H	H	3H	F
volume resistivity	Ω cm	IEC 93	–	$>10^{16}$	$>10^{16}$	$>10^{16}$	$>10^{16}$	$>10^{16}$
dielectric breakdown strength	kV/mm	ASTM D149	Short-time method, 1 mm	40	40	40	40	60
dielectric constant	–	IEC 250	1 MHz	2.3	2.3	2.3	2.3	2.5
dielectric tangent	–	IEC 250	1 MHz	0.0002	0.0002	0.0002	0.0004	0.0002
flammability	–	UL standard	–	94HB	94HB	94HB	94HB	94HB
major applications	–	–	–	medical equipment, optical components	lenses, optical components	lenses, optical components	lenses, optical components	lenses, optical components
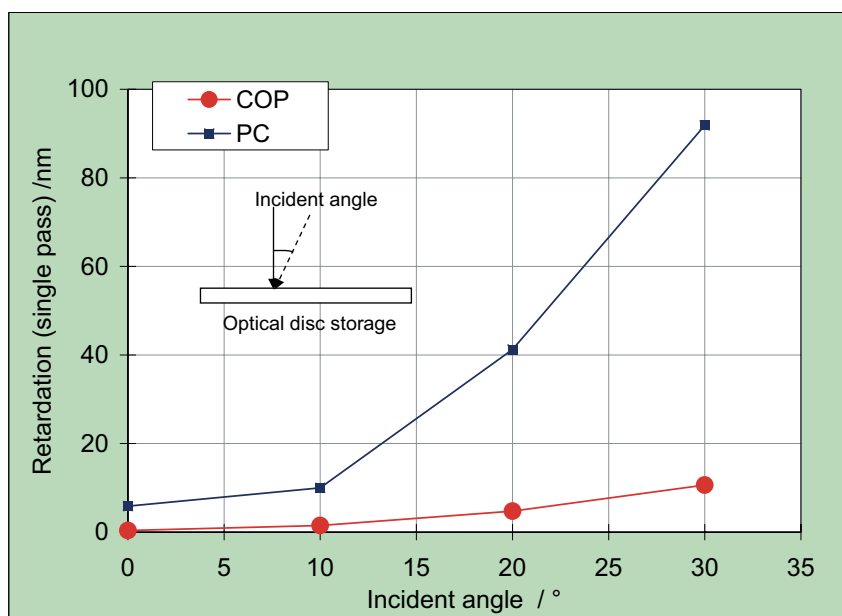
Figure 5.13 Comparison of incidence angle dependence of birefringence (retardation) of COP (ZEONEX® 480R) and PC. Sample: optical disc storage with diameter 86 mm and thickness 1.2 mm; measurement point: 30 mm distance from the center of the optical disc.

The transparency of ZEONEX® is at the same level or higher than that of PMMA, which is known to have the best light transmittance among transparent plastics. Thus, with this property and also because of its dimensional stability it is used for the prisms of compact cameras.

Recently, Zeon Corporation released ZEONEX® new grades, 340R/350R which designed for the blue laser pick-up lens, F52R for digital camera lens.

Zeon Corporation also offers ZEONOR®, which is a polymer characterized by transparency, high fluidity, and high heat resistance like ZEONEX® without refractive index or birefringence properties. With these characteristics, it is used for the transparent parts of optical discs and light guide plates for LCD backlights (Table 5.9).

Table 5.9 Typical properties of cycloolefin polymer: ZEONOR® (Zeon Corporation).

property	unit	method	condition	1020R	1060R
specific gravity	–	ASTM D792	–	1.01	1451.01
water absorbance	%	ASTM D570	–	<0.01	<0.01
light transmittance	%	ASTM D1003	3 mm thickness	92	92
glass transition temperature	°C	JIS K7121	–	105	100
deflection temperature under load	°C	ASTM D648	1.80 MPa	101	99
coefficient of linear expansion	1/°C	ASTM E831	–	7×10^{-5}	7×10^{-5}
melt flow rate	g/10 min	JIS K6719	280 °C, 21.18 N	20	–
			260 °C, 21.18 N	–	14
flexural modulus	MPa	ISO 178	–	2100	2100
flexural strength	MPa	ISO 178	–	80	76
tensile strength	MPa	ISO 527	–	53	53
modulus of elasticity in tension	MPa	ISO 527	–	2200	2100
tensile elongation	%	ISO 527	–	90	60
Izod impact strength	J/m	ASTM D256	with notch	60	18
Dupont impact strength	J	–	–	36	26
Rockwell hardness	–	ASTM D785	M scale	20	20
volume resistivity	Ω m	IEC 93	–	$>10^{16}$	$>10^{16}$
dielectric breakdown strength	kV/mm	ASTM D149	Short-time method, 1 mm	70	70
dielectric constant	–	IEC 250	1 MHz	2.3	2.3
dielectric tangent	–	IEC 250	1 MHz	0.0002	0.0002
flammability	–	UL-94	–	94HB	94HB
characteristics[a]	–	–	–	high moisture-proofing, high strength	high fluidity

Data represent experimental results and do not guarantee specific performance levels in actual usage.

a) Heat-resistant grades are also available.

5.3.3.2 Cycloolefin Copolymer (COC): APEL™/TOPAS®

As polymers synthesized by copolymerization of norbornenes and alpha-olefins, APEL™ and TOPAS® have been commercialized by Mitsui Chemical Co. Ltd and Topas Advanced Polymer GmbH, respectively.

The characteristics are very much similar to those of COP:

- low specific gravity;
- transparency;
- low water absorption;
- low scattering;
- low birefringence;
- heat resistance; and
- high processability.

They are particularly known for their low birefringence and high fluidity.

APEL™ is synthesized by copolymerization of tetracyclododecene (TCD) and alpha-olefin. Table 5.10 [22] gives the general physical properties. In particular, with a birefringence less than that of PMMA and transparency in the red laser region, it is often used in DVD pick-up lenses. The chemical structure of APEL™ is shown in Figure 5.14.
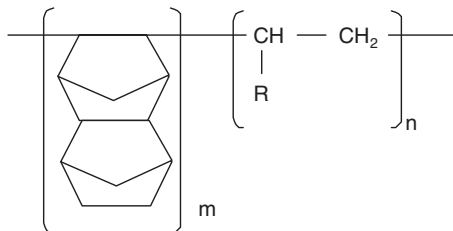

Figure 5.14 Chemical structure of APEL™.

TOPAS® is a copolymer of norbornene and alpha-olefin. Table 5.11 gives the general physical properties and Figure 5.15 shows the chemical structure. The birefringence is similar to that of PMMA; however, the transparency is outstandingly high. TOPAS® is used in various optical lenses.
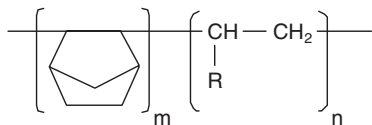
Figure 5.15 Chemical structure of TOPAS®.

Table 5.10 Typical properties of cycloolefin copolymer: APEL™ (Mitsui Chemicals).

property	method	unit	APL8008T	APL6509T	APL6011T	APL6013T	APL5014DP	APL6015T
TMA	Mitsui Chemicals method	°C	80	90	115	135	147	155
glass transition temperature	Mitsui Chemicals method	°C	70	80	105	125	135	145
density	ASTM D792	–	1.02	1.02	1.03	1.04	1.04	1.04
melt flow rate (260 °C, 2.16 kg)	ASTM D1238	g/10 min	15	30	22	15	36	7
heat deflection temp. (1.82 MPa)	ASTM D648	°C	60	70	95	115	125	135
tensile strength	ASTM D638	MPa	50	60	60	60	60	60
tensile elongation	ASTM D638	%	100	30	3	3	3	3
flexural modulus	ASTM D790	MPa	2400	2700	2700	3000	3200	3200
flexural strength	ASTM D790	MPa	90	100	110	110	100	110
Izod impact strength, notched	ASTM D256	J/m	45	35	25	25	25	25
Izod impact strength, unnotched	ASTM D256	kJ/m^2	33	20	15	15	10	10
water permeability	ASTM F1249	g mm/m^2/d	0.09	0.09	0.09	0.09	0.09	0.09
light transmittance	ASTM D1003	%	91	91	90	90	90	90
haze	ASTM D1003	%	2	2	3	3	4	4
refractive index	ASTM D542	–	1.54	1.54	1.54	1.54	1.54	1.54
mold shrinkage	Mitsui Chemicals method	%	0.6	0.6	0.6	0.6	0.6	0.6
applications	–	–	sheets, films	sheets, films	industrial components	hot-fill tainers	con-optical	medical

Table 5.11 Typical Properties of Cyclic Olefin Copolymer :TOPAS® / Topas Advanced Polymer GmbH

property	unit	method	5013L-10	6013S-04	6015S-04
physical					
density	g/cm^3	ISO1183	1.02	1.02	1.02
water absorption(23 °C/24h emersion)	%	ISO 62	<0.01	<0.01	<0.01
volume flow index @ 260 °C 2.16 kg	ml/10min	ISO 1133	48	14	4
mold shrinkage (mold T=60 °C, 2mm)	%	–	0.4–0.7	0.4–0.7	0.4–0.7
		ISO291–23/50 measured under standard conditions			
mechanical					
tensile stress @ yield	MPa	ISO 527 parts 1 and 2	45	63	60
elongation @ break	%		2.7	2.7	2.5
tensile modulus	MPa		3200	2900	3000
charpy impact strength(notched)	kJ/m^2	ISO 179/ eA	1.7	1.8	1.6
thermal					
DTUL HDT/B(0.45MPa)	°C	ISO 75 parts 1 and 2	126	130	150
glass transition temperature	°C	ISO 11357–1,-2,-3	134	138	158
coefficient of linear thermal expansion	°C^{-1}	ISO 11359 part 1 and 2	0.6×10^{-4}	0.6×10^{-4}	0.6×10^{-4}
flammability					
UL flammability rating	Class	UL-94 / 1.6mm	HB	HB	HB
optical					
light transmittance	%	ISO 13468–2	91.4	91	91
refractive index	–	–	1.53	1.53	1.53
Abbé number	–	–	56	–	55

5.3.3.3 Norborne Functional Polymer: ARTON®

JSR offers ARTON® which is a COP with ester groups. The ester groups cause some amount of water absorption compared with other COPs, but lead to easy surface coating, adhesion, and other surface treatments. Table 5.12 [10] gives the general physical properties and Figure 5.16 shows the chemical structure.
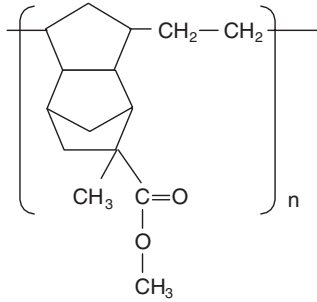
Figure 5.16 Chemical structure of ARTON®.

The characteristics of this polymer are as follows:

- low birefringence;
- high fluidity;
- high heat resistance; and
- easy surface treatment and adhesion.

It is used in optical films, optical lenses, and light guide plates for LCD.

Table 5.12 Typical properties of norbornene functional polymer: ARTON® (JSR).

property	unit	method	condition	F5023	FX4726	FX4727	D4531	D4532
optical								
refractive index	–	ASTM D542	D-line, 25 °C	1.512	1.522	1.523	1.515	1.514
transmittance	%	ASTM D1003	3.2 mm thickness	93	93	93	93	93
haze	%	ASTM D1003	3.2 mm thickness	0.6	0.6	0.6	0.6	0.6
Abbe number	–	ASTM D542	25 °C	57	52	52	57	57
stress optic coefficient	10^{-8} cm^2/N	JSR method	546 nm	3	1	1	4	4
birefringence	nm	ellipsometer	633 nm	<20	<20	<20	<20	<20
thermal								
glass transition temperature	°C	DSC	20 °C/min	167	125	120	135	145
heat deflection temperature	°C	ASTM D648	18.2×10^4 Pa	162	115	110	130	140
mold shrinkage	%	ASTM D955	MD direction	0.5–0.7	0.5–0.7	0.5–0.7	0.5–0.7	0.5–0.7
coefficient of linear expansion	10^{-5}/°C	ASTM D696		6	9	9	8	8
heat conductivity	W/m/°C	JSR method	100 °C	0.17	0.16	0.16	0.17	0.17
melt flow rate	g/10 min	JIS K7210	260 °C, 98 N	8	60	120	45	40
mechanical								
tensile stress	MPa	ASTM D638		75	75	70	75	75
elongation at break	%	ASTM D638		15	10	10	15	15
flexural stress	MPa	ASTM D790		125	120	120	120	120
flexural modulus	MPa	ASTM D790		3000	3000	3000	3000	3000
Izod impact strength	J/m	ASTM D256	$^1/_4$ in notched	20	20	20	20	20
Rockwell hardness	–	ASTM D785	R scale	125	125	125	125	125
pencil hardness	–	JIS K5401		H	H	H	H	H
electrical								
dielectric breakdown strength	kV/mm	ASTM D149	1 mm	30	30	30	30	30
volume resistivity	10^{16} Ω cm	ASTM D257		>1	>1	>1	>1	>1
dielectric constant	–	ASTM D150	1 MHz	3	3	3	3	3
dielectric loss	–	ASTM D150	1 MHz	0.02	0.01	0.01	0.02	0.02
arc resistance	s	ASTM D495	3 mm	190	180	180	190	190
chemical resistance								
dilute sulfuric acid		ASTM D543	soaking, 23 °C, 1 week	1	1	1	1	1
NaOH (10%)			1, tolerant	1	1	1	1	1
methyl alcohol			2, limited tolerance	1	1	1	1	1
isopropyl alcohol			3, not tolerant	1	1	1	1	1
acetone				2	2	2	2	2
toluene				3	3	3	3	3
methyl ethyl ketone (MEK)				2	2	2	2	2
other								
density	–	ASTM D792	–	1.08	1.06	1.06	1.08	1.08
water absorption	%	ASTM D570	23 °C, water, 1 week	0.4	0.2	0.2	0.2	0.3

5.3.4
Other Resin Materials

The challenges with optical plastics include the achievement of low birefringence, high refractive index, and high durability (low moisture absorption and high heat resistance).

5.3.4.1 **Optical Polyester (O-PET)**

A new type of polyester has been suggested for optical use [23]. The chemical structure of an example of such an optical polyester is shown in Figure 5.17 [24]. This polymer is synthesized from 9,9-bis[4-(2-hydroxyethoxy)phenyl]fluorine (BPFE), ethylene glycol, and dimethylterephthalate (DMT).
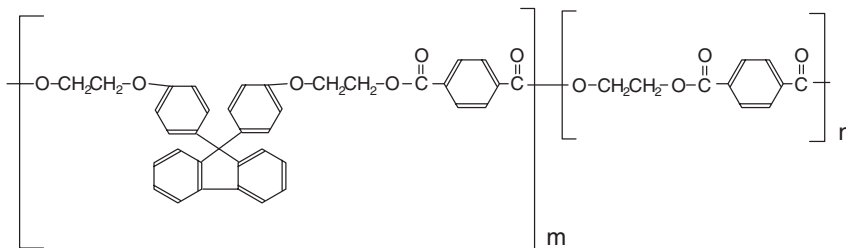

Figure 5.17 Chemical structure of an optical polyester.

Osaka Gas Co. Ltd and Kanebo Ltd have co-developed an amorphous polyester material, OKP-4. It is now available commercially from Osaka Gas Chemical. The characteristics of OKP-4 are as follows:

- high refractive index (>1.6); and
- low birefringence.

Table 5.13 gives the catalog values of some of its properties.

Table 5.13 Typical properties of optical polyester: OKP-4 (Osaka Gas Chemical).

property	unit	method	condition	OKP-4
density	kg/m^3	ISO 1183		1220
water absorption	%	ISO 62	water, 23 °C, 24 h	0.15
light transmittance	%	ASTM D1003	3 mm thickness	90
refractive index	–	ASTM D542	Abbe	1.607
Abbe number	–	ASTM D542		27
tensile modulus	MPa	JIS K7113		2000
tensile yield strength	MPa	JIS K7113		60
tensile yield distortion	%	JIS K7113		4
flexural modulus	MPa	JIS K7203		2300
flexural strength	MPa	JIS K7203		99
heat distortion temperature	°C	ISO 75-1 and -2	1.80 MPa	105
coefficient of linear expansion	10^{-4}/°C	ISO 11359-2		0.7

5.3.4.2 Polysulfone (PSU)

PSU is an excellent engineering plastic with high heat resistance. The characteristics of this polymer are as follows:

- Heat resistance. The heat deflection temperature is 343 °F (174 °C).
- High refractive index (>1.6).
- High intensity.

Typical applications of PSU are in food service components, plumbing fixtures, membranes, and laboratory animal cages. PSU is stable as regards stress, chemicals, and steam or gamma sterilization required for medical applications. PSU is not commonly used for optical purposes because it is colored yellow, but it is used in heat-stable lenses. The general physical properties of the PSU Udel® P-1700 are given in Table 5.14 [25] and its chemical structure is shown in Figure 5.18.

Table 5.14 Typical properties of polysulfone: Udel® P-1700.

property	method[a]	value[b]	value[c]
general			
specific gravity	D792	1.24	1.24
water absorption, 24 h	D570	0.30%	0.30%
melt flow at 343 °C, 2.16 kg	D1238	6.5 g/10 min	6.5 g/10 min
mold shrinkage	D955	0.007 in/in	0.007 mm/mm
mechanical			
tensile strength	D638	10.2 kpsi	70.3 MPa
tensile modulus	D638	360 kpsi	2.48 GPa
tensile elongation at break	D638	50–100%	50–100%
flexural strength	D790	15.4 kpsi	106.2 MPa
flexural modulus	D790	390 kpsi	2.69 GPa
tensile impact strength	D1822	200 ft-lb/in^2	420 kJ/m^2
Izod notched impact strength	D256	1.3 ft-lb/in	69 J/m
thermal			
deflection temperature at 264 psi (1.8 MPa)	D648	345 °F	174 °C
coefficient of linear expansion	D696	31 ppm/°F	56 ppm/°C
glass transition temperature		374 °F	190 °C
electrical			
dielectric strength	D149	425 V/mil	17 kV/mm
dielectric constant at 60 Hz	D150	3.3	3.3
dielectric constant at 103 Hz		2.9	2.9
dielectric constant at 106 Hz		4.1	4.1
dissipation factor at 60 Hz	D150	0.0007	0.0007

Table 5.14 Continued.

property	method[a]	value[b]	value[c]
dissipation factor at 103 Hz		0.001	0.001
dissipation factor at 106 Hz		0.006	0.006
volume resistivity	D257	$3 \times 10^{16} \, \Omega \, cm$	$3 \times 10^{16} \, \Omega \, cm$
color			
NT 11 (natural)		light amber	
NT 06 (natural)		very light amber	
CL 2611 (clear)		nearly water white	
optical			
refractive index	486.1 nm	1.650	
	587.6 nm	1.634	
	656.3 nm	1.623	
Abbe number		23	
light transmittance; 1.8/2.5/3.3 mm thickness	D1003	86/85/84%	
haze; 1.8/2.5/3.3 mm thickness	D1003	1.5/2.0/2.5%	
yellowness index; 1.8/2.5/3.3 mm thickness	D1925	7.0/10/13%	

a) ASTM.
b) US customary units.
c) SI units.
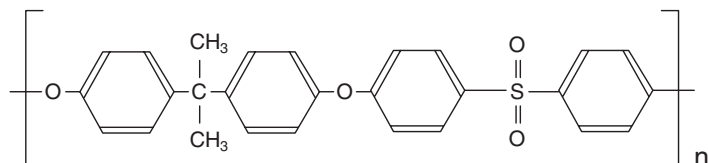
Figure 5.18 Chemical structure of PSU.

5.4
Summary

Table 5.15 gives the physical properties of various plastics for optical use. Table 5.16 gives the refractive index data reported by plastics suppliers. Figure 5.19 shows the retardation data for various plastics. Table 5.17 gives a comparison of some optical plastics. We select the materials that have characteristics in accordance with quality requirements.
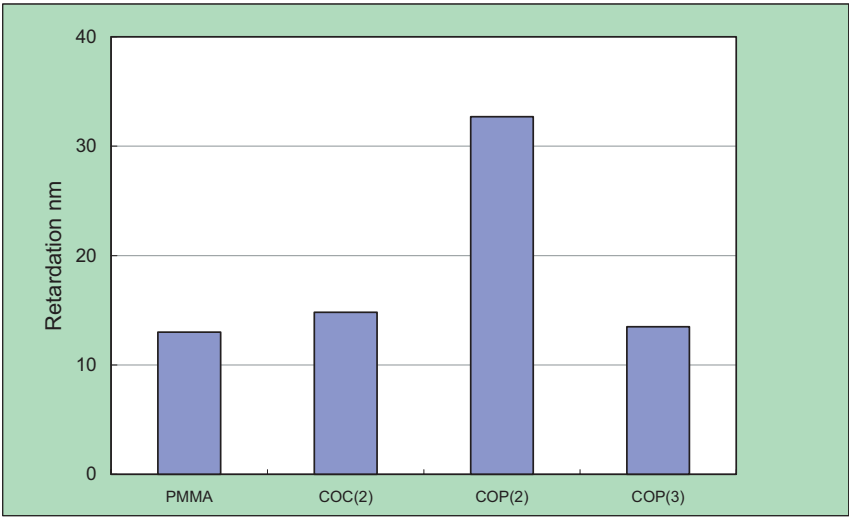
Figure 5.19 Retardation data for various polymers.
PMMA: ACRYPET™ VH; COC(2): TOPAS® 5013; COP(2): ZEONEX® E48R;
COP(3): ZEONEX® 330R.
Measurement by minute area automatic birefringence analyzer: KOBRA CCD, wavelength 590 nm. Sample: injection molded plate, size 65 × 65 × 3t mm. Measurement point: diagonally 75 mm distance from the gate which is located at one corner of the sample plate.

Table 5.15 Properties of various optical polymers.

property	unit	condition	PMMA: ACRYPET™ VH (Mitsubishi Rayon)	PC: PANLITE® AD5503 (Teijin Chemicals)	COP: ZEONEX® E48R (Zeon)	COP: ZEONEX® 330R (Zeon)	COC: APEL™ 5014DP (Mitsui Chemicals)	COC: TOPAS® 5013 (Topas Advanced Polymer GmbH)	COP: ARTON® FX4727 (JSR)	O-PET: OKP-4 (Osaka Gas Chemical)	PSU: Udel® P-1700 (Solvay)
specific gravity	–		1.19	1.2	1.01	1.01	1.04	1.02	1.06	1.22	1.24
water absorption	%		0.3	0.2	<0.01	<0.01	<0.01	<0.01	0.05*	0.15	0.3
light transmittance	%	3 mm thickness	92.5	89	92	92	90	92	93	90	84
refractive index	–		1.49	1.585	1.53	1.509	1.54	1.53	1.523	1.607	1.634
Abbe number	–		58	30	56	56	56	56	52	27	23
glass transition temperature	°C		106*	147	139	123	135	136	120	–	190
deflection temperature under load	°C	1.80 MPa	101	124	122	103	125	123	110	105	174
coefficient of linear expansion	1/°C		6×10⁻⁵	7×10⁻⁵	6×10⁻⁵	9×10⁻⁵	–	6×10⁻⁵	9×10⁻⁵	7×10⁻⁵	5.4×10⁻⁵
melt flow rate	g/10 min		2	–	25	15	36	56	120	–	6.5
		temperature:	230°C		280°C	230°C	260°C	260°C	260°C		343°C
		load:	37.3 N		21.18 N	21.18 N	2.16 kg	2.16 kg	98 N		2.16 kg
birefringence	nm	Zeon method	13	>80	32.7	13.5	2.0	14.8	42.6	–	–

* Measured by Zeon corporation.

Table 5.16a Refractive index of PMMA: PARAPET® HR1000S
(Kuraray Co. Ltd).

temperature (°C)	wavelength (nm)						Abbe number, V_D
	435.8	**486.1**	**546.1**	**587.6**	**656.3**	**827.3**	
23	1.5019	1.4972	1.4933	1.4193	1.4888	1.4848	58.5

Instrument: Kalnew KPR-20 precision refractometer.
Conditions: range = no. 1 (1.25–1.7); mode = auto stand.,
intermediate solvent; $n_d = 1.49$.

Table 5.16b Refractive index of PC: PANLITE® (Teijin Chemicals Ltd).

temperature	theoretical wavelength (nm)			Abbe number, V_D
	486 n_F	**587** n_d	**656** n_C	
room temp.	1.5966	1.5836	1.5782	31.7

Measurement: Atago 2T Abbe refractometer.
Light source: Mitsubishi Rayon ELI-050 halogen lamp.
Homogeneous light from JOBIN YVON H.20 UV;
wavelength 400–700 nm.

Table 5.16c Refractive index of cycloolefin polymer: ZEONEX® 480R (Zeon Corporation).

temperature (°C)	wavelength (nm)															Abbe number, V_D
	h 404.7	g 435.8	f 486.1	e 546.1	d 587.6	C 656.3	r 706.5	780.0	LD 780 785.1	LD 830 824.0	s 852.1	t 1013.2	1083.0	LD 1310 1310.1	LD 1550 1548.1	
−15	1.5456	1.5412	1.5359	1.5315	1.5293	1.5265	1.5250	1.5232			1.5219	1.5200	1.5194			56.3
0	1.5440	1.5396	1.5343	1.5300	1.5277	1.5250	1.5234	1.5217			1.5204	1.5185	1.5179			56.3
25	1.5413	1.5369	1.5317	1.5273	1.5251	1.5224	1.5208	1.5191			1.5179	1.5159	1.5153			56.2
40	1.5397	1.5352	1.5299	1.5257	1.5234	1.5207			1.5174	1.5169				1.51225	1.51123	56.6
60	1.5378	1.5329	1.5276	1.5234	1.5211	1.5184			1.5152	1.5147				1.50993	1.50895	6.6
80	1.5355	1.5308	1.5253	1.5214	1.5189	1.5164			1.5132	1.5126				1.50752	1.50669	58.3

Table 5.16d Refractive index of cycloolefin polymer: ZEONEX® E48R (Zeon Corporation).

temperature (°C)	wavelength (nm)															Abbe number, V_D
	h 404.7	g 435.8	f 486.1	e 546.1	d 587.6	C 656.3	r 706.5	780.0	LD 780 785.1	LD 830 824.0	s 852.1	t 1013.2	1083.0	LD 1310 1310.1	LD 1550 1548.1	
−15	1.5514	1.5469	1.5415	1.5371	1.5348	1.5320	1.5304	1.5286			1.5273	1.5253	1.5247			55.7
0	1.5501	1.5456	1.5402	1.5357	1.5334	1.5306	1.5290	1.5276			1.5260	1.5240	1.5234			55.8
25	1.5477	1.5432	1.5378	1.5334	1.5311	1.5283	1.5268	1.5250			1.5237	1.5217	1.5211			55.7
40	1.5454	1.5417	1.5363	1.5319	1.5296	1.5268			1.5234	1.5230				1.5182	1.5170	56.1
60	1.5446	1.5395	1.5342	1.5299	1.5275	1.5247			1.5214	1.5209				1.5161	1.5151	55.9
80	1.5421	1.5375	1.5320	1.5278	1.5254	1.5228			1.5195	1.5191				1.5141	1.5130	56.9

Table 5.16e Refractive index of cycloolefin polymer: ZEONEX® 330R (Zeon Corporation).

temperature (°C)	wavelength (nm)															Abbe number, V_D
	h 404.7	g 435.8	f 486.1	e 546.1	d 587.6	C 656.3	r 706.5	780.0	LD 780 785.1	LD 830 824.0	s 852.1	t 1013.2	1083.0	LD 1310 1310.1	LD 1550 1548.1	
−15	1.5293	1.5251	1.5200	1.5157	1.5136	1.5109	1.5094	1.5077			1.5065	1.5045	1.5040			56.5
0	1.5278	1.5235	1.5185	1.5143	1.5121	1.5094	1.5079	1.5062			1.5050	1.5031	1.5025			56.4
25	1.5250	1.5208	1.5157	1.5116	1.5094	1.5067	1.5052	1.5036			1.5024	1.5004	1.4999			56.5
40	1.5236	1.5192	1.5141	1.5101	1.5079	1.5052			1.5019	1.5016				1.4970	1.4960	57.0
60	1.5217	1.5169	1.5118	1.5078	1.5056	1.5030			1.4997	1.4993				1.4947	1.4937	57.3
80	1.5194	1.5145	1.5094	1.5053	1.5031	1.5004			1.4973	1.4969				1.4923	1.4913	56.2

Table 5.16f Refractive index of cycloolefin copolymer:
APEL™ 5014DP (Mitsui Chemicals Inc.).

temperature (°C)	wavelength (nm)					Abbe number, V_D
	g-line 435.8	F-line 486.1	d-line 587.6	C-line 656.5	LD 786.5	
5	1.5571	1.5518	1.5450	1.5421	1.5385	56.2
25	1.5556	1.5503	1.5434	1.5406	1.5371	56.0
50	1.5532	1.5478	1.5410	1.5382	1.5347	56.4
75	1.5505	1.5451	1.5383	1.5355	1.5320	56.1
dn/dT ($\times 10^{-5}$/°C)	−9.5	−9.7	−9.6	−9.5	−9.4	

Table 5.16g Refractive index of TOPAS® 5013L-10/
Topas Advanced Polymer GmbH

temperature °C	wavelength nm						vd Abbe number
	g	f	e	d	c	LD	
	435.8	486.1	546.1	587.6	656.3	780	
10	1.5462	1.5410	1.5365	1.5343	1.5315	1.5281	56.2
25	1.5450	1.5398	1.5352	1.5331	1.5303	1.5270	56.1
40	1.5437	1.5383	1.5339	1.5316	1.5288	1.5255	56.0
60	1.5417	1.5364	1.5320	1.5297	1.5269	1.5236	55.8
80	1.5397	1.5344	1.5300	1.5277	1.5249	1.5217	55.5

Table 5.16h Refractive index of optical polyester:
OKP-4 (Osaka Gas Chemical).

temperature (°C)	wavelength (nm)					Abbe number, V_D
	436	486	546	589	656	
30	1.6370	1.6230	1.6130	1.6070	1.6010	27.6

Table 5.16i Refractive index of polysulfone: Udel® P-1700.

temperature (°C)	wavelength (nm)			Abbe number, V_D
	486.1	587.6	656.3	
25	1.650	1.634	1.623	23.5

Table 5.17 Comparison of various optical polymers.[a]

property	polymer: brand name (supplier)									Glass
	PMMA	PC	COP: ZEONEX® E48R (Zeon)	COP: ZEONEX® 330R (Zeon)	COC: APEL™ 5014DP (Mitsui Chemicals)	COC: TOPAS® 5013 (Topas Advanced Polymer GmbH)	COP: ARTON® FX4727 (JSR)	O-PET: OKP-4 (Osaka Gas Chemical)	PSU: Udel® P-1700 (Solvay)	
optical										
light transmittance	5	3	5	5	4	5	5	3	2	5
birefringence (retardation)	4	2	3	4	5[b]	4[b]	3[b]	4	1	5
refractive index	low	high	medium	low	medium	medium	medium	high	high	high–low
Abbe number	high	low	high	high	high	high	high	low	low	high–low
stability										
water absorption	1	3	5	5	5	5	4	3	2	5
coefficient of linear expansion; dn/dT	3	3	3	3	3	3	3	3	3	5
deflection temperature	3	4	4	3	4	4	3	3	5	5
moldability										
flowability/injection molding	4	4	4	4	5	5	5	–	3	1

a) Score: 1, bad; 5, good.
b) Gathered from catalog.

As stated previously, improved polymers are now under consideration as a result of various recent technology developments. These polymers are very good as regards mass-productivity compared to glass; however, they do not necessarily reach the same level of environmental stability and variety of refractive index as glass. Currently, appropriate materials are selected for each use. In the future, further developments of materials are expected, enabling more applications in various fields. The main areas of research and development concern

- high-refractive-index materials;
- low-birefringence materials; and
- materials with higher environmental stability, mainly heat resistance.

References

1 F. Ubrbach, *Phys. Rev.* **92**, 1324 (1953).
2 F. Ide, Refractive index control of transparent high polymers, *Kikan Kagaku Sosetsu* **39**, 3 (1998).
3 T. Kaino, M. Fujiki, and K. Jinguji, *Rev. ECL* **32**, 478 (1984).
4 T. Kakezawa, et al., *J. Appl. Polym.* **46**, 1835 (1992).
5 N. Tanio, *Koubunshikakou* **46**, 210 (1997).
6 Catalog of PANLITE® AD5503 furnished by Teijin Kasei.
7 Technical data of PARAPET® furnished by Kuraray.
8 Technical data of APEL™ 5013DP furnished by Mitsui Chemicals.
9 Technical data of TOPAS®, Topas Advanced Polymer GmbH.
10 Catalog of ARTON®, JSR.
11 Technical data of Udel® furnished by Solvay Japan.
12 Catalog of OKP-4, Osaka Gas Chemical.
13 JP2002–283426, JP8–015503, JP7–325206, JP7–281003.
14 T. Inonu and H. Saito, *Funct. Mater.* **3**, 25 (1987).
15 Catalog of ACRYPET™, Mitsubishi Rayon.
16 H. Kawaki, *Technology and Application of Plastic Lens System* (CMC Publishing, 2003), pp. 80–86.
17 H. Yoshioka, Refractive index control of transparent high polymers, *Kikan Kagaku Sosetsu* **39**, 118 (1998).
18 E. Matsui and T. Makimoto, *Recent Transparent Plastics and the Market* (CMC Publishing, 2001), pp. 70–80.
19 *Optical Plastics; Kougaku-you-toumeijusi* (Gijutu-jouhou Kyoukai, 2001), pp. 63–67.
20 T. Kohara, Refractive index control of transparent high polymers, *Kikan Kagaku Sosetsu* **39**, 133 (1998).
21 K. Minami, *Recent Transparent Plastics and the Market* (CMC Publishing, 2001), pp. 23–37.
22 Catalog of APEL™, Mitsui Chemicals.
23 Y. Yoshida, et al., *JSR Tech. Rev.* **103**, 34 (1996).
24 M. Fuji, et al., Refractive index control of transparent high polymers, *Kikan Kagaku Sosetsu*, **39**, 122 (1998).
25 Catalog of Udel®, Solvay.

6
Coating on Plastics

Ulrike Schulz (Fraunhofer Institut IOF, Albert Einstein Str. 7, 07745 Jena, Germany)

6.1
Introduction

Injection-molded or hot-embossed optics replace glass optics whenever improved properties or a cost reduction can be achieved with plastic parts. In contrast to glass optics where optical coatings are state-of-the-art technology, most plastic optics are used uncoated today. Most experiences with coating exist in the field of eyeglass coatings. First results of research in the field of coating plastics were published about 20 years ago [1, 2]. Today a number of review articles are available that cover the general task [3–5]. Despite of "classical" precision optical applications, the coating of organic polymers is essentially required for the development of optoelectronic devices like organic solar cells and organic light-emitting diodes (OLEDs) [6].

With respect to coating, organic polymers are much more complicated materials than inorganic glasses. Naturally, the temperature applicable in coating processes is limited. This is a difficulty for classical evaporation processes just as for wet-chemical coatings, which require high temperatures for hardening. Consequently, coating technologies well established for glass cannot be used for polymers. An overview about procedures and techniques used for the deposition of coatings on rigid thermoplastics is given in Section 6.2.

It is obvious that miscellaneous interactions have to be taken into account if polymers are exposed to plasma and high-energetic radiations during coating processes. These interactions have to be investigated for the manifold of polymers with different chemical compositions. Especially vacuum ultraviolet radiation can damage surface or volume of polymers and initiate degradation of the coating–substrate interfaces at a later date. A summary of this task is given in Section 6.3 followed by a section covering the basic concerning of the mechanical and thermal stress of coatings on plastics (see Section 6.4). Both plasma interactions and stress have a substantial influence on the lifetime properties of coated plastics.

The most frequent requirement in optical systems production is to increase light transmission by antireflective (AR) layers. However, antireflection properties can not only be provided by coating but also by generating suitable nanostruc-

tures. Because of the importance to reduce surface reflection on plastic optics, several modern techniques are discussed in detail in Section 6.5.

Another motivation for coating plastics results from the mechanical and chemical properties of organic polymers. Coatings are intended to compensate various disadvantages. Protective coatings should increase the abrasion resistance and provide protection against chemical attacks. Barrier layers can reduce the gas flow through or from the polymer part. The requirements to be met by protective layers, particularly in respect of hardness and scratch resistance, depend strongly on the kind of application. In addition, coatings can be helpful to modify surface energy and thus to adjust surface wettability by water or oil. Some examples to provide such additional functionalities on plastic parts are summarized in Section 6.6. The most important thermoplastics for optical applications are each discussed separately in Section 6.7. Section 6.8 is focused on test and evaluation tools.

6.2
Deposition Techniques

Conventional coating processes established on glass substrates typically work at substrate temperatures at about 300 °C. An enhanced substrate temperature is responsible for the activation of the surface and a high mobility of condensing thin film atoms [7]. Therefore, high-density coatings providing stable optical and mechanical properties can be obtained. The dependency of thin film growth and microstructure on deposition temperature is predicted by so-called structure zone models [8].

Naturally, coating on plastics has to be done at temperatures below their heat distortion temperature. For most thermoplastics, this means a temperature limit of about 120 °C. Without substrate heating, only porous coatings would be obtained from most oxide and fluoride thin film materials. Especially fluoride films evaporated at room temperature do not even pass the least severe tests for hardness and abrasion resistance. Moreover, the coatings typically show insufficient adhesion because of the meager substrate activation. Unstable optical properties during the life of the optical parts have to be reckoned with due to a water uptake, depending on environmental conditions.

During the last years, important innovations have been established for coating plastics. The basics of present-day coating technologies are the application of ion assistance in evaporation processes, the possibility to use cold plasma in chemical vapor deposition (CVD) processes, and wet chemical coatings that can be cured by using UV radiation instead of thermal treatment. The corresponding coating techniques are discussed in the following sections.

6.2.1
Physical Vapor Deposition

Physical vapor deposition (PVD) of oxide materials is still the commonly used method for manufacturing optical coatings. The term PVD covers a number of coating techniques, all of them characterized by a transfer process of the thin film material from a solid phase into a vapor phase at low pressure and the condensation of vapor as thin solid film on a substrate. The both fundamental process types are evaporation and sputtering. Several special techniques allow a layer deposition at low temperatures as required for plastics. The fundamental method to provide the growing layers with energy is the use of low-pressure plasma, often emitted by an ion source [9–13].

Evaporation processes are carried out typically inside the closed steel chambers equipped with evaporation sources, substrate holder, and some measurement equipment, that is, for the determination of film thickness. The typical pressure range before the start of evaporation is 10^{-5} to 10^{-6} mbar. The film deposition takes place at about 10^{-4} mbar. Because of the free way path in this pressure range, the thin film particles will move to the substrate in a direct linear way without collisions. This is the main condition to achieve a layer thickness with precision in the range of only a few nanometers as required for optical interference coatings.

An advantage of evaporation techniques is the comparably high deposition rate achievable for many dielectric materials as well as for metals. Several methods such as resistive (filament heating), inductive (radio frequency – RF), electron beam, or laser heating can be used to attain the high temperature required to vaporize the thin film materials. Resistance heating is often used for the metallization of plastics. The substrates are placed on the walls of a cylindrical chamber and aluminum is evaporated from a prolate boat in the center.

High-melting oxides like SiO_2, Ta_2O_5, and Al_2O_5 can only be evaporated by electron beam guns. Modern coating systems for optics are equipped with both resistance and electron beam evaporators and additionally with an ion source. As an example for ion-assisted processes, the plasma-ion-assisted deposition (PIAD) technique carried out with coating plant advanced plasma source (APS) 904 (Leybold-Optics) is mentioned here [14]. The main components and an exterior view are shown in Figures 6.1 and 6.2.

During the PIAD process, the growing film is bombarded with argon ions emitted from the APS with the help of a magnetic field. The ion energy is in a range of about 60–180 eV. For coating plastics, only values below 120 eV can be recommended. Apart from the plasma source, the coating chamber consists of a conventional e-beam evaporation arrangement. For further PVD techniques that use low-pressure plasma for activation, see Ref. [7].

Magnetron sputter deposition is another method of physically depositing inorganic materials. The coating material is physically knocked off from a target surface and condenses on substrate surface some distance away. This process is driven by the kinetic energy of ions generated in plasma. The source of ions is the differentiating factor between diverse hardware such as ion beam sputtering appa-

Figure 6.1 APS 904 conventional batch coating system for optics (Leybold Optics).
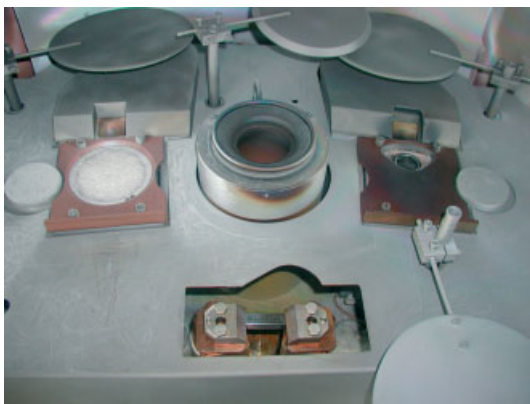
Figure 6.2 Electron-beam arrangement and APS ion source of the APS 904 coating system (Leybold Optics).

ratus and a magnetron sputter source. Typically, a high-voltage DC power supply or, for nonconductive substrates, RF plasma in an argon vacuum system is used. The plasma is established between the substrate and the target and transposes the sputtered-off target atoms to the surface of the substrate. For technical basics, see Refs. [15, 16].

The domain of sputtering is the deposition of coatings with very high density and a good homogeneity of layer thickness that can be simply controlled by time. For this reason, sputtering is also commonly used to deposit optical interference coatings on glass [17, 18]. Because of its comparably high heat and radiation emissions, the sputtering of dielectrics is critical for coating thermoplastics.

Some new concepts use the advantage of high precision for the production of AR layers on eyeglasses and display covers. Pulsed magnetron sputtering was applied to deposit AR and HR coatings on PET at 150 °C [19]. "Closed-field" mag-
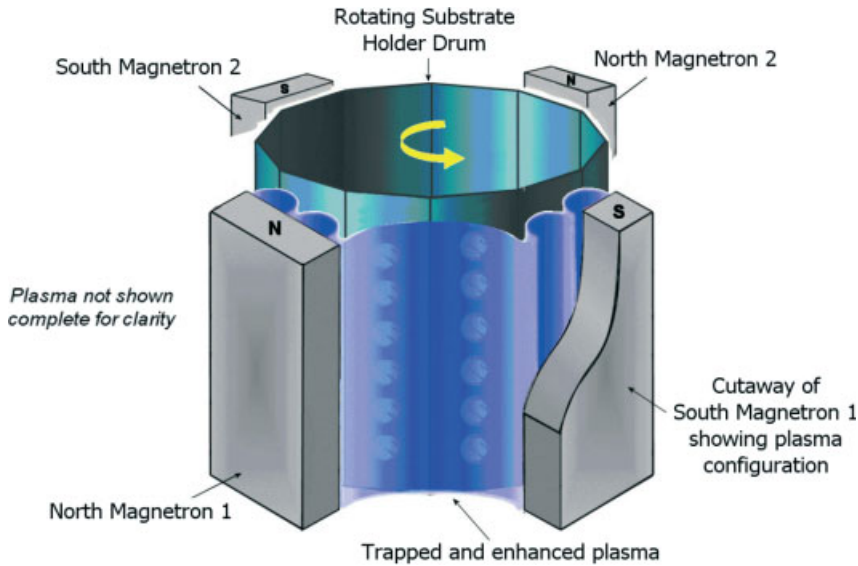
Figure 6.3 Arrangement of closed-field magnetron sputtering [20]. This process does not need a separate ion source. Adjacent magnetrons are made of opposite polarity to trap the plasma all the way around a drum.

netron sputtering offers a flexible low-temperature process for optical coatings on plastics [20, 21]. This process does not need a separate ion source. Adjacent magnetrons are made opposite polarity to trap the plasma all the way around the drum (Figure 6.3). Sputter deposition processes of AR coatings can be preceded by a PECVD process step that deposits a scratch-resistant layer [22]. The Opticus-concept of Singulus was developed to exhibit fully automated coating of eyeglass lenses with a hard coat, an AR layer stack and a clean coat in that way. But, in 2008, this concept was discontinued.

Metal sputter coating systems are well established in the manufacturing of car lighting and indoor lighting reflectors [23]. Figure 6.4 shows a modern coating machine that is typically used for wipe-resistant reflector coatings on complex shaped plastic parts for vehicle headlamps [24]. This machine enables vacuum metallization by sputtering with PECVD hard coat layers in one process.

Moreover, sputtering is the basic technology in web coaters for flexible substrates. In that case, undesired heating of the polymers can be prevented by cooling the web over a drum [25–27]. State-of the art is RF magnetron sputtering of ITO on PET and polycarbonate (PC) foil (see Section 6.6.2).

Figure 6.4 PylonMet VXL reflector coating machine (Leybold Optics).

6.2.2
Plasma-Enhanced Chemical Vapor Deposition

Chemical vapor deposition (CVD) is based on the decomposition and chemical reaction of gaseous compounds in vacuum near the substrate surface. One of the reaction products is a solid that precipitates onto the surface forming a thin film. PECVD techniques use a microwave and/or RF plasma for the activation of the reacting gases [28, 29]. High temperatures, typical for classical CVD processes, are therefore no longer necessary. For complex optical multilayers, PECVD processes do not deliver the same thickness accuracy and homogeneity as PVD processes. Moreover, the materials suitable as precursors are limited and have to be handled carefully. An advantage for coating plastics, on the other hand, is the possibility to produce partly organic coatings with a gradient of hardness and elasticity. The generally observed better adhesion has been attributed to a more uniform distribution of stress throughout the interface, to the interface mechanical stabilization, and to the formation of strong covalent bondings [30]. PECVD was successfully applied to produce Si containing diamond-like carbon films on PC [31]. There are also efforts in progress to use PECVD for the deposition of siloxane protective coatings on PC for automotive applications [32].

A special variety of PCVD is plasma-impulsed chemical vapor deposition (PICVD), developed by the German Schott Hicotec company. In the process, a gaseous precursor is decomposed by microwave plasma pulses [33]. A short ignition of plasma is repeated many times until the required layer structure has been

built up. PICVD was proved to be suitable to coat small complex-shaped substrates homogeneously. It was successfully applied in the production of plastic cold-light reflectors for a couple of years. However, in 2006, the Hicotec facility was closed.

6.2.3
Wet-Chemical Coating or Sol–Gel Coating

The first patent based on sol–gel processes was granted to Jenaer Glaswerk Schott&Gen. in 1939. Coatings for AR applications on glass have been commercially produced since the 1960s. The wet-chemical coating is deposited by dip coating or spin coating on rigid flat or slightly curved substrates. During spin coating, the coating solution is deposited onto the sample surface and spun off to leave a uniform layer. Dip coating is a process where the substrate to be coated is immersed in a liquid and then withdrawn with a well-defined speed under controlled temperature and atmospheric conditions.

Sol–gel process classically involves the use of inorganic salts or metal alkoxides as precursors. Typical an elevated temperature up to 400 °C is needed for hydrolysis and polycondensation to accomplish the network and the chemical decomposition until the oxide is formed [34]. An alternative way is to combine the properties of very different materials and produce organic–inorganic composite materials. Typical examples are organically modified silanes, or the incorporation of organic molecules into the essentially inorganic matrix [35]. Silicate-based inorganic–organic hybrid polymers (ORMOCER®s) have attracted considerable attention due to their optical and mechanical properties [36]. The synthesis comprises a chemical modification of organic components to covalently attach them to the inorganic network. The principle of composition is shown in Figure 6.5.

The final polymerization can be performed either photochemically or thermally, or by a combination of both. The principle possibilities to vary the composition and the properties of hybrid sol–gel-derived materials are reviewed by Schottner and Posset [37]. Hard polysiloxanes and related silica-containing formulations
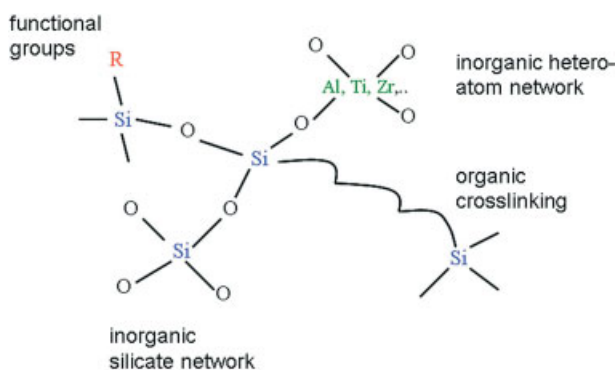
Figure 6.5 ORMOCER®: principle of composition.

were developed several decades ago. The coating formulations and coated products are known (e.g., AS4000, AS4700, PHC587 by Momentiv Performance Materials GmbH, Germany) and sold in large quantities worldwide. However, further new materials are still in development especially to improve the abrasion resistance of thermoplastics [38]. Most industrial companies involved in the ophthalmic lens business produce thermosetting films on top of CR39 and PC by wet chemical coating [39].

The spin-coating process as the typical deposition process is limited to flat or slightly curved substrates to achieve a layer thickness precision in the nanometer range as required for optical coatings. Injection-molded parts of complex forms are not suitable for this deposition method. Moreover, the preparation of multilayers is complex if the depositing and hardening steps have to be repeated many times. Therefore, AR coatings produced by wet-chemical methods consist of one, two, or three layers typically. The following single-layer and two-layer systems are described in patents and literature:

- An alcohol-based inhomogeneous AR layer produced by soaking in acidic or alkaline etchant to dissolve oxide colloids partly from the layer [40].
- A single composite layer containing organic fluoropolymer for curing at 120 °C [41].
- A single composite layer consisting of fluorine-containing binder-aided colloidal silica [42].
- A single composite layer consisting a porous glass film that does not require heating or etching [43].
- An interference two-layer comprises alkoxide or acrylate compounds of Ti, Al, or Zn and hydrolysable organic silicon compounds as low-index material [44].
- A two-layer AR coating and an NIR reflective coating curable by UV irradiation containing polymerizable nanoparticles modified with alkoxy-silanes and mixed with photoinitiator are described in [45].

The application of wet-chemical material for AR is a fast-growing field. During the last two years, a large number of new sol–gel materials for AR applications were described in the scientific literature. Techniques to generate the high-index component by embedding nanoparticles of ZrO_2 or TiO_2 into the lacquers play an important role in this development [46, 47]. AR coatings with additional characteristics such as hydrophobicity, self-cleaning, and antistatic properties have been reported [48, 49]. Furthermore, sol–gel techniques are basic for so-called moth-eye patterns inscribed into hybrid sol–gel-derived polymers forming an AR nanostructural pattern (see Section 6.5.3).

6.3
Plasma Effects on Polymers

The interactions between polymers and plasma and ultraviolet radiation taking place especially in vacuum coating processes but also during hardening of sol–gels are manifold and can have an influence on the properties of coated plastic parts. Many review articles and books deal with plasma treatments of polymers [50, 51], and with plasma deposition of coatings [52–54].

Plasma conditions applied for pretreatments of polymers are normally gas discharges at low pressure [55, 56]. Reactions on polymer surfaces can be caused by high energy electrons, ions, and neutrals as well as electromagnetic radiation in the deep ultraviolet spectral range (vacuum UV – VUV, $\lambda < 180$ nm) emitted during the slowing down of electrons. The treatments cause chain scission, ablation, crosslinking, and oxidation to a depth of typically 5–50 nm [57]. Mostly, it is very difficult to distinguish which reactions have been excited by different plasma particles or by radiation. Which kind of effect dominates is mainly dependent on the molecular composition of the substrate and can be also influenced by the kind of plasma applied [58]. Important plasma parameters for a treatment are the plasma excitation frequency, the gas pressure and composition, and the treatment time.

6.3.1
Effects Caused by UV-Radiation

Electromagnetic radiation at wavelengths below 200 nm has enough energy for breaking any polymer bond, and for wavelengths below about 120 nm, the photon energy is sufficient to ionize most organic molecules [59]. But only radiation that is selectively absorbed by a chosen polymer can initiate chemical effects on it. The penetration depth of the radiation depends on the absorption coefficient and varies between a few nanometers and some millimeters. Depending on the absorption properties, electromagnetic radiation may result in interface and surface reactions without influence on the bulk, or in changes of the bulk polymer without effects on the surface [60, 61].

The polymer radicals formed during plasma treatments are long-lived and typically react with water or oxygen from the gas background. Plasma treatments are therefore able to introduce polar oxygen groups even if carried out in inert gases. Adhesion improvement of coatings has been attributed variously to the improved wettability.

The degradation of polymers caused by global UV radiation is well investigated because of the danger of yellowing of many polymer materials [62, 63]. Particularly, PCs are prone to yellowing, whereas polyacrylates are more stable to global radiation [64–66]. The discoloration is due to photooxidation reactions. Photooxidation and yellowing have also been observed after low-pressure plasma treatments of polycycloolefins [67]. Important for coating processes are VUV radiations at wavelengths below 180 nm. Argon in the system has primarily VUV emissions below 160 nm due to energy transfer from excited-state argon metastables to

hydrogen from water and organic materials, but also higher energy emissions [68, 69]. Many investigations show that crosslinking reactions during low-pressure plasma treatments are mainly initiated by the VUV radiation [70, 71]. Cross-linking dominates on polymers containing at least one hydrogen atom bonded on adjoining carbon atoms. This condition is satisfied for thermoplastics like polyethylene, polypropylene, polystyrene, and polyamide. Polymethylmethacrylate (PMMA) and PC do not belong to that group. Especially for PMMA and other acrylics, scission of bonds and the formation of weakly bonded layers have been observed after many different plasma treatments (see Section 6.8.1).

6.3.2
Ion Bombardment Effects

Modern PVD processes often use ion sources for substrate activation and the densification of growing films. Besides the radiation effects, the ions typically initiate etching processes that are associated to changes of surface topography [72]. Figure 6.6 shows the topography of Zeonex plates before and after an ion bombardment carried out with a Leybold APS ion source. The parameters applied are common for cleaning and activating glass surfaces before the PVD process starts. A slight increase in roughness can be observed. However, a noticeable decrease in transmission caused by increased stray light has to be reckoned with only if high-energy ions and long treatment times are applied. In case of the cycloolefin polymer Zeonex, the change of topography has no influence on the adhesion properties (see Section 6.8). In some cases, ion bombardment effects are utilized to create or assist superhydrophobic (Section 6.7.3) or AR properties (Section 6.5.3).
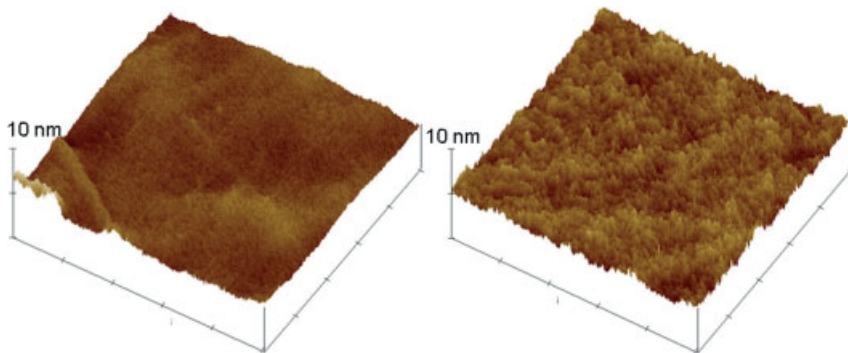
Figure 6.6 AFM image of an injection-molded Zeonex surface before (a) and after (b) 300s Ar-plasma treatment applying an ion energy of 80 eV.

6.3.3
Conclusions for Coating Adhesion

When an adhesive bond breaks at a low applied stress, it is said to have a "poor" adhesion. The fracture may have occurred exactly at the interface, in a thin layer close to the interface, or as cohesive fracture in the bulk phase [57]. Correct identification of the locus of failure is of great importance. If the break occurs cohesively in a thin bulk layer near the interface, efforts should be directed toward strengthening this weak boundary layer rather than increasing the interfacial attraction. Plasma treatments typically produce polar groups on polymer surfaces. The wettability is therefore always improved to various degrees [73]. An adhesion improvement by plasma treatments has been attributed variously to this improved wettability, surface crosslinking or interfacial diffusion. If poor coating adhesion is observed after a plasma treatment because of a cohesive fracture in the bulk, the main problem may be the weak boundary polymer layer formed during the treatment. Taking into account the very short treatment times sufficient for the activation of most polymer surfaces and the danger of formation of weakly bonded layers, all treatments should be as short as possible.

6.4
Stresses and Crack Formation

Behind the problems resulting from the interactions of polymer surfaces with high-energy radiation, mechanical coating stresses can make it difficult to produce coated plastics that do not show cracking or ablation during their later life. Residual stresses in thin films are due to the mechanical growth stress of the thin-film material and the thermal mismatch between the film and the substrate when the system is heated during film deposition and cooled from its fabrication temperature to room temperature [74, 75]. As known from many studies, the mechanical growth stress of thin oxide layers depends mainly on the parameters of the vacuum deposition process and can be adjusted within a certain range [76–79]. Even though a lot of investigations into stress in coatings have been made, less experience exists in the special case of inorganic coatings on polymer substrates. A differing total stress behavior compared with coatings on inorganic glass has to be considered for oxide coatings deposited on polymer substrates because of the difference in the thermal expansions of substrate and film, which is the origin of high-level thermal stress.

In PVD and PECVD processes, the substrate temperature is determined as the combination of heat received from the evaporation sources and the plasma sources used in the process [80]. A gradual increase in substrate temperature during vacuum deposition causes a thermal stress gradient across substrate and coating. To understand the complex stress behavior of coatings on polymer substrates, the temperature has to be controlled carefully during the deposition process. For example, the thermal load on a substrate during PIAD results from both the
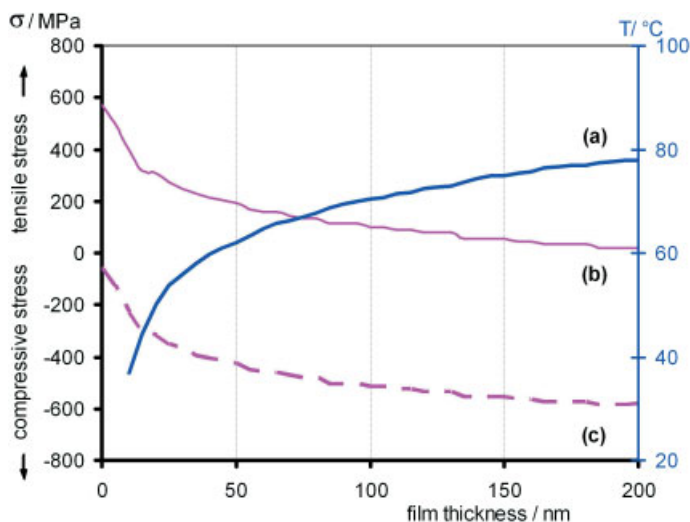
Figure 6.7 Development of thermal stresses during ion-assisted deposition of a TiO$_2$ layer onto a polymer substrate: (a) increase in substrate temperature during the evaporation process, (b) distribution of tensile stresses at the end of the deposition process, and (c) distribution of the residual compressive stresses after cooling to room temperature.

power of the electron beam gun and the thermal emission of the ion source. The e-beam power, which depends on the evaporation temperature, melting behavior, and thermal conductivity of the materials, is much higher for most high-index materials than for the low-index SiO$_2$. An increase in the maximum temperature on polymer surface occurs with increasing film thickness at constant ion energy as shown for an e-beam-evaporated TiO$_2$ layer in Figure 6.7 [81].

Due to the fact that the temperature rises gradually during film deposition, great differences between the stress levels at the coating–polymer interface and on the outer surface have to be expected. The stress σ_{th} of each thin film segment of a coating can roughly be calculated using the equation

$$\frac{d\sigma_{th}}{dT} = \frac{E_f}{1 - v_f}(a_s - a_f), \tag{6.1}$$

where E_f, v_f, and a_f are Young's modulus, Poisson's ratio, and thermal expansion coefficient of the film, respectively, and a_s is the thermal expansion coefficient of the substrate [77]. The thermal expansion coefficient of a polymer is typically about $10^{-5}\,K^{-1}$ and at least one order of magnitude higher than for inorganic layers. It has to be considered in a rough evaluation that a temperature change during the deposition process may generate a stress component of about 5–20 MPa K^{-1}. The stress is tensile during heating and becomes compressive by cooling as demonstrated in Figure 6.7.

More precise calculations are possible by using complex thermal stress models taking into account the elasticity theory [82–84].
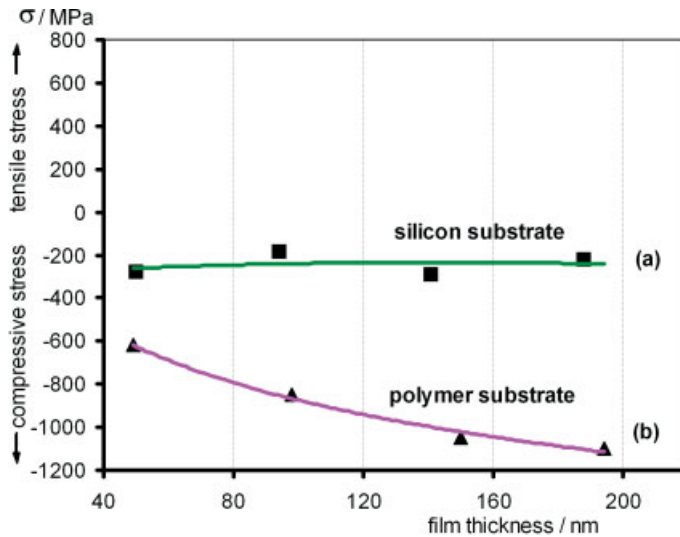
Figure 6.8 Residual stresses in TiO_2 layers of various total thicknesses deposited on (a) silicon and (b) polymer substrates under equal conditions. For layers deposited on polymer substrates, the influence of the thermal stress component on the residual stress level increases with thickness.

Residual stress values for coatings deposited simultaneously on silicon substrate and on a polymer substrate are plotted in Figure 6.8. If changes of growth stress are neglected, all differences between both curves have to be ascribed to the additional thermal stress component in case of a polymer substrate. Considering the significant deviations, stress measurements on silicon are inappropriate to describe the complex properties of coated polymer substrates and to explain, for example, the cracking of coatings during environmental tests.

Figure 6.9 shows a typical stress cracking observed on PMMA coated with $1\,\mu m$ SiO_2. Although the coatings themselves have compressive growth stress, stress cracking caused by thermal tensile stress can occur during the deposition of thick layers on polymer substrates. In Figure 6.9(a), the coating has cracked during the deposition process because of high temperature (tensile stress cracking). Figure 6.9(b) shows the typical buckling of a coating in form of "wormtracks" caused by a high compressive growth stress in combination with insufficient coating adhesion. Note that this kind of damage typically occurs if the coating adhesion is low. The mechanical growth stress of coatings can often be limited by restricting the film thickness and changing the deposition parameters. Water vapor absorbed in porous layers after coating may reduce or increase the intrinsic film stress and affect the adhesion in this way [85, 86]. In case of ion-assisted deposition, a low level of ion energy (Figure 6.10) and the use of water vapor as reactive gas can be very helpful to reduce the growth stress [79].

(a)   (b)
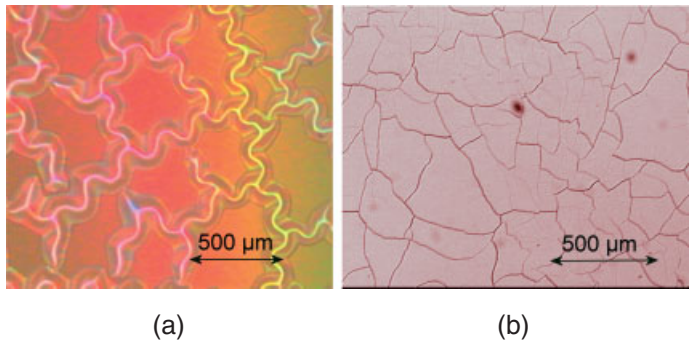
Figure 6.9 Stress cracking of inorganic coating deposited on a polymer substrate: (a) buckling of coating as a consequence of high compressive growth stress and insufficient coating adhesion and (b) tensile stress cracking caused by different thermal expansions of substrate and coating.
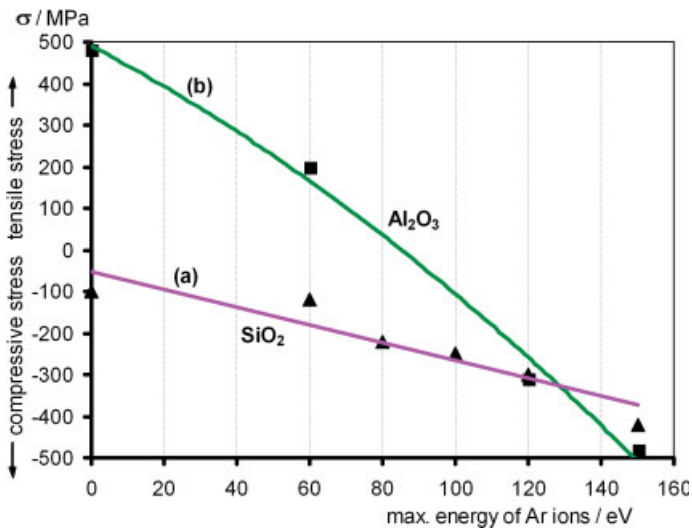
Figure 6.10 Compressive growth stress in (a) SiO_2 and (b) Al_2O_3 thin films as a function of the ion energy. Layers are deposited by electron beam evaporation in a PIAD process (APS 904, Leybold Optics; deposition rate 1 nm/s).

6.5
AR Properties

The manufacturing of optical coatings on polymers started about 35 years ago. The driving force for the development of AR coatings was the ophthalmic industry, and the demand for industrial coating techniques developed with an increasing circulation of plastic eyeglasses.

AR coatings are a necessity on optical lenses and windows especially if multiple interfaces between optical parts have to be considered. Their function is to decrease the amount of radiation reflected and thus to increase the transmitted amount. The Fresnel amplitude reflection coefficient (*r*) for an interface between two media can be represented by the equation

$$r = \frac{n_1 - n_2}{n_1 + n_2}, \tag{6.2}$$

where n_1 and n_2 are the real indices of refraction of the two media [87]. The intensity can be treated as the square of the amplitude. As a rule of thumb, about 4% of the perpendicularly incident light will be reflected at the glass–air interface. For example, an optical system consisting of four uncoated lenses with refractive index 1.5 shows a transmittance of only 75% because of reflection losses. AR coatings or microstructures that decrease the reflectance below 0.5% for each surface would increase the transmitted light up to 96%.

Most AR coatings are based on optical interference as explained in Section 6.5.1. Some polymer-typical properties have to be considered for evaluation of an AR layer stack (coating design). Suitable coating designs for plastics optics are discussed in Section 6.5.2. Surfaces with inhomogeneous refractive indices for AR purposes and methods to produce such surfaces will be described in Section 6.5.3.

6.5.1
Optical Interference Coatings

This section briefly reviews some of the basic principles of thin-film design for AR coatings and should make it easier to get access to the relevant literature. The term "optical thin film" typically indicates coatings with physical thicknesses in the range of a few to several hundreds of nanometers. In the optical sense, a film is called "thin" when interference effects can be detected in the transmitted or reflected light. An arrangement of multiple layers with well-defined indices of refraction and thicknesses that realizes a desired spectral characteristic by interference effects is called a coating design. For most common applications, it is sufficient to consider absorption-free thin films at a near-normal incidence of light. For the more general case of absorbing media with complex refractive indices, see Refs. [87, 88].

Figure 6.11 shows the principle of interference coatings for a single layer deposited on a substrate. When a beam of light is incident on a film, some of the light will be reflected off the front surface and some off the rear surface. The reminder will be transmitted. The light reflected off the boundaries interferes constructively if the path difference is an integral multiple of the wavelength, or destructively if it is an odd multiple of the half wavelength. The path difference depends on the optical thickness of the layer and the angle of incidence. The optical thickness is given by

$$t_{op} = d \cdot n, \tag{6.3}$$

where *d* is the physical thickness and *n* the refractive index of the material.
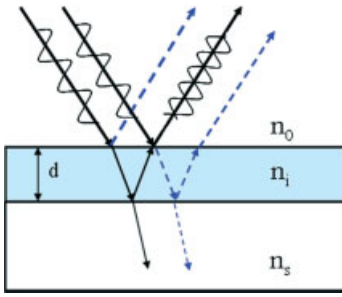
Figure 6.11 Schematic image of reflections at a single layer of physical thickness d deposited on a substrate.

The reduction in reflectance due to interference phenomena is a function of the wavelength of the incident radiation and of the angle of incidence of the light on the surface. The simplest case to obtain AR properties on a material with refractive index n_s at a defined wavelength λ_0 is to deposit a thin film with lower refractive index n_i and a thickness that is one-quarter of that wavelength ("quarter-wave" – QW layer). The amplitude reflection coefficient for that case is given by

$$r = \frac{n_i^2 - n_0 n_s}{n_i^2 + n_0 n_s}. \tag{6.4}$$

Perfect AR at one wavelength would be achieved with a quarter-wave layer or uneven numbers of this layer having the refractive index n_i

$$n_i = \sqrt{(n_0 \cdot n_s)}. \tag{6.5}$$

In practice, by depositing a quarter-wave layer of MgF_2 with $n = 1.38$, the reflectance of a PC surface ($n = 1.56$) can be reduced to about 1%. A better result with a single homogeneous layer is not possible because a real material with lower refractive index is not available.

In order to have an improvement or a broad wavelength range of low reflectance, multiple layers of high and low-index materials must be used to form the AR design. A double AR coating is able to perform zero reflectance at exactly one desired wavelength λ_0 (design wavelength). This so-called V-coating shows a narrower bandwidth than the single layer solution and is designated by a quarter-wavelength (QW) thick layer having a defined medium refractive index followed by a QW of low refractive index ("quarter–quarter" design). Because of the limitation of practically available materials, the medium refractive index material can be replaced by parts of high-index and low-index layers. Materials such as Ta_2O_5, TiO_2, Nb_2O_5, ZrO_2, and SiN ($2.0 < n_H < 2.5$) are used as high-index layers, whereas mainly SiO_2 ($n = 1.46$) and MgF_2 ($n = 1.38$) may be used as low-index materials. Two solutions for this replacement are possible, giving zero reflectance at the same single wavelength. In Figure 6.12, the performance of a theoretical "quarter–quarter" design is plotted.

Most frequently used broadband AR coatings for the visible spectral range nowadays are adapted from a "quarter-half-quarter" design, whereby the first QW layer of medium refractive index is replaced in different ways by parts of high-
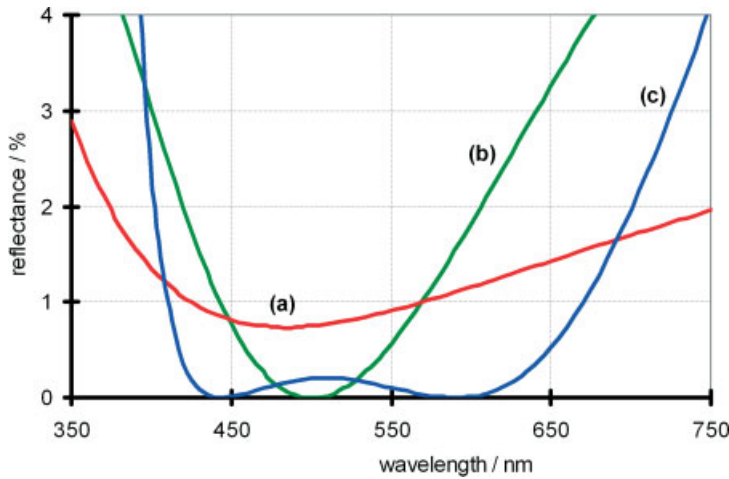
Figure 6.12 AR coatings for glass and polymers ($n_s = 1.5$): (a) single MgF$_2$ layer, (b) two-layer coating or "V"-coating, and (c) quarter-half-quarter or "W"-coating.

index and low-index QW layers followed by a two QW (half-wave) thick high-index layer and a low-index QW layer on top. Most coatings of that type consist of four to six layers and show typically a performance similar to the letter "W" (W-coating, see Figure 6.12) [89, 90].

Many other designs for implementing optical interference coatings like dielectric mirrors, filters, or beam splitters are layer stacks that consist of alternating high-index and low-index layers with a thickness each of one QW at a defined design wavelength (see Ref. [87]). For those applications, no special design developments for plastic optics are known up to now.

Much of design work nowadays is carried out by automatic methods using design software, and this is a very efficient development [91, 92].

6.5.2
AR Design for Plastics

For coating plastics, special requirements have to be taken into account during generating AR designs:

- The layer materials have to be selected in order to achieve radiation protection of interfaces or of the bulk polymer depending on the polymer substrate type.
- The layer materials and thicknesses have to be adjusted considering the mechanical and thermal film stresses and the total heat development during the deposition process.
- Process parameters for the materials used have to be suitable to avoid damages of polymer bulk and interface during thin film deposition.

- Sometimes changed optical properties of interfacial zones due to plasma treatments have to be taken into account for design calculation.
- Designs should be suitable for integrating additional functions like improved scratch resistance, barrier function, antistatic function, or hydrophobic properties.

It is supposed that experience to produce high performance AR coatings on polymers exists mainly in the field of eyeglass coating. Unfortunately, only little of this very special knowledge is published [93–95]. Plastic eyeglasses have to pass strong environmental and abrasion tests to demonstrate their suitability. AR layers (a quarter-half-quarter AR design is preferred) and hydrophobic top coatings are arranged on top of several micron thick hard coatings. Usually, the hard coatings are lacquers based on silanols, or organic modified silica layers applied by vacuum deposition processes. Thus, hard-coated surfaces act as substrate so that the vacuum deposition of the AR coating need not be done onto the more sensitive polymer itself.

The use of evaporated MgF_2 single layers as an inexpensive alternative to multilayer AR coatings suffers from the bad mechanical properties of layers deposited without substrate heating and the high-level tensile growth stress of MgF_2. Some improvements have been obtained by applying a "soft" ion assistance during thermal evaporation [96], but the coating is not common on plastics today.

The development of AR coatings using wet-chemical processes comprises mainly single-layer and two-layer systems (see Section 6.2.3). Unfortunately, the basic research in this field is focused on the coating material rather than the kind of polymer substrates or optical designing. Only few results are open for publication.

A new design type named AR-hard® has been developed especially for plastic optics, to produce AR coatings with high scratch resistance [97, 98]. The basic idea of AR-hard® is to treat symmetrical layer periods as equivalent layers to replace layers with unobtainable refractive indices lower than the index of the low-index material. Each period consists of a very thin high-index layer H sandwiched between two thick low-index layers L. Figure 6.13 shows this principle schematically. The equivalent layers build up a so-called step-down design, matching the refrac-
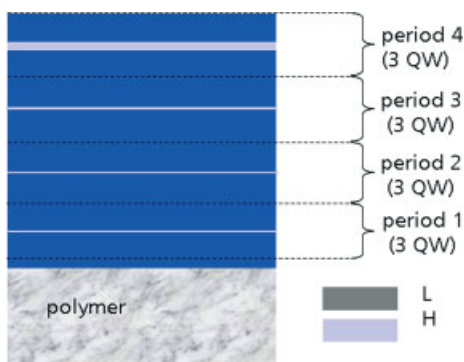
Figure 6.13 Schematic illustration of AR-hard® scratch resistant AR coating showing the arrangement of symmetrical periods that builds up a so-called step-down design of equivalent layers (H, high-refractive index material; L. low-refractive index material).

tive index of the substrate to that of air. A basic example of this coating is an arrangement of symmetrical three-layer periods, each having three times the QW optical thickness (three QWs).

The mathematical relationship between the equivalent index of a three-QW period and the respective thicknesses of the single high-index and low-index layers used to build up such a period has been deduced as a condition for design synthesis [99, 100]. Advantages of the AR-hard® design are the variable bandwidth for different spectral ranges, adjustable hardness by using layer stacks of different total thickness, and a colorless residual reflection if desired. Figure 6.14 shows the residual reflectance available with AR-hard® layer stacks for different bandwidths.
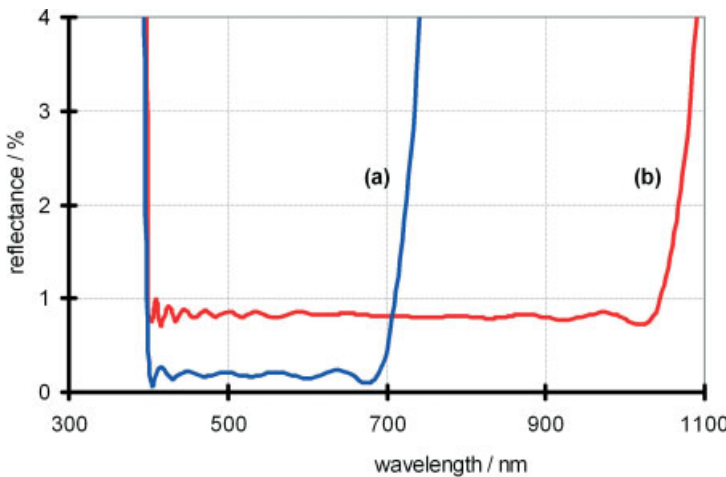
Figure 6.14 Performance of AR-hard®-coatings for (a) the 400–700 nm visible and (b) the 400–1000 nm visible/near-infrared range. Both examples calculated without back surface.

6.5.3
AR Surface Structures

Over the last decade, many attempts have been made to produce broadband antireflective properties applying single layers, in which the refractive index varies gradually from that of the bulk material to unity. Unfortunately, a bulk material with a considerably lower refractive index than the substrate index, as necessary for perfect antireflection of a material with a refractive index near 1.5, does not exist. The principle to overcome this problem is always the same. An available low-index material (e.g., glass or silica) is mixed with air on a subwavelength scale that needs to make a compromise between optical and mechanical properties. Layers with decreasing effective index from substrate site to air can be performed by porous sol–gel coatings or by stochastic and periodic surface structures as shown in Figure 6.15.
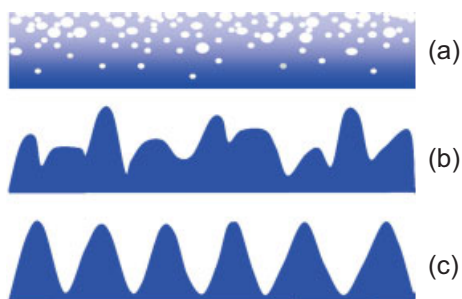
Figure 6.15 Schematic illustration of alternatives to achieve AR properties utilizing a decreasing effective refractive index from the bulk substrate to air: (a) porous coating, (b) stochastic nano-structure, and (c) periodic moth-eye pattern.

Antireflective surface structures on polymers may have the potential to be inexpensive because they can be replicated by embossing. The spacing of a suitable array has to be smaller than the wavelength concerned, but the depth is a significant fraction of that wavelength. First periodic subwavelength surface structures with antireflective properties have been observed in nature on the eyes of the night-flying moth [101]. First technical solutions have been generated by using the interference pattern at the intersection of two coherent beams of light from a laser. Today, master structures for surface areas up to about 0.5 m^2 can be created in a holographic optical process, and efforts are in progress to increase this area [102]. Furthermore, microreplication techniques like UV imprinting are in development to form periodic AR structures at wafer scale [103].

A plasma-etching process to generate an antireflective structure on PMMA has been developed recently at Fraunhofer IOF in 2001 [104]. Applying a new procedure that uses a thin initial layer prior to the etching step in different types of AR structures can now be generated in a shorter period and without limitations on the type of polymer [105]. Both technologies are labeled with the joint trade name AR-plas®. Figure 6.16 shows scanning electron micrographs of AR surface structure generated on PMMA and on Zeonex by plasma etching. The AR properties for normal and oblique light incidence are much better than obtainable by a com-
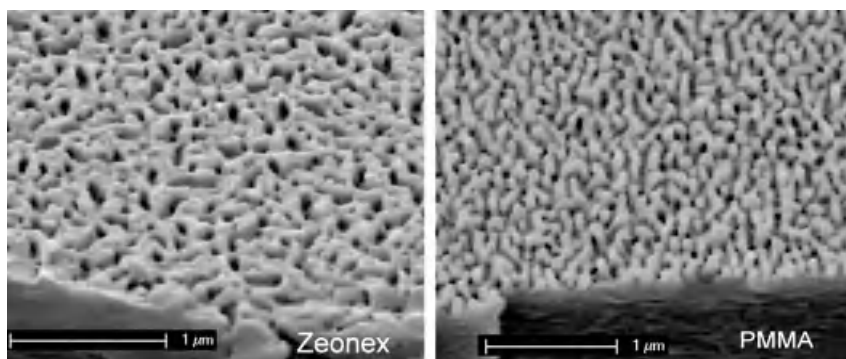
Figure 6.16 SEM images of AR structures on PMMA and Zeonex generated plasma etching.
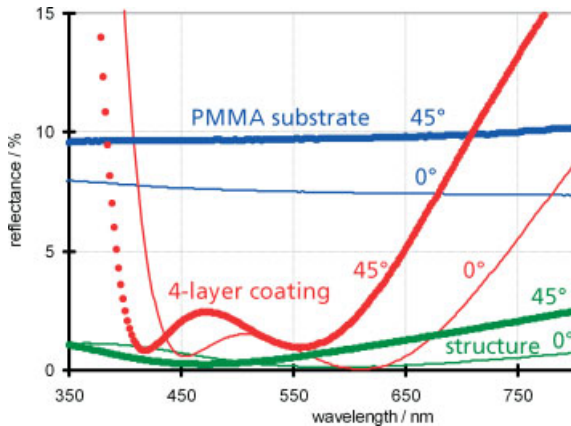
Figure 6.17 AR properties at normal and at oblique light incidence for
a plasma-etched AR structure as shown in Figure 6.16 for PMMA and
for a typical vacuum-deposited AR coating.

mon interference coating (Figure 6.17). Curved lenses with such structures on
both sides appear colorless and clear.

During the last years, a number of technologies to generate AR nanostructures
have been described in literature, among them, few are given below:

- A single porous PMMA film was produced by spin-coating and microphase separation between two PMMA blocks [106].
- Another single porous PMMA film was produced by spin coating of a polystyrene/PMMA blend followed by selective etching the PS phase [107].
- A polymer spin coating containing silica spheres was ion etched to achieve a master structure for replication [108, 109].
- Stochastic nanostructures suitable for AR were generated directly on the tool for hot embossing by an anodic oxidation process of an oxide or metal layers deposited on the tool [110].
- A PMMA latex with AR properties was synthesized by emulsion polymerization of methyl methacrylate and spin coating [111].

6.6
Additional Functional Coatings

6.6.1
Mirrors

The metallization of hot-molded polymer surfaces is a common method to produce front surface and back surface mirrors as well as beam splitters. One of the
most popular applications of metalized thermoplastics is injection-molded reflec-

tors for automotive headlights. Aluminum and silver are the best reflector materials in the visible range, and gold is a good reflector in the infrared range. A good metallic film will completely reflect or absorb the incident light if it is about 100 nm thick, whereas thinner films are partly transparent.

Frequently discussed in the literature are procedures to provide a good adhesion of the metallic layers to special polymers. Nonstoichiometric oxide interlayers of chromium and silicon as well as many different plasma treatments are mentioned [112–115]. In fact, the formation of covalent bonds between atoms of the polymer structure and a metallic atom is the most widely accepted mechanism for high adhesion forces [116–118]. Thin dielectric layer stacks deposited on top of metal layers are common to enhance the reflectivity in a certain spectral range and to prevent chemical and mechanical attacks (Figure 6.18). Typical materials to protect aluminum layers onto a polymer from atmospheric corrosion substrates are SiO_2 and its organically modified compounds [23].
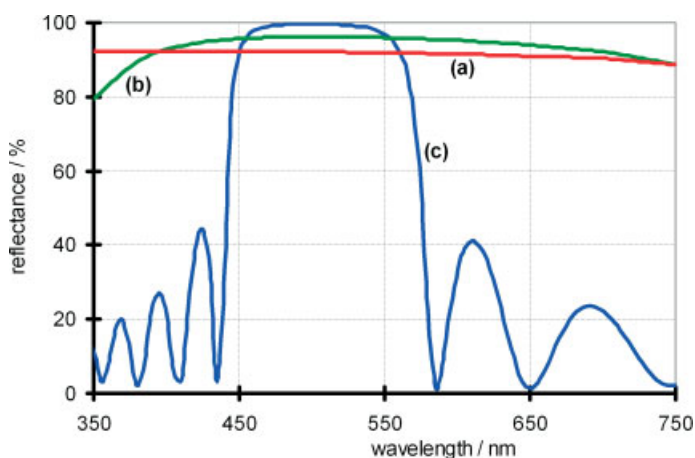
Figure 6.18 Metallic and dielectric mirrors: (a) single-layer aluminum, (b) enhanced mirror consisting of a metallic layer and a dielectric two-layer stack, and (c) multilayer (HL)8H consisting of alternating quarter-wave oxide layers of high and low refractive index.

The metal reflecting layers suffer from a considerable absorption loss. Pure dielectric mirrors are common on glass optics. They consist of alternating oxide layers of high (H) and low refractive index (L) that form a QW stack. This is because the beams reflected from all interfaces are of equal phase when they reach the front surface. They therefore combine constructively. Depending on the number of the HL layer pairs, a reflectivity higher than 99.5% in a small spectral range can be achieved as shown in Figure 6.18. The physical thickness of dielectric mirrors is typically in the range of several microns. Because of problems with adhesion and stress-cracking, they are not often produced on thermoplastics. One example is a cold conversion reflector on ULTEM plastic substrate developed by OC Oerlikon Balzers, Ltd. [119].

A new generation of mirrors consists of multilayer polymer film [120]. Up to several hundred polymer layers with alternating refractive indices are attached together and stretched to become increasingly thinner until a desired interference effect is achieved. Such mirrors can reach a reflectivity greater than 99% of both incident polarizations at all incident angles over a wide wavelength band.

6.6.2
Electrically Conductive and Antistatic Layers

Electrostatic dust attraction and fingerprint soiling can cause significant problems for plastic optics. The most common transparent thin film material used to implement a sufficient conductivity is indium tin oxide (ITO). While it is typically deposited at a higher temperature, various processes have been developed for coating plastics including ion-assisted deposition [121–123] magnetron sputtering [124–127], and sol–gel processes [128]. It was found that a maximum surface resistivity of $10^{10}\,\Omega$ sq.$^{-1}$ is required to prevent a notable airborne dust attraction. A thin ITO layer to provide the enhanced conductivity can be provided at the base of a design incorporating at least 1000 nm of over-coating silica without significant degradation of the electrical properties. The placement of an ITO layer within the AR stack can therefore be optically accommodated [129]. Low-resistivity transparent coatings on polymer substrates are required for EMI shielding of plasma displays and as electrodes. ITO-Ag-ITO layer stacks have been optimized to have sheet resistances below $16\,\Omega$ sq.$^{-1}$ with total light transmissions over 80% at 550 nm [130]. Nowadays, the development of cold deposition processes for ITO and indium zinc oxide is mainly driven by the development of OLEDs. Typical substrates are PC and PET foil [131, 132].

6.6.3
Hydrophobic Topcoats

To reduce the fingerprint problem on AR-coated plastics, so-called topcoats have been developed that are typically used on plastic eyeglasses today. The layer on top of the AR coating, just a few nanometers thin, typically consists of fluorine-containing silanes or siloxanes (fluoroalkyl silanes). These materials form layers providing water contact angles up to 120° and contact angles to hexadecane up to 80°. Hydrophobic and oleophobic topcoats should make it easier to remove fatty fingerprints. The state-of-the-art technique is vacuum evaporation of the organic precursors from a ceramic target [133, 134] as well as dip-coating procedures [135–137] on top of the AR-coated surface. Topcoats that do not contain fluorine are slightly less efficient but can be produced cost effectively by a short plasma polymerization process using organosilicone compounds, that is, hexamethyldisiloxane. Super- (or ultra-)water-repellent polymer surfaces with water contact angles higher than 150° can be obtained by depositing hydrophobic materials (mostly fluoroalkyl silanes) onto a number of different nanostructured or microstructured surfaces [138]. Probably all structured surfaces as discussed for AR pur-

poses in Section 6.5.3 are additionally suitable for generating superhydrophobic surfaces. A new hydrophobic hard coating produced by sol–gel process is described in [139].

6.7
Coating Experiences with Different Thermoplastics

In principle, the group of transparent rigid polymers that can be replicated to optical parts comprises many types of acrylics, PCs, polyamides, polyether sulfones, polystyrene, polycycloolefins, and others. But for most of them, publications that would describe their properties for coating do not exist. Only acrylic and PC are well investigated with regard to their behavior to plasma treatments and vacuum-coating processes. Experience regarding these materials is discussed in Sections 6.7.1 and 6.7.2. The information shown in Table 6.1 summarizes some experience gained by the author. The results are validated for the PIAD process applying e-beam evaporation for the deposition of optical interference coatings. More recent transparent thermoplastics like polycycloolefin polymers and copolymers (types of Zeonex™ [140] and Topas™ [141) are very interesting for coating [142]. It is esti-

Table 6.1 Suitability (+ + +, very good, ~, unsatisfactory) of selected thermoplastic materials for vacuum coating taking into account the adhesion properties and the environmental stability of dielectric layers deposited by electron-beam evaporation (broadband AR-coating, PIAD process).

thermoplastic polymer	supplier	suitability
PMMA 6N, 7N, 8N	Evonik	~
Plexiglas HW55	Evonik	+ +
Pleximid 8817	Evonik	~
Makrolon CD2005	Bayer MaterialScience	+ +
Makrolon LQ2847	Bayer MaterialScience	+ +
Lexan LS2	GE Plastics	+ +
Apec HT9351	Bayer MaterialScience	+
Grilamid TR55LX	EMS-Grivory	+ + +
Trogamid CX7323	Evonik	+ + +
Ultrason E 2010	BASF AG	+ + +
Zeonex 480R	Nippon Zeon	+ + +
Zeonex E48R	Nippon Zeon	+ + +
Zeonex 330R	Nippon Zeon	~
Zeonor 1020R	Nippon Zeon	+ + +
Topas 5013	TOPAS advanced polymers	+ + +

mated that these materials have the potential to replace especially PMMA for precision optical applications where complex interference coatings are required.

6.7.1
Polymethylmethacrylate

PMMA is the main thermoplastic material for optical applications. For vacuum coating, however, this material is the most problematic. Many different plasma treatments have been investigated for PMMA [143–147]. Exposed to VUV radiation, PMMA shows a degradation behavior that depends strongly on the wavelength of irradiation. Photons with energies of about 8.5 eV (145 nm) cause a split-off of the methylester group, whereas radiation below this wavelength can break the main polymer chain [148, 149]. Every uncontrolled exposure to plasma generates weak boundary layers of decomposition products on the surface that lessen the adhesion of subsequently evaporated layers dramatically. Some strong plasma treatment conditions are able to remove the ester groups nearly completely and create a polyolefine-like surface composition. These treatments have been described to improve the coating adhesion on PMMA [150–152].

Adhesion layers described in patents for PMMA coating comprise organic compounds [153–155], silicon oxides [156–158], as well as thin metal layers [159, 160]. To enhance the adhesion of sputtered metal layers, plasma treatments using a CH_4/Ar mixture [161] or CO_2 [162] as reactive gases have been used. A new process suggested the deposition of a VUV protective layer without any presence of plasma. In a second step, optical interference coatings are deposited on this base layer with plasma assistance [163].

Further coating results obtained for PMMA are specified in Sections 6.2.3 and 6.5.3.

6.7.2
Polycarbonate

PC of bisphenol A (Makrolon™, Lexan™) is especially important for automobile applications because of its high fail-safety. On the other hand, the material is very soft and sensitive to scratches. Various efforts are under way to develop scratch-resistant transparent layers. On automobile parts and eyeglasses, one scratch-resistant sol–gel coating based on a highly filled nanocomposite material with surface-modified AlOOH nanoparticles is applied below many different wet-chemical coatings. A haze value of about 10% is reached using a 5-μm-thick layer and a filler content of about 40% [164]. Protective coatings on PC based on silica and siloxane (hexamethyldisiloxane or tetraethoxysilane) can be obtained by applying different PECVD processes [165–167] and ion-assisted deposition of silica [168]. Optical coatings produced by PECVD that consist of SiN_x and SiO_2 are described, as well as classical oxide layer stacks [52, 169–171]. Different plasma treatments are successfully applied to increase the coating adhesion on PC [32, 86, 172, 173]. In fact, there are fewer problems with coating adhesion on PC compared with

PMMA. But, the chemistry of PC due to plasma and UV radiation interactions is very complex [174, 175]. During plasma treatment, both basic processes, crosslinking and degradation, can occur that make the adhesion stronger or worse.

For outdoor applications, coatings on PC have to be protected against UV radiation to prevent a later gradual destruction of the interfaces. This problem is significant and sometimes underestimated. PC is quite sensitive to radiation at wavelength above 330 nm [174]. Evaporated coatings without UV-protecting function lose there adhesion after some days of weathering. TiO_2 thin films do not provide sufficient protection [176]. Suitable UV protection coatings for PC contain organic absorbers (as component of a lacquer or of a vacuum coating [32]), ZnO_x [177] or reflect the damaging wavelength range [176].

6.8
Test and Qualification Methods

6.8.1
Optical Properties

In general, methods to evaluate optical properties like transmission, reflection, and absorption are the same for plastic optics as for glass optics. Suitable instruments are the commercially available UV-visible spectrophotometers [178]. A sample is placed in the UV/Vis beam and a graph of the transmittance or reflectance versus the wavelength is obtained. Optical constants of thin films can be calculated from the spectrophotometric or ellipsometric measurements by applying different physical models as described in the basic literature [179, 180]. Care has to be taken if a spectrophotometer works with partly polarized light. Most of molded polymer parts are able to circle the area of polarization because of anisotropically distributed internal stress during manufacturing. Measured transmission values would be different on different positions on a sample. Sometimes, the refractive index of polymers is influenced by processing parameters of the molding process. High-resolution refractive index and index anisotropy can be characterized by m-line spectroscopy [181, 182].

6.8.2
Adhesion

The characterization of coating adhesion is fundamental in the process of developing high-quality coatings as described in detail in Section 6.3. Generally, the apparent adhesion is determined by applying an external mechanical stress. Most common adhesion tests are the tape-peel test, the pull test, and different scratch tests.

In the pull test, a stud is glued onto the sample surface and removed in vertical direction while the failure force is measured. The test is specified in comparable terms in the international standards MIL 883, ASTM D4541, and EN ISO 4624.

The main problems in applying this test to rigid thermoplastics coated with inorganic layers are interactions between the adhesive or solvents inside it and the coated system; such problems can never be excluded.

The mostly applied tape-peel test can be carried out as a "pass/fail" test (EN ISO 9211, ASTM D1876), or as a six-step classification test if applied on a right angle lattice pattern (cross-cut test according to EN ISO 2409 or ASTM D3002). Note that the numbers 0–5 for evaluating the result are defined in opposite directions in the ASTM D3002 (5 for best adhesion) and EN ISO 2409 standards (0 for best adhesion).

For coated polymers, it is suggested to make a microscopic inspection of the tested sample area to identify the location of failure in the interface, either in a near-surface region or in the bulk polymer. Examples are shown in Figure 6.19.
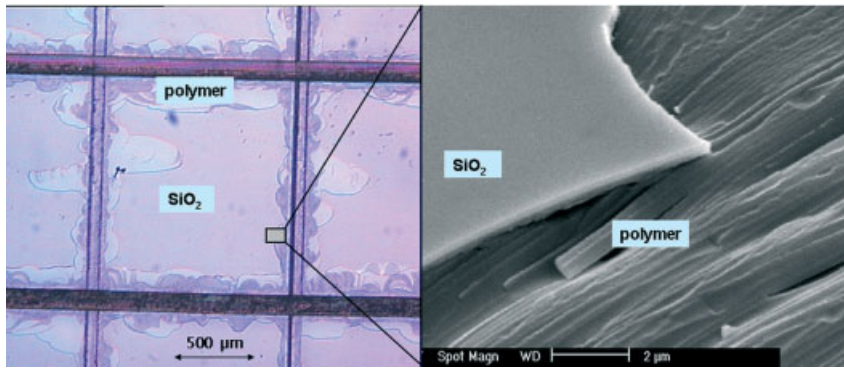
Figure 6.19 Microscopic and SEM images of a coated PMMA surface after tape-peel test carried out on a cross-cut: adhesion loss because of cohesive fracture in the polymer phase.

Some other very special measurements have been developed for testing the adhesion of brittle films on flexible substrates including the investigation of the cracking behavior [183] or electrical properties [184]. In general, adhesion tests are used as comparative tests immediately after coating deposition. Taking into account slow changes of film stress and chemical changes possibly initiated during the deposition process, adhesion tests on coated polymers should be repeated after environmental testing as well as after a given storage time.

6.8.3
Environmental Durability

Environmental tests for coating plastics have to be specified deliberately, taking into account the conditions of application as well as certain polymer-typical properties. In many cases, it is not adequate to adopt test procedures that have been defined for coated glass optics. If a polymer part is coated with an inorganic layer, temperature changes cause comparatively high-level thermal stresses on coatings and substrates (see Section 6.4). Crack formation as a consequence depends on

the total linear expansion and, therefore, the geometry of the coated part. Environmental tests for plastic optics therefore have to be carried out on the original part rather than on standardized sample sizes. Furthermore, test conditions especially for long-term properties have to take into account the durability of the polymer material itself. For example, during a long-term test at an elevated temperature, polymer additives may diffuse to the interfaces and damage them without any participation of the coating itself.

Besides the common climatic test conditions (e.g., high humidity and temperature cycling according to ISO 9022 or MIL-C-675), outdoor applications especially require the testing for resistance to global radiation, which contains UV radiation. For plastic eyeglasses, the so-called quick UV test (Weathering-QUV ASTM D4329, D4587, ISO 4892) is very common. During the test, cycles during storage at high humidity alternate with the condition where the sample is exposed to strong UV irradiation. The test conditions may be stronger than necessary for much optics made of thermoplastics but can be helpful during the development of high-quality coated parts.

6.8.4
Abrasion and Scratch Resistance

Abrasion resistance is of considerable importance especially for many plastic optics and yet extremely difficult to define in any term. Abrasion resistance is a combination of factors such as hardness, packing density, elasticity, adhesion, and others. On polymer surfaces, a thin inorganic film may act like an eggshell. Especially the results of scratch tests that use a spiky scratch pin are dependent on the total thickness of coating more than on physical hardness. However, hard coatings on soft plastic surfaces like PC are often characterized by using nano-indentation tests, scratch tests, and the pencil hardness test [185–188].

Various standard tests involve a pad that is drawn under a controlled load for a given number of strokes. The "scratching" media involve soft clothes as well as rubber and steel wool. But, most tests suffer from the fact that they do not give a measurable value of abrasion resistance. In most cases, the test sample is visually compared with a number of standard samples and ranked. The main techniques generally accepted by industry are the Bayer testing [129] and the Taber Abraser test. The Taber Abraser test produces a crosswise surface damage that can be evaluated by the modified scattering level ("Haze," ASTM D1003). For high requirements concerning mechanical strains, as are typical for eyeglasses, for example, it is common to define combinations of tests that should simulate the real situation of application as well as possible. Some standardized test conditions and suitable applications are summarized in Table 6.2.

Table 6.2 Standardized test methods for abrasion resistance and scratch resistance suitable for coated plastics.

test method/standard	short description/comparability
eraser Test; ISO 9211–4 "Optics and optical instruments – optical coatings, part 4: specific test methods"	• moderate abrasion with cotton cheesecloth • severe abrasion with standard eraser • 20–100 strokes with force: 5–10 N • qualitative classification into stability classes • comparable to parts of MIL-C-48497A
Taber Abraser Test; ASTM D 4060 *"Standard Test Method for Abrasion Resistance of Organic Coatings by the Taber Abraser"*	• abrading the surface by rotating the panel under weighted, abrasive wheels • evaluation by "haze" measurement (scattering of light as it passes through a transparent material) • comparable to ISO 9352 • comparable to ASTM D1044 (specifies the weight loss as measuring quantity)
falling sand abrasive test; ASTM D 968 *"Standard Test Methods for Abrasion Resistance of Organic Coatings by Falling Abrasive"*	• falling of an abrasive (or silicon carbide) from a specified height through a guide tube onto the coated sample • measuring quantity: amount of abrasive used per unit film thickness (abrasion resistance) • comparable to ISO 3537 (uses silica sand and evaluation by "haze" measurement)
air blast abrasion test; ASTM D 658 *"Standard Test Method for Abrasion Resistance of Organic Coatings by Air Blast Abrasive"*	• abrasion produced by an air blast of abrasive on coatings applied to a plane, rigid surface • measuring quantity: amount of abrasive used per unit film thickness (abrasion resistance)
scratch test; ISO 4586–2 *"High-Pressure Decorative Laminates, Part 2: Determination of Properties – Resistance to Scratching"*	• circular scores applied by a motorized diamond stylus subjected to a known load • scratching resistance: distance between scores over which flaking occurs or load at the first visible scratch
pencil test; ISO 15184 *"Paints and varnishes – Determination of film hardness by pencil test"*	• establishing the hardest of 20 pencils that does not mark the coating ("Pencil Hardness") • comparable to ASTM D 3363 (14 pencils)

6.9
Summary and Outlook

The development of optical coatings on plastics is subjected to an enormous pressure from applications. Under the conditions of globalization, the time to develop a new marketable product becomes shorter and shorter. The introduction of easy-

to-form polymer materials becomes important for cost saving in the production of consumer electronics and automobile parts as well as of complex-shaped, high-end precision optical parts. In addition, the development of coating technologies for plastics is driven by the growing field of organic electronics (i.e., OLEDs).

From the viewpoint of the material sciences, organic–inorganic hybrid materials and corresponding gradient layers offer the most promising properties to implement hardening coatings on soft plastic surfaces that are also durable under climatic changes for a long time. Sol–gel techniques as well as several vacuum coating techniques are, in principle, capable of producing such coating materials. Sol–gel coating techniques also provide a potential for mass production. New materials with hard inorganic nanoparticles inside the wet-chemical coatings have been launched during the last few years. In addition, the part of wet-chemical coating for AR purposes has been increased.

Vacuum coating is still the most appropriate technique up to now to produce high-end optical interference coatings on glass and plastics. It is the reliable way to achieve the required high layer thickness precision in the range of 1 or 2 nm. The use of different low-pressure plasmas to assist the processes has become quite common. Plasma treatments are applied to modify the layer materials in a desired way. At the same time, various interactions with the polymer surfaces have to be taken into account. To minimize the risk and to reduce development costs for the optical part, applications that need complex coatings are focused on those polymers that provide the highest process stability. For example, lenses for scanner applications are made from Zeonex rather than from PMMA because of easier coating conditions.

The application of nanostructures ("moth-eye structures") is a suitable alternative compared to coating procedures, where AR properties in the visible spectral range are required and where soft surfaces are not the problem. The optical properties of structured polymer surfaces are often superior compared with that of coated parts. Several new techniques to produce AR structure are in development. The hot embossing of AR patterns has proved to be highly cost-effective especially for mass production.

Presently, there is a demand for techniques to implement multifunctional optical interference coatings on rigid plastic parts with medium size in mass production. For example, there is no cost-effective technology available to realize scratch resistant AR coatings on complex-shaped dashboard covers made of PC. Reactive magnetron sputtering may become more important for coating plastics. The sputter provides an area source that is ideal for scaling processes to any production volume. Particularly, for applications where glass is to be replaced by plastics in order to reduce product costs, expensive coating processes are counterproductive. In the coming years, this demand may give new impulses to the industry for the further advancement of coating machines suitable for plastic optics.

References

1 R.W. Schaffer, *Proc. SPIE* **896**, 140 (1988).

2 K.H. Günther, *Proc. SPIE* **896**, 134 (1988).

3 L. Martinu and J.E. Klemberg-Sapieha, Optical coatings on plastics, in: *Optical Interference Coatings*, edited by N. Kaiser and H.K. Pulker (Springer, Berlin/Heidelberg, 2003).

4 U. Schulz, *Appl. Opt.* **45**, 1608 (2006).

5 Y. Taga, *Appl. Opt.* **32**, 5519 (1993).

6 J.-J. Simon, *et al.*, *51st Ann. Tech. Conf. Proc. Soc. Vacuum Coaters*, 2008, pp. 502–505.

7 H.K. Pulker, *Coatings on Glass* (Elsevier, Amsterdam/New York, 1984).

8 N. Kaiser, *Appl. Optics*, **41** 3053 (2002).

9 P.J. Martin and R.P. Netterfield, Optical films produced by ion based techniques, in: *Progress in Optics*, Vol. 32, edited by E. Wolf (Elsevier, Amsterdam, 1986).

10 J.A. Devasahayam, I. Agatic, B. Druz, H. Hegde, I. Zaritsky, S.R. Das, M. Boudreau, T. Yin, R. Mallard, and S. LaFramboise, *J. Vac. Sci. Technol. A* **20**, 1135 (2002).

11 S. Mohan and M.G. Krishna, *Vacuum* **46**, 645 (1995).

12 P.J. Martin, *Vacuum* **36**, 585 (1986).

13 O. Zabeida, J.E. Klemberg-Sapieha, L. Martinu, and D. Morton, *42nd Ann. Tech. Conf. Proc. Soc. Vacuum Coaters*, 1999, pp. 267–272.

14 S. Pongratz and A. Zöller, *J. Vac. Sci. Technol.* **A10**, 1897 (1992).

15 P.J. Kelly and R.D. Arnell, *Vacuum* **56**, 159 (2000).

16 S.M. Rossnagel, Sputter deposition in: *Opportunities for Innovation: Advanced Surface Engineering*, edited by W.D. Sproul and K.O. Legg (Technomic Publishing, Switzerland, 1995).

17 S.J. Nadel, P. Greene, J. Rietzel, and J. Strümpfel, *Thin Solid Films* **442**, 11 (2003).

18 G. Kienel, *Thin Solid Films* **77**, 213 (1981).

19 D. Glöß, P. Frach, C. Gottfried, S. Klinkenberg, J.-S. Liebig, W. Hentsch, H. Liepack, and M. Krug, *Thin Solid Films* **516**, 4487 (2008).

20 J.M. Walls, I.T. Brinkley, D.R. Gibson, and E.M. Waddell, *4th Ann. Tech. Conf. Proc. Soc. Vacuum Coaters*, 2005, pp. 36–40.

21 M. Walls and D. Gibson, *Photonics Spectra* **42**, 56 (2008).

22 R. Beckmann, K.-D. Nauenburg, T. Naumann, U. Patz, G. Ickes, H. Hagedorn, and J. Snyder, *44th Ann. Tech. Conf. Proc. Soc. Vacuum Coaters*, 2001, pp. 288–294.

23 H. Grünwald, W. Dicken, K. Nauenburg, R. Adam, J. Bartella, T. Gebele, S. Mitzlaff, U. Patz, and J. Snyder, *Metallized Plastics 7: Fundamental and Applied Aspects*, edited by K.L. Mittal (VSP BV, Utrecht/Köln/Boston/Tokyo, 2001).

24 T. Schmauder, S. Küper, and K. Kruse, *50th Ann. Tech. Conf. Proc. Soc. Vacuum Coaters*, 2007, paper O-13.

25 A. Azens, E. Avendaño, J. Backholm, L. Berggren, G. Gustavsson, R. Karmhag, G.A. Niklasson, A. Roos, and C.G. Granqvist, *Mater. Sci. Technol. Eng. B* **119**, 214 (2005).

26 S. Schiller, V. Kirchhoff, N. Schiller, and H. Morgner, *Surf. Coat. Technol.*, **125**, 354 (2000).

27 H.W. Wang, C.J. Tang, and C.C. Lee, *Appl. Opt.* **47**, C79 (2008).

28 J.C. Rostaing, F. Coeuret, B. Drevillion, R. Etemadi, C. Godet, J. Huc, J.Y. Parey, and V.A. Yakovlev, *Thin Solid Films* **236**, 58 (1993).

29 H.K. Pulker, *Surf. Coat. Technol.* **112**, 250 (1999).

30 L. Sabatini and P.G. Zambonin, *Surface Characterization of Advanced Polymers* (Wiley-VCH, Weinheim, 1993.

31 C.T. Guo, *Thin Solid Films* **516**, 4053 (2008).

32 T. Schmauder, K.-D. Nauenburg, K. Kruse, and G. Ickes, *Thin Solid Films* **502**, 270 (2006).

33 M. Kuhr, S. Bauer, U. Rothhaar, and D. Wolff, *Thin Solid Films* **442**, 107 (2003).

34 H. Dislich, *J. Non-Cryst. Solids* **57**, 371 (1983).

35 D. Chen, *Solar Energy Mater. Solar Cells* **68**, 313 (2001).

36 R. Houbertz, G. Domann, C. Cronauer, A. Schmitt, H. Martin, J.-U. Park, L. Fröhlich, R. Buestrich, M. Popall, U. Streppel, P. Dannberg, C. Wächter, and A. Bräuer, *Thin Solid Films* **442**, 194 (2003).

37 G. Schottner, K. Rose, and U. Posset, *J. Sol–Gel Sci. Technol.* **27**, 71 (2003).

38 L.Y.L. Wu, E. Chwa, Z. Chen, and X.T. Zeng, *Thin Solid films* **516**, 1056 (2008).

39 D. Blanc, A. Last, J. Franc, S. Pavan, and J.-L. Loubet, *Thin Solid Films* **515**, 942 (2006).

40 K. Asai and M. Kikuchi, US Patent 5116644, 1992.

41 Y. Sakai, H. Norimatsu, Y. Saito, H. Inomata, and T. Misuno, *Thin Solid Films* **392**, 294, (2001).

42 H.G. Floch and P.F. Belleville, *J. Sol–Gel Sci. Technol.* **1**, 293 (1994).

43 S.S. Ashley and S.T. Reed, US Patent No. 4929278, 1988.

44 T. Taniguchi and J. Mibae, US Patent No. 4590117, 1986.

45 M. Mennig, P.W. Oliveira, and H. Schmidt, *Thin Solid Films* **351**, 99 (1999).

46 M. Sangermano, B. Voit, F. Sordo, and K.J. Eichhorn, G. Rizza, High refractive index transparent coatings obtained via UV/thermal dual-cure process, *Polymer* **49**, 2018 (2008).

47 Y.F. Liu, C.L. Lu, M.J. Li, L. Zhang, and B. Yang, *Coll. Surf. A* **328**, 67 (2008).

48 Z. Liu, X. Zhang, T. Murakami, and A. Fujishima, S*olar Energy Mater. Sol. Cells* **92** 1434 (2008).

49 L. Zhang, Y. Li, J. Sun, and J. Shen, *Langmuir* **24**, 10851 (2008).

50 E.M. Liston, L. Martinu, and M.R. Wertheimer, *J. Adhesion Sci. Technol.* **7**, 109 (1993).

51 L. Gerenser, Surface chemistry of plasma-treated polymers, in: *Handbook of Thin Film Process Technology*, edited by D.A. Glocker and S.I. Shah (CRC Press, Boca Raton, FL, 2003).

52 D. Poitras and L. Martinu, *Appl. Opt.*, **39** 1168 (2000).

53 M. Konuma, *Plasma Techniques for File Deposition* (Alpha Science Int., Oxford, UK, 2006).

54 L. Martinu, D. Poitras, *J. Vac. Sci. Technol. A* **18**, 2619 (2000).

55 M.R. Wertheimer, L. Martinu, and E.M. Liston, Plasma sources for polymer surface treatment, in: *Handbook of thin Film Process Technology*, edited by D.A. Glocker and S.I. Shah (IOP Publishing, London, UK,1998).

56 H.V. Boenig, *Fundamentals of Plasma Chemistry and Technology* (Techonomic, Lancaster, 1988).

57 S. Wu, *Polymer Interface and Adhesion* (Marcel Dekker, New York/Basel, 1982).

58 L.H. Lee, *Fundamentals of Adhesion* (Plenum Press, New York, 1991).

59 V. Skurat, *Nucl. Instr. Meth.* **B208**, 27 (2003).

60 M.R. Wertheimer, *et al.*, *Nucl. Instr. Meth.* **B151**, 65 (1999).

61 A.C. Fozza, J.E. Klemberg-Sapieha, and M.R. Wertheimer, Vacuum ultraviolet irradiation of polymers, *Plasmas Polym.*, **4**, 183 (1999).

62 N.S. Allen and M. Edge, *Fundamentals of Polymer Degradation and Stabilisation* (Elsevier Applied Science, London/New York, 1992).

63 J.F. Rabek, *Mechanisms of Photophysical Processes and Photochemical Reactions of Polymers* (Wiley, New York, 1987).

64 A. Rivaton, *et al.*, *Polym. Degr. Stab.* **49**,163 (1995).

65 A. Ram, O. Zilber, and S. Kenig, *Polym. Eng. Sci.* **25**, 535 (1985).

66 G.F. Tjandraatmadja, L.S. Burn, and M.C. Jollands, *Polym. Degr. Stab.* **78**, 435 (2002).

67 P. Munzert, U. Schulz, and N. Kaiser, *Surf. Coat. Technol.* **173–174**, 1048 (2003).

68 J.R. Woodworth, M.G. Blain, R.L.K. Jarecki, T.W. Hamilton, and B.P. Aragon, *J. Vac. Sci. Technol. A* **17**, 3209 (1999).

69 T. Lippert, *Plasma Proc. Polym.* **2**, 525 (2005).

70 A. Holländer, *et al.*, *Surf. Coat. Technol.* **116–119**, 788 (1999).

71 V. Skuratand and Y.L. Dorofeev, *Angew. Makromol. Chem.* **216**, 205 (2003).

72 M.C. Coen, R. Lehmann, P. Groening, and L. Schlapbach, *Appl. Surf. Sci.* **207**, 276 (2003).

73 F. Garbassi, M. Morra, and E. Occhiello, *Polymer Surfaces* (Wiley-VCH, Weinheim, 1998).

74 V. Teixeira, *Thin Solid Films* **392**, 276 (2001).

75 S. Tamulevicius, *Vacuum* **51**, 127 (1998).

76 K.S. Chen, X. Zhang, and S.Y. Lin, *Thin Solid Films* **434**, 190 (2003).

77 M.F. Doerner and W.D. Nix, *CRC Crit. Rev. Solid State Mater. Sci.* **14**, 225 (1988).

78 G.N. Strauss, N.Q. Danh, and H.K. Pulker, *J. Non-Cryst. Solids* **218** 256 (1997).

79 A. Zöller, R. Götzelmann, and K. Matl, *Proc. SPIE* **2776**, 1 (1996).

80 K. Yamamoto, T. Harada, N. Tomikawa, H. Uyama, S.-C. Yang, and H. Fujiyama, *Thin Solid Films* **345**, 94 (1999).

81 U. Schulz and N. Kaiser, *47th Ann. Tech. Conf. Proc. Soc. Vacuum Coaters,* 2003, p. 419.

82 C.H. Hsueh and A.G. Evans, *J. Am. Ceram. Soc.* **68**, 241 (1985).

83 C.H. Hsueh, *Thin Solid Films* **418**, 182, (2002).

84 R.A. Luchata, *Appl. Opt.* **30**, 2252 (1991)

85 A.A. Abdallah, P.C.P. Bouten, J.M.J. den Toonder, and G. de With, *Thin Solid Films* **516**, 1063 (2008).

86 B.W. Muir, H. Thissen, G.P. Simon, P.J. Murphy, and H.J. Griesser, *Thin Solid Films* **500**, 34 (2006).

87 A. Macleod, *Thin-Film Optical Filters*, 3rd edition (IOP Publishing, Bristol/Philadelphia, 2001).

88 R. Willey, *Practical Design and Production of Thin Films* (Marcel Dekker, Basel/New York, 2002).

89 F.C. Rock, US Patent 3432225 (1964).

90 R. Herrmann, *Appl. Opt.* **24**, 1183 (1985).

91 The Essential Macleod, Version 8.2, 2000.

92 http://www.optilayer.com/.

93 J. Allen and A. Tregunna, *J. Appl. Phys.* **21**, 92 (1988).

94 F. Samson, *Surf. Coat. Technol.* **81**, 79 (1996).

95 R. Blacker, D. Bohling, M. Coda, and M. Kosoley, *43rd Ann. Tech. Conf. Proc. Soc. Vacuum Coaters*, 2002, pp. 212–216.

96 U.J. Gibson and C.M. Kennemore, *Thin Solid Films* **124**, 27 (1985).

97 U. Schulz, U.B. Schallenberg, and N. Kaiser, WO 0204374, 2002.

98 U. Schulz, U.B. Schallenberg, and N. Kaiser, *Appl. Opt.* **41** 3107 (2002).

99 U. Schulz, U.B. Schallenberg, and N. Kaiser, *Appl. Opt.* **42**, 1346 (2003).

100 U.B. Schallenberg, *Appl. Opt.* **45**, 1507 (2006).

101 C.G. Bernhard, *Endeavour* **26**, 79 (1967).

102 A. Gombert, W. Glaubitt, K. Rose, J. Dreibholz, B. Bläsi, A. Heinzel, D. Sporn, W. Döll, and V. Wittwer, *Thin Solid Films* **351**, 73 (1999).

103 C. Ting, C. Chen, and C.P. Chou, *IEEE Phot. Technol. Lett.* **20**, 1196 (2008).

104 A. Kaless, U. Schulz, P. Munzert, and N. Kaiser, *Surf. Coat. Technol.* **200**, 58 (2005).

105 U. Schulz, P. Munzert, R. Leitel, I. Wendling, N. Kaiser, and A. Tünnermann, *Opt. Express* **15**, 1308 (2007).

106 M.S. Park, Y. Lee, and J.K. Kim, *Chem. Mater.* **17**, 3944 (2005).

107 S. Walheim, E. Schäffer, J. Mlynek, and U. Steiner, *Science* **283**, 520 (1999).

108 N.C. Linn, C.H. Sun, and P. Jiang, *Appl. Phys. Lett.* **91**, 101 (2007).

109 C.H. Sun, A. Gonzalez, N.C. Linn, *et al.*, *Appl. Phys. Lett.* **92**, Article Number 051107 (2008).

110 T. Yanagishita, K. Yasui, T. Kondo, *et al.*, *Chem. Lett.* **36**, 530 (2007).

111 H. Jiang, K. Yu, and Y.C. Wang, *Opt. Lett.* **32** 575 (2007).

112 P. Schissel, C. Kennedy, and R. Goggin, *J. Adhesion Sci. Technol.* **9**, 412 (1995).

113 R. Cueff, *et al.*, *Thin Solid Films* **270**, 230 (1995).

114 C. Bichler, H. Langowski, U. Moosheimer, and B. Seifert, *J. Adhesion Sci. Technol.* **11**, 233 (1997).

115 J. Friedrich, *et al.*, *J. Adhesion* **71**, 297 (1999).

116 F. Bodino, *et al.*, *Thin Solid Films* **241**, 21 (1994).

117 S. Ben Amor, *et al.*, *Thin Solid Films* **293**, 163 (1997).

118 Y. Leterrier, *Progr. Mater. Sci.* **48**, 1 (2003).

119 http://www.oerlikon.com/ecomaXL/index.php?site=OPTICS_EN_irblocker_-calflex

120 M.F. Weber, C.A. Stover, L.R. Gilbert, T.J. Nevitt, and A.J. Ouderkirk, *Science* **287**, 2451 (2000).

121 S. Laux, N. Kaiser, A. Zöller, R. Götzelmann, H. Lauth, and H. Bernitzki, *Thin Solid Films* **335**, 1 (1998).

122 J.S. Kim, J.W. Bae, H.J. Kim, N.-E. Lee, G.Y. Yeom, and K.H. Oh, *Thin Solid Films* **377–378**, 103 (2000).

123 K. Fuchsel, U. Schulz, N. Kaiser, *et al.*, *Appl. Opt.* **47**, C297 (2008).

124 C. Yang, S. Lee, T. Lin, and S. Chen, *Thin Solid Films* **516**, 1984 (2008).

125 Z. Yang, S. Han, T. Yang, L. Ye, H. Ma, and C. Cheng, *Appl. Surf. Sci.* **161**, 279 (2000).

126 C.S. Moona and J.G. Han, *Thin Solid Films* **516**, 6560 (2008).

127 C. Guillén and J. Herrero, *Semicond. Sci. Technol.* **23**, 075002 (2008).

128 N. Al-Dahoudi, H. Bisht, C. Göbbert, T. Krajewski, and M.A. Aegerter, *Thin Solid Films* **392**, 299 (2001).

129 D. Bohling, M. Coda, R. Blacker, R. Gove, *43rd Ann. Tech. Conf. Proc. Soc. Vacuum Coaters*, 2000, pp. 222–229.

130 M. Fahland, P. Karlsson, and C. Charton, *Thin Solid Films* **392**, 334 (2001).

131 T.K. Yong, T.Y. Tou, R.B. Yang, B.S. Teo, and H.K. Yow, *Vacuum* **82**, 1445 (2008).

132 S.-W. Cho, J. Jeong, J.-H. Bae, *et al.*, *Thin Solid Films* **516**, 7881 (2008).

133 R. Dombrowski and M. Friz, European Patent EP0770699B1, 1998.

134 http://www.cotec-gmbh.com.

135 T. Teranashi, K. Kamitani, and Sunada T., US Patent 6033738A1, 2000.

136 Y. Yan, D.-G. Chen, WO9919084A1, 1999.

137 A.M. Almanza-Workma, S. Raghavan, S. Petrovic, B.Gogoi, P. Deymier, D.J. Monk, and R. Roop, *Thin Solid Films* **423**, 77 (2003).

138 A. Hozumi and O. Takai, *Thin Solid Films* **334**, 54 (1998)

139 L.Y.L. Wu, G.H. Tan, X.T. Zeng, T.H. Li, and Z. Chen, *J. Sol–Gel Sci. Technol.* **38** 1573 (2006).

140 H. Cherdon, M.J. Brekner, F. Osan, *Angew. Makromol. Chemie* **223**, 121 (1994).

141 G. Khanarian and H. Celanese, *Opt. Eng.* **40**, 1024 (2001).

142 P. Munzert, U. Schulz, and N. Kaiser, *Surf. Coat. Technol.* **173–174**, 1048 (2003).

143 T.J. Hook, J.A. Gardella, and L. Salvati, *J. Mater. Res.* **2(1)**, 117 (1987).

144 T.G. Vargo, J.A. Gardella, and L. Salvati, *J. Pol. Sci. A* **27**, 1267 (1989).

145 O. Chiantore, L. Trossarelli, M. Lazzari, *Polymer* **41**, 1657 (2000).

146 P. Gröning, *et al.*, *Appl. Surf. Sci.* **89**, 83 (1995).

147 A. Licciardello, *et al.*, *Nucl. Instr. Meth. Phys. Res. B* **116**, 168 (1996).

148 K. K Okudaira, *et al.*, *J. Electr. Spectr. Rel. Phenom.* **88**, 913 (1998).

149 S. Küper, S. Modaressi, and M. Stuke, *J. Phys. Chem.* **94**, 7514 (1990).

150 U. Schulz, P. Munzert, and N. Kaiser, *Surf. Coat. Technol.* **142–144**, 507 (2001).

151 S. Koh, H. Jung, S. Song, W. Choi, Y. Yoon, and J. Cho, US Patent US5783641, 1998.

152 J.E. Klemberg-Sapieha, L. Martinu, N.L.S. Yamasaki, and C.W. Lantman, *Thin Solid Films* **476**, 101 (2005).

153 J. Terhuerne, A. Zoeller, R. Goetzelmann, H. Gruenwald, and F. Scherrer, German Patent DE59710224D, 2003.

154 F. Kimock, B. Knapp, and J. Finke, WO9206843, 1992.

155 U. Hayat, Improved process for producing well-adhered/abrasion-resistant optical coatings on an optical plastic substrate, *J.M.S. – Pure Appl. Chem. A* **31**, 665 (1994).

156 H. Ichikawa, German Patent DE3818341, 1988.

157 A. Zoeller, K. Matl, R. Goetzelmann, and G. Sauer, German Patent DE4128547, 1993.

158 N. Couget, European Patent EP1112981, 2001.

159 Y. Lian, K. Leu, S. Liao, and W. Tsai, *Surf. Coat. Technol.* **71**, 142 (1995).

160 C.L. Lau, K. Gibbons, and F. Woodard, US Patent US5589280, 1996.

161 M. Hennessey, US Patent US4957603, 1990.

162 Ph. Duchatelard, *et al.*, *Thin Solid Films* **250**, 142 (1994).

163 P. Munzert, U. Schulz, and N. Kaiser, *Plasma Process. Polym.* **4**, 1036 (2007).

164 S. Sepeur, N. Kunze, B. Werner, and H. Schmidt, *Thin Solid Films* **35**, 216 (1999).

165 H. Amma, Y. Yoshimoto, M. Warshina, and Y. Hatanaka, *Appl. Surf. Sci.* **175–176** 484 (2001).

166 D. Rats, V. Hajek, and L. Martinu, *Thin Solid Films* **340**, 33 (1999).

167 L. Zajickova, V. Bursikova, and J. Janca, *Vacuum* **50**, 19 (1998).

168 U. Schulz, S. Jakobs, and N. Kaiser, *Proc. SPIE* **2776**, 169 (1996).

169 A. Bergeron, J.E. Klemberg-Sapieha, and L. Martinu, *J. Vac. Sci. Technol. A* **161**, 3227 (1998).

170 F. Sarto, M. Alvisi, E. Melissano, A. Rizzo, S. Scaglione, and L. Vasanelli, *Thin Solid Films* **346**, 196 (1999).

171 H. Bartzsch, P. Frach, K. Lau, and J. Weber, *51st Ann. Tech. Conf. Proc. Soc. Vacuum Coaters*, 2008, pp. 455–437.

172 S. Vallon, *et al.*, *J. Adhes. Sci. Technol.* **10**,1287 (1996).

173 J.H. Lee, J.S. Cho, S.K. Koh, and D. Kim, *Thin Solid Films* **449**, 147 (2004).

174 A. Rivaton, B. Mailhot, J. Soulestin, *et al.*, *Eur. Polym. J.* **38**, 1349 (2002).

175 P. Fabbri, C. Leonelli, M. Messori, F. Pilati, *et al.*, *J. Appl. Polym. Sci.* **108**, 1426 (2008).

176 U. Schulz, K. Lau, and N. Kaiser, *Appl. Opt.* **47**, C83 (2008).

177 A. Moustaghfir, E. Tomasella, M. Jacquet, A. Rivaton, B. Mailhot, J.L. Gardette, and E. Bêche, *Thin Solid Films* **515**, 662 (2006).

178 http://las.perkinelmer.com/.

179 H.M. Lidell, *Computer-Aided Techniques for the Design of Multilayer Filters* (Adam Hilger, Bristol, 1981).

180 J. Borgogno, Spectrophotometric methods for refractive index determination, in: *Thin Films for Optical Systems*, edited by F.R. Flory (Marcel Dekker, New York, 1995) pp. 269–328.

181 M.B. Pereira and F. Horowitz, *Appl. Opt.* **42**, 3268 (2003).

182 H. Anma, Y. Yoshimoto, M. Warashina, and Y. Hatanak, *Appl. Surf. Sci.* **175–176**, 484 (2001).

183 Q. Guo, H. Osaki, L.M. Keer, and D.R. Wheeler, *J. Appl. Phys.* **68**, 1649 (1990).

184 D. Nardducci; in: *Metallized Plastics 5&6: Fundamental and Applied Aspects,* edited by K.L. Mittal (VSP BV, Utrecht, 1998), pp. 409–423.

185 C. Zhong, L.Y.L. Wu, E. Chwa, and O. Tham, *Mater. Sci. Eng. A* **493**, 292 (2008).

186 L.Y.L. Wu, E. Chwa, Z. Chen, and X.T. Zeng, *Thin Solid Films* **516**, 1056 (2008).

187 C. Charitidis, A. Laskarakis, S. Kassavetis, C. Gravalidis, and S. Lgothetidis, *Superlattices Microstruct.* **36**, 171 (2004).

188 U. Schulz, V. Wachtendorf, T. Klimmasch, and P. Alers, *Prog. Org. Coatings* **42**, 38 (2001).

7

Production of Optical Components Using Plastic Injection Molding Technology

Thomas Walther (Arburg, Lossburg, Germany)

7.1
Introduction

Optical systems made of transparent plastics stand in strong economical competition to their glass counterparts. Because of the technological advantages that plastic materials offer, they are increasingly gaining ground over glass materials in the field of optical applications. The potential for substitution results from the large range of freedom these materials offer with regard to design of the optical function surfaces, integration of multiple functional parts, integration of frames or fixing elements, low material costs, as well as low specific weight.

Using the injection molding technology, high-quality products can be manufactured at a comparatively reasonable price in only one processing step. With the suitable mold and machine technology, functional optical components can be encapsulated with frame or fixing elements of compatible transparent or nontransparent materials using multicomponent injection molding technology, to produce an assembly of components made of different materials with varying characteristics at an economically reasonable price. Besides the injection molding technology, it could be necessary to use the injection compression molding (ICM) technology, also called compression injection molding or coining.

The method of manufacture is to be regarded on a holistic level because a high degree of expertise is required in various fields of technology. In the design and development stage of the components, calculation methods and the plastic materials to be used are of prime importance. The shaping process requires expertise in mold technology and injection molding technology whereby here the focus is on the injection molding machine and the suitable processing methods. Beyond this, profound knowledge in metrology is vital for lasting quality assurance.

For manufacturers of injection molded parts, optical components are a particular challenge, because in addition to the usual dimensional stability, the optical functions are also relevant.

This documentation starts with a brief introduction to the techniques of plastic injection molding, followed by an explanation of the range of demands placed on these techniques by the varying optical components. The complete, relevant pro-

cess chain is then introduced before defining the processing technology in more detail, in particular the use of ICM and the relevant machine concepts.

7.2
Plastic Injection Molding

The technology of plastic injection molding is a discontinuous process. In addition to the injection molding machine, a mold is required with a cavity in the respective form (Figure 7.1). The cavity is the negative form of the part to be produced.

The mold consists of two halves which when closed are joined together in the so-called parting line. This separation of the two mold halves makes it possible to access the cavity when the mold is open to eject the part. To fill the cavity when the mold is closed, sprue channels are worked into the mold. Depending on the requirements and size of the part, a mold can have one or multiple cavities.

The injection molding machine consists mainly of a plasticizing unit for processing the plastic material and a clamping unit with two mounting platens for accommodating the mold.
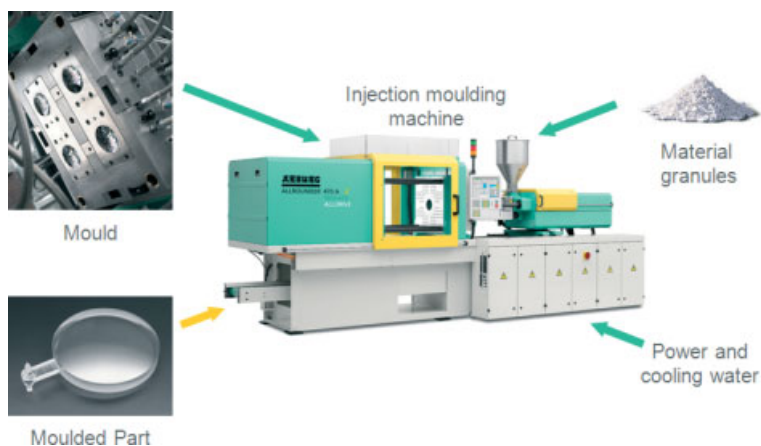
Figure 7.1 The principles of injection molding.

An injection molding cycle is distinguished by various processing steps (Figure 7.2). At the start of the cycle, the mold is closed and the clamping force is built up. With the aid of the plasticizing unit, a thermoplastic material, which is fed to the machine in granular form at room temperature, is heated and processed to a hot, viscous plastic melt. Depending on the type of plastic material used, the temperature of the molten plastic can range between 180 °C and 320 °C (356–608 °F). In the injection phase, this hot melt is introduced under pressure into the cavity of the closed mold.

Inside the mold, the melt cools down until the plastic reaches a dimensionally stable state. The immediate shrinkage in volume that occurs as a result of this cooling down phase can be compensated during the holding pressure phase until the injection point is sealed.

The holding pressure phase is followed by the cooling phase that continues until the part has reached a sufficiently stable state for demolding. During this time, the material for the next cycle is processed inside the plasticizing unit. At the end of the cooling phase, the mold is opened and the part is ejected or removed.
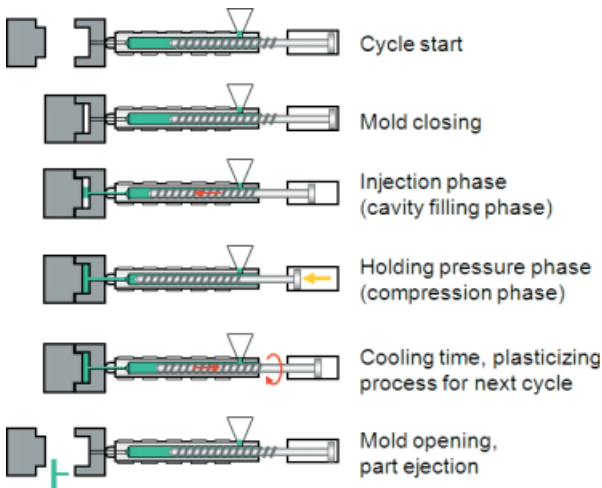
Figure 7.2 Phases of an injection molding process.

After demolding, the part cools down to room temperature. During this time, further shrinkage effects can occur, depending on the type of plastic material.

Material-specific *p-V-t* diagrams show the relationship between the specific volume and the temperature and pressure.

7.3
Classification of Optical Components

In the field of injection molded parts, the term "optical components" includes a wide range of various types of products with different requirements. An important characteristic is the transparency for visual light. In the following classification, which is not deemed to be complete, examples are listed that explain the requirements placed by the varying applications on the processing methods of injection molding.

The components can be grouped according to their application. We differentiate between "nonimaging optics" and "imaging optics," whereby generally speaking

nonimaging optics are referred to as "lighting optics" and imaging optics as "picture-processing optics."

For both groups, the absolute transparency and clarity of the component is a prerequisite.

Nonimaging optics include, for example, automotive head lamp glazing or watch faces, whereby importance is placed on the outer geometry and the transparency of the component. Light conductors are a similar case; here light is picked from a light source and transported.

With imaging optics, light rays are also transported, however, in a controlled form. For the fulfillment of the optical function, the refraction index of the materials used is decisive. A highly precise image of the outer layers at which light is coupled in and out is required, that is, the highest possible imaging accuracy must be achieved. In addition, inner tension can affect the transport of rays and thus impair the quality of the part. This means that instead of the outer geometry deciding the quality of injection molded parts, as is usually the case, the optical function becomes more important, the quality of which must also be assessed.

One characteristic that is particularly important in the processing of plastics is the wall thickness of the part, see ordinate of Figure 7.3. The wall thickness determines the cooling time required in the injection molding process until the plastic reaches a dimensionally stable state. It thus has a decisive influence on the shrinkage effects.

When designing a component, the first goal is usually to achieve the function of the part. The wall thickness should be as low and evenly distributed as possible, in order to be able to control the shrinkage effects.

Wall thickness			
Magnifying glass lenses	Light and rain sensors	Lighthouse optics	Projector lenses, spectacle lens blanks
Decorative optics, light conductors	Sun glasses	Automotive glazing	Camera lenses, spectacle lenses
Advertisement glazing	Steering angle sensors	Watch faces, mirrors	Ruler, optical data carriers

Process requirements

☐ Non-imaging optics   ☐ Imaging optics

Figure 7.3 Classification of optical components.

As a rule, the technical aspects of the plastic materials are not decisive in the design of optical components. Their functionality is derived from the ability to conduct the light in the material. Thick-walled parts and parts with big differences in wall thickness are the result of this ability.

For the injection molding process, this means comparatively long cycle times and the monitoring of warping and shrinkage becomes a challenge. The shrinkage effects must be considered as early as the design stage so that the final geometry of the parts actually corresponds to the specified geometry.

In the abscissa in Figure 7.3, process requirements are listed in increasing order.

Because of the requirement of the highest possible imaging accuracy, together with the side effects of thick-walled parts, a comprehensive know-how is of vital importance in the entire process chain. The classical injection molding method using conventional methods of mold temperature control reaches its limits. Variothermic mold temperature concepts and ICM technology with all its variations are finding increased application.

7.4
Process Chain of the Injection Molding of Optical Parts

In the manufacture of high-quality optical components, it is essential to observe the process chain and the system technologies involved as a whole. For this purpose, profound knowledge of each process step in the process chain must be available or acquired.

The process chain comprises, besides the actual injection molding process, in which the mold and machine are of prime importance, the material conditioning as well as downstream operations such as part removal, quality assurance, and other subsequent processes (Figure 7.4) These can be coating, assembly, or packaging processing designed to finally achieve a manageable product.

Figure 7.4 Process chain.

7.4.1
Basic Rules: Cleanliness and Repeatability

Any form of soiling, inclusions, or streak formation in transparent parts is immediately recognizable and therefore evaluated as a quality-impairing fault. Tracking the cause does not always lead to definite findings. For this reason, absolute cleanliness and reproducibility must take top priority in all process steps.

Every potential for contamination must be eliminated or minimized. Top-level clean room conditions will only be required in the rarest of cases; however, some measures derived from the requirements for clean-room technology could well be beneficial.

7.4.1
Material and Material Feed

With regard to available materials, the processor has not much leeway. The optical and mechanical characteristics of the raw material are adapted to the particular application. Nevertheless, there are some differences. For instance, some material manufacturers offer special charges with "optical grade" rating, in which a high level of purity and dust-free content is guaranteed at this stage already.

An excessive dust content can cause problems because dust particles have different melting characteristics from the material or cannot be melted down at all. They are then transported in the melt and can be deposited as impurities under certain circumstances.

It is important to ensure that both the granule drying system and the conveying system are dust-proof and that they (a) do not exercise an abrasive effect on the material and (b) cannot suffer any erosion from the material they are conveying. The distance from the material hopper to the screw feed opening should be short and easy to navigate. Designs in which an enclosed circuit is used are particularly suitable. The processing air used in the systems must be finely filtered and free of contaminants.

These are the critical requirements for keeping the melt free from dust and impurities.

7.4.2
Mold

High-precision optical components require a respectively superior mold technology to withstand the long, high-pressure holding pressure phases and high mold temperatures involved. The mold must therefore be designed and constructed with sufficient stability. For mold construction, corrosion resistant mold steel is used as well as standard mold steel with chemically deposited corrosion protection coatings.

The high-precision functional areas are usually realized in the form of exchangeable mold inserts (Figure 7.5). The surfaces of these, as in the case of free-form designs, lens arrays, or reflector prisms are usually produced with diamond machining equipment. In spite of the inserts being interchangeable, an effective temperature control must be guaranteed. Molds for optical parts are to be regarded under the aspect of clean-room technology. Here the basic rule is to minimize unnecessary surfaces, which would be subject to contamination. Electric and hydraulic supply lines and temperature-control hoses must not be dragged along with the opening and closing movements of the mold. In order to keep the mold supply lines short, suitable interfaces are provided on the moving mold mounting platen of the injection molding machine (see Figure 7.6).
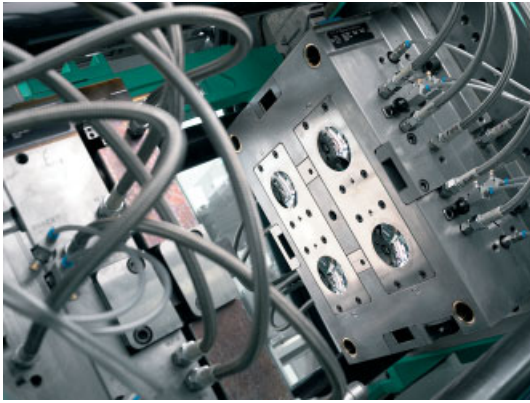
Figure 7.5 Four cavity mold with inserts.
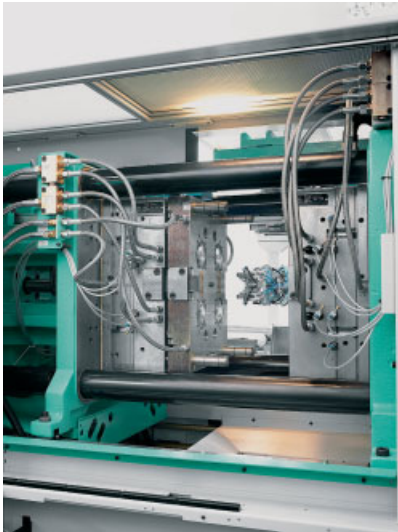
Figure 7.6 Direct connection to the supply lines.

Mold temperatures and information from the sensors are recorded in the machine controller and are monitored. For this purpose, the data of the mold temperature devices are transferred to the machine control system via standard interfaces and are used for QA evaluation. To increase the safety of the process, flow monitoring of the temperature control fluid is recommended, as well as the operation of a fluid evacuation system prior to insert changes or mold removal.

The injection compression technology (main/auxiliary axis coining) used for the technical requirements of each machine is specified by the construction of the coining mold.

7.4.3
Injection Molding Machine

With regard to the general machine concept and the machine technology involved, there are no typical aspects for optical applications. Suitable machine concepts are derived from the size of the part to be produced, the clamping force, the mold, and processing technologies required.

7.4.3.1 **Design of the Machine**
The decisive aspect determining the size of the machine is the mold. The size of the mold and the clamping force requirement determine the mounting dimensions and clamping force and thus primarily the size of the machine. When calculating the clamping force requirement, the often large wall thicknesses must be taken into consideration because these require a longer and stronger holding pressure.

The injection unit is a module that can be chosen to match the individual requirements. The criteria for this are the shot weight, raw material to be used, the expected cycle time, and the required injection force.

The shot weight and the expected injection pressure are relevant for the choice of screw diameter. The process-relevant shot weight should ideally lie between 20% and 80% of the maximum possible output of the screw diameter selected. The dwell time of the plastic melt in the screw can be determined by the screw diameter and the cycle time. This must be kept within the range recommended by the manufacturer of the raw material [2, 3].

In actual practice, it is often necessary to reach a compromise in order to achieve the recommended dwell time. Thick-walled parts require longer cycle times, which means the melt stays longer in the plasticizing cylinder (Figure 7.7). Too long dwell times can lead to thermal oxidation, which is noticed by an increasing yellowing discoloration of the material. This impairs the quality of the finished part. Furthermore, the risk of contamination of the melt is increased. Decomposed and discolored particles are transported in the melt and are visible in the finished parts as "black spots."

Figure 7.7 Plasticizing components.

For the components of the plasticizing unit, that is, cylinder module, screw, and check valve, only highly wear-resistant materials are used as a rule. Typical transparent plastic materials such as polycarbonate have the tendency to stick to the plasticizing components. To counteract the possibility of deposits that could also appear later in the finished parts as "black spots," the screw and check valve are coated with resistant layers of a hard material. For this purpose, physically applied layers of chromium nitride or titanium nitride are used [6].

7.4.3.2 Machine Technology

Basically, the production of optical components is not bound to a certain machine technology. Injection molding machines equipped with today's standard of technology, that is, processor-controlled control systems and the respective sensors fulfill the necessary stipulations for a reproducible injection molding process.

When injection compression processes are to be applied however, additional requirements must be met. With regard to the drive technology, the required coining function must be realizable and the machine control system must be equipped with the respective options.

7.4.3.3 Equipment Installed on the Machine

In a few cases, clean-room conditions are required for the production environment of optical components.

In order to guarantee such a production environment, options from the clean room technology sector are applied.

Examples of clean-room measures (Figure 7.8) :

- Clean-room flow box over the clamping unit to avoid contamination in the vicinity of the cavity.
- Higher machine feet to facilitate cleaning under the machine.
- Short supply lines to the mold temperature control device by installing the hose connections on the machine side directly on the mounting platens.
- All machine parts painted in light colors to facilitate recognition of soiling.
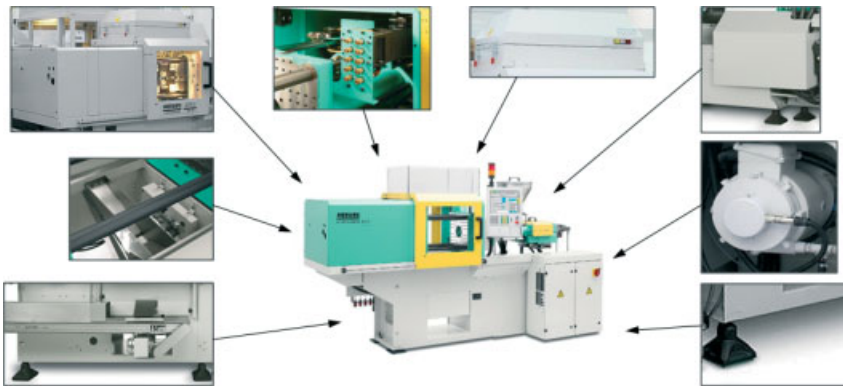
Figure 7.8 Machine options for clean manufacturing conditions.

- Fluid-cooled drives to reduce air streams that could swirl dust.
- Minimization of machine and mold surfaces, e.g., by completely enclosing hydraulic manifolds.

7.4.4
Automation and Downstream Processes

The manufacturing of sophisticated optical components requires a holistic manufacturing concept. Free-fall applications with parts being transported on conveyor belts to large containers are seldom used, as a rule. More typically, robotic systems integrated in the machine control system are used for part removal. The components are either taken out of the cavity by the so-called removal grippers or passed to the removal gripper by an ejection system. Latest technological appliances here range from simple pneumatic gripper axes up to servo axes synchronized with the ejector.

The decisive factor for the removal technology is the complexity of the downstream processes and the method of part set-down. This can range from a simple placement of the parts directly onto a conveyor belt, through set-down in defined patterns, up to in the filling of trays with up/down stacking facilities.

Further processes can follow. In such cases, defined cooling stations are often used. The molded parts that are removed from the mold at still high temperatures are placed in defined positions for cooling, where they can cool down evenly to room temperature before measuring facilities check and document the quality of the parts. Depending on the application, assembly steps with other components or set-down in a protected environment are possible.

Figure 7.9 shows a turn-key production system for the manufacture of blanks for ophthalmic lenses.
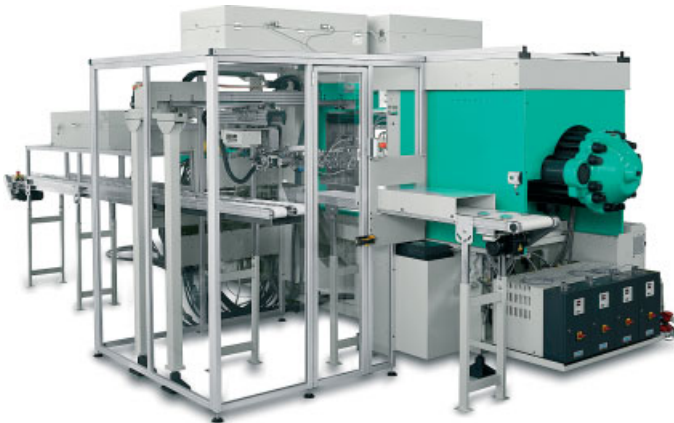
Figure 7.9 Production cell for the manufacture of ophthalmic lenses.

7.5
Injection Molding–Injection Compression Molding

When stress-free or low-tension characteristics are required in the injection molding of thick-walled or optical parts, ICM often becomes an issue.

During the injection compression step, the cavity volume is adapted. A requirement of the machine is that it must be able to move the injection unit and the mold or mold components simultaneously. The mold must be designed so that the cavity is sealed from the outside even when the mold is not completely closed.

The differences between conventional injection molding and ICM are explained in more detail below.

7.5.1
Fundamental Difference

In a classical injection molding process, a constant volume of melt is injected into a closed cavity through a runner (see Figure 7.12, *red arrow*).

As the cavity is filled, the pressure drops along the flow path from the runner (high pressure) to the front of the melt or end of the flow path (low pressure). To compensate the volume shrinkage, this pressure drop is boosted during the holding pressure phase. At the end of the holding pressure phase, that is, when the gate solidifies and the holding pressure has no more effect on the component, the pressure drop freezes. This causes a residual stress profile in the component. This inner tension in the component can cause deformation of the part after demolding. In the case of optical parts, these inner tensions can impair the light conducting characteristics.

Figure 7.10 shows a diagram of the injection molding process. The cavity is filled centrally from the sprue bushing. "p1" represents a point in the flow path near to the sprue and "p2" a point further away from the sprue. In the diagram, the pressure gradient from the injection point via "p1" to "p2" is shown.
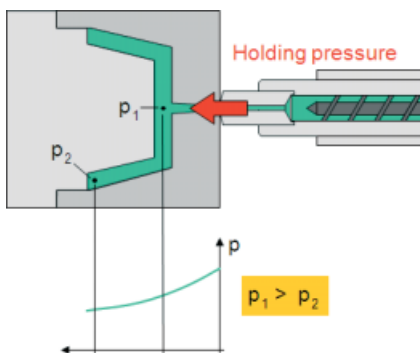
Figure 7.10 Diagram of the injection molding process.

In a ICM process, the cavity volume changes during and/or after the injection/ holding pressure phase. As a rule, the mold is not completely closed at the beginning of the injection process, that is, when the plastic melt is first injected into the cavity. The mold is not closed completely until all the melt is inside the cavity. In this way, less pressure is required to fill the cavity and the pressure gradient is already reduced in the filling phase. When the mold closes, the pressure acting on the complete cavity area of the shrinking part is reduced (see Figure 7.11). Ideally, the pressure is constant inside the cavity, that is, the pressure level remains constant from the injection point through p1 to p2.
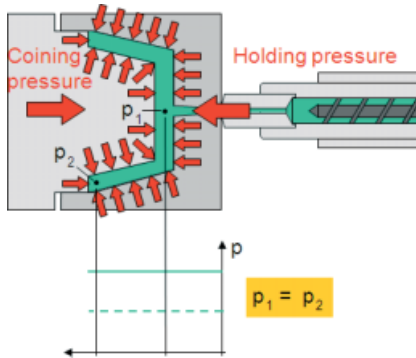
Figure 7.11 Diagram: injection compression molding.

In this way, larger ratios of flow path to wall thickness can be realized and possible sinks and voids are avoided and the risk of shrinkage and warpage reduced. Further advantages include the reduction of inner tension in the part and the minimization of birefringence effects.

This fundamental difference between the effect of the holding pressure through the gate during injection molding and the effect of the coining pressure acting on the whole surface of the part during coining can be practically realized in many different ways. Consequently, there are many variants of injection coining. In available literature on injection coining various, overviews are given in which the different coining techniques are explained. The continual further development of the machine control systems means the number of variants is still increasing.

7.5.2
Differences in Mold Technologies

There are several possibilities of varying the volume in the cavity. In mold technology, we differentiate between the so-called Main axis coining and Auxiliary axis coining – expressions that are taken from the machine technology.

The main axes in an injection molding machine refer to the mold movement axis, the injection axis, and the dosing process.

The auxiliary axes include the ejector axis, the nozzle movement axis, and the core pull axes.

7.5.2.1 Main Axis Coining

In main axis coining, the cavity changes are realized by the movement of the clamping unit.

The sealing of the cavity can be achieved with a moat surround, whereby a core dips into a matrix and seals the cavity off from the inside (see Figure 7.12(a)). Alternatively, it is possible to seal off the cavity with an axially moving cavity ring or coining frame. As long as, the mold is not completely closed, this lies in the parting line and seals the cavity off from the outside. The cavity ring can either be pressed on with springs or hydraulic force. For the coining process, the cavity ring can be moved axially (see Figure 7.12(b)). This method is suitable for flat parts with an even wall thickness. Undercuts or perforations across the direction of coining are, however, more problematic.
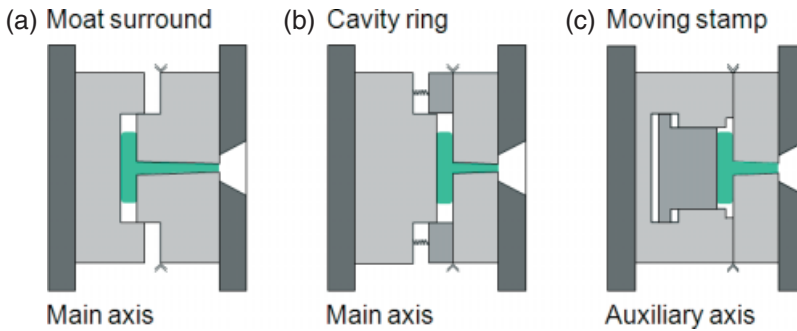
Figure 7.12 Mold concepts.

7.5.2.2 Auxiliary Axis Coining

When coining with the auxiliary axes, the mold is completely closed. The volume of the cavity is adapted by moving plungers inside the cavity. The stamp movements are controlled hydraulically using the core pull functions. It is also possible to use the mechanical ejector devices in the injection molding machine for the coining process.

Auxiliary axis coining is particularly suitable for coining only partial areas of the part because the buoyancy forces arising in the noncoined areas are absorbed by the clamping force of the machine.

When coining only partial areas of the part with the main axis, mold concepts using cavity rings are applied. With this construction, the buoyancy forces are absorbed by the hydraulic force or by the spring force supporting the cavity ring. The maximum possible supporting forces acting on the cavity ring are substantially lower than the clamping force of the machine. For this reason, the processing window is very limited in partial-area coining with the main axis.

7.5.2.3 **Conclusion**

Compared with coining in the mold, coining with the clamping unit has the advantage that much higher forces are available for this purpose. In this connection, it must be noted that the achievable quality with regard to reproducibility of the process largely depends of course on the repeatability of the axis movements.

7.5.3
Using the Clamping Unit for Injection Coining

The various construction types of clamping units offer different advantages with regard to the injection coining process.

With hydraulic clamping units, coining strokes equal to the maximum movement path of the clamping stroke are possible. The maximum coining force is available at every stroke position provided that there is a counter pressure. In general, this force corresponds to the maximum clamping force (Figure 7.13).
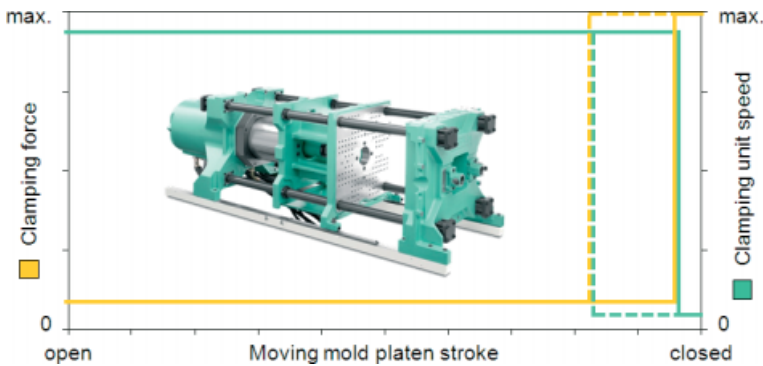
Figure 7.13 Hydraulic concept: force and speed pattern.

The speed of the movement, not counting the acceleration ramps, can be kept at the maximum value over the entire opening stroke while reducing the clamping force. In this case, the movement is usually realized with the moving cylinder. If a large clamping force is required, the movement is carried out using the large pistons of the closing cylinder, which permit a high perforce at a comparatively low speed. With the respective control technology, the coining profiles can be easily realized. Hydraulic clamping units are equipped with systems that measure the distance, usually with a resolution of 0.1 mm, thus guaranteeing a precision of the coining position in the 1/10 mm range.

On toggle-type clamping units, the clamping force and the speed of the movement are dependent on the opening stroke, due to the kinematics of the toggle joint. The full clamping force is not achieved until the toggle is fully expanded and locked. High coining forces can thus only be realized with short coining strokes (Figure 7.14).
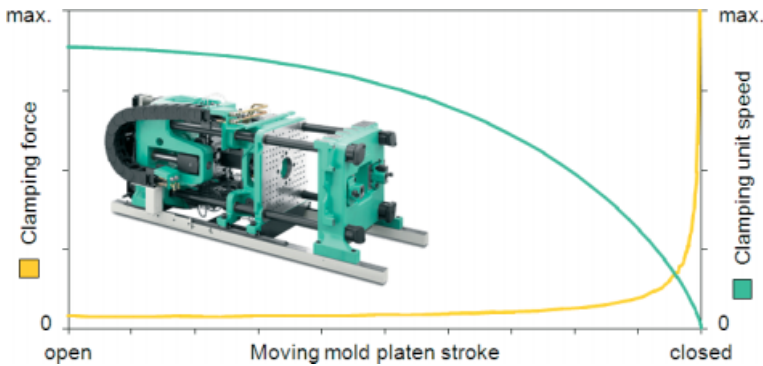
Figure 7.14 Toggle concept: force and speed pattern.

Electrically driven machines must in some cases be equipped with a large-sized drive motor to achieve adequate coining forces. A typical coining stroke of an electric clamping unit ranges around 1 mm. Reaction speed and coining velocity are, however, comparatively fast compared to hydraulic drives because pressure build up times are practically nonexistent.

With toggle drives, the positioning of the clamping unit is realized using the crosshead of the toggle joint and with electrically driven clamping units via the incrementation of the drive motor. Positioning accuracies in the range of well below 1/100 mm can be achieved. The repeatability is also considerably higher than with hydraulic systems, due to the position-controlled driven systems.

7.5.3.1 Summary

Hydraulic clamping units are mainly used for longer coining strokes (1–10 mm) because the achievable precision of the coining position is usually adequate for these applications.

For applications requiring coining strokes in the range of 1 mm, electrically driven toggle systems are unbeatable due to their fast reaction time and coining speed and their high-precision coining positioning and repeatability.

For the manufacture of optical components, these drive systems are not mutually exclusive but complementary, depending on the application.

7.5.4
Process Variants of Injection Compression Molding

The fundamental marginal conditions for injection coining are determined by the mold concepts and the machine technology. The numerous variants of the injection coining process arise from the capabilities of the drive technology and the machine control system.

The process variants are generally distinguished by three degrees of freedom: the type of coining axis, the direction of coining, and the chronological course (Table 7.1) .

Table 7.1 Overview of coining variants

Coining axis	Main axis
	Auxiliary axes
	Combination of main and auxiliary axes
Direction of coining	Closing coining
	Opening coining
	Combination of opening and closing coining
Chronological order	Sequential
	Simultaneous

As explained in Section 7.5.2, the process can be divided into various coining axes, depending on the mold technology used. Besides the clear difference between the main axis and auxiliary axis coining, a combination of the two is also possible, providing the mold concept can be realized.

As the second degree of freedom, the coining direction is also important. Here we speak of "opening coining" or "closing coining," depending on whether the cavity volume is to be increased or decreased during the process [1].

As the last degree of freedom, the chronological course is characteristic for the process. Here the chronological course is seen in relation to the filling of the cavity, that is, the screw movement.

The coining process can be carried out sequentially or simultaneously [7]. In a sequential coining process, the coining position is first approached, then the melt is injected into the cavity and then the coining process is carried out, one step after the other. In a programmed sequence illustrated, the upper picture shows a
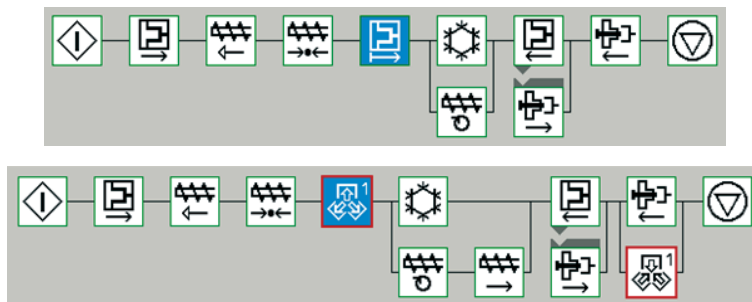
Figure 7.15 Sequence: sequential coining.

consecutive coining sequence with the main axis, and the lower picture shows a sequence using an auxiliary axis. In this example, the auxiliary axis is controlled by a core pull function (Figure 7.15).

In contrast, with simultaneous coining, these processing steps overlap each other. With regard to the filling of cavity, simultaneous coining has the decisive advantage that the melt front does not come to a standstill, thus reducing the risk of flow marks.

Figure 7.16 illustrates such a sequence using the main axis. The coining step starts at the same time as the injection step starts.

Figure 7.16 Sequence: Simultaneous coining.

The condition for starting the coining process can be selected individually, depending on the mold, component, process, and available sensors (Figure 7.17).

Figure 7.17 Start conditions for coining functions.

In a modern control system, the following start conditions are available:

- in relation to a delay time
- in relation to a screw position
- in relation to the injection pressure
- in relation to the cavity pressure
- in relation to the mold wall temperature
- in relation to any external signal.

The state-of-the-art technology comprises a machine controller which is not related to a specific case of application but enables the user to program the required machine sequence individually for each case. All variants of the described coining methods can be covered with one controller version.

7.5.5
Example of Coining Tasks

7.5.5.1 Manufacture of Ophthalmic Lenses

One case of application is the manufacture of low-tension, dimensionally stable, thick-walled spectacle lens blanks for the ophthalmic industry. A sequential coining sequence with the main axis is applied (Figure 7.18).
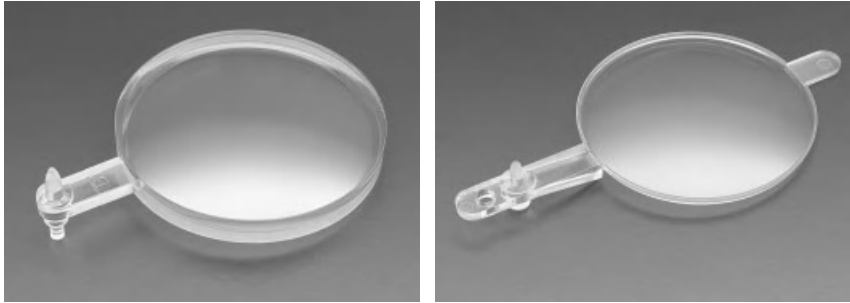
Figure 7.18 Spectacle lens blanks.

For this purpose, a mold with coining frame is used. The mold is closed up to a defined coining gap. The screw injects the melt at a low pressure and moves to the advanced end position. The mold then closes fully (coining) and the melt is distributed over the cavity.

In this case, the mold is equipped with quick-changing mold inserts. The thickness of the lens is adjusted by the variation of the coining gap.

With regard to the machine drive technology, no simultaneous movements of clamping unit and screw are necessary with this method.

7.5.5.2 Optical Data Carriers

Typical examples of products of daily use are optical data carriers such as CDs and DVDs. While the CD substrate with a diameter of 120 mm features a wall thickness of 1.2 mm, a DVD with the same diameter comprises two substrates each with a wall thickness of 0.6 mm.

For the molding process of a DVD substrate, a very high ration of flow path to wall thickness is given. For this reason, a simultaneous injection coining process is applied. The mold is equipped with a cavity ring and the main axis carries out the coining process that is started when a defined screw stroke is reached. In this way, the coining process is carried out together with the filling of the mold cavity (Figure 7.19).

The injection compression process is able to compensate the unfavorable ratio of flow path to wall thickness and it also improves the pit replication in the outer area. Further effects are reduced birefringence and an achievement of the required smoothness.
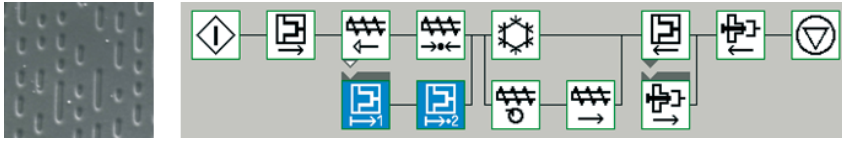
Figure 7.19 Optical data carrier: DVD substrate, 0,6 mm wall thickness.

CD blanks in contrast can be produced with the classical injection molding method. A mold without coining options is used. To reduce the cycle time however, so-called "flying-start injection" is applied (Figure 7.20).
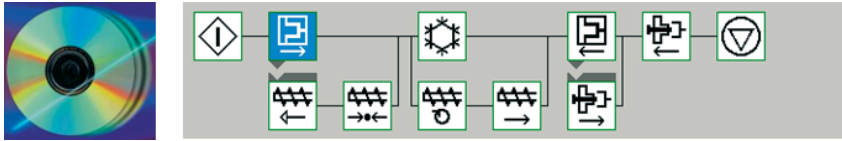
Figure 7.20 Optical data carrier: CD substrate, 1,2 mm wall thickness.

"Flying-start injection" does not necessarily require a coining mold [4]. In principle this method is a simultaneous screw stroke-related closing coining process carried out with the main axis. The mold is closed and during the closing process, the screw movement, i.e., the injection process, is started when a defined stroke position is reached. Flying-start injection is suitable for symmetrical, flat components which are injected from a central point. The injection pressure requirement in the cavity filling phase is reduced and the melt distribution is supported by the final mold closing movement. This method is applied in the production of thin-walled parts with a high flow path to wall thickness ratio in order to positively influence the cavity filling process and thus the quality of the part.

It can also be applied in conventional, fast-running processes because the enable signal for injection is given before the mold has fully closed.

In both the cases, the machine must be equipped so that the clamping unit and the injection unit can be operated simultaneously.

7.5.5.3 Active breathing

"Active breathing" refers to a process using conventional injection molds and the production of flat parts [5]. This works on the principle of "simultaneous opening/closing coining" with the main (Figure 7.21).
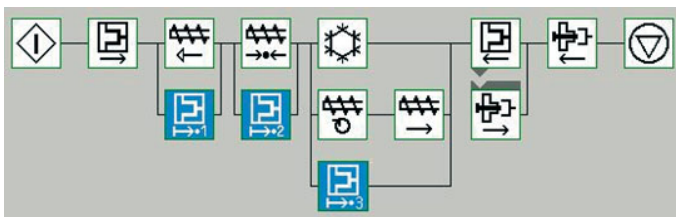
Figure 7.21 Active breathing.

During the cavity filling phase, the clamping pressure exerted by the clamping unit is reduced under the control of a multistage programmable clamping profile and then is increased again. This enables the mold to "breathe" over a stroke a few hundredths of a millimeter. With this slight breathing process, the holding pressure is distributed over a wider area and a coining effect is produced (Figure 7.22).
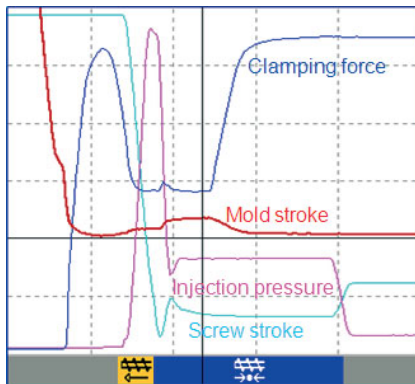
Figure 7.22 The course of a process with active breathing.

In the case of transparent, flat components birefringence in particular can be reduced and the smoothness of the component enhanced. The inner tensions are also minimized that in turn has a positive effect on the subsequent galvanic treatment of the parts.

Special coining molds are not always required.

7.6
Conclusion

The production of optical components in injection molding technology is a sector that is still strongly developing. Successful production requires comprehensive knowledge not only in injection molding and mold construction but also in the field of optics and the respective metrology.

In contrast to the conventional injection molding, injection coining in all its variations offers several significant advantages, in particular for optical parts. The requirements for this, however, are high-quality and complex mold and machine technology. This makes the process technology considerably more extensive and calls for a high level of sustained knowledge in this field. This is required not only for the development and validation of the processes but also right through to the supervision of the processes in serial production.

For injection coining, injection molding machines with high-precision positioning and a high level of repeatability are applied. The choice of machine technology

depends on the concept of the coining mold. Today's machine control systems are already designed to cope with challenging coining mold concepts of the future.

References

1 "Spritzgiessen, Der gläserne Innendruck – Qualitätsmasstab für optische Teile", Schnerr, O.; Bürkle, E., Klotz, B., Sonderdruck aus Kunststoffe 5/2007, Carl Hanser Verlag, München

2 Bestimmung der Verweilzeit beim Spritzgießen technischer Thermoplaste, ATI, Bayer AG, Leverkusen, 1988

3 Handbuch Spritzgießen, Johannaber, F., Michaeli, W., Hanser Verlag, 2002

4 Today – The ARBURG magazine, Issue. 25, 2004

5 Today – The ARBURG magazine, Issue. 39, 2008

6 Anforderung an Werkzeugoberflächen für die Kunststoffverarbeitung, Mumme F., Galvanotechnik 8/2008, Eugen G. Leuze Verlag

7 Injection molding handbook, Tim. A. Osswald, Lih-Sheng Turng, Paul J. Graham, Hanser Verlag.

8
Cost Modeling of Injection-Molded Plastic Optics

Jukka-Tapani Mäkinen (VTT Technical Research Centre of Finland, Oulu, Finland)

8.1
Introduction

Injection molding is a cyclic process, in which 3D geometries are formed from the raw material with a single process step. This simplicity makes it possible to produce large quantities of complex and accurate parts fast and cost efficiently. As a manufacturing technology, injection molding is competing with other technologies capable of making components with similar function. There are some inherent benefits such as integration of mechanical features that can make plastic optics more attractive by lowering the cost of assembly [1], but then there are also other factors such as mold cost that may restrict the use of molding to high-volume applications. Cost modeling can be used for playing "what if" games to determine if the part is worth the trouble and cost of producing it or for finding an optimum design at the device level [2]. In some cases such as mobile phone camera optics, the choice is obvious as there are only few low-cost manufacturing methods available that can produce the huge quantities of lenses needed for the annual production volumes of phones. However, there are plenty of other optical applications that do not have large volumes, but still the potential benefits of injection molding make it worthwhile investigating the possibility to use it.

Plastics injection molding is a several decades old manufacturing technology and there are many tools available for calculating the molding costs of parts. Some of these tools can be used freely at the websites of, for example, companies that are involved in injection molding [3] or plastic material manufacturers [4]. Some of the tools are quite simple and easy to use, but there are also cost models that are very sophisticated and complex [5]. Unfortunately, there is no standardized way of calculating molding costs and for this reason all of the tools are somewhat different from each other. In each case, there is a set of input parameters that determine the cost via a series of simple arithmetic operations. What makes the tools complicated is the fact that many of the input parameters are connected to the output parameters through more than one route. For example, molding yield is used in the formulas for material, machine, and labor costs. This complexity makes it difficult to use the readily available models as the relations between

input and output parameters are not clear for the user who has not made the calculation tool himself.

The first part of this chapter deals with cost calculations of three key processes in injection-molded optics production: mold tooling, molding, and coating. However, the main emphasis is on the injection molding itself. The issue is approached by making a tear-down analysis of an example cost calculation tool. Main purpose of the analysis is to explain how the different input parameters are defined and to show how they affect the outcome of the calculations. Second part of this chapter is dedicated to three case studies, which are illustrating the possible uses of cost calculation tools, or in other words, the actual cost modeling.

8.2
Different Uses and Users of Cost Modeling

All injection molding companies have their own tools for estimating and calculating production costs. The first and most obvious use of these tools is in price estimation, which is done when customer needs a quotation for a specific set of parts. The estimate can be made quite intuitively if the product is very similar to a previous part made in the factory, but if the part or module is totally different or if it has higher or lower accuracy requirements, the estimate will have to be made by balancing the worst-case cost scenario with assumed market price. More precise calculations can only be made when there is enough feedback from the first molding trials and both the part and process are well defined. There is also always room for some improvement in a normal production process. Cost modeling can be used to pinpoint the exact location or parameter in the process chain, where improvements will have the largest impact on overall cost. Several process adjustments can be made during the lifetime of a high-volume product. Every time the process can be improved without compromising quality, the profit margin can be increased and/or the sales price can be lowered to keep the customer satisfied.

The second user of cost modeling is a person working in the sourcing department of a device or module manufacturing company. Cost modeling can provide a useful tool for increasing the transparency of a supplier's pricing practices. A profit margin will always be added to the calculated manufacturing cost in a molding company to determine the final sales price of a component or module. In some application areas such as mobile phone camera optics, the margins can be very low because the high volumes are attractive to many companies and the competition is fierce. In some other areas such as medical analysis devices, the volumes are lower and there can be more room for good margins when the customer is putting more emphasis on quality and reliability than on cost. Profit margins on specific products are one of the best kept secrets in any company, but some educated guesses can also be made on the buyer's side if the manufacturing costs can be estimated with the help of a cost model. Modeling can also be used in determining whether molding is a suitable production method for the company's low or medium volume optics product or not. The same information can also be

compiled by cross-checking the quotations from different suppliers, but a much deeper understanding of the relation between volume and cost can be obtained by building a functional model for cost estimation. This understanding will make supplier discussions easier and speed up decision making.

The third main user is a designer who can utilize cost modeling in bridging the gap in design optimization between cost and performance. According to some estimates, as much as 50–80% of manufacturing productivity can be determined at the design stage [6, 7]. Design for manufacturing (DFM) is the term generally used for the art of "global optimization," where the main goal is to find an optimum design in respect to manufacturing cost of the component, module, or a whole system. Optical design software is routinely used in simulating performance of optical systems with high accuracy. Totally different designs or just small variations of one solution can be compared by simulating them in a ray tracing software without the need of building expensive prototypes. Tolerance analysis routines can be used to determine the probable production yield based on performance distributions and the design can be optimized for maximum yield instead of maximum nominal performance that can never be reached in real life. Cost models can be used for simulating the effects of design variations to manufacturing costs in a similar manner. A cost model closes the feedback loop between design decisions and resulting manufacturing cost in very much the same way than an optical design software closes the loop for performance optimization. By using these two tools concurrently, a designer can make the jump from part optimization to true module or system-level optimization.

8.3
Calculating Plastic Optics Manufacturing Costs

Table 8.1 shows a view from a simplified cost calculation tool created in MS Excel for estimating production costs of injection-molded optical parts. In this example tool, separate cost calculations are made for three plastic optics key processes: mold tooling, injection molding, and coating. The results are calculated per single manufactured piece in large-scale production, in which the mold cost can be easily amortized. The total cost is calculated simply by adding the three separate process expenses together. Manufacturing quantity is not present in the calculations as the main idea is to add up the costs of a smoothly running continuous process. However, this tool can be used to calculate costs also for smaller production series by taking the volume into account when setting the input parameters for the tooling costs and batch size.

Daily production capacity can be calculated from the number of working hours per day, number of cavities, and cycle time. Machine uptimes will also need to be included as well as the yield parameters from all of the successive processes. Although production capacity calculations do not have an effect on the cost, they are indispensable in determining the throughput of one injection-molding machine. If the monthly capacity is not large enough with just one machine and a multicav-

Table 8.1 A view from a simplified example cost calculation tool created in Excel.

basic information		tooling cost calculations	
product	viewfinder optics	mold design cost	2 000 €
material	Zeonex E48R	mold cost	30 000 €
		optical insert cost	1 000 €
molding input parameters		mold life	500 000 cycles
materials price	25 €/kg	insert life	100 000 cycles
product weight	1.8 g	inserts per cavity	3
machine rate	18 €/h	**tooling costs**	**0.0460 €/piece**
machine uptime	85 %		
yield	90 %	**molding cost calculations**	
number of cavities	4	material	0.0500 €/piece
cycletime	240 s	machine	0.3950 €/piece
work cost1 (operator)	10 €/h	labor	0.1121 €/piece
work cost2 (skilled)	20 €/h	Tool R&M	0.0032 €/piece
indirect costs	70 %	indirect	0.3573 €/piece
workers per machine	0.5	**molding costs**	**0.9176 €/piece**
batch size	50000		
batch setup time	8 h	**coating cost calculations**	
repair and maintenance	8 h/batch	coating batch cost	250 €/batch
		pieces per batch	1 600
capacity calculations		coating yield	95 %
day (24h)	1 047 pieces	coatings per piece	1
week (7 days)	7 326 pieces	**coating costs**	**0.2104 €/piece**
month (year/12)	29 303 pieces		
year (48 weeks)	351 631 pieces	**Total cost**	**1.17 €/piece**

ity mold, the number of injection units will need to be increased. This also means balancing between labor, machine, and tool costs in which cost modeling can be a very useful instrument.

The example pie-charts of Figure 8.1 were drawn for the calculation case shown in Table 8.1. In the example case, the production volume was considered so high that the lifetime of the four-cavity mold was totally used up. With high-volume products, the tool cost can be a fairly small part of the total manufacturing cost, which is dominated by the molding costs as shown in Figure 8.1(a). However, this relation is highly sensitive to volume and with small production series the tooling costs can be much more pronounced or even dominating. This is a question that often comes up when a small series of plastic optical parts are needed for proto-

(a) **Total manufacturing costs**
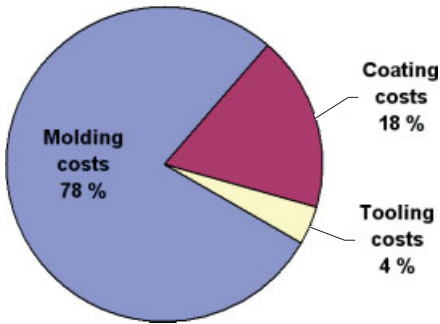
(b) **Molding costs**
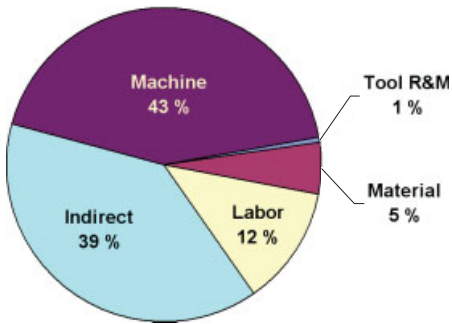
Figure 8.1 Example pie-charts show (a) how the total cost is divided between the three key processes and (b) how the molding costs are divided to the major cost factors.

typing or for a limited number of products. The next section in this chapter is dedicated to the relation between mold costs and production volume to illuminate this issue further.

Figure 8.1(b) shows how the molding costs are divided in the example case. The three main parts are machine, indirect, and labor costs. Material costs represent only 5% of the total molding costs. However, this does not mean that the material choice is an insignificant cost factor when the optical design is made. In this particular case, the cost of molding can be as much as 60% higher if the piece is made from PMMA instead of Zeonex even though the latter material is several times more expensive than the former. This apparent contradiction has its roots in the way a material's physical properties affect the process parameters of injection molding. If an optical designer wants to fully utilize the potential of DFM ideology, he or she will need deep understanding of the manufacturing process and the factors lying behind the cost structure. One section of this chapter is dealing with cycle time and its purpose is to dig deeper into the functioning of the example calculation tool to clarify the relations between optical part features and

molding cost. The cost factors shown in Figure 8.1(b) are all explained in better detail in their own subsections under the topic of molding costs.

Usually, coatings form a significant part of the manufacturing cost of an optical piece and notable savings can be made if they are not needed in the system. In many cases they are simply mandatory to meet the optical specifications set for the design. In addition to the processing costs themselves, coatings will increase the total manufacturing costs by introducing another process into the production chain. As in any real-life manufacturing process, there is a yield factor associated with it and the parts that are coated with defective layers will have to be wasted and the costs factored into the sales price.

Some additional processes such as metrology, which are crucial to plastic optics production, are not analyzed thoroughly in this chapter as the purpose is to focus on the actual core-manufacturing processes. There are numerous procedures and functions that are needed in running a plastic optics factory which all add up to the manufacturing costs of parts. A full coverage of these topics would fill up a whole book of its own.

8.4
Mold Costs and Production Volumes

The injection molding process makes a near 100% copy of the tool. The main benefit of this technology comes from the fact that the high-accuracy shape and finish of the part will need to be tooled only once into the mold and then it can be replicated to a very large number of nearly identical pieces. With standard injection-molded parts, an annual production volume under about 25 000 pieces is considered "low volume" [8] and it can be questionable if it is sensible to use molding technology at all to make parts at lower quantities than this. In optics, the competing traditional glass-based manufacturing processes have fairly high costs associated to them, due to the fact that each high-precision piece is manufactured separately. For this reason, the threshold of acceptable production series size can easily be lower in plastic optics than with plastic parts without optical function.

There are several different methods for estimating the cost of an injection mold [9]. Some of these methods are based on tooling time and some are based on geometric features. The estimation itself can also be made by intuition based on the mold maker's experience, or it can be calculated with a dedicated computer software or calculation tool [10]. In general, molds can cost anything from a few thousands of euros to a few hundreds of thousands of euros depending on, for example, the size and complexity of the part, number of cavities, and accuracy requirements [11–13]. Optical parts tend to be relatively small and the production volumes are usually not that high, which means that optical molds are generally not the biggest and most expensive ones. High demands for accuracy have a two-fold effect on optical mold costs. On one hand, the tight tolerances for surface finish, shapes, and dimensions increase the costs by making it necessary to use separate precision inserts for optical surfaces and also resort to special mechanical fea-

tures to ensure accurate positioning of the mold halves. On the other hand, the parts may be kept relatively simple in their geometry to avoid, for example, shape distortions and birefringence effects that are caused by unpredictable shrinkage during the molding cycle. A simple mold is less expensive to make than a complicated one, which has a lot of moving parts or mechanical details.

The cost risk associated to the sensitive optical surfaces is managed by using separate insert pins or pieces as part of the mold cavity. The cost of renewing an exchangeable pin is much less than the cost of reworking a whole mold half. A pin can also be replaced quite fast, whereas tooling of a mold half will stop the production for a considerably longer period of time. Spare inserts can be manufactured along with the set required for filling all of the mold cavities. Typically, a single insert is more expensive than a series of identical pieces. It takes some time to get the settings right for, for example, the diamond turning machine, but when the preparations are done the successive parts will take less time to prepare and cost per insert is smaller. In a multicavity mold, the fact that the cavities are identical will give definite cost advantage [13]. This means that the cost of, for example, an eight-cavity mold is much less than two times the cost of a four-cavity mold. Exact relation of mold cost to the number of cavities is quite difficult to estimate without a large database of actual purchased molds. The best way to estimate costs is to discuss with a mold maker and ask for ballpark figures. Same applies to the choice of mold material, complexity, etc.

Equation (8.1) shows how the tooling costs are calculated from the input parameters of the example calculation tool shown in Table 8.1. The first part of the formula deals with the mold costs and the second part takes care of the optical insert costs. Main reason for this division is that the mold and the inserts have different lifetimes associated to them. The mold itself can be made to withstand even millions of molding cycles, but the inserts will need to be replaced or renewed much more frequently. Good care should be taken so that the mold material choice, construction, and chosen number of cavities are done with the volume and projected life of the tool in mind. Proper steel choice and durable nickel layers will prolong the life of the tool considerably.

$$\text{Tooling} = \frac{\text{Mold design} + \text{Mold cost}}{\text{Mold life} \times \text{Number of cavities}}$$
$$+ \frac{\text{Optical insert cost} \times \text{Inserts per cavity}}{\text{Insert life}}. \tag{8.1}$$

Calculation tools for mold costs are needed especially for estimating the costs connected to low- or medium-volume products where the main concern is the amortization of the tool. One major input parameter in injection molding cost calculations is the number of cavities used. This variable is closely connected to production volume and it is also present in the cost calculations of the two key processes, tooling and molding. A complicated mold with several cavities will cost more than a mold with just a single cavity. However, with a multicavity mold several pieces will be made simultaneously, whereas a single cavity mold will produce

only one piece at a time. This means that the cost of molding is lower with several cavities as the time it takes to make one piece is shorter. The proper number of cavities is calculated by balancing the costs of the mold tooling and molding with the expected volume of the product in mind.

As an example, Table 8.2 shows calculated tooling and molding costs over a large range of production volumes with four different mold options for the same product (presented later in Figure 8.7(a)). The four molds had one, two, four, and eight cavities and their total costs including inserts were €18 000, €34 000, €56 000, and €76 000, respectively. Tooling cost values in the table were obtained simply by dividing the price of the mold with the production volume in each case. Molding costs were calculated with the example calculation tool. At very low volumes, the molding cost is dominated by the costs associated to the start of a new production batch. Assembly of the mold to the injection-molding machine and successive test runs require some work time which costs money. The starting costs are divided by the number of pieces in the production batch and if the batch is very small the molding cost is high. At higher volumes, the cost of molding comes down and levels off to a certain value that is dependent on the number of cavities. With multicavity molds, the initial costs are higher as the assembly and testing take more time and therefore also the molding costs come down somewhat slower than with a single cavity mold.

Table 8.2 Tooling and molding costs calculated for one product at different production volumes with molds that have one, two, four, and eight cavities (the costs are presented as €/piece).

production volume		1	10	100	1 000	10 000	100 000	1 000 000
1-cavity	tooling	18 000	1 800	180	18.0	1.80	0.18	0.02
	molding	546	56.1	7.14	2.25	1.76	1.72	1.72
	total	**18 546**	**1 856**	**187**	**20.2**	**3.56**	**1.90**	**1.73**
2-cavity	tooling	34 000	3 400	340	34.0	3.40	0.34	0.03
	molding	654	66.6	7.84	1.96	1.37	1.32	1.32
	total	**34 654**	**3 467**	**348**	**36.0**	**4.77**	**1.66**	**1.36**
4-cavity	tooling	56 000	5 600	560	56.0	5.60	0.56	0.06
	molding	790	79.8	8.79	1.69	0.98	0.92	0.92
	total	**56 790**	**5 680**	**569**	**57.7**	**6.58**	**1.48**	**0.97**
8-cavity	tooling	76 000	7 600	760	76.0	7.60	0.76	0.08
	molding	1 170	118	12.5	1.97	0.92	0.83	0.83
	total	**77 170**	**7 718**	**772**	**78.0**	**8.52**	**1.59**	**0.90**

Figure 8.2 shows four graphs calculated for the same case as presented in Table 8.2. The logarithmic scales used for production volume and cost per piece show
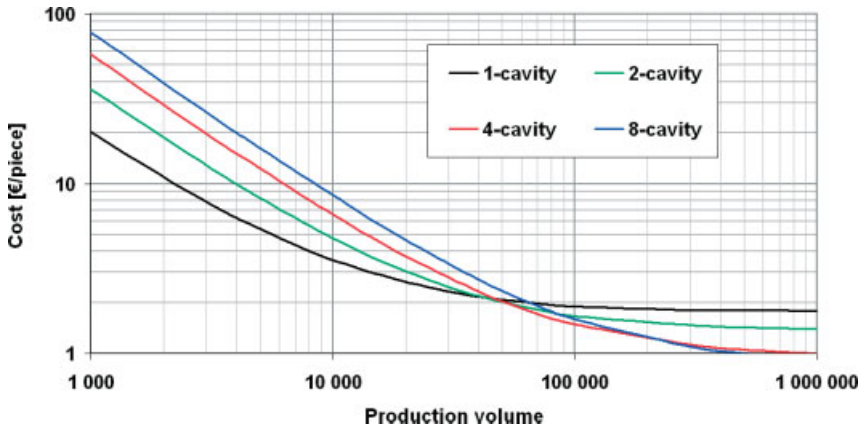
Figure 8.2 Calculated total manufacturing costs for one product at different production volumes with molds that have one, two, four, and eight cavities.

the trends better at low volumes. The costs per piece are first dropping rapidly as the volume is increased and then they are leveling off close to the large volume molding cost value. As the initial high cost of tooling dominates the low-volume figures and the molding costs dominate the high-volume figures, the graphs cross at some specific points. These points can be used to determine the suitable number of cavities of the mold for a specific production volume. For example, in this case the one-cavity mold is the lowest cost option below a production volume of about 45 000 pieces and the eight-cavity mold will become economical at volumes greater than around 220 000 pieces.

From the previous example it is quite obvious that a single-cavity tool will most likely be the best choice for prototyping or for very low-volume products. With high volumes, more cavities are needed as the cost of molding starts to dominate and multicavity molds will produce pieces more cost effectively. Similar calculations can be performed for any product intended for injection molding. If just a few prototype pieces are needed, molding will always be an expensive method to make them due to the high cost of tooling and molding initial costs. Many of the other plastic manufacturing processes such as fused deposition modeling that are suitable for low production volumes [14] are not possible for optical parts due to the poor surface finish quality and material inhomogeneity. Prototypes diamond turned directly from plastics can offer a cheaper solution if just a few (tens) of pieces are needed. However, as the manufacturing method is different, the diamond turned pieces differ in many ways from their molded counterparts. Another method that can be used for manufacturing components for low-volume modules is to make a so-called family mold. This is a type of mold that has different cavities for similar parts. For example, a casing with two near-mirror-image halves could be made with such a method. Family molds can utilize the cost benefits of a multicavity mold and still fulfill the need for different parts geometry in one module.

8.5
Calculating Molding Costs

The molding cost calculation tool input parameters deal with both process and product related issues. Examples of process related parameters are the hourly wages of workers, machine rate, machine uptime, yield, price of electricity, etc. Many of these parameter values are based on knowledge that has been built up inside a molding company during its operational years or they can be obtained from the company's accounting department. These are also the parameters that can be very difficult to estimate from outside of the company. Examples of product related parameters are thickness and weight of the part. Only those parameters that are related to the product features can be directly affected by the design.

Figure 8.3 presents the absolute change in cost when each variable in the example molding cost calculation tool is changed by 1%. This sensitivity graph shows that the five most influential factors in the model are yield, cycle time, machine uptime, number of cavities, and machine rate. Cycle time is the most important parameter directly related to the design of the manufactured component. For example, cycle time has 12 times higher impact to the cost of molding than the price of material. This does not mean that material choice is an insignificant factor in plastic optics production, but it just indicates that it is much more effective to reduce part costs by shortening the cycle time than by selecting a lower cost material. And as we can see in the next paragraph, material choice has a big impact to this time factor and therefore also to the production cost.
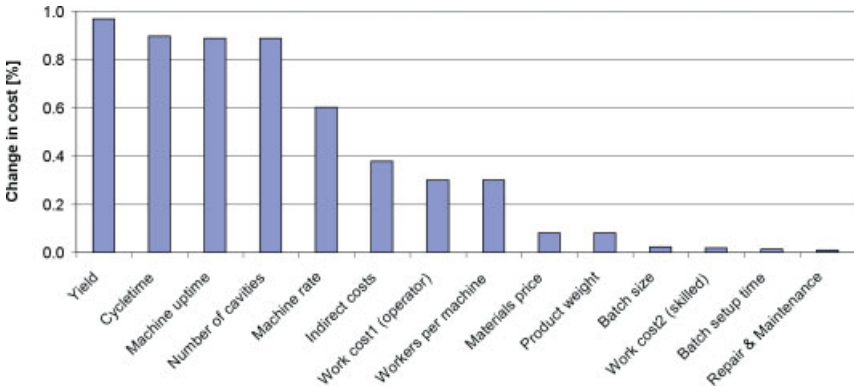
Figure 8.3 Molding cost calculation tool sensitivity to parameter change. The graph shows how much the molding cost of the example product changed (absolute value) when each input parameter was changed by 1%.

8.5.1
Cycle Time and Cooling Time

Cycle time is the time that it takes from the injection-molding machine to make a single part, or in the case of a multicavity mold, a set of parts. Any changes in this time factor, usually measured in seconds, will be multiplied by the number of produced parts. As the size of the production series can be as high as tens of millions, the time spent for making a single piece will have a drastic effect on the time spent for the production of the whole series. A simple example calculation can be made to illustrate this effect. If a product with total production series size of 10 million pieces and an eight-cavity mold will have its cycle time increased by one second, the resulting difference in total production time is 1 s × (10 000 000/8) ≈ 22 workdays (16 h/day). During this time, all of the machines will have to be maintained, workers salaries will have to be paid, etc. The increased cost of production will then be reflected in the increased sales price of the product.

The basic injection-molding cycle consists of several parts. Closing of the mold, forward movement of the injection unit, mold filling, mold opening, and part ejection build up a time factor, which is practically constant for each type of injection-molding machine [15]. As the parts get thinner and cooling times shorter, the relative importance of this factor will increase and some technological development is needed to shorten it. The varying time factor, cooling time, consists of parts such as holding pressure and recovery time. These factors are dependent on the material used, part geometry, mold design, and accuracy requirements. It is possible to eject the piece from the mold before it has been totally cooled, but then it will experience some small uncontrolled shape changes. If the shape accuracy requirement for the part is not high, this can be accepted as it will shorten the cycle time and bring down the cost. Because of demands of high precision, cooling time is usually the dominating factor in cycle time of plastic optics manufacturing and also the main driver for cost.

The simplest theoretical formula for calculating cooling time is used for the geometry of a flat plate. The formula is written as [16]

$$t_c = \frac{h^2}{a\pi^2} \ln \left[\frac{4}{\pi} \left(\frac{T_m - T_w}{T_e - T_w} \right) \right], \tag{8.2}$$

$$a = \frac{k}{\rho c}, \tag{8.3}$$

where t_c is the time for part centerline to reach ejection temperature T_e, after which the solidified material will not deform anymore at ejection. The other variables in the equation are h the plate thickness, T_m the melt temperature, and T_w the mold temperature. Thermal diffusivity factor a consists of k thermal conductivity, ρ density, and c specific heat of the material.

Figure 8.4 shows the relation between cooling time and part thickness for four commonly used optical plastics, as calculated from the previous Eq. (8.2). The difference between, for example, polymethyl methacrylate (PMMA) and polycarbonate (PC) is clear. For example, a 4-mm-thick piece of PMMA will have a cooling
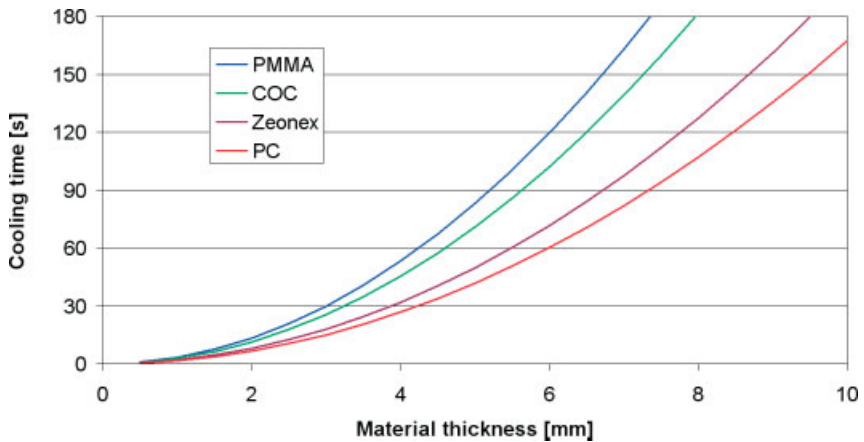
Figure 8.4 Relations between cooling time and material thickness calculated for four optical plastic materials with common material characteristics and molding process parameters.

time of ~53 s, which is two times longer than the ~27 s of PC. This means that the same plate manufactured from PMMA may cost almost two times as much to mold as it would cost if it would be made from PC. With all materials, the cooling time will increase exponentially when the thickness is increased. For this reason, the most important geometric factor in plastic part design is wall thickness [8].

There are several ways of estimating the cooling time of a piece. Equation (8.2) is one example of an analytic approach, which can be used with simple geometries like plate, cylinder, cube, and sphere. Unfortunately, injection-molded pieces are usually much more complex and the analytic approach can only give crude ballpark figures. Another possibility is to use molding simulators such as Autodesk Moldflow or Moldex3D, which use finite element modeling (FEM) to calculate how fast the heat is transferred from the plastic material to the mold and cooling system. This numeric method can be used with complex 3D part geometries and molds with custom designed cooling channels. Accuracy of the estimated cooling time depends on the accuracy of the simulation input parameters and consistency of the model with reality. The third way of estimating cooling time is to use a database of previous products that are similar in size, shape, and precision. These kinds of databases can only be found from injection-molding companies specialized in plastic optics. Naturally, all of these methods can be used simultaneously to find a good estimation for the cooling time of a new part. The exact cycle time can only be determined by making the actual mold and doing some test runs during which the process parameters can be optimized.

8.5.2
Yield and Machine Uptime

As shown in Figure 8.3, yield and machine uptime are among the most important factors that determine the molding cost. Yield defines the proportion of manufactured components that function as specified or which pass the different inspection stages. In every production process, the goal is to reach a yield value of 100%. If all the manufactured parts fulfill the specifications, there is no need, for example, to sort out the defective ones, material loss is at minimum and no machine time is wasted. In real-life production, this is practically impossible to reach.

With plastic optics there are many ways a component can fail to meet the high requirements set to it. Typically, at the start of a new production batch, the first pieces will need to be discarded as the mold and the machines take some time to adjust to the optimal process conditions. If the cavity count of a mold is increased, the risk for one of the inserts becoming damaged is also increased. When the cost of having a repair and maintenance break in the production is balanced with the cost of lowered yield, it is sometimes more cost effective to continue the production until the next scheduled break and just sort out the pieces from the faulty cavity. This leads to the fact that the expected yield is slightly lower for molds that have more cavities. Size of the optics may also have an effect on the yield if there is a specification for the allowed number of defects on the surface of the piece or inside it. As the size of the piece is increased, also the risk of having these defects increases.

Machine uptime is the proportion of time that the machine is used in full production of a particular product. Occasional tool repair and maintenance breaks are necessary especially with plastic optics as the sensitive inserts will need to be cleaned and checked to ensure good quality. Again, with larger number of cavities, the machine uptime can be considered to be somewhat lower as it takes more time to do the maintenance and the risk of something happening to the mold is higher. The breaks themselves are a risk to the inserts as they can be damaged during handling. In the simplified example calculation tool the machine uptime is not connected to the repair and maintenance calculations and it is just used as a single estimated figure. Equation (8.4) presents the formula used for the tool repair and maintenance cost calculation.

$$\text{Tool repair and maintenance} = \frac{\text{R\&M time} \times \text{Workcost2}}{\text{Batch size}}. \tag{8.4}$$

8.5.3
Machine and Labor Costs

Machine rates can also be determined in many ways. It is possible to include to this variable everything from the cost of factory floor area occupied by the machine to the price of electricity that it uses inside an hour of operation. In some cases, the cost of an operator or a robot and profit are also built in to this

single number [8]. The main trend in machine cost is that it follows the size of the machine [13]. This is only natural as a bigger machine will cost more, it will use more floor space, etc. One place to look for examples of machine rates with different tonnages can be found from the PlasticsTechnology website [17]. The site contains updated data from a US survey on machine rates. The machine size (and therefore the rate) is also connected to the size of the molded piece and rules of thumb are generally used to pick the right-sized machine for a particular product. This is done by considering the volume and total projected surface area of the product with all the mold cavities and the runner system [15].

Machine costs in the example calculation tool are calculated from Eq. (8.5). The first part of the formula calculates the machine costs during production and the second part adds the costs of setting up the machine for a new production batch.

$$\text{Machine} = \text{Machine rate} \times \frac{\text{Cycle time}}{\text{Number of cavities}}$$
$$\times \frac{1}{\text{Yield} \times \text{Machine uptime}} + \text{Machine rate} \times \frac{\text{Batch setup time}}{\text{Batch size}}.$$
$$(8.5)$$

In the example tool, the labor costs are calculated separately from the machine rate. Equation (8.6) shows the formula. The first part calculates the cost of operation over the time that the machine is running and an operator is working next to it. If the cycle time of the piece is very short and/or number of cavities is large, more than one operator may be needed for one machine to, for example, separate the parts from the sprue, perform simple visual inspection, or place the parts to a holding tray. If the cycle time is very long and the tasks performed next to the machine are fast, it is also possible that a single person operates several machines simultaneously. The second part of the formula deals with the cost of starting a production or changing the mold for a new production batch. The setup time and hourly wages of the specialized technicians define the cost of this operation. In the formula, work cost1 is dedicated to a person who performs simple tasks and work cost2 is used for skilled personnel with higher wages. The exact values to be used in calculations will need to be estimated on the basis of the location of the production plant. In low-labor-cost countries like China, the hourly wages of workers can be a small fraction of their Europe of US-based counterparts.

$$\text{Labor} = \text{Work cost1} \times \text{Workers per machine}$$
$$\times \frac{\text{Cycle time}}{\text{Number of cavities}} \times \frac{1}{\text{Yield} \times \text{Machine uptime}} \qquad (8.6)$$
$$+ \text{Work cost2} \times \frac{\text{Batch setup time}}{\text{Batch size}}.$$

8.5.4
Indirect Costs

In the example cost calculation tool, the indirect costs are included just as a simple percentage figure. This percentage is calculated from the total sum of the machine, labor, and tool R&M costs as shown in Eq. (8.7). The main idea is that the figure contains all of the indirect costs associated to running a production plant. This simplistic practice makes the calculation tool more approachable. Another option would be to include most of the costs associated to, for example, the necessary clean room facilities and measurement equipment to specific machine costs. In that case the overhead would be used only for calculating the costs of, for example, management, storage workers, or other plant personnel not directly involved in the production of a specific product, but still necessary for running the whole plant. As a single figure, the overhead percentage in the example tool is quite difficult to estimate from outside of an injection molding company. Molders themselves can obtain this number from the company's accounting department.

$$\text{Indirect} = \text{Indirect costs} \times (\text{Machine} + \text{Labor} + \text{Tool R\&M}). \qquad (8.7)$$

8.5.5
Material Costs

Calculating the cost of material per single manufactured piece is a straightforward task when the materials price and product geometry are known. Equation (8.8) shows the formula. The product weight can be calculated from density value of the material and geometric volume of the piece. The volume of runners and sprue will also need to be included as this may represent a very large portion of the material usage, especially with small pieces and molds with many cavities. Yield is also included in the equation as some of the produced parts will always fail to meet the high-quality criteria. In optics injection molding, the material cannot be usually recycled into the process due to the fact that it needs to be homogeneous and clean. The molding and material regrinding introduce, for example, dust particles to the plastic, which affect the optical properties. For this reason, a large portion of material is wasted in plastic optics production.

$$\text{Material} = \text{Materials price} \times \text{Product weight} \times \frac{1}{\text{Yield}}. \qquad (8.8)$$

There can be big differences in the cost per kilogram between two optical plastics such as PMMA and Zeonex. At first glance this may tempt a designer to choose a cheaper material if the optical functioning of the piece allows this. However, as shown in the sensitivity analysis of the molding cost calculation tool (see Figure 8.3), the materials price has a much smaller impact to the cost than cycle time, which is also directly linked to the choice of material. In many optical cases, the direct cost of material is only a small part of the total molding cost and the

selected material affects the molding cost mostly through the physical properties of the plastic, which define the cycle time.

8.6
Calculating Coating Costs

Similarly to the tooling costs, a very simple approach is taken to the estimation of coating costs in the example tool. The costs are calculated by taking into account the batch cost and piece holder size of the coating chamber. Equation (8.9) presents the formula. The main idea is that a holder or a tray that is put into the coating chamber has a certain size that is limiting the number of molded pieces that can be fitted to it. As the size of the optics grows, a lower number of pieces can be fitted to one batch and the cost per piece increases. The coating batch cost is associated to the machine rate of the coating device. In this case, the labor costs connected to coating are included in the batch cost. A much more sophisticated model can be developed with more in-depth knowledge of the coating process, but for the purposes of this article the presented model was considered adequate.

$$\text{Coating} = \frac{\text{Coating batch cost}}{\text{Pieces per batch}} \times \frac{1}{\text{Coating yield}} \times \text{Coatings per piece}$$
$$+ \text{Molding costs} \times (1 - \text{Coating yield}). \quad (8.9)$$

As in the case of any production process, coating will also have a yield factor associated to it. The second part of the formula deals with the fact that a defective coating will also make the injection-molded piece itself unusable. As the defective pieces will need to be discarded, the costs of manufacturing these failed parts will need to be included in the calculations. If there are many successive manufacturing stages where the previous products can be irreversibly ruined, the importance of high yield at each stage becomes even more pronounced. In the case of plastic optics, molding and coating form such a chain.

The distinct difference between molding and coating is that the former is a continuous process whereas the latter one is a batch process. This means that a group of components is coated as a single batch in the coating chamber under identical processing conditions. If the conditions are not ideal and something goes wrong with the coating, the whole batch will have to be discarded. It also means that coating can be a very expensive process for just a few pieces. The batch cost will remain the same even if the chamber has only few components in it and the high batch cost will need to be divided between a small number of parts.

8.7
Additional Processes

In addition to the three key processes mentioned in the previous sections, there are several other processes that belong to the whole production chain of plastic optics products [8, 15]. Some processes such as sprue cutting can be very similar with optical components than with normal mechanical molded parts. However, as the requirements for the functionality are different, there are also lots of differences in some of the subsequent processes that are needed in building whole plastic optics modules and systems.

One example of an additional process that is very specialized for optics is inspection. As explained in the metrology section of this book, there are numerous ways to measure the components or modules that come out of the production lines of plastic optics factories. A large number of devices are needed to make these measurements along with the skilled personnel that can use them. The cost of all this equipment, the floor space that they occupy, electricity that they use, etc. will need to be factored into the sales prices of products made at the factory. Some of these costs are buried in the overhead, but for some cases specialized equipment is needed for a particular product and the costs associated to measurements will need to be included to the sales price directly. For this purpose, individual cost calculation tools are needed also for the metrology processes.

Another additional process that has the potential to clearly increase the cost of plastic optics products is packaging. Optical surfaces in plastic pieces are very sensitive to scratches and contamination, which means that special care must be taken to protect the parts during shipment to the module or device integrator. Usually, special trays are needed for this purpose. As these trays are custom made for each product type, they will also add to the costs directly. This type of expense can also be influenced by design. If the part is designed with mechanical features that protect the optical surfaces, the pieces can be packaged faster and more efficiently without extra packaging material. More pieces can possibly also be fitted to a container, which will then reduce the cost of shipping.

8.8
Case Study 1: Comparing Different Design Concepts

The purpose of the first case study is to illuminate the use of cost modeling at the concept creation phase of a new optical product. Figure 8.5 shows two alternative design concepts for a viewfinder. Both of the designs are able to perform the same required optical functions: the optical path is tilted by 90° and the image is magnified by a factor of 1.5. Additional specifications state that the sharp image Field of View (FOV) is 4.8°, aperture diameter is 8 mm, and transmission of the optics is higher than 88%. The first design in Figure 8.5(a) is a more traditional one in the sense that it is made from separate components by using two lenses and a surface mirror. This design could also be made with glass lenses, but to have adequate

(a)

(b)
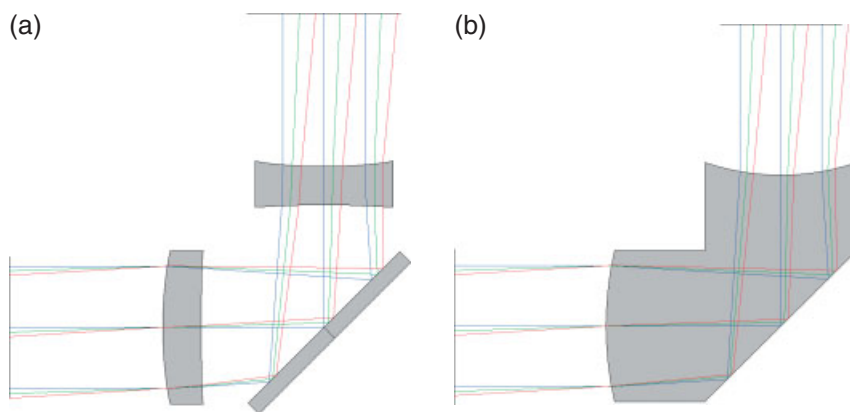
Figure 8.5 Two alternative optical designs for a telescopic viewfinder: (a) made with separate optical components and (b) made with a single integrated optical component.

(a)

Ø11.00

2.27

Ø11.00

2.88

(b)
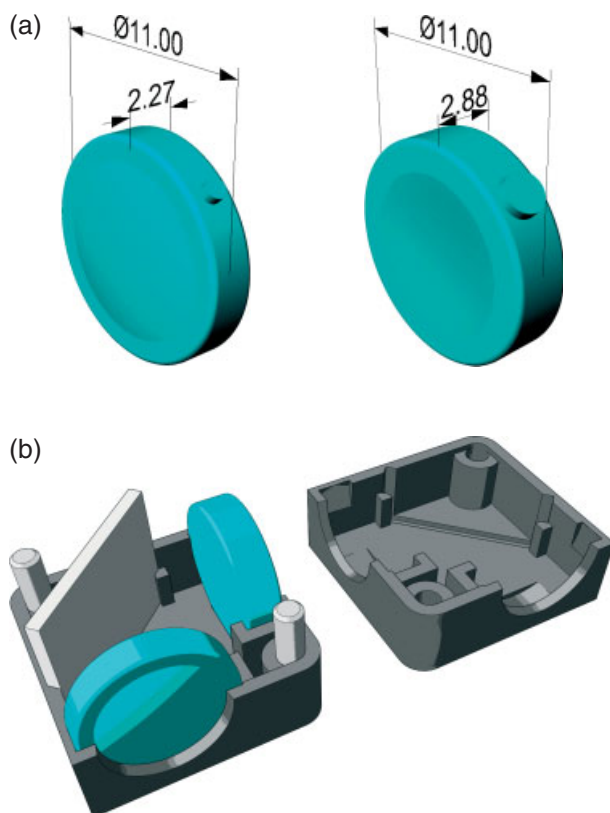
Figure 8.6 Parts needed for the first design option: (a) two plastic lenses and (b) the whole module.

performance the surfaces will need to be aspheric and plastic offers a lower cost solution for the intended volumes of this application. The second design utilizes the potential of plastic optics more extensively by integrating three optical surfaces to a single monolithic piece.

As both of these design concepts are capable of producing basically the same optical performance, the designer is left with the difficult task of choosing the one which can be made with lower cost. The first design is more complicated and requires more parts as the separate components will need to be assembled into a module, as shown in the concept module design at Figure 8.6(b). The higher part count and assembly process will definitely add cost. In the second monolithic approach, the optical component is a very thick piece, as shown in Figure 8.7(a). This means that the cycle time will be very long and the manufacturing costs of this single piece are relatively high.

The first design will require at least three molds: one for the two symmetric casing halves that hold the optical elements together and two for the different lenses. However, the two optical molds can be very simple, whereas in the second case the mold for the imaging prism will be much more complicated with three optical surfaces that will need to be aligned in a single cavity.

If the required transmission of the system is >88%, the first design will need AR coatings on all of the lens surfaces due to the fact that the surface mirror will
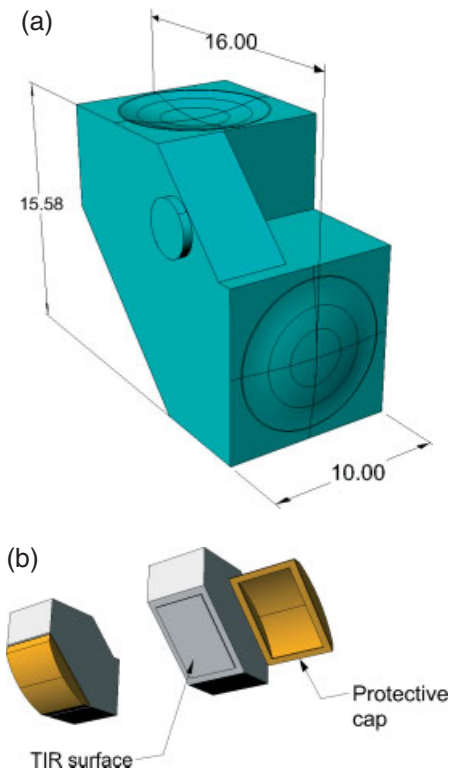
Figure 8.7 Parts needed for the monolithic design option:
(a) the imaging prism and (b) optional protective cap.

loose some light (~8%) on the optical path. In the monolithic approach, there are actually two alternative ways to make and protect the mirror surface. A protective cap (concept shown in Figure 8.7(b)) can be used to protect the surface that works by the principle of total internal reflection (TIR). In this case, no coatings are needed and the reflectance is nearly 100%. A second option is to put a simple aluminum mirror coating on the tilted surface, but this would make the reflectance worse and some coatings on the two lens surfaces would be needed to meet the specified transmission. If the mirror coating would be used, there would be no need for the molding and assembly of the protective cap. Overall, it is very difficult to come to any kind of conclusion on which design to choose for further development without first doing some cost estimation.

Table 8.3 shows the input parameters that were used in the calculation tool to estimate the component manufacturing costs of the three design concepts. The materials price for lenses 1 and 2 are different, because the first one should be made from PC and the second one from Zeonex. The monolithic imaging prism is also made from Zeonex, but the casing for the separate parts module and the protective cap can be made from a lower cost material such as PMMA, which suits better to the mechanical function. Product weights were estimated with the help of a CAD-program that was able to determine the volume of the piece from the concept design models. As the lenses and imaging prisms have both roughly the same projected area, a similar injection-molding machine can be used for both and the machine rates can be set to the same value. As the casing of the first concept design is somewhat larger in size, it will also need a larger machine and the machine cost is higher. Machine uptimes and yields depend on the complexity of the pieces and molds. These can be set to somewhat higher values for the single lenses than for the imaging prism, which is a more complicated piece with three optical surfaces. In this exercise the number of cavities was set to four for all of the produced pieces, but this value as well as the production volume could also be varied to make a more thorough comparison. Cycle times for each piece were estimated on the basis of their geometry and material properties. The imaging prism is a very thick part and therefore it will need a lot of cooling time whereas all the other pieces are much thinner and cool down faster. All the other input parameters for the molding were set the same to keep the calculations simple.

The mold costs for the two lenses were set to somewhat lower values than the cost for the casing mold, because they are more simple and smaller. However, in the lens molds there are two expensive optical inserts in each cavity, which makes a total of eight inserts per mold. In the monolithic prism case, the molds are more complicated and there are also three optical inserts per cavity, which makes them clearly the most expensive tools in this example set.

As the lenses have smaller area than the imaging prisms, a larger amount of them can be fitted to a single coating batch. Because of the transmission specification, both of the lenses need AR coatings on both sides, whereas the imaging prism does not need any coatings if the protective cap is used. If the monolithic component is coated with a mirror coating, it will also need AR coatings on the two lens surfaces to ensure adequate transmission.

Table 8.3 Input parameters used in the manufacturing cost calculations

molding input parameters		viewfinder made from separate components			monolithic with protective cap		coated monolithic
		lens 1	lens 2	case h1/h2	imaging prism	protective cap	imaging prism
materials price	€/kg	10	25	5	25	5	25
product weight	g	0.24	0.25	0.62	1.8	0.62	1.8
machine rate	€/h	18	18	25	18	18	18
machine uptime	%	87	87	90	85	93	85
yield	%	92	92	95	90	97	90
number of cavities		4	4	4	4	4	4
cycletime	s	27	35	22	240	14	240
work cost1 (operator)	€/h	10	10	10	10	10	10
work cost2 (skilled)	€/h	20	20	20	20	20	20
indirect costs	%	70	70	70	70	70	70
workers per machine		1	1	1	0.5	1	0.5
batch size		50 000	50 000	50 000	50 000	50 000	50 000
batch setup time	h	8	8	8	8	8	8
repair and maintenance	h/batch	8	8	8	8	8	8

tooling input parameters		lens 1	lens 2	case h1/h2	imaging prism	protective cap	imaging prism
mold design cost	€	2 000	2 000	3 000	3 000	1 000	3 000
mold cost	€	30 000	30 000	40 000	50 000	20 000	50 000
optical insert cost	€	1 000	1 000	–	1 000	–	1 000
mold life	cycles	1 000 000	1 000 000	1 000 000	1 000 000	1 000 000	1 000 000
insert life	cycles	100 000	100 000	–	100 000	–	100 000
inserts per cavity		2	2	0	3	0	3

coating input parameters		lens 1	lens 2	case h1/h2	imaging prism	protective cap	imaging prism
coating batch cost	€/batch	250	250	250	250	250	250
pieces per batch		2 000	2 000	2 000	1 600	1 600	1 600
coating yield	%	95	95	100	100	100	95
coatings per piece		2	2	0	0	0	3

Table 8.4 shows the calculated manufacturing costs for the three presented module options. In the separate components case, the time it takes to assemble the module was estimated to 30 s, and this was used in calculation of the assembly cost. Also the cost of the additional components was estimated to calculate the total cost of the module. The protective cap was considered as a part manufactured in the same factory, but this could also be a component that is purchased outside the company that makes the optical modules. In this case, the cap assembly time was estimated to be 10 s.

Table 8.4 Calculated manufacturing costs of the three module design concept cases.

assembled from separate components

	tooling	molding	coating	total
lens 1	0.028	0.130	0.270	0.428
lens 2	0.028	0.167	0.272	0.467
case h1	0.011	0.127	0.000	0.138
case h2	0.011	0.127	0.000	0.138
pins	–	–	–	0.020
mirror	–	–	–	0.100
assembly	–	–	–	0.083
total	**0.078**	**0.552**	**0.541**	**1.374**

monolithic imaging prism with protective cap

	tooling	molding	coating	total
imaging prism	0.043	0.918	–	0.961
protective cap	0.005	0.070	–	0.076
assembly	–	–	–	0.028
total	**0.049**	**0.988**	**0.000**	**1.064**

monolithic imaging prism with coatings

	tooling	molding	coating	total
imaging prism	0.043	0.918	0.539	**1.500**

The lowest cost (1.06 €/piece) is achieved with the monolithic prism that has a protective cap. A module made from separate components would cost ~30% more and the fully coated imaging prism would be over 40% more expensive to make. Figure 8.8 shows with graphics how the costs are divided in each case between the different factors. The biggest difference between the two main design concepts is the cost of molding. The separate parts can be molded with approximately 60% of the cost of the imaging prism. Coating is a major cost factor in the separate parts case. If the specification for transmission would be relaxed to, for example, a value of 82%, then the separate parts concept would be competitive with the cap-protected imaging prism as only two AR coatings would be needed for the system and the manufacturing cost would drop to a value of 1.11 €/piece. Similar cost/performance tradeoff would not be possible with the imaging prism as the cost of molding is dominating the overall cost of the system. In the monolithic case, the size of the optical piece would have to be made smaller to get a lower cost module.
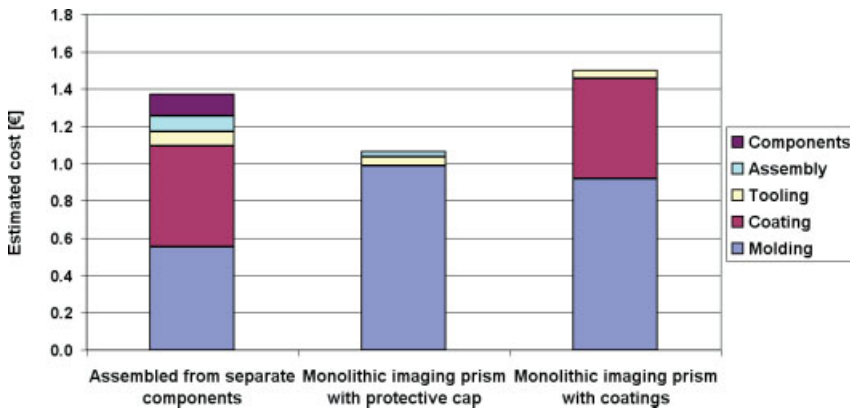
Figure 8.8 Ratios of different cost factors for the three design concept cases.

8.9
Case Study 2: Evaluating Manufacturing Process Improvements

In the second case study, the monolithic viewfinder imaging prism shown in Figure 8.7(a) is used as an example on how to use cost modeling as a support for decision making in manufacturing process optimization. Figure 8.9 shows the simulated modulation transfer function (MTF) of the nominal viewfinder design. A specification for the acceptable resolution of the optics was set at a minimum MTF value of 0.3 at 2.4° field half-angle and at 20 cycles/deg. According to a
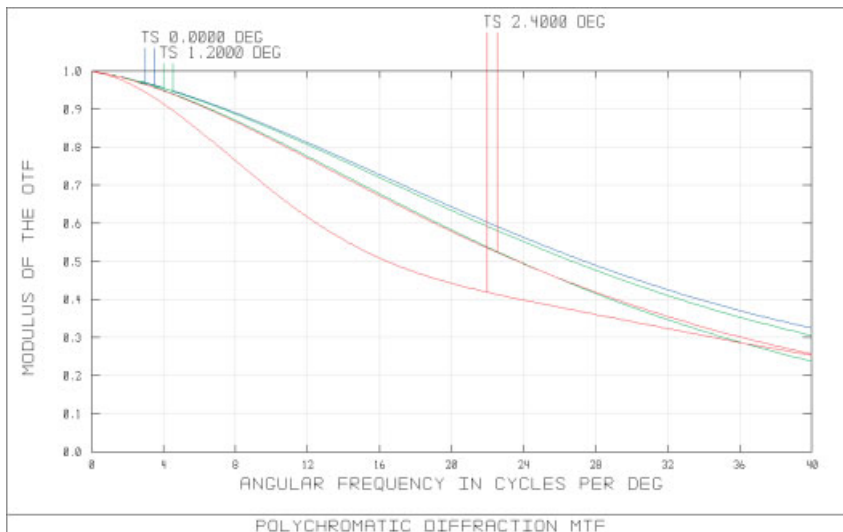
Figure 8.9 Calculated MTF graphs of the nominal design.

Zemax simulation, the nominal design reached a value of 0.44 @ 2.4 deg @ 20 cycles/deg, which is clearly above the specification.

Tolerance analysis was made as a part of the optical design for the example view-finder. Table 8.5 shows three different tolerance value sets that were used in the analysis. The first set can be considered as easy-to-reach values for this particular mold design. The second and third sets were made by first analyzing the sensitiv-ities of the individual tolerance variables and then tightening the most sensitive ones. Purpose of this was to reduce the expected performance variations of the manufactured optical parts. The values are tighter than in the first tolerance set, but they can still be considered feasible if more effort is put into building the mold.

Table 8.5 Three sets of tolerance parameter values used in the analysis.

parameter	tol. set 1	tol. set 2	tol. set 3
radius of curvature	$\pm 25\,\mu m$	$\pm 10\,\mu m$	$\pm 5\,\mu m$
center thickness	$\pm 50\,\mu m$	$\pm 20\,\mu m$	$\pm 10\,\mu m$
surface decenter	$\pm 50\,\mu m$	$\pm 40\,\mu m$	$\pm 40\,\mu m$
surface tilt	$\pm 0.5°$	$\pm 0.4°$	$\pm 0.2°$
refractive index	± 0.001	± 0.001	± 0.001
abbe number	$\pm 1\%$	$\pm 1\%$	$\pm 1\%$

Figure 8.10 shows the results of Monte Carlo (MC) tolerance runs made with the three tolerance sets. The graphs are histograms that show normalized perfor-mance distributions of 100 000 simulated systems in each case. As expected, the second tolerance set produced a more narrow distribution than the first set and
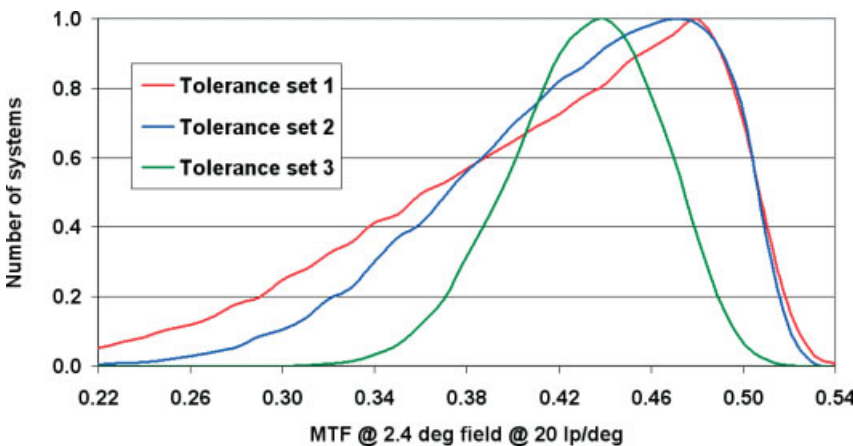
Figure 8.10 Simulated MC performance distributions.

with the third set the distribution became most restricted. The first two distributions have their peaks at about the same value of MTF ~0.48 @ 20 cycles/deg, but with the first tolerance set there are clearly more systems that fall below the specified pass/fail limit of 0.3. With the third tolerance set, the distribution peak is at a lower value of MTF ~0.44 @ 20 cycles/deg, but this time all of the systems are above the specified performance limit.

Figure 8.11 shows the cumulative yield values calculated from the three performance distributions. At tolerance set 1, the yield is ~90% at MTF 0.3, whereas with the tighter tolerance set 2, the yield is a good ~98%. The tightest set 3 produces a tolerance yield of full 100%. When these values are used in the cost calculation tool the following molding costs are obtained: 90% yield €0.92, 98% yield €0.84, and 100% yield €0.83. From these estimated numbers we can calculate that the cost difference between the first two tolerance sets in manufacturing will result to €40 000 with a production volume of 500 000 pieces. This means that if, for example, €20 000 more is invested to a higher accuracy mold, the cost saving will be another €20 000, because the better yield will save money in the long run. However, in both of these cases the yield is such that all of the manufactured pieces will need to be measured in order to be able to separate the good pieces from the bad ones. Although the molding cost difference between tolerance sets 2 and 3 is only €5000 at 500 000 piece volume, the overall savings can be much higher, because with 100% tolerance yield a sampling measurement is enough to ensure acceptable performance. In real life optics injection molding, a 100% yield is practically impossible to reach, but with a good design it is possible to reduce the amount of needed measurements to a minimum. Cost modeling can be used in finding a balance between these factors.
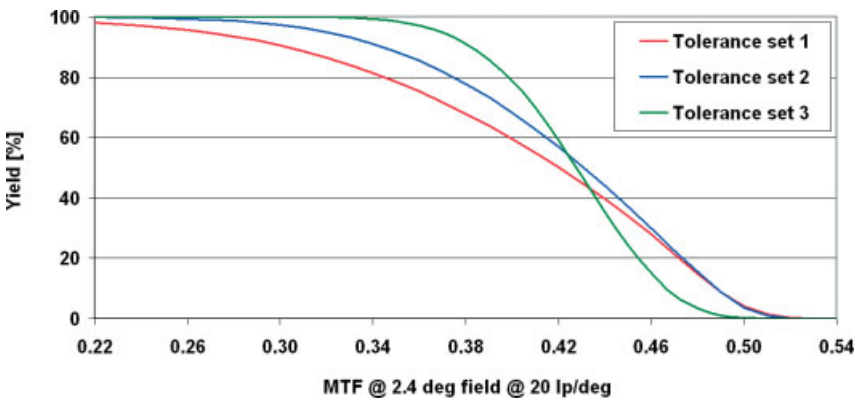
Figure 8.11 Yields calculated from the simulated performance distributions of the three tolerance sets.

8.10
Case Study 3: Optimizing an Optical Design at Module Level

In the third case study, a concentrating photo voltaic (CPV) module is used as an example for showing how an optical component can be designed for module level optimum. The main idea in a CPV module is to concentrate light with low-cost optics to a small multilayer solar cell, which can operate at much higher conversion efficiency than a standard silicon panel. In such a module, only a small area of expensive semiconductor surface is needed to convert the Sun's radiation to electricity. A lot of mechanics is needed to make the module and tracking system that keep the optics in line with the solar cell and pointed to the direction of the moving Sun. One type of such systems uses Fresnel lenses as the primary optical element (POE). A secondary optical element (SOE) such as a CPC (compound parabolic concentrator) is used to relax the aiming tolerances of the tracking system, but the POE is responsible for the concentration of light [18].

An aspheric Fresnel lens with a certain aperture size, focal length, and spot size can be designed in several different ways. If the lens is injection molded, the thickness of the piece becomes very important. Figure 8.12 shows three examples of POE designs, which are 50 mm × 50 mm in size and have basically the same optical function. As the number of rings is increased, the thickness of the piece is also reduced. Figure 8.13(a) shows this relation between the number of rings and thickness calculated for eight designs. All of the lenses were designed with a 2-mm-thick base layer and the ring structure was formed on top of this layer as shown in Figure 8.14. As the total thickness dropped from the 8.1 mm of the one-ring case to the 2.5 mm of the 26-ring case, also the molding cost went down as the cycle time was reduced. Figure 8.13(b) shows the relation between the number of rings and molding cost. The graph shows that the design with only one ring costs over four times as much to mold than the design with 26 rings.

From the component cost point of view, the thinnest design would be an obvious choice. However, as the number of rings is increased, also the area covered by the rounded ring tips, troughs, and drafted walls between the rings is increased. This area is wasted because the light falling on it is not focused to the solar cell but is instead scattered around as stray light. The relation between the
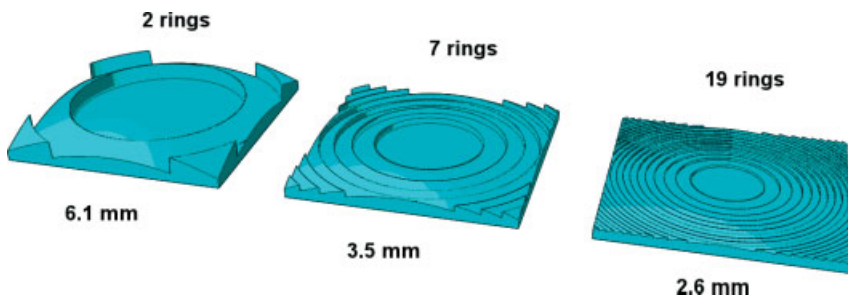
Figure 8.12 Three example 50 mm × 50 mm Fresnel lens designs for POE.

(a)

(b)
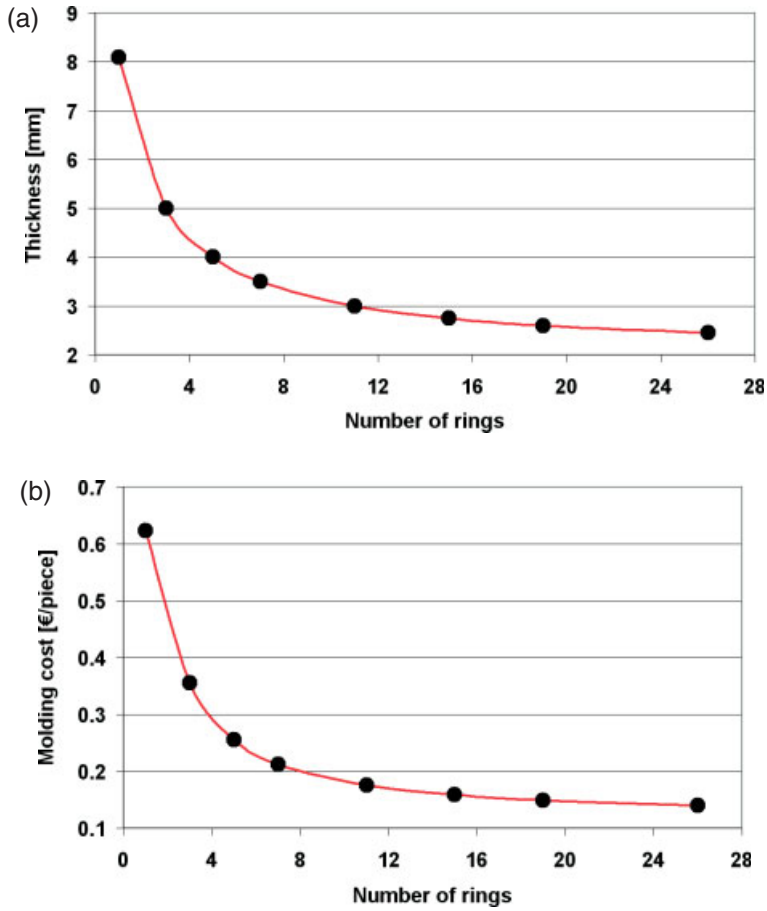
Figure 8.13 Relations between the number or POE rings and (a) thickness and (b) molding cost calculated with eight-example Fresnel designs.
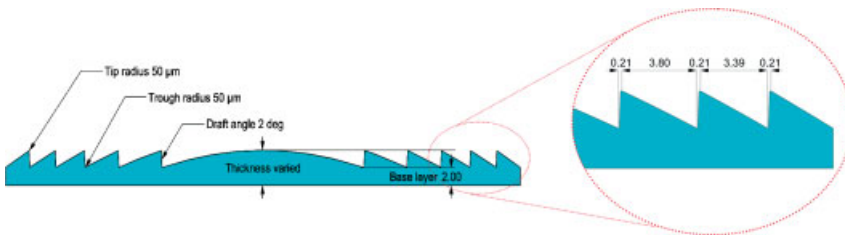
Figure 8.14 Design parameters of the example POEs: base layer thickness 2 mm, tip and trough radius 50 μm, and draft angles of 2°.

number of rings and component transmission, as shown in Figure 8.15(a), was simulated with optical design software Zemax. When the values shown in Figure 8.14 were used, the one-ring case had a transmission of 90% as the 26-ring design transmitted only 81% of the light. Therefore, from the performance point of view, the one-ring case would definitely be the best choice.

Figure 8.15(b) shows the relation between POE transmission and molding cost. This "value for money" graph shows that the relation between performance and cost is not linear. The costs start to rise fast after about 88% transmission value. As all of the light falling on the solar cell comes through the POE, the performance of the whole module is affected by the transmission of the Fresnel. This means that the component performance and cost will need to be balanced with the performance and cost of the whole module.
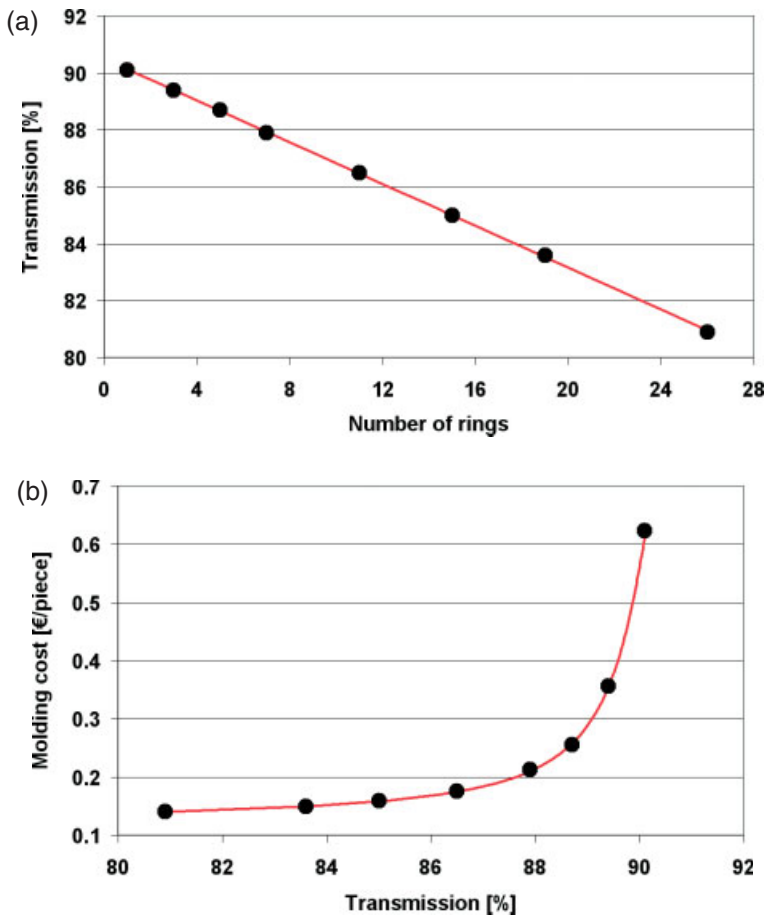
Figure 8.15 Relations between (a) the number or rings and transmission and (b) transmission and molding cost calculated and simulated for the example POEs.

If we assume that the maximum amount of light falling on the CPV module is 1000 W/m^2, module conversion efficiency is 25% (without the Fresnel) and module cost is €600/m^2, the graph shown in Figure 8.16 can be calculated for the eight-example designs. The graph shows that the minimum module manufacturing cost in €/Watt is achieved with a POE design that has 10 rings. If the design with the best performance would have been chosen, the module cost would have been as much as 22% higher. If the component-level cost optimum design would have been chosen, the module cost would have been 5% higher than with the intermediate design that is now optimized for module-level performance and cost.
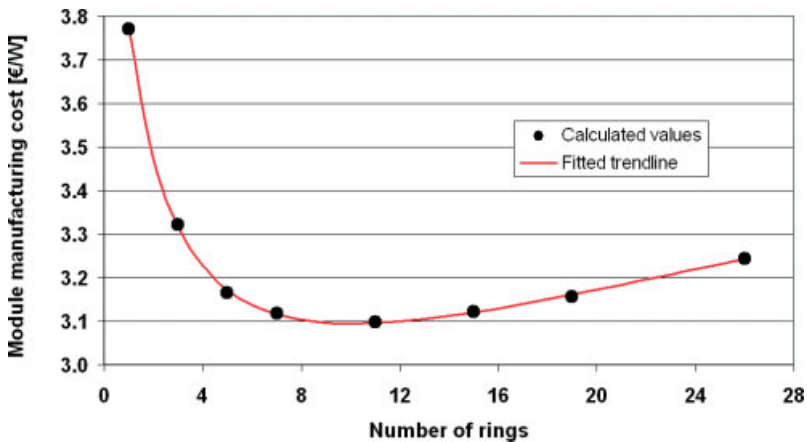
Figure 8.16 Relation between the number of POE rings and module manufacturing cost calculated for the example designs.

8.11
Discussion and Conclusions

As with any other simulation tools, the results obtained with cost models should not be trusted blindly. It is very easy to make mistakes with the input parameters due to lack of knowledge or simple misconception on the functioning of the tools. The cost models that are used should always be "calibrated" against real-life data that can be obtained from various sources. The parameter values used in this chapter were just generic ballpark figures not connected to any specific geographical region or factory. There is a lot of material available for estimating the processing parameters and costs associated to normal injection-molding production. Unfortunately, optics is only a small subsection of this field of manufacturing and there is clearly less information available for plastic optical parts. Because of different functional requirements, not all of the injection-molding data is applicable to optics and good care should be taken when the different rules of thump are used in estimating the parameters for cost calculations.

One major result from the analysis presented in this chapter was that in respect to cost the two most important design-dependent features for plastic parts are the wall thickness and material selection. This is a general rule for all injection-molded pieces. Unfortunately, the selection of optical plastics is very limited and no fillers can be used to enhance the properties of materials as is done with standard mechanical parts. Optics is also all about geometry. Propagation of light is manipulated with the help of different surface shapes and the flat plate geometry, which is ideal for the injection-molding process, cannot be utilized effectively in optics. Diffractive structures, in which the optical geometry is reduced to a minimum, are a rare exception to this rule. However, as in the Fresnel lens case, the flatness of diffractive optics is followed by deterioration of performance. For some applications this is acceptable if the functional specifications are not strict and the cost is the major driving force, but for some applications no reduction of performance is possible. And as in any field of product engineering, the optical design needs to be optimized by balancing performance with cost by considering the whole module or device.

Concurrent engineering is a philosophy, which aims for better products and lowered costs by improving the whole product development process [19]. This holistic approach is based on the principles of communication and concurrent decision making. Many features of concurrent engineering such as DFMA (Design for Manufacturing and Assembly) and QE (Quality Engineering) can actually be found from standard optics development practices. Optical designs have always been restricted by manufacturing possibilities, which means that out of necessity, DFMA has become a natural part of the process. For example, glass lens systems are usually designed by avoiding aspherics, because they are expensive and their quality is more difficult to control. Also the assembly process of complex or high-quality optics is often considered during tolerancing when the variables and compensators are set for the analysis [20]. Although, the term concurrent engineering is not usually mentioned in connection to optics, the main idea of interdisciplinary cooperation is clearly the same. The fact that plastic optics components are buried into more and more complex devices creates a need for guidelines and tools that make this design integration possible. Cost modeling of optics manufacturing offers just one extension to this practice.

A good optical design is optimized to meet the tolerances of the intended manufacturing process. This means that some of the peak performance of the ideal design can be sacrificed to make the performance distribution inside a production series more narrow and/or yield higher. In a similar way, the cost models could be used for tolerancing costs. Parameters such as cycle time are sometimes very difficult to predict accurately for optics as the high requirements may drive the values to extremes. With false predictions the estimated costs can be either too high for, for example, a competitive quote or too low for, for example, feasible profit margin. Both qualitative and quantitative analysis can be made with a parameterized cost model. The sensitivity analysis of the injection molding process shown in this chapter is an example of the former case. The latter case could be covered with a Monte Carlo analysis in which the input parameters of the model are varied

according to an estimated distribution and the outcome would be the probability distribution of cost. These kind of simulations could make cost-risk management a little easier.

References

1 J.G. Bralla, *Design For Manufacturability Handbook*, 2nd ed. (McGraw-Hill, NY, USA, 1999).

2 P. Dewhurst, *Cutting Assembly Costs with Molded Parts* (Machine Design, Cleveland, OH, USA, July 21, 1988).

3 IDES CostMate® – Injection molding part cost estimator: www.ides.com/costmate/.

4 BASF Quick Cost Estimator for Injection Molding Thermoplastic Parts: iwww.plasticsportal.com/quickcost/

5 Y.-M. Chen and J.J. Liu, Cost-effective design for injection molding, *Robot. Comput.-Integrated Manufact.*, **15**(3), 1–21 (1999).

6 N.P. Suh, *The Principles of Design* (Oxford University Press, Oxford, 1990).

7 L.B. Newnes, A.R Mileham, and H. Hosseini-Nasab, On-screen real-time cost estimating, *Int. J. Prod. Res.*, **45**(7), 1577–1594 (2007).

8 D.M. Bryce, *Plastic Injection Molding: Vol. II, Material Selection and Product Design Fundamentals* (Society of Manufacturing Engineers, ME, USA, 1997).

9 Nagahanumaiah, B. Ravi, and N.P. Mukherjee, An integrated framework for die and mold cost estimation using design features and tooling parameters, *Int. J. Adv. Manufact. Technol.*, **26**(9–10), 1138–1149 (2005).

10 S.F. Chan, C.K. Law, and K.K. Chan, Computerised price quoting system for injection mould manufacture, *J. Mater. Process. Technol.*, **139**, 212–218 (2003).

11 A. Fagade and D.O. Kazmer, Early cost estimation for injection molded parts, *J. Inject. Mold. Technol.*, **4**(3), pp. 97–106 (2000).

12 D.M. Bryce, *Plastic Injection Molding: Vol. III, Mold Design and Construction Fundamentals* (Society of Manufacturing Engineers, ME, USA, 1998).

13 P. Dewhurst and D. Kuppurajan, Determination of optimum processing conditions for injection moulding, *Int. J. Prod. Res.*, **27**(1), 21–29 (1989).

14 R. Karania and D. Kazmer, Low volume plastics manufacturing strategies, *J. Mech. Design*, **129**, 1225–1233 (2007).

15 D.M. Bryce, *Plastic Injection Molding: Vol. I, Manufacturing Process Fundamentals* (Society of Manufacturing Engineers, ME, USA, 1996).

16 K. Beiter, J. Cardinal, and K. Ishii, Design for injection molding: balancing mechanical requirements, manufacturing costs, and material selection, *Proceedings of the ASME Computer Integrated Concurrent Design Conference*, Boston, MA, USA (1995).

17 *PlasticsTechnology*, Gardner Publications, Inc: www.ptonline.com

18 U.S. Department of Energy: www1.eere.energy.gov/solar/concentrator_systems.html.

19 B. Prasad, *Concurrent Engineering Fundamentals Vol. I: Integrated Product and Process Organization* (Prentice-Hall, New Jersey, 1996).

20 P.R. Yoder Jr., *Opto-Mechanical Systems Design*, 3rd ed. (Marcel Dekker, New York, 2006).

9
Applications of Injection-Molded Optics

Stefan Bäumer (Philips Applied Technologies, Eindhoven, The Netherlands)

9.1
Introduction

There are many applications of injection-molded optics all around us. It starts off by personal communication items: mobile phone cameras, web cameras, entertainment applications such as CD, DVD, or Blu-ray players, head-mounted displays (HMD) for viewing or gaming experiences, more and more lighting applications mostly in conjunction with LED technology, all kinds of sensor technologies ranging from remote controls to industrial distance or level sensors. Solar energy and medical diagnostics are newer application areas as well. Once one observes the environment minutely, the list seems endless. In many cases, the reason for injection-molded optics is either cost advantage in volume manufacturing, integration of function in combination with freeform type of optics, or weight. Sometimes, it is a combination of two or more of these items. This chapter visualizes some of these applications. All the products have been manufactured (some as prototypes) and show how versatile injection-molded optics can be. Going through the chapter, one gets a quick overview of what different possibilities are feasible using injection-molded optics. It should also become clear, that injection-molded optics is way past the state of low quality toy-like optics. For the different contributions, the following format has been applied:

- application
- why plastic optics?
- challenges.

Following these three guidelines, the essence of plastic optics in the applications is revealed. However, before going to the examples, trends in different industries where injection-molded optics is important will be discussed. Most of the trends will also be supported by one or two examples in this chapter. Further details can be found in the literature [1].

9.1.1
Lighting Industry

Following a global trend toward more energy efficiency and -saving, the lighting industry is undergoing a major change from incandescent lighting to more energy-efficient lighting. One of the main contributors to more energy-efficient lighting is LEDs. Using LEDs in general lighting requires different optical systems than in the past. LEDs are relatively small in lateral dimensions and the bare die has got a radiation pattern different from incandescent sources. The radiation pattern extends only over one hemisphere and not into the 360° space like incandescent sources. And due to the relatively small chip dimensions, lenses capturing and shaping the light come into play. Optical systems involving LEDs have to be designed differently. One main difference is that quite often a two-step approach is taken. The so-called primary optics is positioned very close to the chip and put boundaries on the radiation angle. Sometimes the LED chip is even encapsulated by transparent material with an optical shape [2]. Once the radiation is bound by the primary optics, a secondary optical element is used to shape the light further into the form it is desired. In many cases, the primary optics is made of injection-molded transparent silicon-based material; see example on silicone primary optics. The reason for the silicone material is mainly heat resistance and temperature stability at elevated temperature that occurs close to the LED chip. The secondary optical element can be made from thermoplastic optical material. Figure 9.1 schematically illustrates the situation.
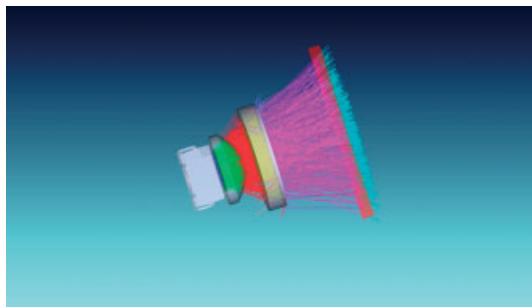
Figure 9.1 LED with primary and secondary optics.

Since often many LEDs are needed in one application, the number of optical elements for the LEDs is high as well. Therefore, a cost-effective way of producing these optical elements has to be found, and injection-molded optics could be the manufacturing method of choice. Another advantage that goes together with the molded optics is the freeform capabilities. In more and more applications, LEDs are used in combination with so-called freeform optics. Because of the diamond turning capabilities of today's state-of-the-art single-point diamond turning machines, these unconventional shapes can be realized a lot better [3]. Figure 9.2 shows a typical LED collimator, making use of total internal reflection (TIR) and refractive surfaces.

Figure 9.2 Typical LED collimator optics (Photo courtesy of LEDXtreme, Vancouver, Canada).

Applications of LED illumination systems are manifold: indoor, outdoor, portable, and automotive is a possible top-level classification (see, e.g., street lighting).

Other examples of using LEDs in conjunction with injection-molded optics can be found in functional and accept lighting as well. Logos of companies are being illuminated or projected by a few LEDs. An example is shown later in the chapter. Yet another LED application is the mobile phone flash, of which a product is shown later as well.

The automotive industry already adapted LEDs in rear lights and brake lights. Front lighting might follow. The first series cars with full LED head lighting are released [4]. In general, lighting in and around the automobile has become a strong design element and distinguishing factor. Many of these applications are LED based and require more or less complicated optics, which can be realized very well using injection molding.

9.1.2
Mobile Communications

Mobile communication and entertainment has been at the cradle of high-volume manufacturing of injection-molded optics. Starting in the 1980s with optics for CD players, injection-molded optics got a real boost in precision, volume, and also in acceptance. CDs are being followed by DVDs and now Blu-ray technology. In all the systems, injection-molded optics plays a major role and was to some extent enabling the commercial successes because of the cost-effective way of producing these parts. Later, at the beginning of this century, mobile phone cameras followed. Today in this whole sector, probably most of the injection-molded optics is produced. Driving forces are cost, volume and integration capabilities, and weight (see, e.g., mobile phone camera, phone flash, add on lens mobile phone, HMD).

9.1.3
Security

Security is a sector that has shown consistent growth over the last years. Cameras are widely used in this sector. Although surveillance cameras are usually equipped

with glass lenses, there are some examples where plastic optics is applied as well (see, e.g., security camera). Besides surveillance cameras, there exists a wide variety of biometric applications: iris scanners, fingerprint readers, and access point scanners are some examples. In many of these sensors, molded optical parts are being applied. Reason for the molded optics again is cost and integration capabilities.

9.1.4
Healthcare

Healthcare is being perceived as the growth industry of the 21st century. One of the main trends in healthcare is the so-called personalized healthcare. For that patients need to gain access to more diagnostic devices and aids. Many of the devices for self-testing are based upon optical technologies. Glucose measurement for diabetes is one of the most known examples. Another trend in healthcare is earlier and faster diagnostics of various diseases. For that to happen, various test methods of DNA and proteins are being developed. Quite a few of them are based upon optical technology. For these tests to break through, cheap disposables are a necessity. Injection-molded parts (not necessarily optics only) are very well feasible options [5]. An application that is penetrating the market as well is a miniature camera that can be swallowed. With the aid of this camera, investigations of the intestines are carried out [6].

Another large volume application of molded optics is the spectacle lens industry. Today many spectacles are produced out of polycarbonate, because of the good optomechanical properties of polycarbonate (nonbreakable and light weight). For spectacle lenses, an example is shown in this chapter. Contact lenses as well and the manufacturing process of them can be counted in the wide field of application of molded optics. Since many of these designs and applications are fairly sensitive, it is very difficult to publish any case studies at this point. However, many sources can be found on corporate websites and in the literature [7].

9.1.5
Sensors and Other Applications

Besides the categories mentioned above, there is also the wide field of sensors where injection-molded optics has got its place: barcode scanning devices at the cashiers, optical mice for computers, HMD for virtual reality and gaming experiences, optical level sensors in construction, light gates in automation, vision systems, simple optical systems in toys, and micro projection (see micro lens array (MLA) example). In this category, automotive applications have to be mentioned as well. There is a whole series of cameras, sensors, and displays that can be found in modern cars. Head up displays (HUDs) can be found in more and more vehicles. Rear view and side view cameras are being applied in cars. Security systems like lane departure cameras and systems that detect the presence of passengers for airbag release are being developed and applied. Many of these systems make at least partial use of injection-molded optics. The reason is mostly cost-savings compared to glass optics in the same volume.

9.1.6
Photovoltaic

In recent years, photovoltaic regained lots of attention and importance. Among the photovoltaic systems, the so-called concentrated photovoltaic systems (CPV) link nicely with high volume, low cost optics. In CPV, a small amount of silicon or GaAs semiconductor material is used for the conversion of light into current. However in order to collect as much light as possible onto the small semiconductor surface, optical systems are being used. From a principle point of view, these optical collector systems show a certain similarity with LED illumination systems, here only used the other way around. Most of the CPV optical systems that are being manufactured today make use of a primary optical element, that is, a large Fresnel lens and a secondary optical element close to the photocell, something like a compound parabolic concentrator (CPC). Potentially, this market segment could develop into another high-volume segment for molded optics (see example). Also in the field of CPV, the freeform capability of injection-molded optics might play a major role in the future. Several novel design concepts involving freeform optics are emerging and being presented at scientific conferences, see for example the conference on Nonimaging Optics and Efficient Illumination Systems V [8].

Although the list of application of injection-molded optics is long, it is most of the time quite difficult to convince people to publish their application – at least at the level of detail done here. Therefore, the author is extremely grateful to all the contributors who found the time and were willing to contribute to this project. Hopefully this chapter will inspire readers to think about injection-molded optics in their own applications.

References

1 W.S. Beich, "Injection molded polymer optics in the 21st Century," *Proc. SPIE* **5865**, 58650J, (2005).

2 T. Brukilacchio and C. DeMilo, "Beyond the limitations of today's LED packages: optimizing high-brightness LED performance by a comprehensive systems design approach", *Proc. SPIE* **5366**, 161–172, (2004).

3 F. Muñoz, P. Benítez, O. Dross, J.C. Miñano, and B. Parkyn, "Simultaneous multiple surface design of compact air-gap collimators for light-emitting diodes", *Opt. Eng.* **43**, 1522–1530, (2004).

4 T. Whitaker, "LED headlamps illuminate the way forward", *LED Mag.* **Nov./Dec.**, 18–19 (2007).

5 G.S. Fiorini and D.T. Chiu, "Disposable microfluidic devices: fabrication, function, and application," *Biotechniques* **38**(3), 429–446, (2005).

6 Given Imaging, www.givenimaging.com

7 F.S. Ligler, "Perspective on optical biosensors and integrated sensor systems," *Anal. Chem.* **81**(2), 519–526, (2009).

8 A. Cvetkovic, M. Hernandez, P. Benítez, J.C. Miñano, J. Schwartz, A. Plesniak, R. Jones, and D. Whelan, "The SMS3D photovoltaic concentrator," *Proc. SPIE* **7059**, (2008).

9.2
Architectural LED Accent Lighting

Application

Architectural accent lighting is a very good application for LEDs. The expected lifetime, small size, low energy consumption, and rich color of LEDs can be considered as strengths. Yet, the amount of light an LED emits combined with its price defines a new set of rules for product development and optics design in the luminaire business. High optical efficiency together with well-prescribed light patterns defines a new challenge to optical design. The price for the optical parts has to compare to standard illumination optics. Figure 9.3 shows a luminaire for highlighting the soffit of a window, the window frame in a façade. The light of two LEDs is mixed in a color mixing rod. A 3D tailored freeform mirror redirects the mixed light toward the target, a strip with 20 cm width and 280 cm height. Tailored freeform optics allows to yield the prescribed illuminance pattern without clipping any radiation. For a specific architectural project, approximately 3000 luminaires are needed to be built in a tight time schedule. Three elevations of a representative building are artfully illuminated with approximately 3 kW of electrical power.
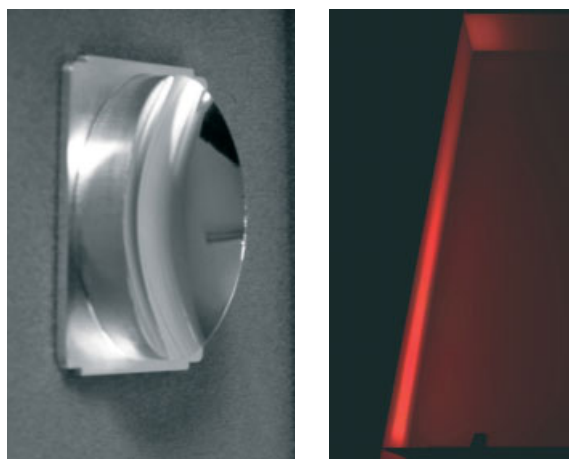
Figure 9.3. 3D tailored freeform mirror (a) casting the light into a thin strip inside an external window frame.

Why Plastic Optics

The two parts of the hollow mixing rod as well as the freeform mirror were produced by injection molding. The plastic construction allowed an easy extension of all parts with frames and mechanical holders, slipping into a main frame of laser cut sheet metal. Single-point diamond ball end milling of the tool for the freeform

mirror allowed a precise tooling of the freeform mold, while injection molding of the part promised a good replication of this complex geometry in the first loop. For the comparably low volume, it was sufficient to use a soft tool. This approach allowed yielding both targets for time as well as costs.

Challenges

The optics design for this demanding project needed to be done quickly and accurately. The 3D tailoring of freeform surfaces supplied a straightforward approach for calculating the mirror surface. Integrating the optical surfaces into the mechanical design helped reducing the number of parts to a minimum of three for the optical system, easily connecting them to the mechanical structure. Translating the NURBS of the freeform surface into a machine path required specifically programmed CAD–CAM tools. Metrology for the freeform surface of inset as well as for the parts was not available, so precision had to be achieved in the first run. Meeting the schedule as well as the price targets was the biggest challenge. Identifying the optimal manufacturing approach for the small volume was a critical point in this project.

Contact Information

Andreas Timinger, OEC AG, timinger@oec.net, www.oec.net
Horst Wodak, UPT Optik Wodak GmbH, h.wodak@upt-optik.de,
www.upt-optik.de

Reference

H. Ries and J. Muschaweck, "Tailored freeform optical surfaces", *J. Opt. Soc. Am. A* **19**(3), (2002).

9.3
Freeform Lens for Logo Forming Illumination

Application

The use of freeform surfaces in illumination has been increasing tremendously over the last 15 years. Freeform surfaces allow forming a well-prescribed and complex illuminance pattern at a target surface with a single optical element. The applications range from automotive head lighting over machine lighting to general illumination. In the last decade, different algorithms for the design of freeform surfaces have been proposed and implemented. Ray-tracing simulations and single piece prototypes show very good performance of the resulting parts. Yet, to prove the validity of freeform optics in industrial processes with high-volume output, the complete chain from optics design to a part, fit for mass manufacturing had to be proven.

Experts for optics design, ultraprecision tooling, and precision injection molding teamed up for this demonstration project to produce a series of plastic lenses with a freeform surface to cast logos of light. Figure 9.4 shows two of the resulting lenses with their light distribution. The front surface of each lens is a spherical surface with large radius. The rear surface is a 3D tailored freeform surface forming the light into the intended pattern.
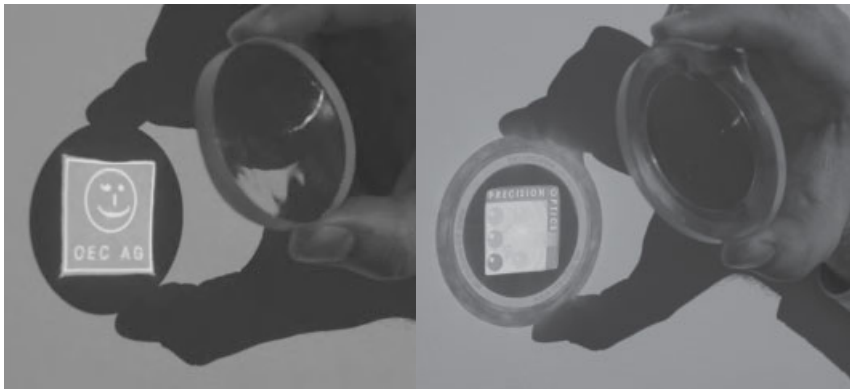
Figure 9.4 (a) and (b) Photos of freeform lenses casting their illuminance patterns.

Why Plastic Optics

The tooling of freeform surfaces is in most cases a time-consuming process. In all cases, it is significantly more expensive than tooling for spherical or rotationally symmetric surfaces. Illumination applications usually need a high-volume output at moderate or very low costs. Hence reproduction processes for the optical elements must meet moderate cost targets. On the other hand, to keep their perfor-

mance edge, freeform optics need to meet tolerance targets, which are tighter than usual for illumination optics. For cost reasons and the ability to integrate mechanical parts into the optical parts as well, plastic optics already have a large market share in illumination optics. Injection molding and compression injection molding of plastic provide replication processes, which allow controlling the balance between accuracy and prices.

Challenges

Calculating freeform surfaces for illumination requires up-to-date algorithms and computing power. The 3D tailoring approach provided very adequate means for this challenge. The translation of the NURBS representation of an optical surface into a machining path for single-point diamond ball end milling is not a standard procedure and had been tackled with in-house programming at the tooling partner. The process control for compression molding needed to be elaborated to yield a good balance between quality and holding time. Since metrology of optical freeform surfaces was not available in the project, a reliable process for tooling was needed. The quality of the molded parts could be assessed by a visual test.

Contact Information

Andreas Timinger, OEC AG, timinger@oec.net, www.oec.net
Horst Wodak, UPT Optik Wodak GmbH, h.wodak@upt-optik.de,
www.upt-optik.de
Oliver Grönlund, IKV Aachen,groenlund@ikv.rwth-aachen.de,
www.ikv-aachen.de

References

H. Ries, and J. Muschaweck, "Tailored freeform optical surfaces", *J. Opt. Soc. Am. A* **19**(3), (2002).

9.4
Optics for Street Lighting Luminaires

Application

In the coming decade, it is expected that the technology for street lighting will undergo a drastic change from the current use of conventional light sources (e.g., low-pressure sodium) to LED-based light engines. The driving force behind this will be mainly power consumption. LED-based luminaires are already considerably more power efficient than conventional types. Also the LED-based luminaires generally provide a much better color rendering making it possible to achieve the same visual acuity (visibility distance for small objects) with a lower amount of lumens, hence contributing again to power savings. In addition, energy savings can be obtained through selective lighting control that becomes more easily accessible because LEDs can be dimmed rather easily.

Why Plastic Optics?

The challenges of street lighting applications are manifold. One of them is the expected lifetime extending easily beyond 15 years. Cost-effectiveness is another one, and clearly the earlier mentioned power savings are crucial. In the latter respect, it is important to exploit the advantage that LEDs have over conventional light sources – that is, LEDs are very small in size. A small source in principle enables a much better control of the light directions, thereby preventing light from being wasted into areas where it is not needed. This can be realized with appropriate small optics close to the LED. Given the boundary conditions of efficiency, accuracy, and cost, the production method suited best for such optics is injection molding. In the inset of Figure 9.5(b), an example of such an optic is shown.
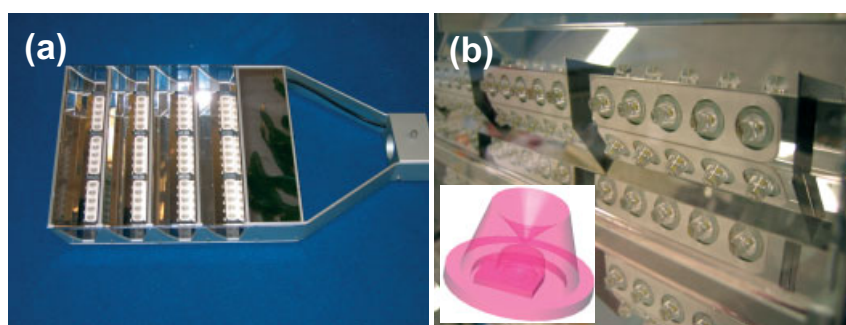
Figure 9.5 (a) Photo of an LED-based street lighting luminaire. (b) Close-up view of the luminaire with the inset showing one of the plastic lenses placed around a LUXEON Rebel LED.

Challenges

The optics designs of street lighting luminaires are demanding in terms of the combination of simultaneous realization of high surface quality (preventing glare), accuracy in shape (ensuring good uniformity in illumination), low manu-facturing cost, durability over lifetime against UV light, and elevated temperatures and ease of assembly. All these challenges can be met using injection-molded optics of the type shown in Figure 9.5.

Contact Information

Stefan Bäumer, Philips Applied Technologies, s.m.b.baumer@philips.com
www.apptech.philips.com
Author: Pascal Bloemen, Philips LumiLeds, info@lumileds.com

Reference

http://www.philipslumileds.com/solutions/outdoor-lighting/

9.5
Injection-Molded Transparent Silicone for High-Temperature and UV-Stable Optics

Application

The number of applications is increasing where temperature load and/or UV load are so high that standard transparent plastic material (e.g., PMMA, PMMI, PC) is not feasible any more. Typical applications are high brightness LEDs, where already radiation densities of 1 W/mm^2 are achieved. Multichip arrays are already on the market (e.g., for automotive headlamps), where the longevity of the primary optics is a challenge for standard plastics. Another field of application is secondary optics for CPV, where highly concentrated sunlight is collected by plastic optics before hitting the solar cell (see Figure 9.6).
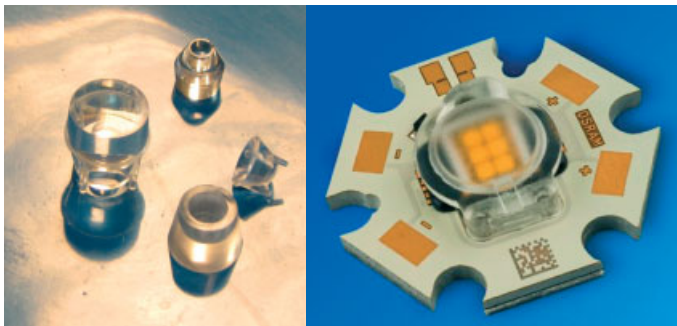
Figure 9.6 (a) Silicone lens prototypes for secondary CPV applications.
(b) Serial silicone lens application for high power multichip LED.

Why Plastic Optics

The large quantities needed for LEDs and solar cells make it necessary to use a scalable production process feasible of producing millions of parts per year at very high quality and simultaneously at a reasonable price. Additionally, the optics needs to function for the full lifetime of the product, which can be 20 years or more (for CPV). Thus, injection molding is the suitable process for these applications, but not with standard polymers, but with injection moldable silicone. This material is proven to provide long lifetime and good UV and heat stability, with a transparency even higher than that of polymethylmetacrylate (PMMA).

Challenges

Silicone hardens by a curing process. Thus the mold design differs significantly from thermoplastic mold design. Since the polymerization is initiated by temperature, cold runners are used to prevent the resin from curing already in the injec-

tion machine. The mold itself is heated, and thus the contact of the silicone resin with the hot mold starts the curing.

The resin consists of two components and is mixed just before injection. It has very low viscosity, which requires a very careful design of the mold to avoid leakage and flashes. Sliders are typically not feasible in a mass production silicone mold due to the risk of flashes blocking the sliders after some injections.

To achieve the accuracy necessary for the high precision demands, diamond turning inserts are typically used. Due to the low viscosity, silicone reproduces very good, even extremely tiny structures, e.g., diffractive optical elements are possible as well. To compensate shrinking of the silicone when curing, insert corrections are inevitable, resulting in one or two iterations in the optimization process.

For high-volume output, multicavity tools are possible. Eschenbach has produced up to 64 cavity tools, resulting in a maximum annual output of several tens of millions parts per mold. Also thick parts are possible with silicone. A big advantage of silicone in that case is that the curing time is not increasing with the thickness like it is the case for thermoplastic injection molding.

Due to the soft surface of silicone, mechanical dimensional measurements are not possible; only optical measurement and control devices are possible.

Contact Information

Thomas Luce, Eschenbach Optik GmbH , Thomas.luce@eschenbach-optik.com
www.eschenbach-optik.com

9.6
Compact Camera for Mobile Applications

Application

During the last decade, integrated cameras have become a standard asset for mobile telephones. These cameras are very compact and yet show a remarkable image quality for their form factor. Also the number of pixel has been increasing steadily, leading to more demanding optics. Autofocus and zoom capabilities have been added into some models as well. This makes these camera modules complete micro-optical electrical mechanical modules (MOEMS). Figure 9.7 shows a typical image of such a camera.

(a)   (b)
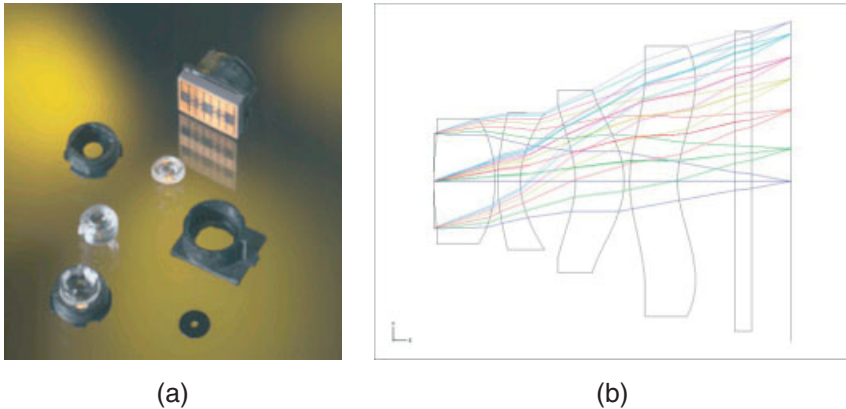
Figure 9.7 (a) Photo of a typical mobile phone lens.
(b) Optical cross-section of a typical mobile phone lens.

Why Plastic Optics?

The challenges for mobile phone applications are manifold. One of them is the manufacturing volume involved. Mobile phone cameras are produced by millions per month. Also the cost price for the optics needs to be very competitive. Therefore, the production method suited best for this application is injection-molded optics. Another more technical reason is that given the form factor and the desired performance of such a camera optic, the use of aspheric optical elements is absolutely necessary. In order to produce aspheric optical elements in large quantities at low cost, again injection molding optics is the most suitable way of doing so. Integrating optical and mechanical features for these lenses has to be done as well. Only a good enough optomechanical design will provide sufficient yield during assembly. Therefore, integrating some mechanical features in the plastic lenses will aid tight tolerance assembly.

Challenges

The optics designs of the mobile phone cameras are very demanding in terms of tolerances. The biggest challenge is to produce lens elements in multicavity tools with a high enough yield. The surface alignment and contour accuracy needs to be of micron and submicron accuracy. This needs to be combined with an assembly strategy designed for yield. A good process control and suitable metrology should be in place. On the design side, the challenge is to match tolerance and manufacturing capabilities. Balancing the lenses thermal and also in chromatic aberrations is quite a task given the limited amount of materials in plastic optics.

Contact Information

Author: Stefan Bäumer, Philips Applied Technologies,
Contact: Rien de Schipper, Penta HT Optics; r.de.schipper@penta-ht-optics.com
www.apptech.philips.com

9.7
Macrolens for an Add-on Microscope Device

Application

An add-on device (Figure 9.8(a)) that can be used to make a simple mobile micro-scope has been developed. A standard camera phone can be turned into a micro-scope simply by placing the device on top of the phone's camera aperture. Inte-grated macrolens design (Figure 9.8(b)) contains both the imaging and illumina-tion optics in a single piece. In the latest prototype, the bifunctional lens was also injection molded directly on a circuit board [1] containing the illuminating LEDs (Figures 9.9(a) and (b)). Pictures taken with the second generation prototype have shown that the phone and add-on device combination can resolve $10\,\mu m$ features on a $4 \times 3\ mm^2$ object surface. A mobile microscope, such as this, holds the bene-fits of an instant microscope image at any site and wireless transfer of data via, for example, Bluetooth or e-mail. Some potential applications for "telemicroscopy" are inspection (e.g., paper/print quality), security markings, telemedicine, envir-onmental monitoring, and education [2].
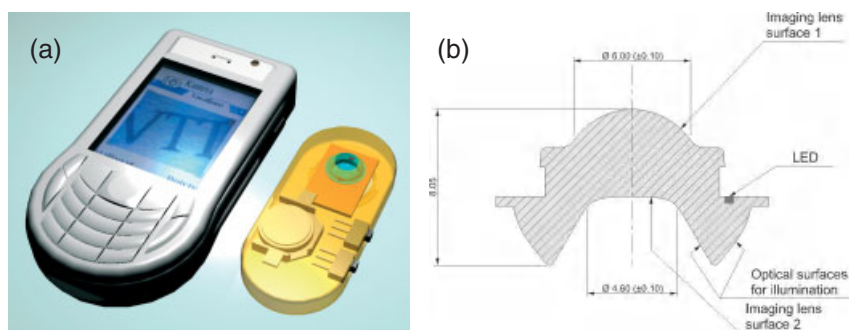
Figure 9.8 (a) Add-on microscope device for a mobile phone and (b) the bifunctional lens component.
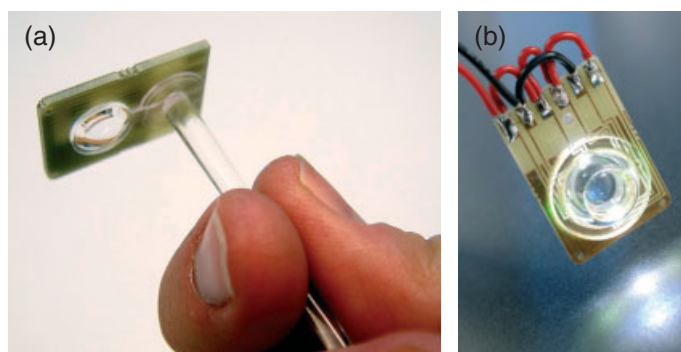
Figure 9.9 The lens has been injection molded directly on top of a circuit board with illuminating LEDs.

Why Plastic Optics

Plastic optics offers a cost-effective way to integrate the two different optical functions needed in a microscope system, imaging and illumination, to a single component. The central imaging lens is double-aspheric and it functions as an extreme macrolens for the phone camera optics. The surrounding illumination system consists of parabolic and conical shapes that collect and direct the light from the LEDs to the area to be imaged with the camera. These four complex optical shapes can be effectively combined by building a single tool that is used to replicate all the features to the 3D shape with one shot of the injection molding machine. By combining the functions to a single component, one can also avoid the need for assembly and relative adjustment of the two optical structures. In this example, the level of integration has also been brought to another level by combining active optoelectronics with the passive optical structures. A circuit board with wire bonded and packaged LED chips was inserted into the mold and the optical structures were injection molded directly on top of and through the electronic component. The PMMA material was, therefore, also used to package the sensitive semiconductor chips by embedding them into the optics. This insert molding technology makes it possible to use bare chip components that are of lower cost than packaged components and also enables some performance improvements due to the lower number of optical surfaces between the emitter and target.

Challenges

Integration of two different optical functions and embedded electronics imposed some very special challenges to the whole development cycle of the prototype optics. In order to fit all the optical surfaces together into a single manufacturable piece, two different optimization approaches were needed. Standard sequential ray tracing was used in optimizing the imaging lens, and nonsequential ray tracing was used in designing the illumination features. These were performed concurrently in a design and simulation loop that also included mechanical design. This loop ensured that all the geometrical requirements from the optical functions (e.g., resolution, homogeneous illumination, and stray light) and manufacturing method were considered properly. Integration of the electronic circuit board increased the challenges of mold design and injection molding. Special features were designed into the mold to overcome the problem of circuit board thickness variation and particular care was needed in finding the suitable molding process parameters that made it possible to overmold the delicate wire-bonded LED chips.

Contact Information

Jukka-Tapani Mäkinen, VTT – Technical Research Centre of Finland, jukka-tapani.makinen@vtt.fi, www.vtt.fi.

References

1 J-T. Mäkinen, K. Keränen, J. Hakkarainen , M. Silvennoinen, T. Salmi, S. Syrjälä, A. Ojapalo, M. Schorpp, P. Hoskio, and P. Karioja, "In-mould integration of a microscope add-on system to a 1.3 Mpix camera phone," *Proc. SPIE* **6585**, 658507-1 to 658507-10, (2007).

2 J-T. Mäkinen , K. Niemelä, H. Vasama, R. Mattila, M. Aikio, S. Aikio, and J. Aikio, "Add-on laser reading device for a camera phone," *Proc. SPIE* **5962**, 596228-1 to 596228-11, (2005).

9.8
Camera Flash for Mobile Phones

Application

During the last decade, integrated cameras have become a standard asset for mobile telephones. These cameras are very compact and yet show a remarkable image quality for their form factor. Accompanied with this trend is the increasing desire to maintain this high image quality in dark environments and hence also have a compact flash. LED-based flash modules have in recent years proven to be extremely suitable to fulfill this need. By using LED-based modules, the stringent demand for very low form factor is met and at the same time offering more functionality (torch and auto-focus assist light) than ever in this same extremely small volume. Additional advantages are the robustness and being Pb-free. Moreover, the use of Fresnel type of optics provides an appreciable freedom in design impacting phone appearance (see Figure 9.10).
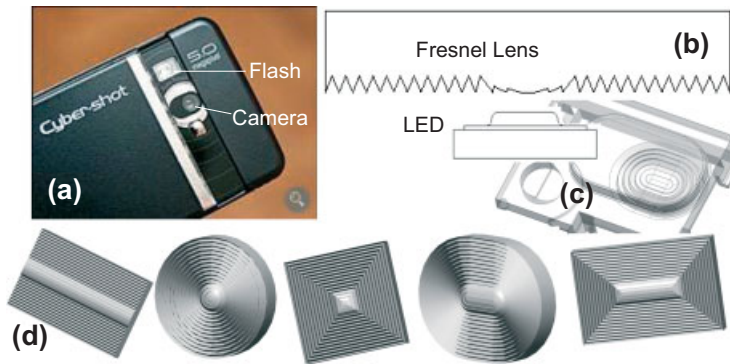
Figure 9.10 (a) An example phone demonstrating the small size of the Flash unit. (b) A cross-section of a typical Fresnel lens. (c) A Fresnel lens integrated in a unit with other mechanical functions. The row in (d) demonstrates the design freedom through different possible lens designs.

Why Plastic Optics?

A major challenge for this type of application is to realize an extremely competitive cost price at a good performance. The lens is commonly integrated into the phone cover and for reasons associated with matched thermal expansion plastic needs to be used as lens material. Also often several alignment and other mechanical features need to be integrated to enable accurate assembly. Therefore, there is no doubt that the production method suited to manufacture such flash optics is injection molding.

Challenges

The optics designs of Fresnel lenses for flash application are demanding in terms of surface profile accuracy. As a result of the ultra-low building height, the lens requires a considerable number of Fresnel teeth that each should have the correct angle, and equally important the teeth should be sharp. When not sharp enough, an appreciable amount of flash light is not directed at the intended scene and hence will not contribute to the image quality. Supplier choice and process conditions need to be checked to ensure a good optical performance. Figure 9.11(b) shows a microscope image of a Fresnel lens with teeth that are rounded too much, whereas Figure 9.11(a) shows a Fresnel having the proper surface quality and sharpness of teeth.
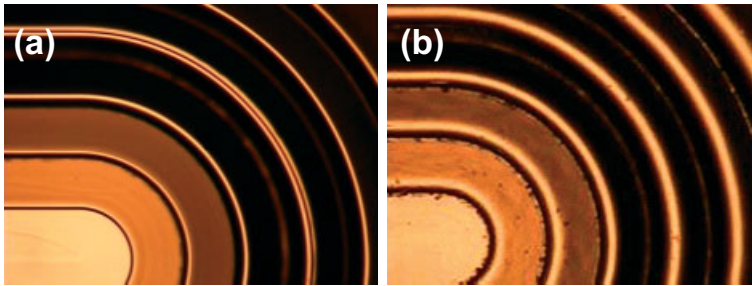
Figure 9.11 Microscope images of (a) a good-quality Fresnel lens and (b) a bad-quality Fresnel lens. The thickness of the transitions is the representative for the sharpness (rounding) of the teeth.

Contact Information

Stefan Bäumer, Philips Applied Technologies, s.m.b.baumer@philips.com
www.apptech.philips.com.
Author: Pascal Bloemen, Philips LumiLeds, info@lumileds.com

References

http://www.philipslumileds.com/solutions/cameraphoneflash/

9.9
Extreme Aspheric Objective for 360° Camera System

Application

The application in this instance is an eight-element (Figure 9.12) 360° omni view imaging system with a depth of field from 12 inches to infinity. The optical design performance demanded multiple biaspheric surfaces but most critically an objective with four active optical zones, including two second surface mirrors and two AR apertures (Figure 9.12). Plastic was also the only obvious choice because of the physical packaging constraints. The entire lens train could be no more than 100 mm. Given the product application market of commercial and home security, a full omni-directional camera without the need of articulating motors or drives, the volume requirements were quite large and the market cost drivers low. Target cost for the entire system was less than $100.00 USD.
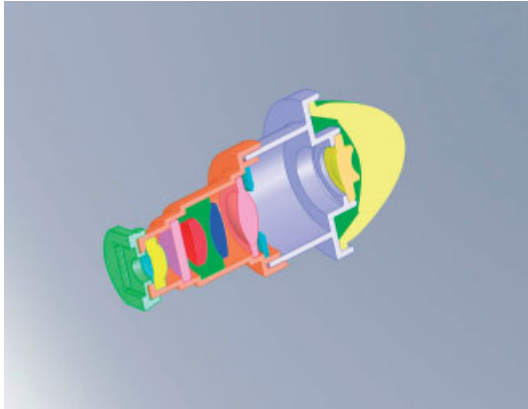
Figure 9.12 CAD model of the security camera assembly.

The exercise became far more than a simple integration of lenses, as the assembly cost would play an important role in the success of meeting the target price.

Challenges

Since the entire lens train were more of conventional polymer optic problems (i.e., good edge thickness to CT ratio, large flange area, and with the exception of one lens meniscus or positive), the real trial was with Element 1. The object had four active optical areas, a center-to-edge thickness ratio of 6.7:1, and an index of refraction requirement that specified cyclic olefin copolymer as the material of choice, see Figure 9.13. Thus the challenges were as follows:

- very thick optic (17.120 mm center thickness);
- biaspheric with steep S1 departure rate;
- COC material – generally requires long cycle time and is not low cost conducive;

$\emptyset 42.74^{+1}_{0}$

$\emptyset 18.12^{+0.50}_{0}$

| ⌾ | $\emptyset$ | .12 | A | B |

$\emptyset 30.44^{0}_{-1}$

$\emptyset 6.42^{0}_{-0.50}$

Zone 2, Annulus
AR Coated

Zone 1, Annulus
Al Coated

E

[30.437]

(13.317)

E

SECTION E-E

$\emptyset 26.40^{+1}_{0}$

| ⌾ | $\emptyset$ | .12 | A | B |

$\emptyset 8.32^{+0.50}_{0}$

| ⌾ | $\emptyset$ | .12 | A | B |

Zone 3,
Multilayer
BB AR

Zone 4, Annulus
Al Coated

		DIMENSIONS ARE IN MM		NAME	DATE		
		TOLERANCES: FRACTIONAL± ANGULAR: MACH± BEND ± TWO PLACE DECIMAL ± THREE PLACE DECIMAL ±	DRAWN	LL			
			CHECKED			Al & AR Coating Print	
			ENG APPR.				
			MFG APPR.				
PROPRIETARY AND CONFIDENTIAL		MATERIAL	Q.A.				
THE INFORMATION CONTAINED IN THIS DRAWING IS THE SOLE PROPERTY OF SYNTEC TECHNOLOGIES. ANY REPRODUCTION IN PART OR AS A WHOLE WITHOUT THE WRITTEN PERMISSION OF SYNTEC TECHNOLOGIES IS PROHIBITED.			COMMENTS				
	NEXT ASSY	USED ON	FINISH			SIZE **A**	DWG. NO. 100403-7	REV. **7**
	APPLICATION		DO NOT SCALE DRAWING			SCALE:1:1 WEIGHT:		SHEET 2 OF 4

Figure 9.13 Technical drawings and specifications.

- multiple thin films BBAR and Al reflective coatings;
- Metrology requirement generally required contact profilometry.

To solve these issues, Syntec Optics assumed innovative approaches initiated with the mold design incorporating an active hybrid cooling system and an evolutionary gating scheme. This allowed a reasonable process window to be created and the option for multicavity tooling development. The ability to accurately control the shrink amount typically associated with such thick optics enabled process diffraction optical element (DOE) to compensate the insert geometries for cycle time reduction, thus significantly reducing the element cost. Robotic end of arm tooling providing labor-free handling and custom-designed null correctors were incorporated with Fisba Interferrometers in line to minimize in process inspection time.

Contact Information

Paul R Tolley , CEO, ITC MEMS www.itcmems.com, paul.tolley@itcmems.com www.syntecoptics.com.

9.10
Snap-Mounted Optics Assembly

Anyone who has been involved in product design for any length of time has experienced efforts that have not made it to market for various technical, marketing, or financial reasons. But in most cases, there were embedded successes in these efforts. Such is the case for the fairly complex structure represented in Figure 9.14; a molded optomechanical subassembly for a head-mounted display intended for minimally invasive surgical procedures.
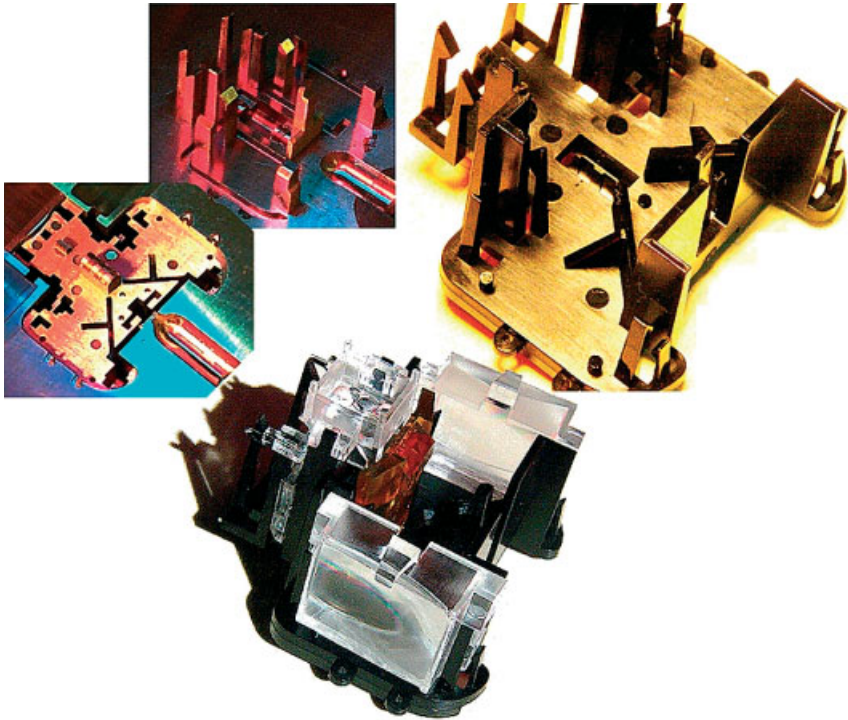
Figure 9.14 Prisma HMD snap – assembly (US patent 6,480,174).

In the end, the chosen optical approach proved to be impractical. But the optomechanical integration techniques were unique and effective. The challenge was to integrate seven individually molded optical functions into a subassembly with least labor and exquisite precision, involving the fewest mechanical interfaces in order to minimize tolerance stacks. Goals included automatically referencing optical elements to one another without any secondary operations such as alignments or bondings.

This was accomplished by using a common mechanical base with integrally molded features including two snap fingers, one spring finger, and three reference surfaces for each inserted optical component. Each optical component had a

corresponding series of eight contact points to achieve alignment in all planes and axes with a three-point plane (rear surface), a two-point line (bottom), and a single-point reference (left side); all loaded into contact with the snaps and spring. This concept is graphically illustrated for a single optical element in Figure 9.15.
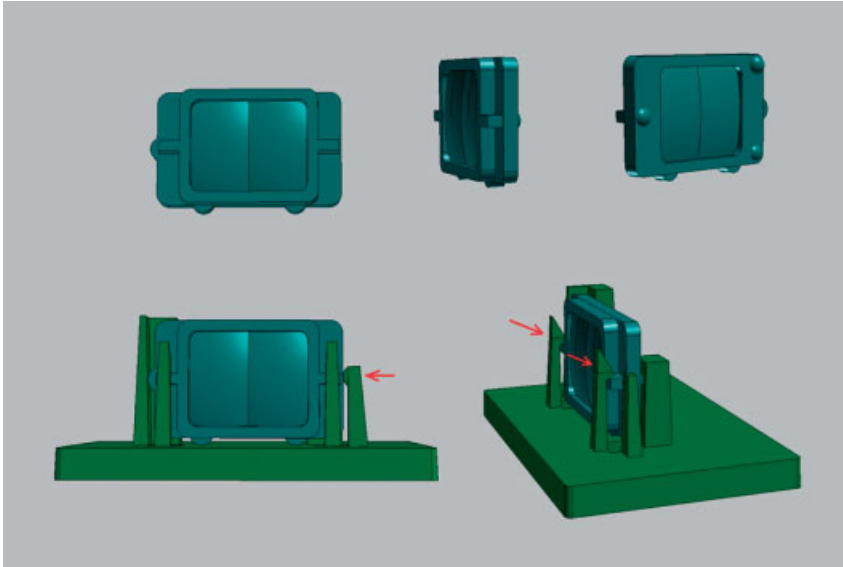
Figure 9.15 Molded snap fit.

Contact Information

Ray Hebert, Prisma Optics, prisma-optics@mindspring.com
www.prima-optics.com.

9.11
Solar Fresnel Lenses

Application

Augustin Jean Fresnel published his treaty on Fresnel lenses for lighthouses in 1822. He understood that only the curvatures of the surfaces of a lens are important. The bulk of the material could be eliminated. Suddenly, it became possible to design and make lightweight large-area Fresnel lenses composed of glass prisms (Figure 9.16). Global and local surface slopes are decoupled.
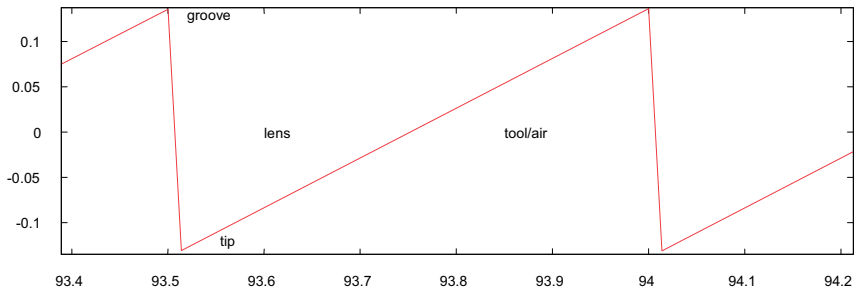
Figure 9.16 Fresnel lens prisms. Step size is 0.5 mm. Light enters from the top and is refracted toward the left.

Lighthouses became obsolete, but Fresnel lenses (now made of plastics) are applied as state-of-the-art concentrator lenses for CPV (Luque 2008). The collection of sunlight demands large-area, lightweight, and durable lenses of high spectral transmissivity and high accuracy. The development of CPV systems is driven by efficiency and cost. The decoupling of slopes allows for the design of non-imaging Fresnel lenses (Leutz 2001).

Why Plastic Optics?

Large-area Fresnel lenses are produced by casting or hot embossing. Single lenses may have any size, but individual lenses are often combined into parquets of areas exceeding 1 m^2 (Figure 9.17). The lenses must be highly transmissive, that is, the geometrical losses due to tip and groove radii, and slope of the draft angle must be minimal. The high surface tension of glass prohibits sharp prism structures when made of cost-effective processes like hot embossing or molding.

Plastic Fresnel lenses can be made in large quantities at a cost below 100 €/m^2. Parquets are made to size, with built-in alignment tolerances. The plastic parquet facilitates mass manufacturing of CPV modules.
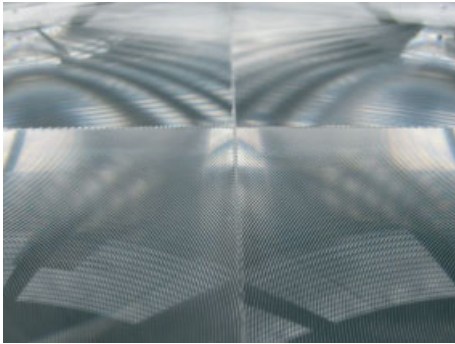
Figure 9.17 Fresnel lens parquet for concentrating photovoltaics (CPV) hot embossed in PMMA.

Challenges

The design of nonimaging Fresnel lenses for CPV is successful only if advanced under a systems approach encompassing the spectral and angular characteristics of the sun, as well as the performances of the parts of the CPV plant in terms of optical efficiencies and tolerances. Lens and secondary (if any) must be designed as one optical train, matching the spectral response, and the uniformity requirements of the multijunction cell.

Tooling of Fresnel lenses is a forgotten art. Making Fresnel tools by modern lathing using diamond points cutting an x–y-profile is a difficult task as prism surfaces must be smooth, and prism grooves must be as sharp as possible with radii under 5 μm.

Solar Fresnel lenses are embossed in PMMA in a hot-and-cold pressing process (Figure 9.18). Other plastics include silicones, which are cured during the embossing process. Mass manufacturing of large-area optics requires time-optimized processes and full automation.

PMMA has a large thermal expansion coefficient of $8.4 \, 10^{-4} \, \mathrm{K}^{-1}$. Differential expansion in CPV modules must be observed. The spectral transmissivity of PMMA can be adapted to the solar spectrum. Enhancement in the UV from 350 nm is a challenge if the material is not to be compromised in its stability. Solar PMMA will be exposed to outdoor conditions for 25 years; its surface hardness of 3–4 H could be improved to better scratch resistance.
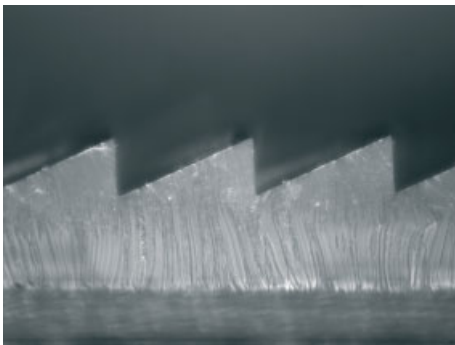
Figure 9.18 Fresnel prism embossed in silicone. Step size 0.5 mm.

The longevity of plastic optics is decisive for the success of the majority of CPV systems: PMMA and some silicones are UV-stable, weatherable, and do not yellow (Figure 9.18). And plastic optics is quite suitable for high-grade solar Fresnel lenses.

Contact Information

Ralf Leutz, Concentrator Optics GmbH, ralf.leutz@concentratoroptics.com, www.concentratoroptics.com.

References

R. Leutz and A. Suzuki, *Nonimaging Fresnel Lenses: Design and Performance of Solar Concentrators* (Springer, Berlin, 2001).
A. Luque (ed.), *Concentrating Photovoltaics* (Springer, Berlin, 2008).

9.12
Refractive–Diffractive Eyepiece

HMDs have had a strong military market for years. But efforts to commercialize their applications have been slow to develop due to limitations and tradeoffs of cost, performance, quality, and ergonomics. This is now changing due to technical advances in combination with miniaturization and mobility of applications that would benefit from large-screen graphic quality. Microdisplays have been shrinking in size, thereby impacting cost, and gaining in resolution with decreasing pixel size.

These considerations place substantial demands on the design of the virtual-display eyepiece optics in terms of performance, size, weight, and cost; demands that generally cannot be met with conventional glass optics. Optical performance requirements include wide field of view, high resolution, low distortion, and minimal color in combination with ergonomic requirements of focal range, substantial eye relief, and large exit pupil for generous eye placement tolerance with minimal eyestrain. In other words, we are talking about very short focal length, low *f*/number designs.

The application of diffractive chromatic correction has been found to be highly beneficial to such designs, best used in combination with some degree of refractive chromatic correction. This combination approach minimizes the characteristic blue or red haze associated with the falloff of diffractive efficiency to either side of the chosen optimization wavelength. At the same time, it reduces overall thickness by taking advantage of the positive optical power of a diffractive surface and reduced required negative power associated with refractive chromatic correction. The combination also tends to keep challenging diffractive cut profiles to a realistic scale (pitch greater than $10\,\mu\mathrm{m}$). Along with aspheric profiles, this minimizes path length, number of elements, weight, and cost.

Figures 9.19 and 9.20 illustrate a refractive–diffractive eyepiece doublet design based on the above principles. In keeping with the principles of refractive achromats, a positive eyepiece of a lower dispersion material (Apel) is followed by a negative element of a higher dispersion material (polycarbonate); in this case, placed in a field lens position for distortion control. The diffractive surface is applied to the inside, environmentally protected surface of the positive element with power appropriate to achieve ideal performance tradeoffs. Based around a 7.7-mm diagonal microdisplay, this 14.9 mm effective focal length (EFL), *f*/1.85 design achieves a 28° field of view with an eye relief of 20 mm and an unobscured exit pupil of 8 mm. Video graphics array (VGA) resolution is achieved with 50% MTF through a 4-mm eye pupil with less than 1% distortion.

Many such designs are now in production, several with further enhancements of field of view (FOV) and resolution with the addition of a third element.

The primary disadvantage of this approach is the limited choice of vendors capable of tooling and molding such designs. There are perhaps no more than a dozen or so such firms in the USA. A precision diamond-turning lathe and specific skills are essential to the prototyping and tooling of diffractive surfaces, as well as
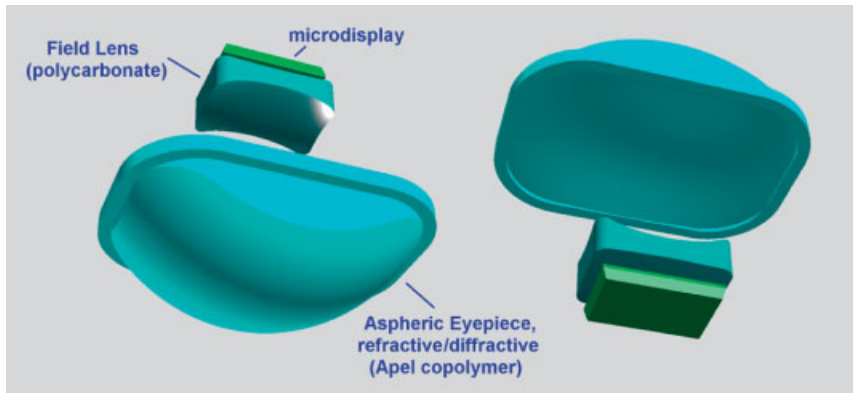
Figure 9.19 Overview design refractive–diffractive eyepiece.
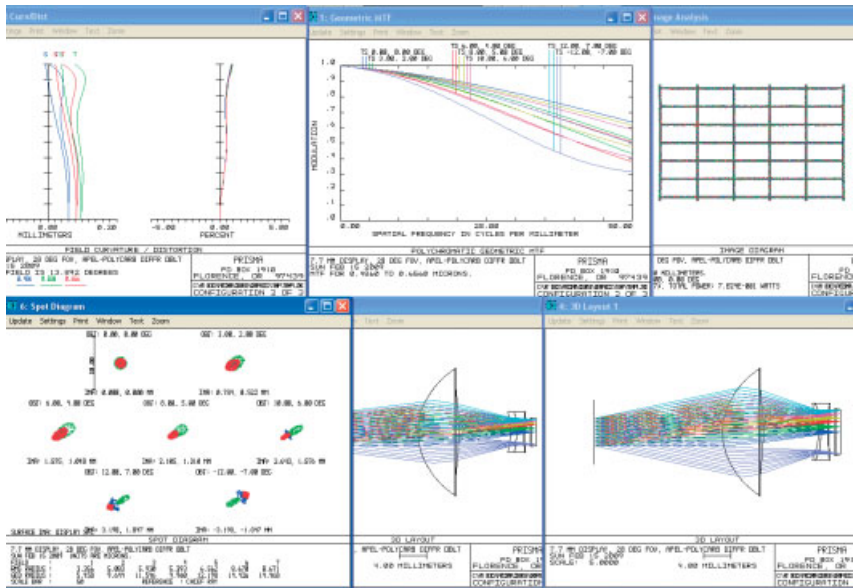
Figure 9.20. Ray trace model refractive–diffractive eyepiece.

appropriate optomechanical metrics for evaluating the results. Diffractive profiles must be turned free of mechanical chatter with near dead-sharp corners to approach theoretical diffraction efficiency and minimize scatter. Softer polymers such as polycarbonate are generally inappropriate for diffractive prototypes.

Contact Information

Ray Hebert, Prisma Optics, prisma-optics@mindspring.com
www.prima-optics.com.

9.13
Pentaprism Assembly

Application

This viewfinder for a professional long-distance measurement device is equipped with a plastic molded pentaprism (Figure 9.21). This prism has integrated molded aspherical lenses as inlet and outlet windows, which take care of the proper magnification and aberration correction. Besides bending the light by 90°, there is also a laser mounted on one mirror side of the prism. This laser is precisely aligned to the center of the image and indicates the measurement spot.

Figure 9.21 Pentaprism for viewfinder.

Why Plastic Optics

Injection molding made it possible to integrate the lenses into the prism, together with mounting features for exact alignment of the assembly in the unit. Adding the laser requires two more plastic parts, a lens/carrier, and an iris. Both parts have a high level of optomechanical integration. Chosen material and processing methods, in combination with used assembly procedures, have led to a price breakthrough for this product, which is going to be produced in relatively high volumes.

Challenges

- *Design aspects*: The optical design of the aspheres is an optimized solution between the requirements of the image made by the viewfinder and the requirement of the target marking laser spot, many aspects needed to be taken into account, including the optical layout of the human eye.
- *Material aspects*: Material choice was by and large related to the requirements of the optical coatings. The chosen coatings are all interference filters, partly transmitting keeping the balance between transmission/reflection, for the white

light of the image and the red light of the laser as well. Choices were made such that the relatively thick coatings withstand the environmental conditions of an outdoor used, handheld application.

- *Processing aspects*: The quality of the image is largely determined by the flatness of the mirror surfaces, which is specified as $\lambda/10$ per mm. In practice, this means a rather long cycle time and a very accurate mold temperature control.

Contact Information

Rien de Schipper, Penta HT Optics; r.de.schipper@penta-ht-optics.com
www.penta-ht-optics.com.

9.14
High-Efficiency Microoptics for Illumination Projection Systems

Application

In close cooperation with MEMS Optical Inc., the JENOPTIK Polymer Systems GmbH has developed a double-sided MLA precisely aligned front-to-back in plastic. A proprietary tooling allows for very accurate alignment of the two sides of the mold. That enables homogenized optical paths. Because of their flexibility in design, the MLAs can be applied in various fields of application (Figure 9.22). They are especially used in micro projection systems, which can be found in data projectors or cellular phones. Jenoptik Polymer Systems has the expertise to attend products with these elements from design to final product as well as the capability to manufacture them in volume production.
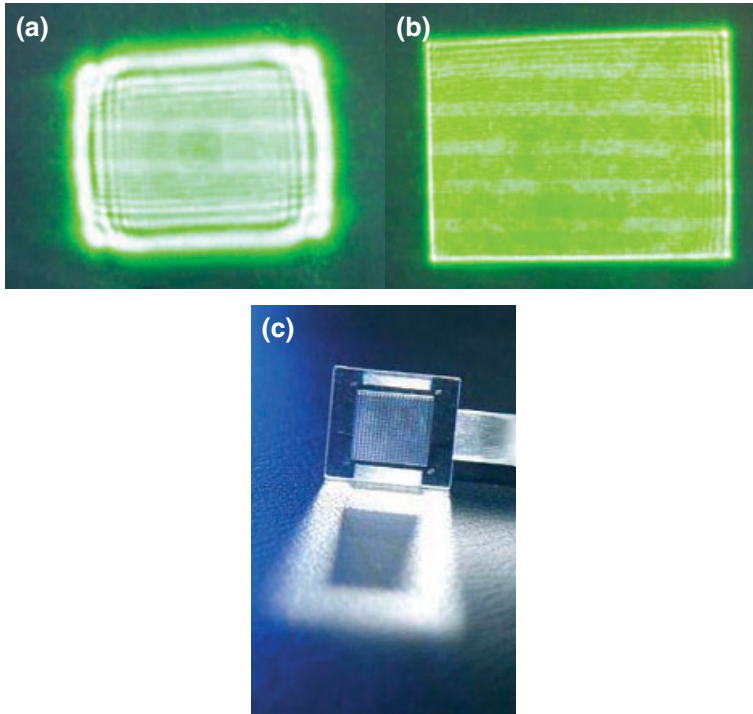
Figure 9.22 (a) Far-field pattern from a single-sided MLA. (b) Far-field pattern from a double-sided MLA. (c) Prototype double-sided MLA produced in plastic (9×7 mm).

Why Plastic Optics

The double-sided MLA can be used in various applications. Especially in the field of consumer applications, it is important to manufacture high volume at low

costs. That is one reason for using plastic optics. Injection molding allows for designing mounting and alignment features as an integral part of the optical component, which then can be assembled in a system or module. Because the same tools are used for each item, a consistent quality is assured. A low risk of breakage of the optics is another important advantage in the use of plastic optics in consumer applications, since they tend to fall down easily.

Challenges

Because the array can be implemented in various products, each application has its own challenges, but a few things have to be thought about in general. While designing the application, it has to be considered that the array has to have some additional lines for clear aperture. There is also some extra space for an ejector needed, because the array itself must not act as an ejector (because the needed backlash would not allow a perfect centering of the arrays).

A bigger challenge is the accurate adjustment of the two arrays. A new proprietary tooling technology allows for the two mold halves, and thus for the arrays, to be adjusted step by step. Depending on the typically small size of the single lenses of the arrays and the required surface accuracy of each lens and the pitch between them, a lithographic process is used to provide a highly accurate master (e.g., made of fused silica). The necessary adjustment marks for the alignment are positioned next to the array in the same process. Afterward, the master is used to manufacture a negative mold insert via electroforming.

Contact Information

JENOPTIK Polymer Systems GmbH,
sales@jenoptik-ps.de, www.jenoptik-ps.de.

9.15
Eye Spectacles

Application

Historically spectacles were made in glass. However in the last century, it was also possible to make them in cast plastic with CR39 as the dominant material [1]. Basically the way of manufacturing was similar. Initially a blank is made and by different process steps, the final spectacle is made.

In the USA, there was a quest to have more impact-resistant spectacles than possible with the cast plastic, and they therefore produced blanks in polycarbonate (PC) and finished them with known processing steps like milling, grinding, and polishing.

Determining the stock keeping units (SKU) distribution, it is clear that a few SKUs are made in high quantities and for these SKUs injection molding is an economic way of manufacturing. Figure 9.23 shows a typical molded lens blank.
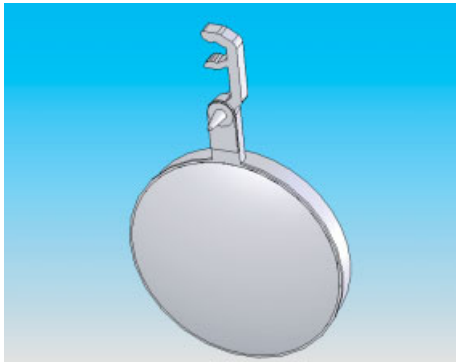
Figure 9.23 Typical injection-molded PC spectacle lens blank.

Recently people also started to mold finished spectacle lenses. For the high volume standard prescription this is even more economical than working with blanks.

Why Plastic Spectacles?

- It allows more freedom in design.
- It is more cost-efficient.
- It is of less weight.
- It has superior shock resistance (PC material).

Besides cost-effective manufacturing, the freedom of design is another important parameter in the choice for plastic spectacles. Modern multifocal and progressive glasses require a very sophisticated surface geometry [1]. Using suitable blanks and the well-understood processes of milling and polishing the forms,
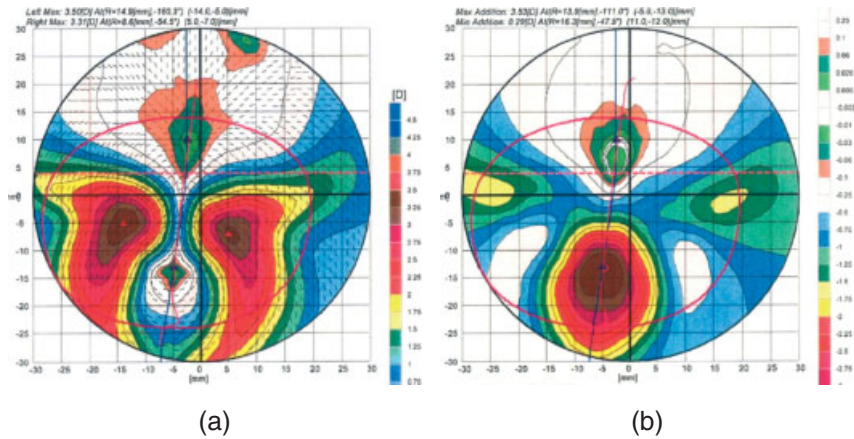
Figure 9.24 (a) Surface power cylinder map. (b) Surface power add map.

more comfortable designs with large progressive areas can be produced. Figures 9.24(a) and (b) show aspects of such a design ((a) surface cylinder power map, and (b) the surface power addition map).

Challenges

- Different SKUs per shot
  Due to the differences in shape between SKUs, there is a difference in the most optimal process per SKU. In case the same process can be used for different SKUs, the cost price of SKUs will decrease.
- Stress-less lenses with big variations in wall thickness.
  There is a contradiction in minimum stress in the lens at one hand and reduction of cycle time on the other hand.
- Controlling and designing for shrinkage

Contact Information

HTP Tooling, Esp 430, 5633 AJ Eindhoven, The Netherlands
Email: info@htptooling.com.

References

1 C.W. Fowler, "Method for the design and simulation of progressive addition spectacle lenses," *Appl. Opt.* **32**, 4144–4146 (1993).

Index